THE NUCLEATION AND GROWTH OF PRECIPITATES IN ALUMINIUM ALLOYS

by

M.H. JACOBS, B.Sc., A.Inst.P.

T.I.RESEARCH LABORATORIES, HINXTON HALL, CAMBRIDGE,

and

UNIVERSITY OF WARWICK, COVENTRY.

A dissertation submitted

to the

University of Warwick

for the

degree of Doctor of Philosophy

August, 1969.

All the original work on aluminium-zinc alloys which is reported in this dissertation was carried out during the period October 1966 to August 1969. The experimental work reported on the aluminium-magnesium-silicon alloy is a continuation of the earlier work mentioned above. For completeness, some of the earlier work is described in this dissertation. Where this is so (particularly Chapter 5) it is clearly stated and it is acknowledged that it was carried out in collaboration with Dr. Pashley. Also, Chapter 3 includes a section in which an electron diffraction investigation of the crystal structure of the needle-shaped precipitates in the aluminium-magnesium-silicon system is described. A few of the electron diffraction patterns which are discussed in that section were obtained by me prior to October 1966, but the detailed analysis of the results was carried out after that date.

Finally, I wish to thank British Aluminium Research Laboratories, Chalfont Park, for supplying the aluminium alloys and, in particular, to thank Miss M.K.B.Day and Dr.A.J.Cornish for the interest they have shown in my work. I also gratefully acknowledge the help of Mr.A.G. Doggett with some of the heat treatments, the assistance of Mr. B. Jaggard and Mrs. Christine Simpkins with the photographic work and Mrs. Beryl Chapman for typing the final manuscript.

I declare that the experimental results described in this dissertation and their interpretation are, to the best of my knowledge, original, except where reference is made to the work of other people. No part of the dissertation has been submitted for a degree at any other University.

M. H. Jacobs.

August 1969.

T.I. Research Laboratories,
Ilinxton Hall,
Cambridge.

ABSTRACT

The aim of the work described in this dissertation was to gain an improved understanding of the basic factors controlling the nucleation, growth and stability of precipitates in age-hardening alloys. The stimulus for the work was provided by the current use of complex ageing heat treatments for modifying (normally with the object of improving) the mechanical properties of alloys. The research was confined to aluminium-base alloys, but it is believed that many of the ideas and concepts yielded by the work will be equally applicable to other alloy systems.

Two aluminium-base alloys were studied in detail: one composition of aluminium-magnesium-silicon alloy and three compositions of aluminium-zinc alloy. The experimental heat treatments were carried out on thin foil samples ($\sim$ 0.01 cm.thickness) and the resulting precipitation was studied by means of thin foil transmission electron microscopy.

The low temperature precipitation sequence of aluminium-zinc alloys has been investigated extensively by other workers and their results are reviewed in Chapter 3. During this investigation, some samples of aluminium-zinc alloy were quenched rapidly to a high ageing temperature and, under these special ageing conditions, a new type of precipitate was observed. The morphology and crystal structure of this precipitate are described in Chapter 3. Also described in Chapter 3 are the results obtained from an extensive electron diffraction investigation into the crystal structure of the small needle-shaped precipitates which are formed, under suitable ageing

conditions, in aluminium-magnesium-silicon alloys.

The types of heat treatment that were studied may be broadly classified into two categories: (1) single-step ageing treatments, and (2) two-step ageing treatments. A large number of single-step and two-step ageing treatments were investigated, with the general objective of obtaining a comprehensive idea of the overall response of the two alloys to the heat treatments. These experimental results provided data for the development of a theoretical model to explain the basic processes affecting the response of both alloys to two-step ageing treatments. It is emphasized that the basis of this model had already been detailed by Dr. D. W. Pashley,F.R.S. to explain the extensive microstructural observations obtained, at T.I. Research Laboratories, with an aluminium-magnesium-silicon alloy, during an earlier research programme (the salient points of this model are discussed in Chapter 5 of this dissertation). Many aspects of this model are extended and amplified in Chapters 4 to 7 and it is shown that there is an excellent qualitative agreement between the predictions of the model and the numerous experimental results which have been obtained. This applies not only to the aluminium-magnesium-silicon system but also to the aluminium-zinc system.

The model has been particularly successful for aiding the semi-quantitative explanation of the observed marked dependence on heat treatment conditions of the width of grain boundary precipitate-free zones in aluminium-zinc alloys. A full account of this aspect of the work is presented in Chapter 6. The model also provides a new insight into the basic processes controlling the phenomenon of reversion in aluminium-zinc alloys, and this is described in Chapter 7

together with an account of the experimental results obtained from "reversion" studies with this alloy.

Finally, in Chapter 8, the theories and concepts developed in this dissertation are compared and contrasted critically with those of other workers.

For brevity, the alloys are denoted throughout this dissertation by their chemical symbols. Except where otherwise stated, all alloy compositions are given in weight per cent.

CONTENTS

CHAPTER 1

INTRODUCTION AND DISCUSSION OF PREVIOUS WORK

1.1 AIMS OF THE RESEARCH

Since almost the beginning of this century the process of precipitation hardening has been used as a method for improving the strength of some alloys and the process has had considerable impact in the light-alloy industry, particularly with aluminium-base alloys. Much of the early progress in the development of stronger and more useful alloys was empirical in nature, although there has been a constant effort to understand the process scientifically.

The work described in this dissertation was aimed at improving the understanding of the factors controlling the formation, growth and stability of the precipitates which are formed during age-hardening heat treatments. Electron microscopy was used throughout the work as the technique for studying the precipitation. Experimentally, the research involved examining the effect of different ageing conditions on the type, size and distribution of the precipitates which were formed in high purity alloy samples.

Two aluminium-base alloys were studied in detail; one composition of Al-Mg-Si alloy and three compositions of Al-Zn alloy. The former alloy is of considerable industrial interest, as it is used as the basis for a number of commercially important alloys. The latter alloy has little direct commercial importance but was chosen for study for a number of reasons:

(1) it is a relatively simple binary alloy system that exhibits considerable solubility of zinc in aluminium at high temperatures and an extensive two-phase region at low temperatures;

(2) the alloy has been studied by many workers, using X-ray and electrical resistivity techniques, and the ageing sequence and ageing characteristics are well documented;

(3) the initial G.P. zones that are formed by low-temperature ageing are spherical in shape and give rise to only small coherency strains, two facts which it was hoped would make easier the development of a semi-quantitative model to explain the precipitation behaviour.

The original aim of the work was to study the response of the alloys to two-step ageing treatments in which a sample is first quenched and aged isothermally at one temperature, T_1, and then given a second ageing treatment at some higher temperature, T_2. Conventional ageing treatments are often a special case of this type of heat treatment, where T_1 is room temperature and T_2 is often referred to as the "artificial ageing temperature". In order to derive a satisfactory model to explain the precipitate distribution at the end of such a two-step ageing treatment it was found necessary to study separately the factors influencing the formation of precipitates, the growth of precipitates at T_1 and the stability of precipitates when the temperature was raised from T_1 to T_2.

The remaining sections in this chapter are devoted to brief surveys of certain topics which have been discussed in the literature and which form necessary background information to the subject matter of later chapters.

1.2 HISTORICAL BACKGROUND

The history of precipitation hardening goes back about sixty

years to the discovery, by Wilm[1] in 1906, that the hardness of a quenched Al-Cu-Mg alloy initially increased with time at room temperature. He was unable to detect, by optical microscopy, any structural changes within the alloy which could account for the increase in hardness and his observations remained unexplained for about a decade, until the work of Merica, Waltenberg and Scott[2], in 1919. In their study of an Al-Cu alloy they demonstrated that the solid solubility of copper in aluminium decreases with decreasing temperature and this led them to propose that the age-hardening was a consequence of extremely small precipitate particles. In a review paper, published in 1932, Merica[3] suggested that hardening in Al-Cu alloys resulted from the assembly of copper atoms into a random array of small groups ("knots") and that these interfere with slip within the grains.

The first direct evidence in support of Merica's "knots" was provided in 1938, when Guinier[4] and Preston[5] discovered, independently, the diffuse X-ray scattering from aged alloys. They interpreted these diffuse effects as being due to very small segregates of solute atoms within a supersaturated matrix and these solute clusters have since been called Guinier-Preston zones (G.P. zones).

In the years following these early discoveries a large number of alloy systems were found to exhibit the precipitation-hardening behaviour, particularly the aluminium-base alloys. The X-ray techniques used originally by Guinier and Preston were developed and became invaluable in the search to understand the precipitation process. Extensive use was also made of the changes which occur in different mechanical properties of an alloy during precipitation-hardening, as a means of following the decomposition process. The change in electrical resistivity of an alloy during ageing was also found to be a useful way of following the process

and this, together with the X-ray and mechanical property techniques mentioned above, are still widely used today. The major drawback of these techniques is that no direct knowledge of the distribution of precipitates in the alloy is readily available from the experimental measurements and it was not until recent years, when transmission electron microscopy became available as a research tool for investigating the microstructure of materials at high magnification (and resolution), that more direct evidence of the changes taking place during precipitation-hardening became possible.

A considerable amount of research effort has been aimed at improving the understanding of the basic processes controlling the precipitation and, in particular, the thermodynamics and kinetics of the associated phase changes (see, for example, the reviews by Hardy and Heal[6], Hardy[7], Newkirk[8], Kelly and Nicholson[9] and Christian[10]).

It is now generally recognised that the precipitation can be divided into different categories, according to the mode of the precipitation. The following modes can be distinguished[10] :

(i) Continuous precipitation ;

(ii) Discontinuous precipitation ;

(iii) Precipitation of metastable phases ;

(iv) Formation of segregates, or G.P. zones.

The first two modes distinguish between two main types of diffusional process. Continuous precipitation is applied to the situation where solute atoms are transported over (relatively) large distances in the matrix to growing precipitates and the reaction proceeds simultaneously at a number of sites throughout the matrix. If the sites are associated with crystal defects (e.g. dislocations, grain boundaries)

the precipitation is said to be heterogeneous; if not, it is said to be homogeneous. In the case of discontinuous precipitation, the distribution of precipitates is non-uniform and the reaction is confined to an advancing interface which separates regions of crystal where the transformation is complete from regions where the transformation has not been initiated. Discontinuous precipitation is always heterogeneous in nature, for example, it is often confined to a grain boundary.

The formation of G.P. zones and metastable phases often precedes the formation of the equilibrium precipitates, particularly if the ageing temperature is low and the initial solute supersaturation is high. A typical ageing sequence is

G.P. zones → metastable intermediate precipitates → equilibrium precipitate.

Two early theories of the ageing sequence can be attributed to Geisler[11] and to Guinier[12]. Geisler based his theory (the "sequence theory") on the observed changes in diffuse X-ray scattering from a number of alloys and concluded that there is a sequence of stages during the decomposition, which correspond to the progressive development of the intermediate precipitate in one, two and then three, dimensions. Guinier interpreted the X-ray effects differently. In his "pre-precipitation" theory he considered that the reaction proceeds in a number of distinct stages, each of which can be associated with a characteristic type of intermediate precipitate. He suggested that the initial stage, the "pre-precipitation" stage, was associated with clustering of solute atoms into zones and that "these occur without the presence of two distinct phases"[13]. Kelly and Nicholson[9] have refuted this idea and consider that G.P. zones should be treated as a second phase, with the general characteristic that the G.P. zone/matrix interface is coherent, and possibly diffuse, in nature (see

section 1.3.3.).

1.3 THE FORMATION OF SOLUTE CLUSTERS

1.3.1 The free energy of the solid solution

Before discussing the possible mechanisms of cluster-formation it is useful to consider briefly the thermodynamic driving force for the decomposition of a supersaturated solid solution.

A system at constant temperature T and pressure P is said to be in equilibrium when its Gibbs Free Energy (G) is a minimum; G is defined by the relation

$$G = H - TS = U + PV - TS \qquad (1.1)$$

where U and S are the internal energy and entropy of the system of volume V and H is the enthalpy. In a condensed system at atmospheric pressure, PV is very small compared with U and TS, thus $G \simeq U-TS$ and $H \simeq U$. The Helmholtz Free Energy (F) is defined by the relation

$$F = U - TS \qquad (1.2)$$

and this is a minimum for equilibrium with respect to changes at constant volume and temperature. For a condensed system at atmospheric pressure, $G \simeq F$.

In order to be able to deduce the equilibrium state of a condensed system of two components, of a given composition and at a given temperature, one needs to know how the free energy varies with these two parameters. Precise evaluations of the necessary thermodynamic quantities are, at present, prohibitively difficult and it is usual to make a number of simplifying assumptions in order to gain a qualitative idea of the behaviour[10, 14, 15].

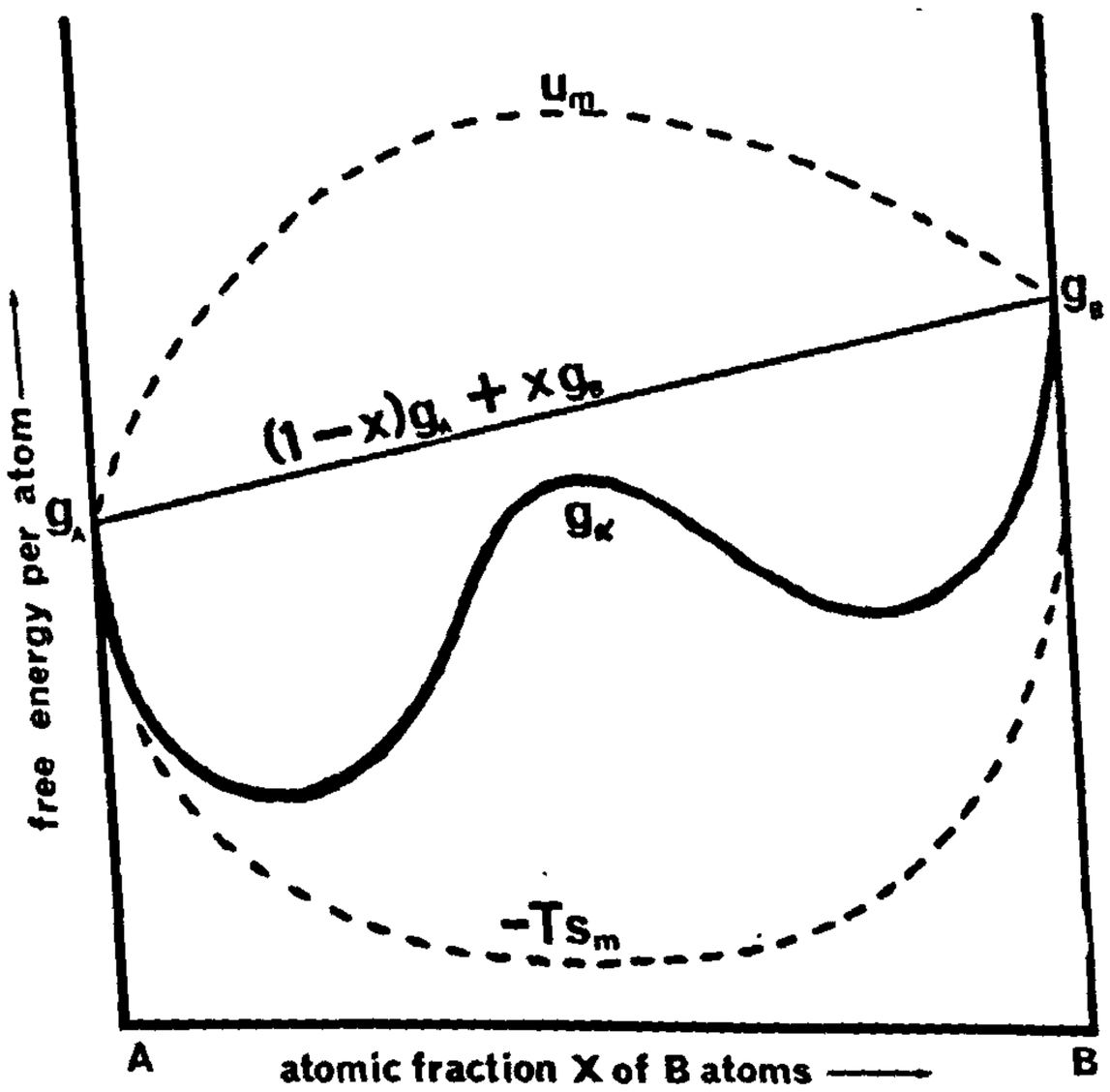

Figure 1.1 The free energy of a binary solid solution as a function of composition.

Consider two pure metals, A and B, which have the same crystal structure and let their free energies per atom, at a temperature T, be g_A and g_B respectively, measured with respect to some arbitrary zero. If we now take a volume (1-x) of A and volume x of B and place them in contact but allow no diffusion to take place, then the mean free energy per atom of the whole system is given by

$$(1-x)g_A + xg_B \qquad (1.3)$$

where x is the atomic fraction of B atoms in the system (see Figure 1.1). If we now allow the A and B atoms to mix freely together to form a random, substitutional, solid solution, we must consider an additional free energy term - the Free Energy of Mixing (g_m) - which may be expressed as

$$g_m = h_m - Ts_m \qquad (1.4)$$

where h_m and s_m are the enthalpy and entropy of mixing. For a condensed system the enthalpy of mixing is practically equal to the internal energy of mixing, u_m, and a complete evaluation of u_m would require the detailed knowledge of the interaction between A and B atoms, which is not feasible at present. An approximate method is to use the "quasichemical approach" in which only chemical effects are considered and these are confined to nearest neighbour interactions[10, 14, 15]. We may then define V_{AA}, V_{BB}, and V_{AB} as the neighbouring bond energies between two A atoms, two B atoms and an A and B atom, respectively. We will be interested in the special case where it is energetically favourable for like atoms to cluster together (i.e. $2V_{AB} > V_{AA} + V_{BB}$). Thus, a random mixture of A and B atoms has a higher internal energy than the same number of A and B atoms separated into two volumes, each containing pure components.

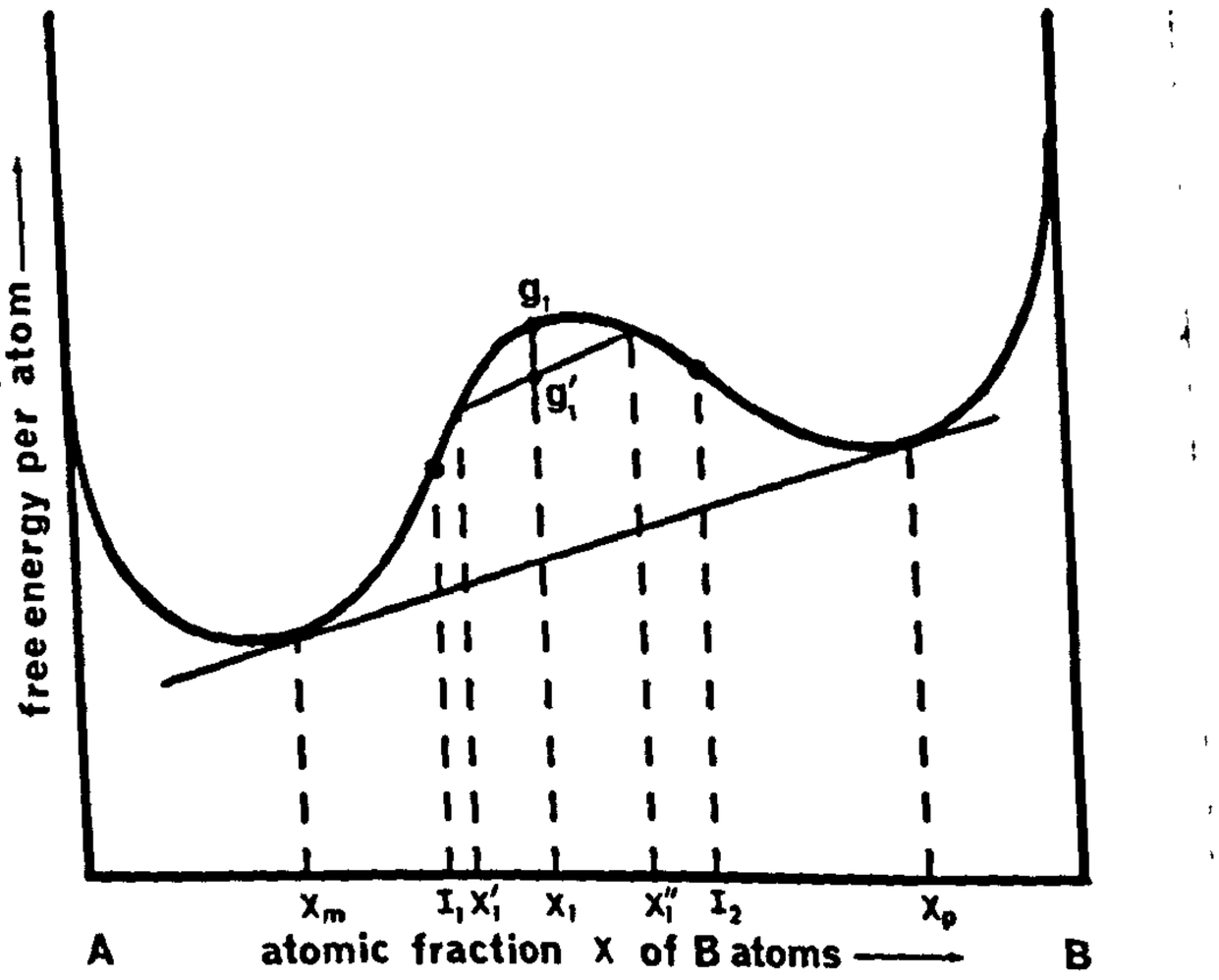

Figure 1.2 A diagram of free energy versus composition illustrating spinodal decomposition.

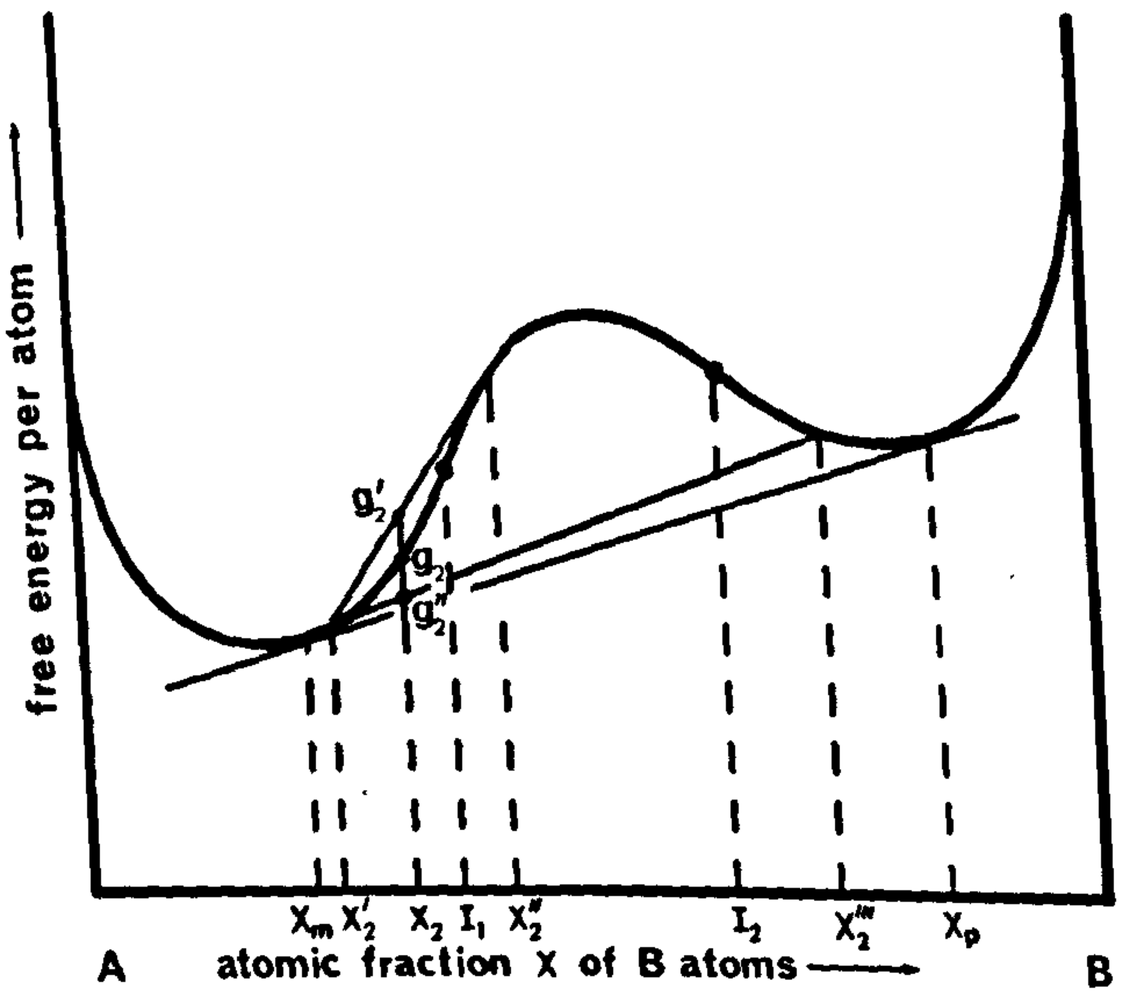

Figure 1.3 A diagram of free energy versus composition illustrating a nucleation and growth transformation.

The mixing of A and B atoms will, however, increase the configurational entropy of the system and this is assumed, according to the "regular solution" model, to be the only contribution to the entropy of mixing, s_m. It is assumed that the vibrational entropy of the components remain unchanged when atoms are transferred from the pure state into a random solid solution.

Since s_m is associated with the temperature in equation 1.4, the second term on the right hand side dominates the free energy of mixing at a high temperature, and the equilibrium configuration of the system is a single phase, random, solid solution. At low temperatures the entropy term is less dominant and, in a solid solution where the clustering of like atoms is favourable, the total free energy curve g_α develops the shape shown in Figure 1.1.

Alloys outside the region of g_α which is limited by the compositions x_m and x_p (see Figure 1.2) are stable as random solid solutions, since these have a lower free energy than any other configuration. Alloys with compositions between x_m and x_p warrant more careful consideration.

Consider an alloy of composition x_1 (Figure 1.2). If a solid solution of this composition decomposes into regions of compositions x_1' and x_1'', the mean free energy of the system is lowered from g_1 to g_1', where g_1' is given by the lever rule as

$$g_1' = \left(\frac{x_1'' - x_1}{x_1'' - x_1'}\right)C + \left(\frac{x_1 - x_1'}{x_1'' - x_1'}\right)D \qquad (1.5)$$

where C and D are the individual free energies per atom of the two phases of compositions x_1' and x_1''. Even if the two phases have compositions which

are only infinitesimally different from x_1, their formation will always lead to a lowering of the free energy of the system, so there is no barrier to decomposition. This mode of phase separation is known as "spinodal decomposition". It is confined to alloy compositions which lie between the points of inflection of the free energy curve (I_1 and I_2 on Figure 1.2), that is, to the region of the free energy curve where

$$\frac{\partial^2 g_\alpha}{\partial x^2} < 0.$$

Consider, next, a solid solution of composition x_2 (Figure 1.3). If such an alloy separates into regions of slightly different compositions, x_2' and x_2'', the mean free energy of the system is increased from g_2 to g_2' and these compositional fluctuations will be unstable. A net decrease in free energy can only be achieved by large compositional fluctuations, for example, into regions of composition x_2' and x_2''', when the mean free energy is reduced from g_2 to g_2''. There is thus a free energy barrier to the formation of small solute fluctuations and the transformation cannot begin until small regions with a sufficiently large fluctuation in solute content (nuclei) are formed. When this occurs, the transformation is said to proceed by a nucleation and growth process and this, and then spinodal decomposition, is discussed in more detail in the next two sections.

1.3.2 Homogeneous nucleation

The large solute fluctuation x_2''', discussed above, was not defined in terms of size or shape. In the more general case of a phase change in a two component system the thermally activated solute fluctuations (embryos) may also differ in crystal structure from the

parent phase and may be chemically non-uniform. Hence, before embarking upon any theory of nucleation for a two-component system, one must decide beforehand which of the embryo parameters are variables. The choice of different variables has led to a number of different nucleation models, each of which attempts to describe the initial decomposition of a super-saturated solid solution. These models were all inspired by the classical nucleation theory of Volmer and Weber[16] and Becker and Döring[17] (the V.W.B.D. theory), which was first formulated for the case of condensation from supersaturated vapours. Before discussing nucleation in a two-component system it is instructive to present a brief outline of the V.W.B.D. theory, which seeks to explain the difficulty of forming liquid droplets in a supersaturated vapour.

The formation of a liquid droplet is associated with a free energy change ΔG. Intuitively, one might expect that the free energy of the system would be increased for two reasons: (1) energy is required to form a liquid/vapour interface; and (2) energy may be expended in the form of strain energy if the transformation involves a volume change. Strain energy may be neglected in the case of a vapour $\rightarrow$ liquid transformation, since any volume change is easily accommodated by vapour flow (it is, however, important in solid-state transformations). In the simple theory, the interfacial free energy is assumed to be isotropic and also independent of droplet size. The droplet is also assumed to have the structure of the bulk liquid. Then, for a spherical droplet of radius r

$$\Delta G = \frac{4}{3}\pi r^3 \Delta G_v + 4\pi r^2 \gamma \qquad (1.6)$$

where ΔG_v is the difference in free energy per unit volume between the

bulk vapour and liquid phases at the temperature considered and γ is the interfacial free energy per unit area. For a supersaturated vapour ΔG_v is always negative, whereas γ is always positive and in this situation the free energy of formation goes through a maximum at a critical radius r_c. Maximizing equation 1.6 gives

$$\frac{\partial \Delta G}{\partial r} = 4\pi r^2 \Delta G_v + 8\pi r \gamma = 0 \qquad (1.7)$$

from which

$$r_c = - \frac{2\gamma}{\Delta G_v} . \qquad (1.8)$$

A stable nucleus may be formed if the droplet achieves the critical radius r_c and this requires an activation energy of formation of

$$\Delta G_c = \frac{16\pi\gamma^3}{3(\Delta G_v)^2} = \frac{4}{3}\pi r_c^2 \gamma \qquad (1.9)$$

If the vapour is treated as an ideal gas it may be shown that (see reference 10, p.391)

$$\Delta G_v = - \frac{kT}{\Omega} \log_e \frac{P_r}{P_\infty} \qquad (1.10)$$

where Pr is the vapour pressure in equilibrium with a droplet of radius r, P_∞ is the vapour pressure in equilibrium with a flat liquid surface, Ω is the atomic (molecular) volume of the liquid and kT has its usual meaning. The ratio $\frac{Pr}{P_\infty}$ is called the supersaturation i. Substitution of equation 1.10 into equation 1.8 gives

$$\log_e i = \frac{2\gamma\Omega}{r_c kT} \qquad (1.11)$$

which is the Gibbs-Thomson equation for the critical nucleus.

The next problem is to deduce the nucleation rate I. Volmer and Weber assumed that the droplets change size by unit processes, that the concentration of embryos and nuclei is the equilibrium concentration and that the shrinkage of super critical nuclei is negligible. They were then able to derive the following expression for the initial nucleation rate :

$$I = A_1 \exp\left(-\frac{\Delta G_c}{kT}\right) \qquad (1.12)$$

where A_1 is a kinetic factor describing the collision frequency of single atoms (molecules) with a droplet of critical size. Becker and Döring improved upon this result by allowing for the possible shrinkage of a critically sized droplet, but this only modified the value of the kinetic factor A_1. From equations 1.9 and 1.11 the initial nucleation rate can be expressed in terms of the supersaturation i, as follows

$$I = A_1 \exp\left[-\frac{16\pi\gamma^3\Omega^2}{3(kT)^3} \cdot \frac{1}{(\log_e i)^2}\right] \qquad (1.13)$$

Thus, we obtain the important conclusion that the nucleation rate is extremely sensitive to the value of the supersaturation.

Becker[18,19] extended the V.W.B.D. theory to a transformation in a solid-state two-component system in which the phase change only involves a composition change. Strain energy was neglected and so the theory only applies if the two solid phases have identical atomic volumes. A binary alloy system which conforms to this restriction would be an ideal alloy, composed of two pure components A and B which have identical crystal structures and atomic volumes. The phase diagram of such a system is

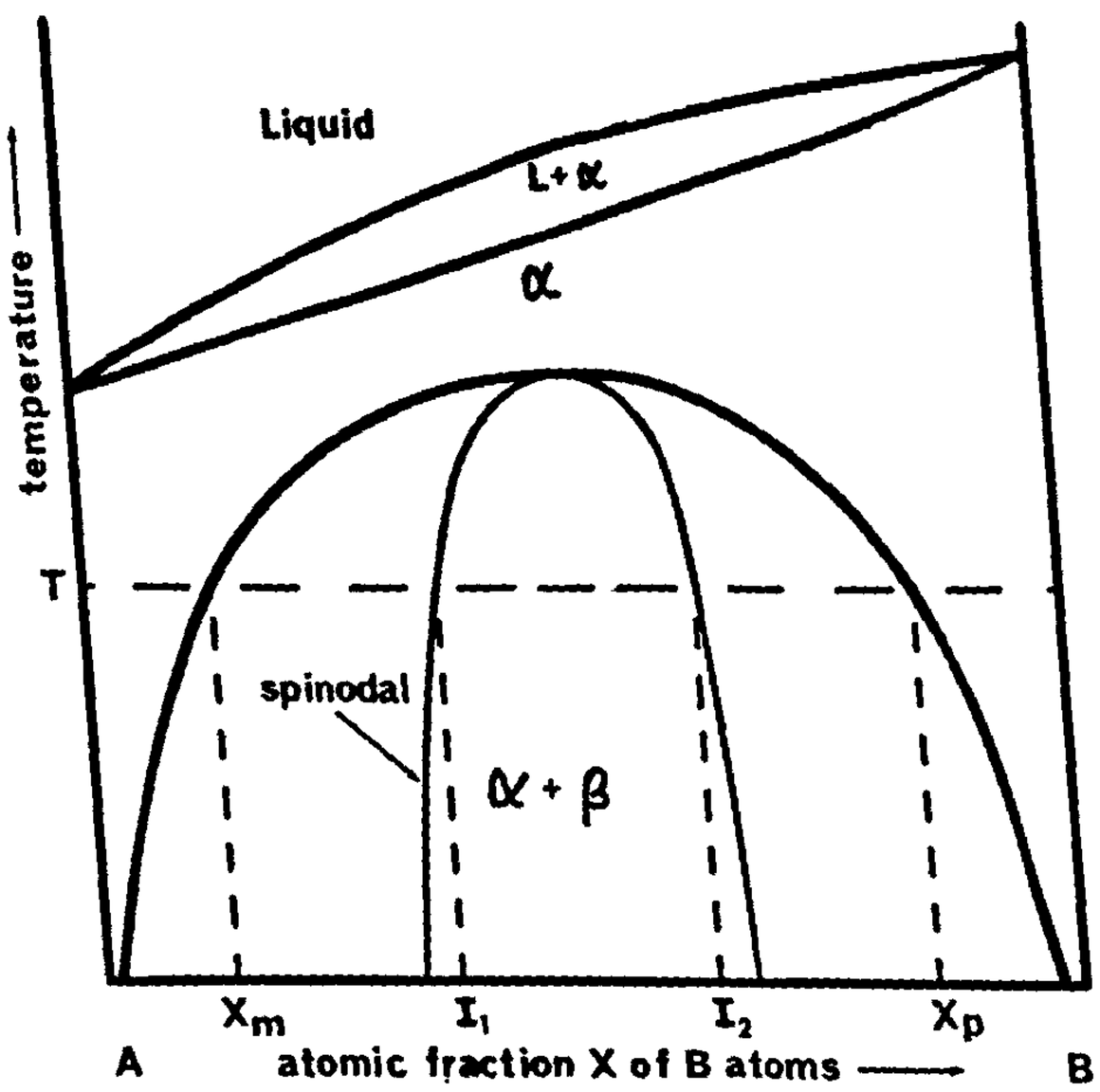

Figure 1.4 A schematic phase diagram for an ideal binary alloy illustrating the solubility and spinodal curves.

shown schematically in Figure 1.4 and displays a miscibility gap at low temperatures. At the temperature T the free energy/composition diagram for this alloy will be similar to that shown in Figure 1.3. Becker obtained the following expression for the initial nucleation rate in such a system:

$$I = A_2 \exp\left(-\frac{Q}{kT}\right) \exp\left(-\frac{\Delta G_c}{kT}\right) \qquad (1.14)$$

where A_2 again is a kinetic factor and Q is the activation energy for diffusion within the solid solution. In order to obtain a value for the activation energy for nucleation ΔG_c, Becker assumed that the composition of the nucleus was that of the equilibrium phase (x_p in Figure 1.3). He then used the theory of regular solutions and the quasichemical approach (see section 1.3.1) to derive the following expression

$$\Delta G_c = 2r_c^2 (x - x_p)^2 \left[2V_{AB} - (V_{AA} + V_{BB})\right] \qquad (1.15)$$

Becker's assumption that the nucleus has the composition of the equilibrium phase precludes the possibility of a compositional barrier to the nucleation. This possibility has been examined by Borelius[20,21,22] who considered the stability of a cluster of atoms of fixed size as a function of its composition. Strain energy and interfacial energy were ignored. He found that the compositional barrier became zero for decomposition within the spinodal region of the phase diagram (see Figure 1.4). Outside the spinodal, but still within the two-phase region, he found that a compositional barrier could exist, but one of the drawbacks of the theory is that the size of the cluster is left as an adjustable parameter and the theory requires the arbitrary assumption of a minimum sized cluster. Both Hobstetter[23] and Scheil[24] have attempted to

overcome this difficulty by considering that the most probable nucleus will have a size and composition corresponding to the least activation energy for formation. They found that the composition of the initial precipitate decreased as the supersaturation was increased.

1.3.3 Spinodal decomposition

During his classic work on thermodynamics, in the late nineteenth century, Willard Gibbs proposed two types of phase change: (a) a change that is small in degree but large in extent, such as a small solute fluctuation spread over a large volume; (b) a change that is large in degree but small in extent, which is familiar in nucleation theory as the super-critical nucleus. The first type of change was largely neglected until recently, when Hillert[25], Cahn and Hilliard[26] and Cahn[27,28,29,30] have attempted to derive quantitatively a unified theory of homogeneous phase separation.

Cahn and Hilliard considered the Helmholtz free energy per unit volume F_v of an isotropic, incompressible, two-component fluid whose composition differed only infinitesimally everywhere from the average composition. They derived the free energy as

$$F_V = \int [f(x) + K (\nabla x)^2] dV \qquad (1.16)$$

where f(x) is the free energy per unit volume for a homogeneous system of composition x and $K (\nabla x)^2$ is an additional free energy term (the "gradient energy"), for which K is a positive constant, which arises if the volume element is in a region of non-constant composition. The gradient energy is the analogue of the surface energy term in the localised fluctuations of nucleation and growth theory, although in this case the

"surface" is diffuse. They then calculated the free energy change, ΔF_v per unit volume, for a compositional fluctuation of infinitesimal amplitude in a system where the atomic volumes of solute and solvent atoms are identical:

$$\Delta F_v = \int \left[\frac{1}{2} \left(\frac{\partial^2 f(x)}{\partial x^2} \right)_{x=x_o} (x - x_o)^2 + K (\nabla x)^2 \right] dV \qquad (1.17)$$

where x_o, is the average composition. Since the gradient energy is always positive, the sign of ΔF_v is determined by the sign of $\frac{\partial^2 f(x)}{\partial x^2}$. They considered two possibilities :

(i) $\frac{\partial^2 f(x)}{\partial x^2} > 0$; ΔF_v is positive and the solution is metastable to all infinitesimal fluctuations in composition - the alloy is outside the spinodal region and a finite fluctuation (a nucleus) is required to render the solution unstable.

(ii) $\frac{\partial^2 f(x)}{\partial x^2} < 0$; ΔF_v can be negative, but only if the gradient energy is sufficiently small - the alloy is inside the spinodal region and is unstable with respect to fluctuations of sufficiently long wavelength (i.e. low gradient energy).

Cahn[27] has extended this approach to an isotropic, solid, two-component system where the two equilibrium phases differ slightly in lattice parameter. This introduces an additional energy term (the elastic strain energy) into equation 1.17, which is as follows

$$\frac{\eta^2 E}{1 - \nu} (x - x_o)^2 \qquad (1.18)$$

where η is the fractional change in lattice parameter per unit change in composition, E is Young's modulus and ν is Poisson's ratio.

He showed that inclusion of this energy term modifies the condition for spinodal decomposition, so that the limit of metastability is now defined by the locus of

$$\frac{\partial^2 f(x)}{\partial x^2} = - \frac{2\eta^2 E}{1-\nu} \qquad (1.19)$$

which he called the "coherent spinodal". If $\eta = 0$, this reduces to the locus of the "chemical spinodal" (see Figure 1.5(b)).

Cahn tackled the problem of determining the permissible wavelengths of the fluctuations by expressing a three-dimensional composition fluctuation in terms of a Fourier series. This simplified the problem, since the total free energy change of an arbitrary composition fluctuation is the sum of the individual free energy changes of its Fourier components. His analysis concentrated on a single Fourier component and in this way he was able to show that, within the coherent spinodal region, the alloy was unstable with respect to a sinusoidal fluctuation of wavelength λ conforming to the following condition,

$$\lambda > - \left[\frac{8\pi^2}{K} \left(\frac{\partial^2 f(x)}{\partial x^2} + \frac{2\eta^2 E}{1-\nu} \right) \right]^{1/2} \qquad (1.20)$$

that is, the wavelength must be greater than a certain critical wavelength λ_c. In general, a whole spectrum of wavelengths greater than λ_c are possible, but Cahn showed that the most rapidly growing wavelength is given by $\lambda = \sqrt{2}.\ \lambda_c$.

In a further extension of this theory, Cahn[28] considered spinodal decomposition in cubic crystals and examined the effect of elastic anisotropy on the compositional fluctuation. He found that fluctuations formed preferentially along directions where E is a minimum. In the case of most

cubic crystals[31] E is a minimum along $\langle 100 \rangle$ and in these systems Cahn suggested that the initial $\{100\}$ fluctuations will give rise to a cubic array of precipitate particles of spacing $\sqrt{2}.\ \lambda_c$. This spacing is expected to coarsen during prolonged ageing.

1.3.4 The nucleation of metastable phases

The discussion of precipitation from supersaturated solid solutions in section 1.3.1 was confined to the ideal case where the two equilibrium phases have identical crystal structures and atomic volumes. In the more general case the equilibrium precipitate has a different crystal structure from the matrix and it is useful to make a distinction between incoherent and coherent precipitation.

An incoherent precipitate is one for which there is a lattice discontinuity at all points over the precipitate /matrix interface. The interface is localised (a few atomic diameters in thickness) and the crystal structure and composition are different on either side of the boundary. The interfacial energy γ is similar in magnitude to that of a high-angle grain boundary ($\sim$ 500-1000 erg/cm^2 [15,32,33,34]) and the critical nucleus size and activation energy for nucleation are large.

If the equilibrium phase is incoherent it becomes energetically favourable for the alloy to decompose initially by the formation of coherent, or partially coherent, metastable precipitates. A coherent precipitate has been defined by Kelly and Nicholson[9] as "one in which all interfaces with the matrix are coherent and the Bravais lattices in the two crystal structures are identical if differences in chemical species and consequent small changes in atomic spacing are neglected". A partially coherent precipitate is defined as "one in which at least one interface with the matrix is coherent". Coherent precipitates are characterized

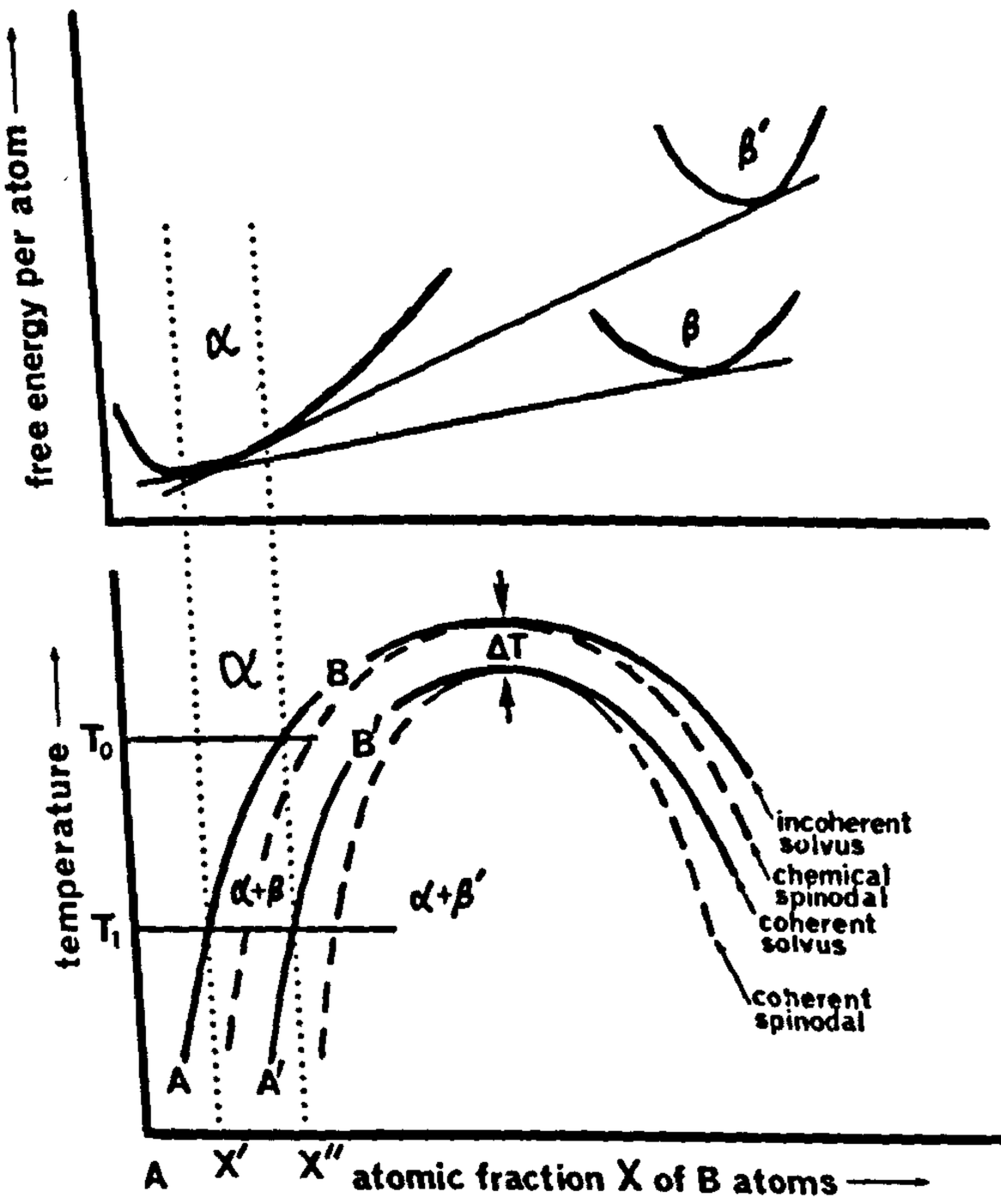

Figure 1.5 (a) a schematic free energy diagram at a temperature T_1 for the α matrix, an incoherent precipitate β and a coherent precipitate β', showing the respective solubility limits x' and x''; (b) is the corresponding phase diagram illustrating schematically the relationship between the incoherent and coherent solvus curves and the chemical and coherent spinodal.

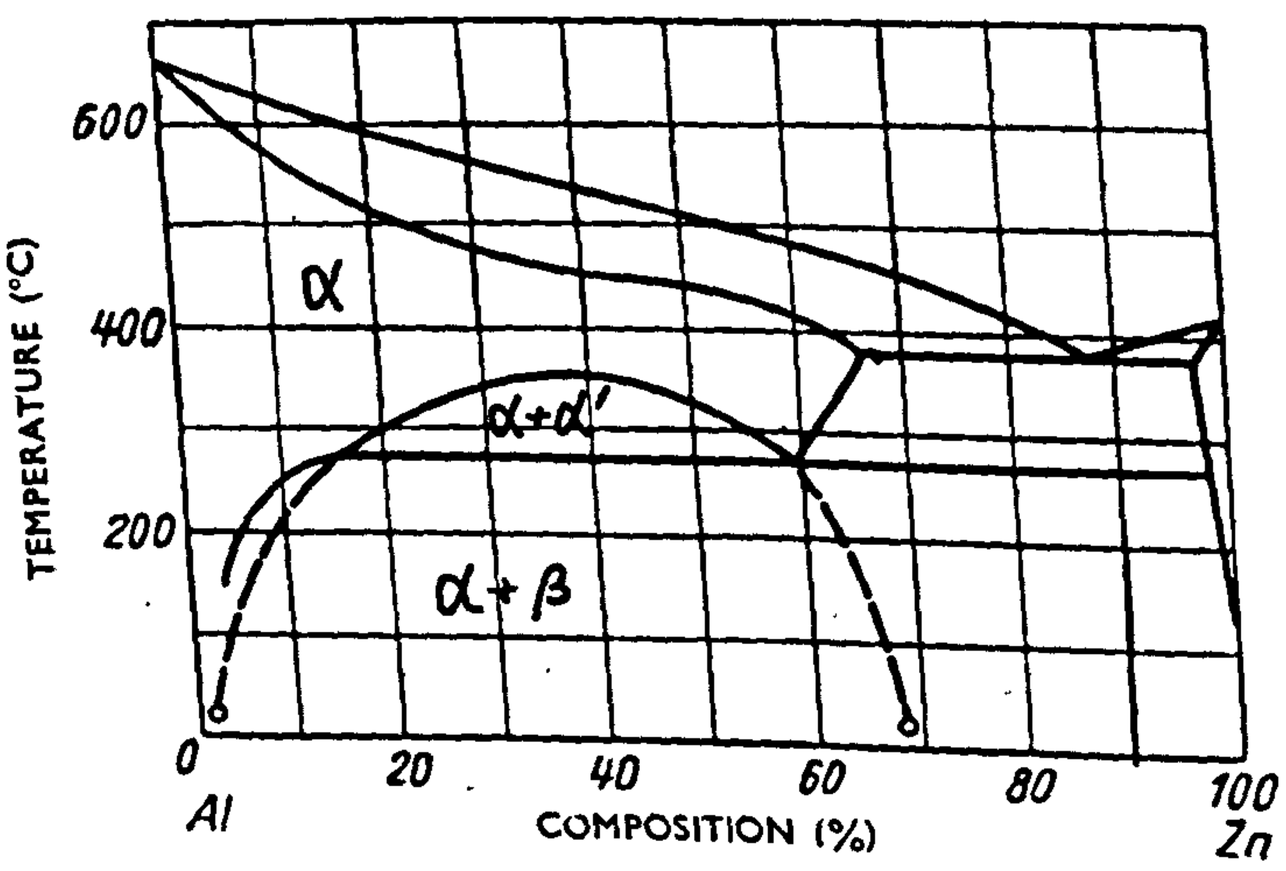

Figure 1.6 The phase diagram of the Al-Zn system illustrating the metastable α'- solvus (the dashed-curve) as proposed by Gerold and Schweizer[41].

by a low value of interfacial energy, which means that their critical nucleus size and activation energy for nucleation are much smaller than for incoherent precipitates and they are therefore formed more readily. If the supersaturation is high enough, so that the alloy is within the coherent spinodal, the alloy may decompose spinodally and it is no longer useful to speak of an interfacial energy γ during the early stages of decomposition when the interface is diffuse.

Since a coherent precipitate is metastable with respect to an incoherent one[35,36], the former will always eventually be replaced by the latter. Another important characteristic is that, since the free energy of a metastable coherent phase β' is higher than the free energy of a stable incoherent phase β, the solute concentration x'' of the α phase in equilibrium with a <u>large</u> cpherent precipitate at a temperature T_1 is higher than that, x', for a <u>large</u> β precipitate at the same temperature[14,37,38] (see Figures 1.5(a) and (b)). Thus, if an alloy of composition x'' is quenched to a temperature which lies between T_0 and T_1 then only incoherent precipitates can be nucleated. If it is quenched to a temperature below T_1 then, in principle, both coherent and incoherent precipitates can nucleate, although in practice the former often nucleate so much more readily than the latter that coherent precipitation may be considered as the only mode of initial decomposition.

The curve A' B' of Figure 1.5(b) may be thought of as a solvus curve for coherent precipitates. This is important in the theory of the nucleation of G.P. zones where it has been identified with the so-called "G.P. zone solvus", which has been the subject of much recent discussion and this topic is discussed again in Chapter 4.

Metastable solvus curves may also be defined for intermediate precipitates. An important example occurs in the Al-Zn system for the

incoherent α' intermediate precipitate. The idea of a metastable miscibility gap has been developed by Gerold [39,40,41] and used by him to aid the interpretation of his X-ray results from Al-Zn alloys. He proposed that the boundary of the high temperature, stable, α + α' miscibility gap can be extrapolated down into the α + β region in the form of a metastable solvus line (see Figure 1.6). Gerold based his deductions on the version of the Al-Zn phase diagram as reproduced by Hansen[42]. More recent experimental work[43,44] has indicated the presence of a peritectic reaction in the Al-Zn system and an associated $(\alpha + \alpha') \rightarrow (\alpha + \gamma)$ transformation within the stable miscibility gap (see Figure 3.2). The α, α' and γ phases are all face centred cubic but differ slightly in lattice parameter. Thus, Gerold's work must be slightly modified to take this effect into account, although the concept of a metastable miscibility gap remains unchanged. Metastable phase diagrams have also been proposed for the Al-Ag[45,46] and Al-Cu[47,48] systems.

1.4 THE GROWTH OF SOLUTE CLUSTERS

1.4.1 The vacancy concentration and diffusion

Precipitation from a supersaturated substitutional solid solution requires the diffusion of solute and solvent atoms through the matrix and this is currently believed to take place by the migration of vacant lattice sites.

The formation of vacancies in a pure metal crystal increases its internal energy and also its configurational entropy. The equilibrium situation is achieved when the vacancy concentration is sufficient to minimise the free energy of the system. The application of standard statistical thermodynamics to this problem[49] yields the result that the concentration of single vacancies C_v in equilibrium in a pure metal at a

temperature $T^{o}K$ is given by

$$C_V = \exp\left(\frac{S_f}{k}\right) \exp\left(-\frac{E_f}{kT}\right) \qquad (1.21)$$

where E_f is the energy of formation of a single vacancy and S_f is the entropy of formation of a single vacancy due to its effect on the vibrational frequencies of its surrounding atoms. The value of the constant term, $\exp\frac{(S_f)}{k}$, is not known accurately but it is usually taken to be between 1 and 10. For pure aluminium, the value of E_f as determined by resistivity measurements[50,51] is 0.76 eV.

The self-diffusion coefficient D_v in a pure metal, when diffusion occurs by the migration of single vacancies, is given by

$$D_V = D_o \exp\left(-\frac{E_f}{kT}\right) \exp\left(-\frac{E_m}{kT}\right) \qquad (1.22)$$

where D_o is a constant and E_m is the activation energy for migration of a single vacancy. The activation energy for self-diffusion Q is defined by the equation

$$Q = E_f + E_m \qquad (1.23)$$

Lomer[52] has considered how the equilibrium vacancy concentration in a dilute alloy, C_v^s, may differ from that of a pure metal and has derived the following equation for the vacancy concentration in a f.c.c. solvent with a concentration x of solute

$$C_V^s = A \exp\left(-\frac{E_f}{kT}\right)\left[1 - 12x + 12x \cdot \exp\left(\frac{E_B}{kT}\right)\right] \qquad (1.24)$$

where A is a constant and E_B is known as the binding energy between a vacancy and a solute atom. The derivation of equation 1.24 supposes that there is a difference in the energy of formation of a vacancy surrounded by solvent atoms only and a vacancy adjacent to one solute atom. The value of E_B is usually a fraction of an electron-volt for aluminium alloys and the experimental methods for measuring it are many and varied[53,54].

1.4.2 The rate of cluster growth

It is now well established[55,56,57] that the rate of cluster growth in alloys, which have been quenched and then aged near to room temperature, is many orders of magnitude ($\sim 10^7$) higher than can be explained in terms of equilibrium diffusion rates. There have been two basic mechanisms put forward to explain this observation.

Turnbull[58,59] devised a mechanism whereby solute atoms migrate rapidly along moving dislocation lines and so enhance the diffusion rate. This mechanism, although plausible, does not readily explain the observed variation of cluster growth-rate with changes in quenching-rate, solution treatment temperature or ageing temperature. It has now been superseded in favour of the second mechanism, the excess-vacancy theory.

Seitz[60], in 1952, suggested that the high diffusion rate observed during clustering could be due to a non-equilibrium vacancy concentration retained during the quench. His idea was subsequently developed by Federighi[61], de Sorbo et al[62] and Turnbull et al[63]. According to this theory, for an ideal quench in which all vacancies are retained, the diffusion coefficient of the solute atoms during the initial stages of ageing is given by

$$D_s = D_0 \exp\left(-\frac{E_f}{kT_s}\right) \exp\left(-\frac{E_m}{kT_A}\right) \qquad (1.25)$$

where T_s is the solution treatment temperature and T_A the ageing temperature. Thus, the alloy initially contains a high supersaturation of vacancies. During subsequent low temperature ageing the excess vacancies migrate to sinks (such as external surfaces, grain boundaries and dislocation lines) to become annihilated and the diffusion rate drops continuously towards its equilibrium value. For a slow quench, or a step-quench, allowance has to be made for the decay of the excess-vacancy concentration during the quenching process.

In the case of pure aluminium[51,64], observations of the change in electrical resistivity of a sample quenched to and then annealed at room temperature indicated that the quenched-in excess-vacancy concentration decays to the equilibrium value in a few hours. Similar experiments carried out with an Al-10% Zn alloy[65] indicated that the clustering reaction in this alloy virtually ceases within a few hours, which is satisfactorily explained by the decay of the excess-vacancies. However, in the case of Al-Cu[62], Al-Mg-Si[66] and Al-Mg-Ge[67] the clustering process continues over a period of days or even weeks. Clustering in these alloys is characterized by an initial "fast reaction" which is subsequently followed by a "slow reaction" during which the growth-rate is appreciably higher than can be accounted for by equilibrium diffusion rates. The "fast reaction" is consistent with a high matrix excess-vacancy concentration which rapidly falls to a lower value, which is then maintained over a long period during the "slow reaction".

Several hypotheses have been suggested to explain the slow reaction: (a) vacancies are trapped by solute clusters and escape slowly[68,69]; (b) excess-vacancies exist in equilibrium with the surface tension of small voids formed by the clustering of vacancies or the line tension of small dislocation loops formed by the collapse of the

voids[63]; (c) a long-range elastic interaction between a vacancy and a solute cluster retards the annealing-out of quenched-in excess vacancies[70,71]. Okamoto and Kimura[72] have recently obtained evidence that mechanism (b) operates during the slow reaction in Al-4%Cu alloys. Mechanism (a), as expounded by Federighi and Thomas[69], generalizes the idea of a binding energy E_B between a vacancy and a solute atom by suggesting that there may also be a binding energy E_B' between a vacancy and a cluster of solute atoms. If E_B' is small, excess-vacancies will not be trapped significantly by solute clusters and will decay as in pure aluminium (as exemplified by Al-10%Zn). If E_B' is large, as appears to be the case in Al-Mg-Si and Al-Mg-Ge alloys, excess-vacancies will be temporarily trapped by solute clusters, which will initially contain a high vacancy concentration. Evidence in support of this is discussed in detail in Chapter 3.

Girifalco and Herman[73] have pointed out that, in order to explain the observed cluster growth quantitatively, each vacancy must transport about 10^3 solute atoms from the matrix to the clusters. They proposed a "vacancy-pump" mechanism whereby vacancy-solute atom complexes arriving at a spherical cluster interface can dissociate and the free vacancies set-up a concentration gradient which tends to drive vacancies back into the matrix, where they can again combine with solute atoms. This process is repeated a large number of times by a vacancy before it eventually becomes annihilated at a sink. They found good agreement between their model and the kinetics of clustering in Al-Zn alloys as determined by Panseri and Federighi[65].

1.4.3. The kinetics of clustering

A complete description of the development of solute clusters

(G.P. zones) during age-hardening requires the detailed knowledge of the variation with ageing time of parameters such as,

(i) the number of clusters per unit volume,

(ii) the size distribution of the clusters,

(iii) the composition of the clusters,

(iv) the volume fraction of solute precipitated.

Three different models have been proposed, each of which attempts to describe the development of clusters during ageing.

If the alloy is within the coherent spinodal region of the phase diagram then the early stages of decomposition can be treated rigorously (see section 1.3.3). The later stages of spinodal decomposition and the beginning of particle coarsening have also been examined by Cahn[74].

lle considered terms in the general diffusion equation that involve a diffusion coefficient which is dependent upon composition. By using a method of successive approximations he was able to show that these non-linear terms give rise to harmonic distortions of the composition fluctuations and that in dilute alloys these give rise to isolated particles which resemble a conventional distribution of large G.P. zones in a depleted matrix.

The two other models arose as a result of independent attempts to explain the observed variation of X-ray small angle scattering, with room temperature ageing, from samples containing spherical G.P. zones (either Al-Zn or Al-Ag alloys). Both models agree that, during and immediately after the quench to room temperature, a process of solute clustering occurs leading to the formation of G.P. zones. The two models differ, however, as to the mechanism describing the solute segregation and these are now discussed separately.

The Gerold model[40,41] assumes that the segregation of the

excess solute atoms, in the form of small solute clusters, is completed during the quench (or within a very short time after the quench) and the solute concentration in the matrix is reduced to the equilibrium value, as determined by the metastable miscibility gap. Thus, apart from a short initial transient, the volume fraction of solute precipitated is considered to remain constant during further growth of the solute clusters, which takes place by a coarsening mechanism. The growth process is then entirely one of competitive growth, with the mean cluster size increasing as the density of clusters decreases. The model is based on the observation that, in Al-Zn and Al-Ag alloys, the total integrated X-ray intensity in absolute units remains constant for all ageing times longer than a few minutes. The integrated intensity Q_o has been defined by Gerold[40] as

$$Q_o = p(m_1 - m_A)(m_A - m_2)\frac{(Z_A - Z_B)^2}{V} \qquad (1.26)$$

where m_1 and m_2 are the solute concentrations inside and outside the zones, m_A is the volume fraction of solute in the alloy, Z_A and Z_B are the atomic numbers of the solute and solvent respectively, V is the average atomic volume and p is the fraction of the alloy which has segregated into clusters. If m_1 and m_2 are assumed to be constant (they are considered to be the equilibrium values as defined by the metastable miscibility gap) then the volume fraction precipitated (p) is constant if Q_o is constant, as was shown to be the case for alloys containing 15, 20.1 and 24.5 wt.%Zn when aged at room temperature for times ranging between 24 and 10^5 minutes after quenching.

According to the Guinier model[13,75] a spherical G.P. zone is initially surrounded by a spherical region depleted in solute atoms.

During and immediately after the quench there is a period during which nucleation of clusters occurs, so that the cluster density initially increases. Each cluster is surrounded by a region depleted in solute atoms with the full matrix supersaturation remaining in between such regions. Subsequent cluster growth causes the depleted regions to overlap and the matrix supersaturation is then progressively reduced to a low value. At this stage, competitive growth starts to occur and the density of clusters progressively decreases, as is characteristic of coarsening reactions.

1.4.4 Two-step ageing

Many commercial age-hardening heat treatments involve an initial isothermal ageing treatment at some low temperature (often room temperature) which is subsequently followed by a second treatment at some higher temperature. In recent years, considerable attention has been paid to this type of treatment since the final mechanical properties of the alloy may be varied over a wide range. Of particular interest are treatments which result in a marked improvement in properties. These results have stimulated a number of workers to examine the effects of two-step ageing treatments on the microstructure of the alloys and this has led to the proposal of several models, all of which attempt to explain the observed precipitation behaviour. Two of the models, those of Nicholson and co-workers[76,77,78,79] and Pashley and co-workers[80,81,82], have attempted an overall description of the basic factors controlling the precipitation behaviour in the alloys that they studied and various aspects of these models are reviewed in Chapters 4 to 8, where they will be critically contrasted and compared. Contributions by other workers will also be examined.

CHAPTER 2

EXPERIMENTAL PROCEDURE

2.1 INTRODUCTION

All the heat treatments described in this dissertation were carried out on thin-foil samples, about 2 cm. x 3 cm. in area, which were cut from rolled-strip of approximately 0.01 cm. in thickness.

The initial stage of all heat treatments was a "solution treatment" during which the sample was annealed at a high temperature, in the single phase region of its equilibrium diagram, for a period of time which was usually one hour. The purpose of this heat treatment was two-fold; firstly, to produce a single solid solution (this probably occurred within the first few minutes of the anneal) and secondly, to recrystallize the cold-rolled structure and so produce a uniform grain size. After solution treatment the grains were equiaxed, with a diameter $\sim$ 0.01 cm., i.e. approximately the thickness of the foil. The grains showed a marked tendency towards a preferred orientation, with a preference for $\{001\}$ planes to be parallel to the foil surface of Al-1.2%Mg_2Si samples and $\{110\}$ planes to be parallel to the foil surface of Al-Zn samples.

After solution treatment the sample was quenched and then given its ageing heat treatment. Details of these processes are described fully in the following sections. At the completion of the heat treatment the sample was cooled in a beaker of cold water. Specimens suitable for transmission electron microscopy were then prepared from the sample by an electropolishing technique.

2.2 THE COMPOSITION OF THE ALLOYS

Two different types of aluminium alloy were studied; one containing additions of magnesium and silicon and the other additions of zinc. The alloys were prepared[+] from high purity aluminium and high purity additions.

The aluminium-magnesium-silicon alloy studied was pseudo-binary, of nominal composition Al-1.2%Mg_2Si. The actual composition is given in Table 2.1.

Table 2.1

Nominal composition	Actual Composition in wt.%			
	Mg	Si	Mg_2Si	Excess Mg
Al-1.2 wt.%Mg_2Si	0.84	0.43	1.16	0.10

The concentration of impurities present in the alloy was very small, as can be seen in Table 2.2.

Table 2.2

Concentration (wt.%) of impurities in Al-1.2% Mg_2Si alloy			
Fe	Mn	Zn	Cu
0.01	< 0.005	< 0.005	< 0.005

[+] The alloys were supplied by British Aluminium Research Laboratories, Chalfont Park.

Three different compositions of aluminium-zinc alloy were studied. An analysis[+] of the zinc concentration of these three alloys was carried out on samples cut directly from the strip in the "as-received" condition and also on samples that had been solution treated (annealed for 1 hour in the temperature range 500°C to 560°C). The results are shown in Table 2.3, where it will be seen that a very small loss of zinc may have occurred during the solution treatment of the two more concentrated alloys.

Table 2.3

Nominal composition	Concentration (wt.%) of Zn	
	As received	After solution treatment
Al - 10% Zn	10.1	10.1
Al - 17.5% Zn	18.1	17.8
Al - 26% Zn	26.3	26.2

The impurity levels in the three alloys are shown in Table 2.4.

Table 2.4

Concentration (wt.%) of impurities in the Al-Zn alloys			
Alloy	Cu	Si	Fe
Al - 10% Zn	0.0005	0.002	0.002
Al - 17.5% Zn	0.0005	0.0025	0.0035
Al - 26% Zn	0.001	0.0025	0.0055

[+] This analysis was carried out by Mr. A. Lacis, of Hinxton Hall. All other analyses were carried out by British Aluminium Research Laboratories, Chalfont Park.

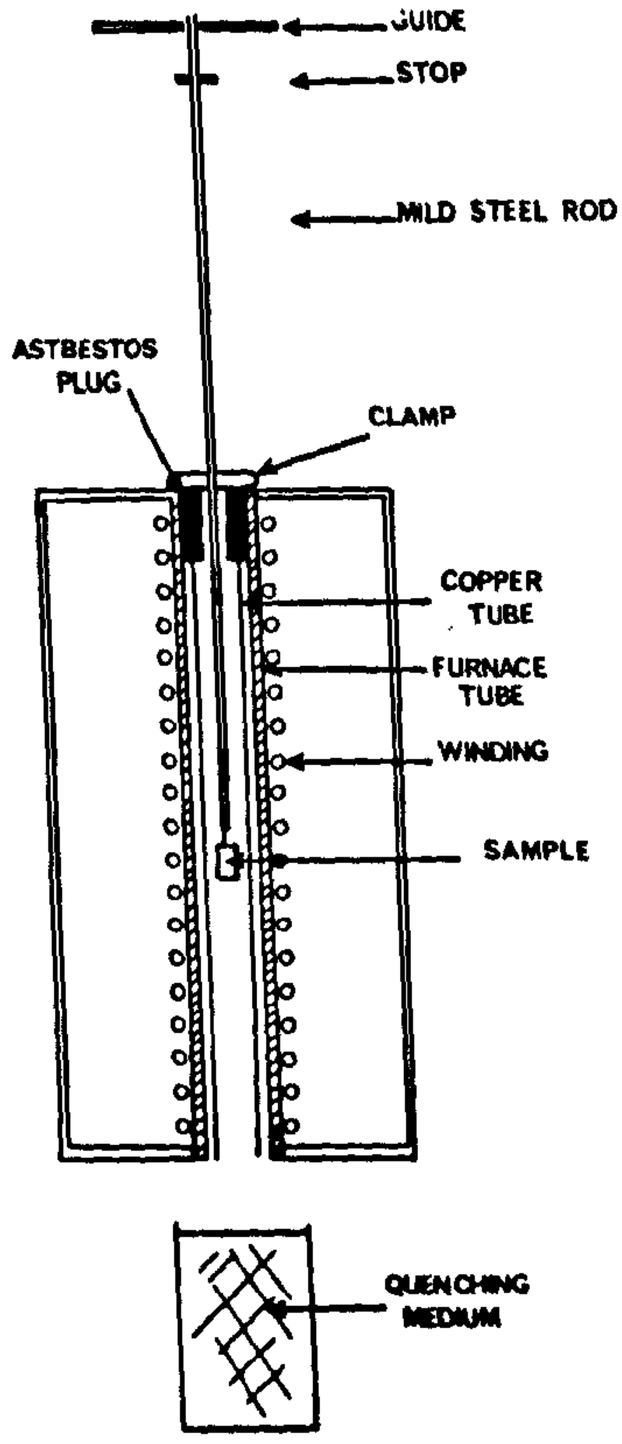

Figure 2.1 A schematic cross-sectional diagram of the solution treatment furnace and quenching apparatus.

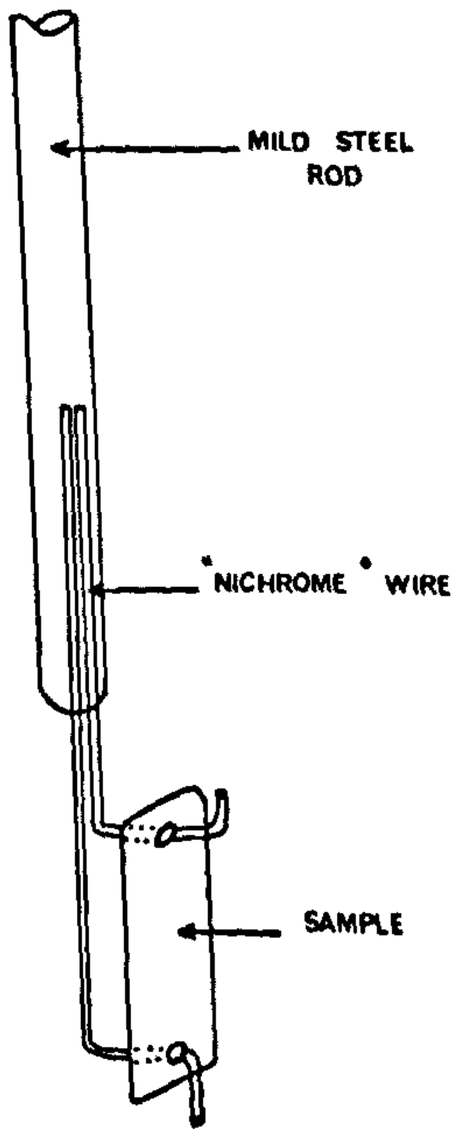

Figure 2.2 A diagram showing the method used for supporting a sample to be quenched into liquid Wood's metal.

2.3 HEAT TREATMENT (APPARATUS AND PROCEDURE)

Solution treatment

The samples were solution treated in a "Wild-Barfield" laboratory tube muffle furnace (type M 93). This was placed on-end so that a sample, suspended inside the vertical heating tube, could be easily quenched by simply dropping it into a quenching bath positioned immediately below the furnace (see Figure 2.1). The heating tube was 20 in. long and 2 in. in diameter. A thin-walled copper tube, 20 in. long and $1\frac{1}{2}$ in. in diameter was inserted inside the heating tube in an attempt to reduce the temperature gradient along the length of the heating tube. An asbestos plug (2 in. long) was inserted at the top of the furnace to reduce heat loss by convection.

The furnace temperature was regulated by means of an "Ether Transitrol" controller which was activated by a chromel-alumel thermo-couple, the hot-junction of which was located half-way down the furnace between the copper tube and the heating tube. Calibration experiments showed that the temperature was controlled to within $\pm$ 5°C of the desired temperature over a distance of $\pm$ 10 cm. above and below the middle of the heating tube. The samples were always placed in this region.

The sample was suspended from the bottom end of a mild steel rod, 100 cm. long and 0.3 cm. diameter, which passed vertically down the centre of the heating tube and projected up through a small hole in the asbestos plug at the top of the furnace. During solution treatment of the sample this rod was raised and clamped in the position shown in Figure 2.1. In order to quench the sample the clamp was removed and the rod allowed to fall until it was arrested by means of a stop, which was adjusted so that the sample became completely immersed within the quenching medium. For quenches into either water, oil or molten salt the samples were attached

to the mild steel rod by means of a short length of fine copper wire. A small brass nut, hung from the bottom of the sample, was all that was required to ensure complete and rapid immersion of the sample into the quenching medium. For quenches into liquid Wood's metal a modified arrangement was necessary because of the high density of this quenching medium. In order to ensure efficient immersion the sample was held rigidly, in the manner illustrated by Figure 2.2. Two lengths of 0.030 in. diameter "Nichrome" wire, about 6 in. long, were spot-welded to the bottom end of the steel rod so that they could be bent and passed through holes punched in the top and bottom of the sample. This arrangement was adopted so that the cooling-rate of the sample would not be significantly affected by the support wires.

The quenching bath was placed immediately below the solution treatment furnace, so that the air-gap between the bottom of the furnace and the surface of the quenching medium was no more than 5 cm. and often less than this.

Quenching

As indicated in the preceding section, various quenching media were used and the choice for a particular experiment was governed by the desired values of quenching-rate and ageing temperature. A list of the quenching media used is given in Table 2.5.

Table 2.5

Quenching medium	Temperature or temperature range	Remarks (see text for further comments)
Water	20°C	Fast quench
Oil (glycerol)	50°C - 250°C	Fast quench at low temperatures but less efficient at high temperatures
Molten Salt (Cassel TS 150)	150°C - 400°C	Fast quench
Liquid Wood's Metal	80°C - 250°C	Very fast quench

Two different quenching procedures were used during the course of this work and these will be referred to as direct-quenching and step-quenching, respectively.

(1) Direct quenching : In this case a sample, held at a temperature T_S in the solution treatment furnace, was dropped directly into the ageing bath held at the desired ageing temperature T_1.

(2) Step-quenching : In this case the quench was interrupted for a short time at some intermediate temperature T_Q between T_S and T_1. This was achieved experimentally by initially quenching the sample into a bath held at T_Q and then, a short time later, it was transferred into a second ageing bath held at T_1. The purpose of the intermediate holding treatment at T_Q was to allow the vacancy concentration to decay to almost its equilibrium value at T_Q and then, provided that the temperature difference between T_Q and T_1 was small, the excess-vacancy concentration present during the initial stages of ageing at T_1 was reduced to a low value. This is discussed in more detail in Chapter 4.

The choice of quenching media for step-quenching was not critical, although in general molten salt was used for the intermediate treatment at T_Q and oil for the ageing treatment T_1. Whereas, in the case of direct-quenching, the choice of quenching medium was very important, since changes in quench-rate were found to have a significant influence on the precipitation behaviour during ageing at T_1. During the early experiments with the Al-1.2%Mg_2Si alloy[81] the samples were direct-quenched into oil at a temperature within the range 180°C to 250°C. Poor reproducibility of precipitation behaviour resulting from these experiments led to the conclusion that localized vapourisation of the oil around the sample, as it entered the bath, was responsible for uncontrollable variations in quench-

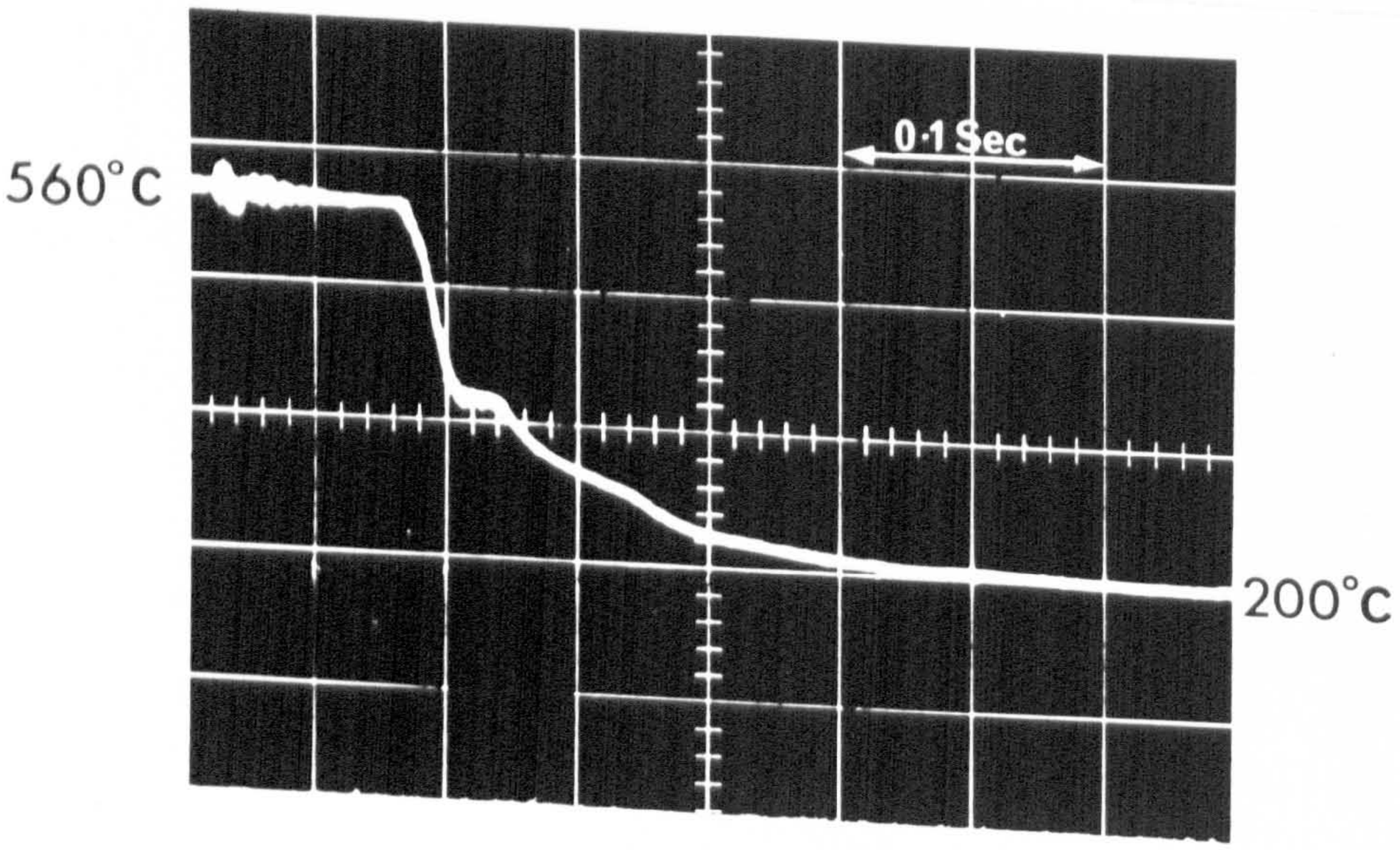

(a)

(b)

Figure 2.3 The cooling-curve obtained by quenching a sample from 560°C into (a) an oil bath at 200°C and (b) a salt bath at 200°C.

rate. Similar heat treatments carried out using a molten salt quenching-bath gave reproducible results. An approximate measurement of the cooling curves from 560°C to 200°C for the oil-quench and the salt-quench was obtained by embedding a fine thermocouple into the centre of a sample and displaying its output on an oscilloscope+. Two typical cooling curves are illustrated by Figure 2.3. The plateau in the cooling-curve for the oil-quench was believed to be associated with the local vapourisation discussed above.

Molten Wood's metal was used as the quenching medium in some experiments and the resulting precipitation behaviour could always be interpreted consistently with this being a very rapid quench. The change in electrical resistance with temperature, of a strip sample, has been used by Lorimer(79) to measure the quenching rate over the temperature range 500°C to 100°C in Wood's metal and water. He obtained values of 40,000°C/sec. for the quenching rate of Wood's metal at 68°C, 12,000°C/sec. for water at 50°C and 2,000°C/sec. for water at 100°C. The experimental results presented in later chapters of this dissertation suggest that Wood's metal retains its high quenching rate properties at least up to temperatures of about 250°C.

The ageing treatments

A large number of different types of ageing treatment were investigated but these may be broadly classified into two groups; single-ageing treatments and double-ageing treatments. Single-ageing involved either step-quenching or direct-quenching the sample to a temperature T_1, followed by an isothermal ageing treatment at T_1, whereas double-ageing (often referred to as two-step ageing) involved an additional ageing treatment at a second temperature T_2.

+ I am grateful to Mr.J.T.Victz for assisting with these experiments.

The isothermal ageing treatments in the temperature range 100°C to 250°C were carried out either in an oil bath or in a salt bath. The oil bath consisted of a brass pot, 15 cm. high and 10 cm. diameter, filled with glycerol and heated by means of an "Eltron" immersion heater (type TRV 5, 500 watts, 230 volts) which was controlled by a "Sunvic" adjustable bimetal thermostat (type TS1, as supplied by AEI Ltd.). The salt bath consisted of a mild steel pot, 15 cm. high and 10 cm. diameter, filled with Cassel TS 150 (a proprietary salt manufactured by ICI Ltd.) which was heated electrically by means of a heating element bolted to its base and regulated by a "Foster Anticipatory Controller". The baths were rapidly stirred during all heat treatments. The accuracy of temperature control was to within $\pm$ 1°C of the desired temperature for periods of ageing of the order of a few hours and for short ageing times ($<$ 10 mins.) the accuracy was probably better than this.

Low temperature ageing treatments (50°C to 100°C) of long duration (several days) were carried out in a muffle furnace regulated by a control unit which consisted of an "Ether Proportional Controller" operating in conjunction with an "Ether Pilot Amplifier" and a saturable reactor. The accuracy of the temperature control was $\pm$ 2°C over a period of two weeks.

2.4 ELECTRO-POLISHING

Prior to electro-polishing, the sample was lightly abraded with fine emery paper to remove the thick surface of oxide film which formed during heat treatment. Samples quenched or aged in Wood's metal were initially immersed in dilute nitric acid for a few minutes to dissolve all traces of Wood's metal adhering to their surface. Thin film specimens, suitable for transmission electron microscopy, were then prepared from the

sample by means of the well-known "window" technique[83,84,85].

The first step of the process was to grip the sample at one of its shorter edges with a small crocodile clip. The edges of the sample were then lacquered with "Lacomit" (manufactured by W.Canning & Co.Ltd.) so that a bare "window" of material was produced. The jaws of the crocodile clip were also coated with Lacomit. The electrolyte used for electro-polishing the Al-Mg-Si and Al-Zn alloys consisted of perchloric acid (specific gravity 1.54), ethyl alcohol and glycerol mixed in the proportions 1:7:2, respectively. During storage this solution was kept in a refrigerator at -20°C and during use its temperature was never allowed to exceed 0°C. The electrolytic cell consisted of about 100 c.c. of electrolyte contained in a glass beaker and surrounded with an ice jacket. The lacquered sample was immersed in the electrolyte and made the anode of the cell with respect to an aluminium cathode at a potential of 20 volts.

During the initial few seconds of electro-polishing a black deposit often formed on the surface of the sample and this was particularly noticeable in the case of the Al-Mg-Si alloy. This was easily removed by temporarily withdrawing the sample from the electrolyte and washing it in cold ethyl alcohol.

Electro-polishing was then allowed to proceed for $\frac{1}{2}$ to $\frac{3}{4}$ hour, after which a perforation usually formed at the top of the sample. This was allowed to grow into a hole until about the upper third of the window had been removed. The sample was then turned upside down and polishing continued until a second perforation occurred near to the surface of the electrolyte. For good results it was essential at this stage to maintain the electrolyte at a low temperature, $\sim -20°C$. The upper and lower holes were then allowed to increase in size until only a thin "bridge" of alloy was left. The sample was then quickly removed from the electrolyte

and immersed in cold ethyl alcohol. Thin flakes of alloy were then picked-up on electron microscope grids.

2.5 TRANSMISSION ELECTRON MICROSCOPY

Specimens were examined in either a Siemens Elmiskop I or an AEI EMGG electron microscope at Hinxton Hall or a JEM 7 electron microscope at Warwick University. All machines were operated at 100 kV. The majority of the work was carried out on the EMGG, full use being made of the high angle tilting specimen stage. As the above electron microscopes are now widely used in a large number of laboratories their operating principles[84, 85, 86] can be taken as standard procedure and so are not elaborated on here. The interpretation of electron diffraction patterns and diffraction contrast effects are more peculiar to individual types of specimen and these are dealt with in later chapters.

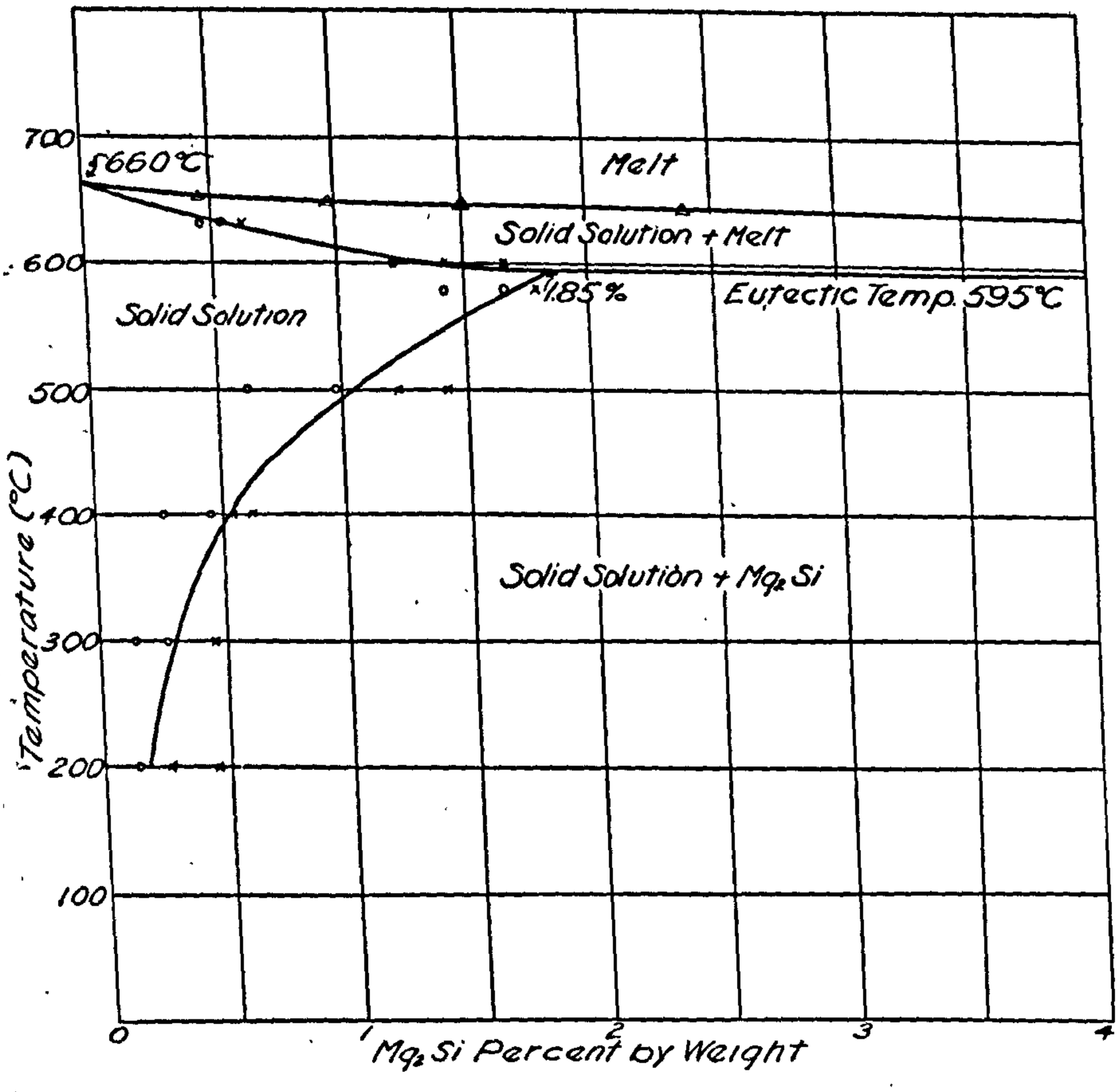

Figure 3.1 The Al-rich side of the pseudo-binary Al-Mg_2Si diagram (after Dix et al[87]).

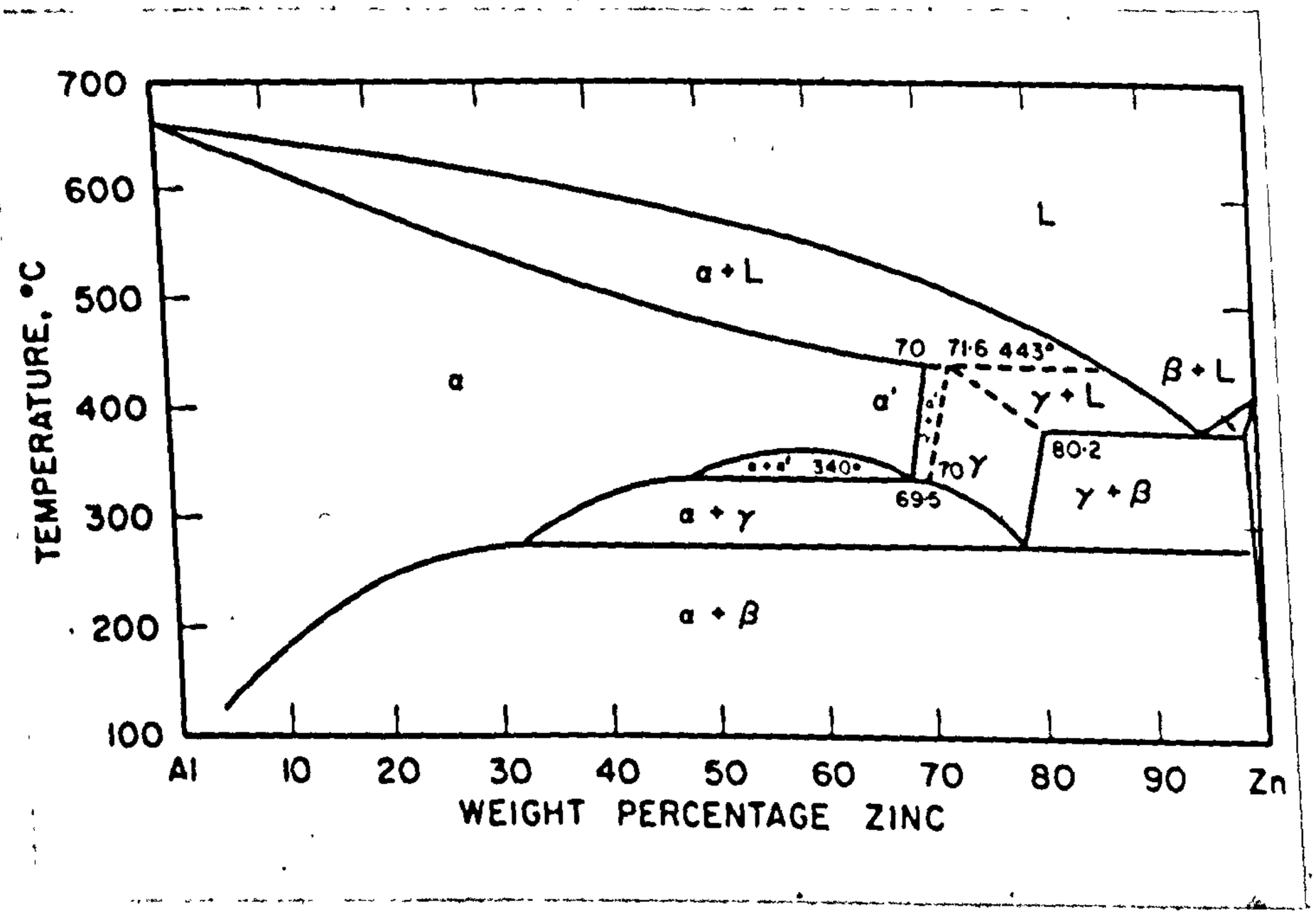

Figure 3.2 The equilibrium diagram of the Al-Zn system (after Presnyakov et al[44]).

CHAPTER 3

THE PRECIPITATION SEQUENCE DURING AGEING OF Al-Mg-Si AND Al-Zn ALLOYS

3.1 INTRODUCTION

It is often convenient to treat the Al-Mg-Si system as a psuedo-binary system because the compound Mg_2Si, which is the equilibrium precipitating phase, is extremely stable. Practically all the work associated with determining the ageing sequence in this alloy has been carried out on so-called balanced alloys in which the magnesium and silicon additions are such that the alloy may be considered as Al-Mg_2Si. The solid solubility of Mg_2Si in aluminium has been studied by Dix et al[87] and their phase diagram is reproduced in Figure 3.1. The maximum solubility of Mg_2Si in aluminium is 1.85 wt.% at 595^{o}C and decreases to 0.1%, or less, at room temperature.

The decomposition of supersaturated Al-Mg_2 Si alloys has been the subject of a number of X-ray[13,88-93] and electron microscopic[80,94-96] examinations. The probable ageing sequence, as given by Kelly and Nicholson[9], is :

Needle-shaped zones along $\langle 100 \rangle$ $\longrightarrow$ needle-shaped zones with internal order $\longrightarrow$ β' $\longrightarrow$ β (Mg_2Si).

The structure of β phase is f.c.c. with the Ca F_2 structure and with a lattice parameter of 6.39 Å. In section (3.2.1) the X-ray studies of the early stages in decomposition are described and this is followed in section (3.2.2) by a review of the electron microscopy carried out on these alloys together with a detailed description of an investigation carried out by the author, on the structure of the needle precipitates.

The decomposition of supersaturated Al-Zn alloys has been studied by a number of techniques (see Kelly and Nicholson[9] for a review). The most recent phase diagram of the Al-Zn system is that proposed by Goldak and Parr[43] and Presnyakov et al[44] and is reproduced here as Figure 3.2. In section (3.3.1) the ageing sequence for dilute Al-Zn alloys ($<$ 30 wt.% Zn), as deduced from recent X-ray and electron microscopic[106-112] examinations, is shown to be :

G.P. zones → rhombohedral α' → cubic α' → β (equilibrium precipitate)

In Chapter 4 experiments are described in which the upper limiting temperature for G.P. zone formation as a function of alloy composition was determined. Part of this work involved quenching samples into Wood's metal or molten salt as a means of quenching-in a high excess-vacancy concentration during the initial stages of ageing. Under these special quenching conditions a new type of precipitate was observed, not accounted for in the ageing sequence given above. The structure of this precipitate is discussed in detail in section (3.3.2).

3.2 PRECIPITATION IN Al-Mg_2Si ALLOYS

3.2.1 The ageing sequence: early X-ray work

The first X-ray examinations, carried out by Geisler and Hill[88] using an Al-1.4% Mg_2Si alloy, and Guinier and Lambot[89] using an Al-0.7% Mg_2Si alloy, failed to detect any abnormal X-ray scattering in samples quenched and then aged at room temperature even though slow changes in mechanical properties were observed. Lutts[90], in a later study, aged samples for as long as one year at room temperature and still was unable to detect any changes in X-ray scattering.

By ageing samples at temperatures between 150°C and 250°C both Geisler and Hill[88] and Guinier and Lambot[89] were able to detect

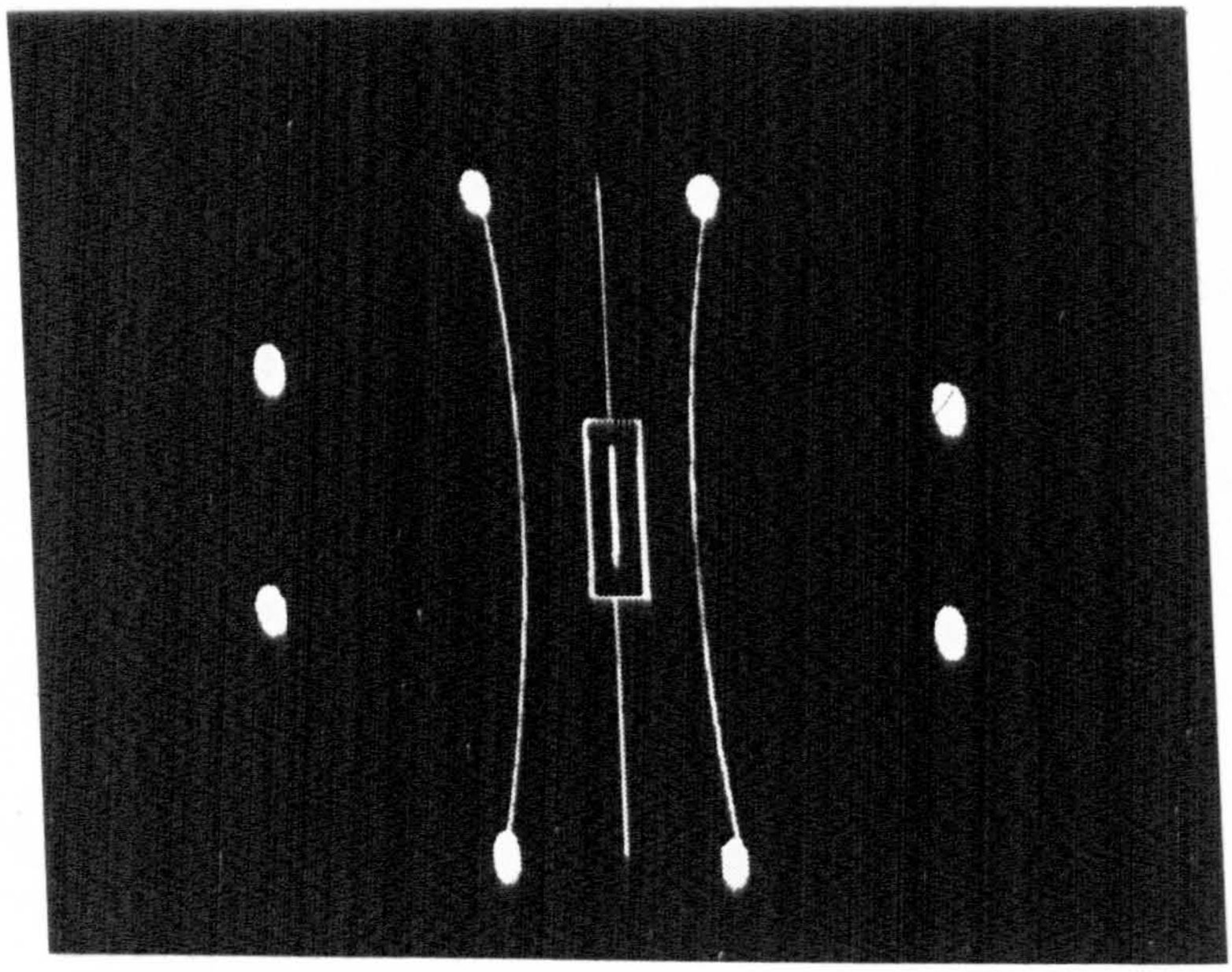

Figure 3.3(a) A schematic illustration of the X-ray pattern obtained by Lutts[90] from an Al-1.0%Mg_2Ge single crystal, aged for 6 hr. at 150°C. Streaks of diffuse scattering pass through, at left, the $(0\bar{1}0)$ and, at right, the (010) matrix reciprocal lattice points.

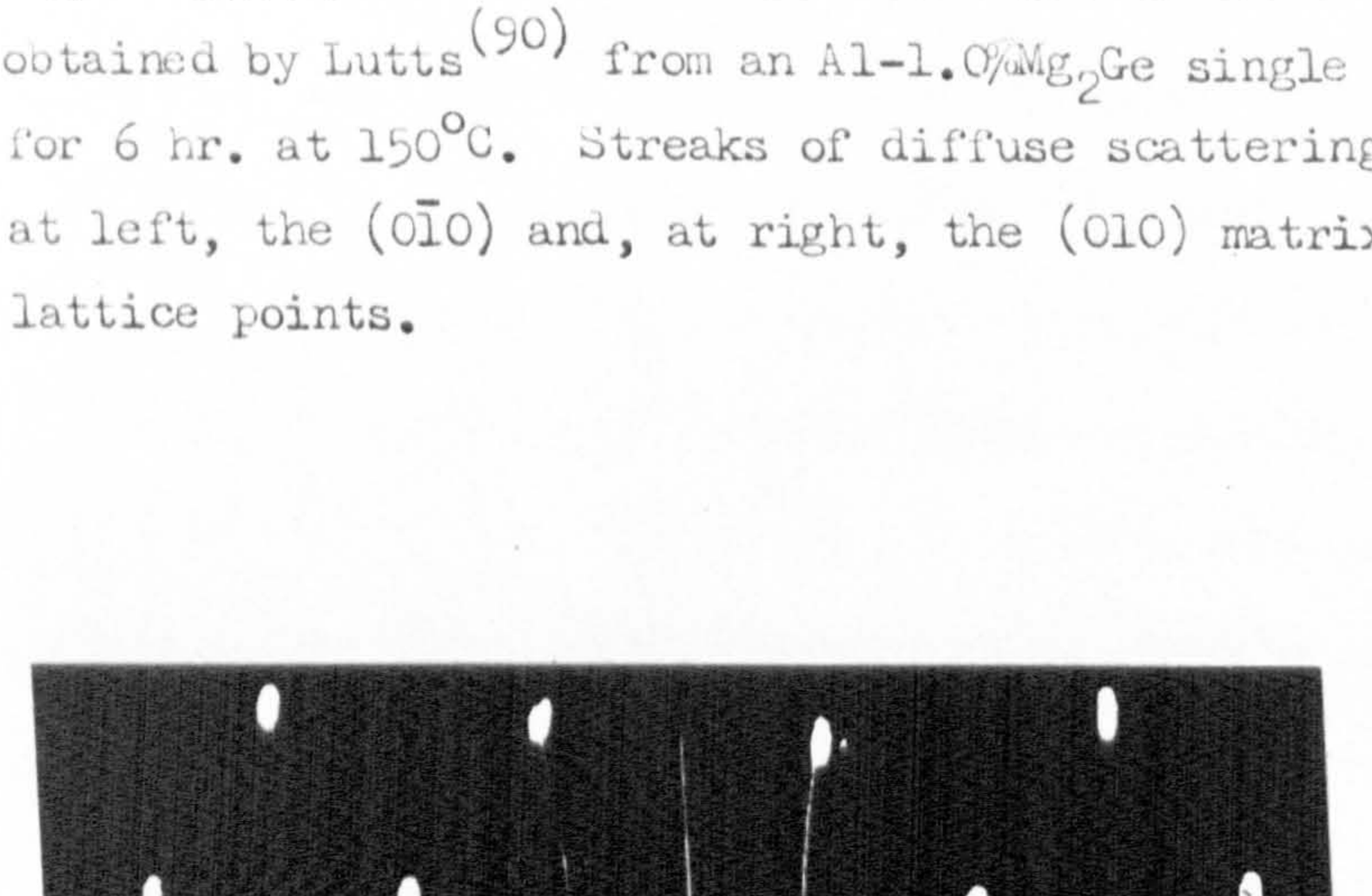

Figure 3.3(b) A schematic illustration of the X-ray pattern obtained by Lutts[90] from an Al-0.7%Mg_2Si single crystal, aged for 10 hr. at 150°C. The intensity of the streaks is very low near to the $(0\bar{1}0)$, (000) and (010) matrix reciprocal lattice points.

diffuse X-ray scattering effects which they attributed to long, but extremely thin, solute clusters whose major axes were parallel to the matrix cube directions. These diffraction effects have been studied by Lambot[91] and more recently in detail by Lutts and Lambot[92] and Lutts[90]. All three papers described the observed changes in diffuse X-ray scattering during ageing and the interpretation of these effects was aided[90,92] by a direct comparison with the similar alloy system, Al-Mg-Ge. One of the difficulties associated with Al-Mg-Si is that the X-ray scattering factors of Al, Mg and Si are all very similar; a fact which led Guinier[13] to conclude that the diffuse scattering arises in this alloy because of a displacement disorder of the lattice. In the case of Al-Mg-Ge, the alloy contains an atom, Ge, which can be distinguished from Al and Mg by virtue of its larger scattering factor and this fact has enabled Lutts[90] to deduce some significant conclusions about the initial clustering in this alloy and also in Al-Mg-Si. He examined single crystal specimens with a monochromatic X-ray beam parallel to either a $[100]$ or a $[101]$ matrix direction. In the case of an Al-1.0%Mg_2Ge aged at 150°C for 3 hours, he observed an extremely faint but continuous line on his X-ray pattern which passed through the (000) reciprocal lattice point. This was interpreted as the intersection of the Ewald sphere with an $\{010\}$ plane of diffuse scattering which passed through the origin of the reciprocal lattice. On further ageing for 3 hours he observed additional lines on the pattern which passed through $(0\bar{1}0)$ and (010), as shown schematically in Figure 3.3(a). After a total of 14 and 30 hours ageing at this same temperature a second and then third pair of lines appeared, which passed through the $(0\bar{2}0)$,(020) and $(0\bar{3}0)$,(030) matrix reciprocal lattice points, respectively. The observed behaviour of an Al-0.7%Mg_2Si alloy, aged at 150°C, was very similar initially in that, after 5 hours ageing, a line appeared through

the (000) reciprocal lattice point. After a further 5 hours ageing a pair of lines appeared through the (010) and $(0\bar{1}0)$ matrix points but with the important difference that their intensity was very low near to the matrix points. At the same time the intensity of the central streak, previously constant along its length, suddenly decreased to an extremely low value near to the central spot (see Figure 3.3(b)). Further ageing to a total of 28 and 80 hours caused lines to appear through the $(0\bar{2}0)$, (020) and $(0\bar{3}0)$,(030) points with noticeable intensity modulations along their length but the intensity near to the central spot remained practically zero. Similar behaviour was observed in samples aged isothermally at temperatures between 135°C and 300°C but at the higher temperatures the time required for each pair of lines to appear was very much shorter. With prolonged ageing at temperatures above 200°C the formation of precipitate Bragg spots was observed, corresponding to the equilibrium precipitate.

Lutts interpreted the initial streak through the (000) spot, which was identical for both Al-Mg-Si and Al-Mg-Ge, as indicating that the early clusters possessed a displacement disorder with no internal order or periodicity. The progressive formation of streaks through $(0\bar{1}0)$,(010); $(0\bar{2}0)$, (020) and $(0\bar{3}0)$,(030) matrix points he interpreted as indicating the progressive formation of an internal periodicity or order along the major axes of the clusters. Since the streaks were confined to $\{100\}$ matrix reciprocal lattice planes, he concluded that the clusters have the periodicity of the matrix only in one direction, along the $<100>$ matrix axes, which is consistent with the idea that the clusters are needle-shaped. Lutts proposed that the initial presence and subsequent decrease,of the intensity close to the origin of reciprocal space in the case of Al-Mg-Si can be explained by the presence of a high vacancy

concentration within the initial clusters. He suggested that an incorporated vacancy acts as a source of scattering with an X-ray scattering factor significantly different from that of Al, Mg or Si. During subsequent cluster growth the vacancies are replaced by Mg and Si atoms, which reduces the intensity scattered at small angles but increases the diffuse scattering at high angles on $\{100\}$ matrix reciprocal lattice planes because of the increased internal order of the cluster. In the case of Al-Mg-Ge the vacancies are replaced by Mg and Ge atoms and, since Ge has a different scattering factor from Al and Mg, the scattering at low-angles remains constant.

These results suggest the following stages for the initial decomposition of an Al-Mg_2 Si solid solution:

1. The solute atoms assemble in lines, with the aid of vacancies, along the $\langle 100 \rangle$ matrix axes :

2. Progressive internal ordering of the cluster occurs as growth proceeds, leading to a needle-shaped zone which has the periodicity of the matrix along its length.

According to Guinier[13,93], the needle-shaped zones may be described as having a "linear disorder". There are three sets of needles, each set parallel to one of the three matrix cube directions. In directions normal to the needle-axis the solute atoms progressively take on an arrangement different from the matrix, which accounts for the modulations in diffusely scattered intensity.

Finally, it should be pointed out that this model is consistent with the hypothesis of Federighi and Thomas[69] in which a strong interaction energy between vacancies and a zone is proposed to explain the rapid transition from the "fast" to "slow" reactions in certain alloys (see Chapter 1), a behaviour which has been observed in Al-1.4%Mg_2Si

by Panseri and Federighi[66] and in Al-2.1%Mg_2Ge by Ceresara and Fiorini[67].

3.2.2 Electron microscopy

(a) Previous work

The earliest electron microscope observations of precipitation in Al-Mg-Si were performed by Castaing and Guinier[94] using the oxide - replica technique. They were able to detect large rod-like structures by ageing samples at a high temperature. Similar structures were observed by Saulnier and Mirand[95] in a thin-foil examination of samples aged for 2 hours at 250°C. The first detailed electron microscopic study of this alloy was carried out by Thomas[96], who worked with a high purity Al-1.53%Mg_2Si alloy. He was able to detect needle-shaped zones by ageing samples at temperatures below 204°C. The needles were aligned along the matrix cube directions. Their length increased from ~200 Å up to > 1000 Å as the ageing time or temperature was increased but their diameter remained fairly constant at ~ 60 Å. The density of the needles was measured as ~ 2 - 5 x $10^{15}/cm^3$. Electron diffraction patterns obtained from these specimens contained streaks which were consistent with the X-ray results of Lutts[90]. At ageing temperatures above 200°C the needles increased in both length and diameter, to become rods, and Thomas reported that the associated electron diffraction patterns indicated that the rods had a f.c.c. superlattice, with a = 6.42 ± 0.07Å. He proposed that this is the structure of the β' precipitate, with the following orientation relationship with the matrix :

$$\langle 100 \rangle \text{ matrix} \;//\; \langle 110 \rangle \; \beta'$$

Subsequent ageing caused the rods to transform into platelets of the β equilibrium phase. Thomas reported that in most cases the Mg_2Si platelets

grew out from the large needles, although occasionally a few may have been nucleated independently. In this investigation he did not observe preferential precipitation on dislocations or the presence of a strain field associated with the needles although this was detected in a later investigation[97].

In a later paper, Pashley, Rhodes and Sendorek[80] gave a brief summary of their observations of the ageing sequence in an Al-1.2%Mg_2Si alloy which differed from the conclusions of Thomas[96] in several respects. Firstly, they observed a radial strain field associated with the needles viewed end-on which was characterised by a double loop of contrast separated by a line of no contrast, parallel to the operating reflecting plane. This contrast became more pronounced as the needles increased in length but was distinguishable around needles of only 150 Å in length. Secondly, precipitation was observed to occur on dislocations. Thirdly, the thicker needles or rods gave rise to discrete spots on selected area diffraction patterns which were not consistent with the f.c.c. lattice proposed by Thomas[96], nor any other cubic structure. They did not obtain a full interpretation of the patterns although it was concluded that the needles never assumed the structure of bulk Mg_2Si.

Recently, the author has studied the ageing sequence of an Al-1.2%Mg_2Si alloy in considerable detail by means of electron microscopy and electron diffraction[98]. This work has revealed that the larger needle precipitates appear to have a hexagonal unit cell with the c-direction of the cell parallel to a matrix cube direction. This result, together with other aspects of the ageing sequence are discussed in the next section.

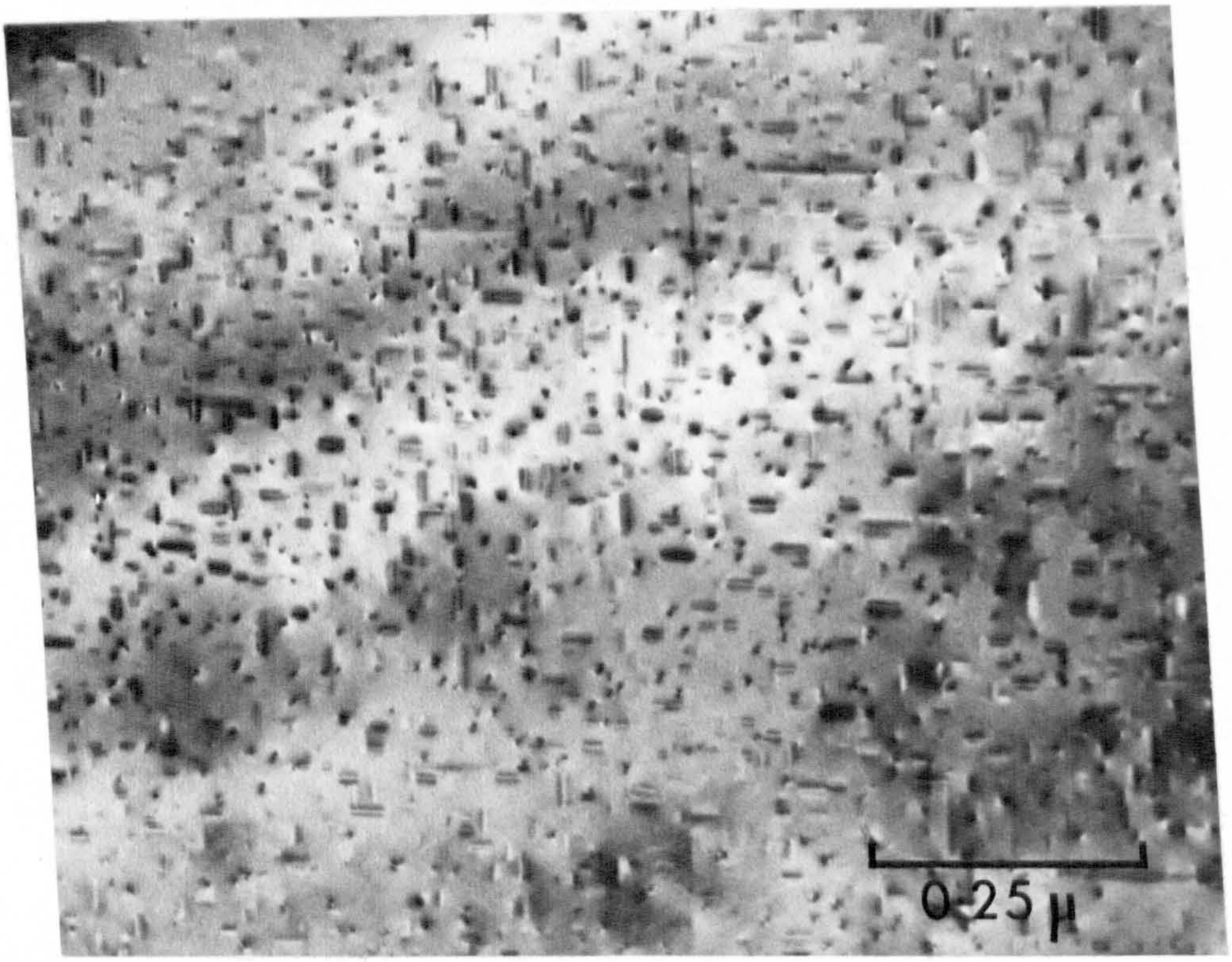

Figure 3.4(a) Al-1.2% Mg_2Si alloy, solution treated at 560°C for 1 hr. and then direct-quenched into oil at 160°C and aged for 24 hr., illustrating the high density of small needles produced by this heat treatment. Foil orientation is (001).

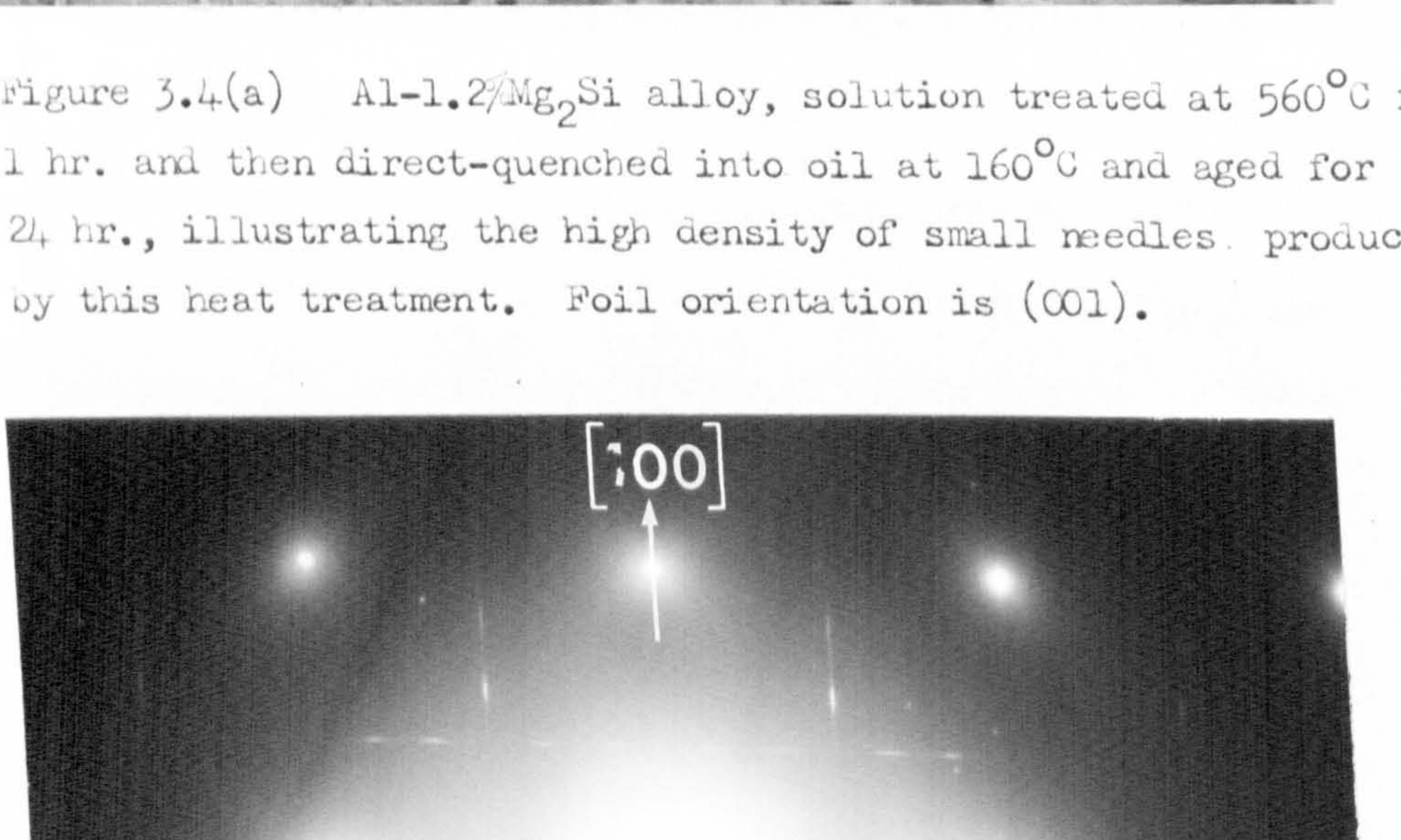

Figure 3.4(b) Typical selected-area diffraction pattern from an area similar to that shown in (a).

(b) Recent experimental results with an Al-1.2%Mg_2Si alloy

In Chapter 4 the concept of an upper limiting temperature for G.P. zone nucleation is discussed at some length. In practical terms, this means that an alloy must be quenched to an ageing temperature below some "critical temperature" before the nucleation and growth of G.P. zones is observed. The upper limiting temperature for the formation of needle-shaped zones in an Al-1.2%Mg_2Si alloy was found to be very quench-rate dependent and varied from about 190°C for a step-quench up to about 240°C for a rapid quench into Wood's metal.

Samples which were quenched directly into oil at 160°C (i.e. well below the critical temperature) and aged at that temperature for 24 hours contained a high density of needle-shaped zones. A typical example is shown in Figure 3.4(a) for a foil in cube orientation. Since the major axes of the needles lie along <100> matrix directions, one set of needles is seen end-on in this micrograph. The needles are 200 - 500Å in length. This and similar samples in this orientation gave rise to streaks on selected-area diffraction patterns, as illustrated by Figure 3.4(b). Similar patterns have been obtained by Thomas[96] and Pashley, Rhodes and Sendorek[80]. The geometry of the streaks indicates that the needles are coherent with the matrix along their length. Further discussion of this pattern is postponed until later in this section.

Much larger needles were produced by quenching samples into water at room temperature and then, after a few minutes, ageing them in the temperature range 250°C to 300°C for up to 30 minutes. The final density of needles was usually quite low (see Figure 3.5) and many of the needles had clearly been nucleated on dislocation lines. Needles longer than $\frac{1}{2}\mu$ were produced by this type of heat-treatment. Many of these needles gave rise to discrete spots on selected-area diffraction patterns obtained from

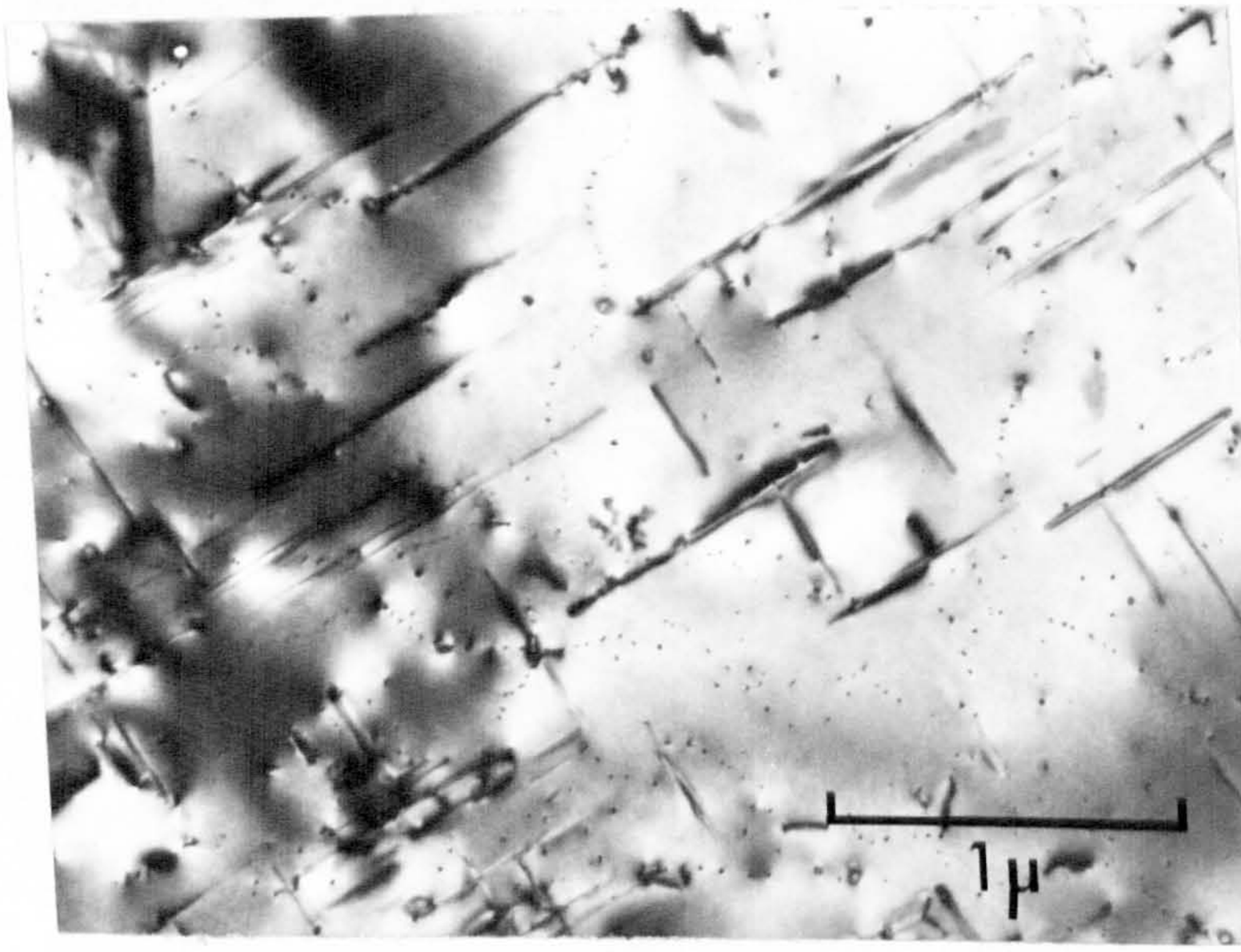

Figure 3.5 Al-1.2%Mg_2Si alloy, solution treated at 560°C for 1 hr., direct quenched into water at 20°C and then aged at 250°C for 6 hr., illustrating the low density of large needles produced by this heat treatment. Foil orientation is (001).

foils in different matrix orientations. Unfortunately it was not possible to obtain spot patterns from needles viewed end-on. This was thought to be because such needles were sufficiently long to intersect both surfaces of a thinned sample and so appeared to suffer preferential chemical attack during specimen preparation. The general approach was, therefore, to obtain a large number of diffraction patterns consisting of plane sections through the reciprocal lattice of the needle when the needle axis was normal to the electron beam direction. These results were supplemented by a significant number of patterns for which the needle axis made an oblique angle with the electron beam. A careful analysis of all such patterns has enabled a three-dimensional construction of the reciprocal lattice to be made. The results of this analysis will now be given and this is followed by a description of the experimental results.

The results indicated that the large needles have a hexagonal unit cell ($a = 7.05 \pm 0.05$ Å ; $c = 4.05$ Å) such that a needle along $[100]$ matrix direction has the following orientation relationship with the matrix:

$$\left.\begin{array}{llll} (001) & \text{needle} & // & (100) \quad \text{matrix} \\ [100] & \text{needle} & // & [01\bar{1}] \quad \text{matrix} \end{array}\right\} \text{ I}$$

If this is called orientation I then, by symmetry, there is a second, equivalent, orientation II given by :

$$\left.\begin{array}{llll} (001) & \text{needle} & // & (100) \quad \text{matrix} \\ [100] & \text{needle} & // & [011] \quad \text{matrix} \end{array}\right\} \text{ II}$$

There are thus two equivalent orientations for each of the three possible sets of needles lying along the three $\langle 100 \rangle$ matrix directions, giving a total of six possible orientations of needle.

Figure 3.6 is a diagram of the (001) reciprocal lattice section

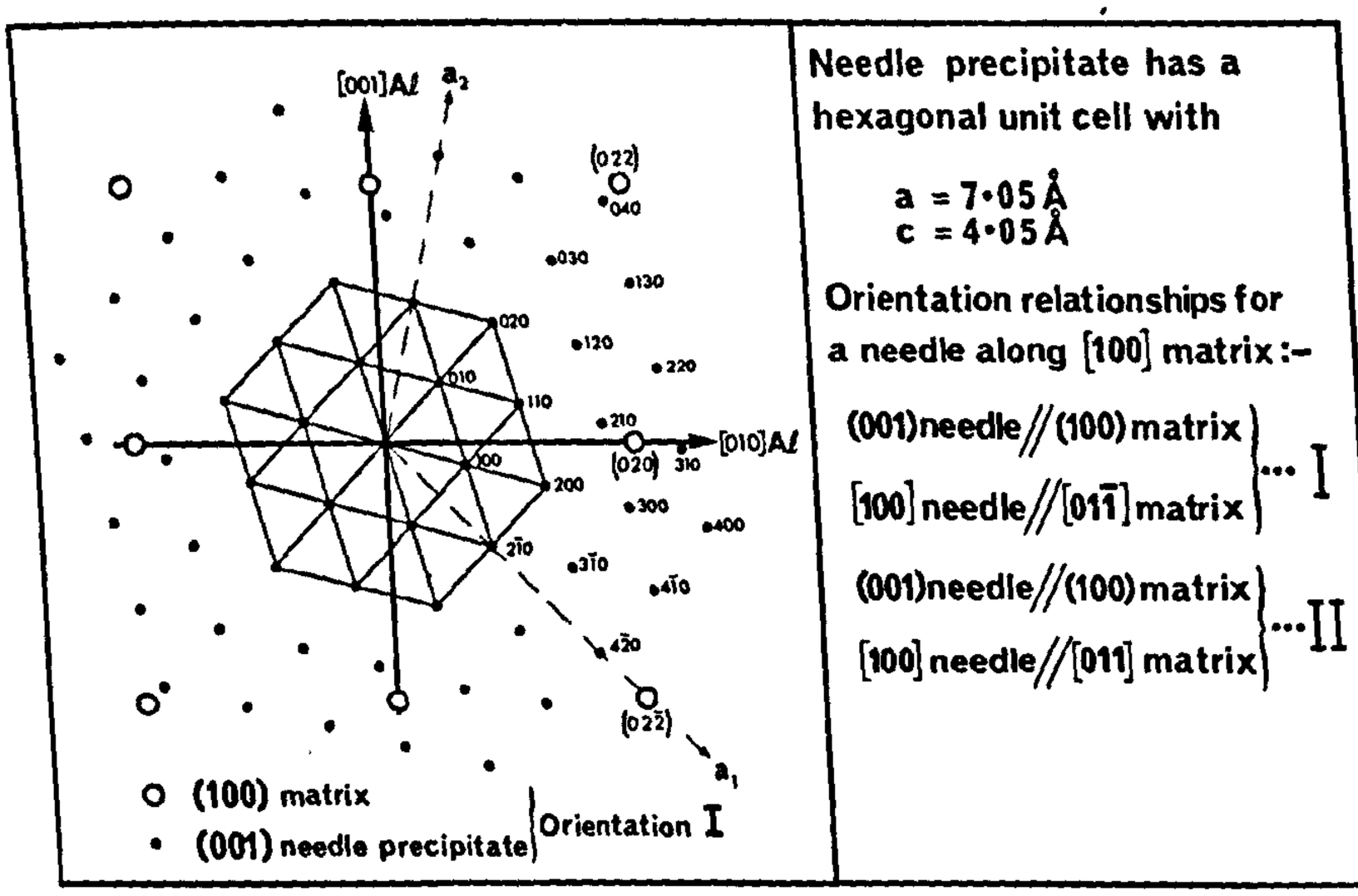

Figure 3.6 Diagram of proposed (001) reciprocal lattice section of a needle precipitate, superimposed on the (100) reciprocal lattice section of the matrix.

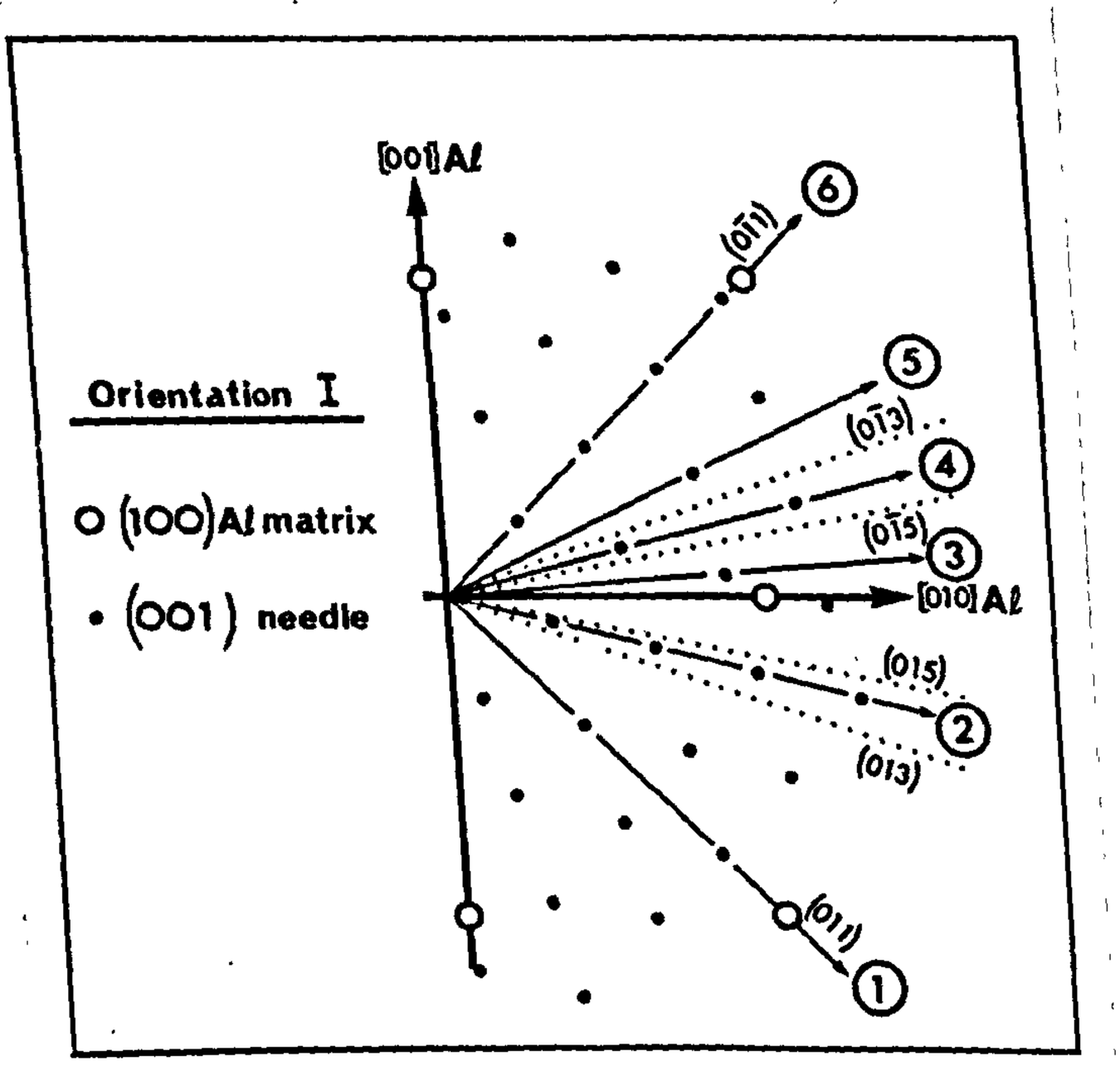

Figure 3.7 Part of Figure 3.6 redrawn to illustrate the sections labelled (1) to (6), which refer to the diffraction patterns Figure 3.8(a) - (f).

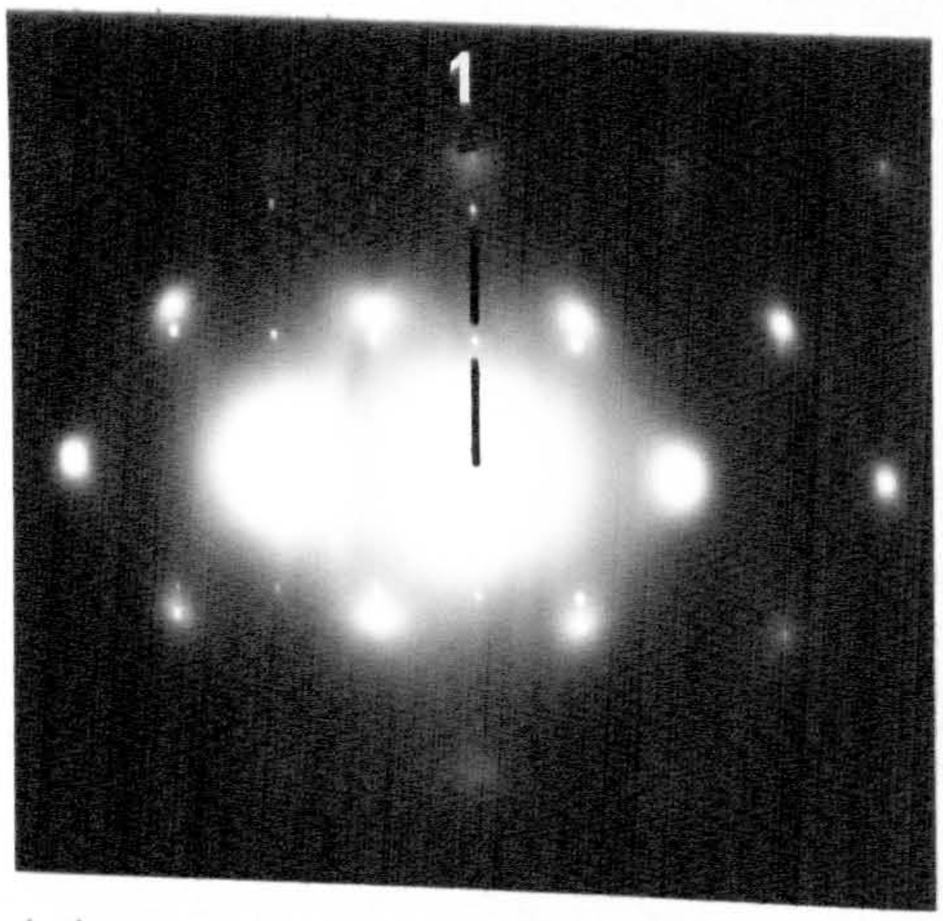

(a) near (011)

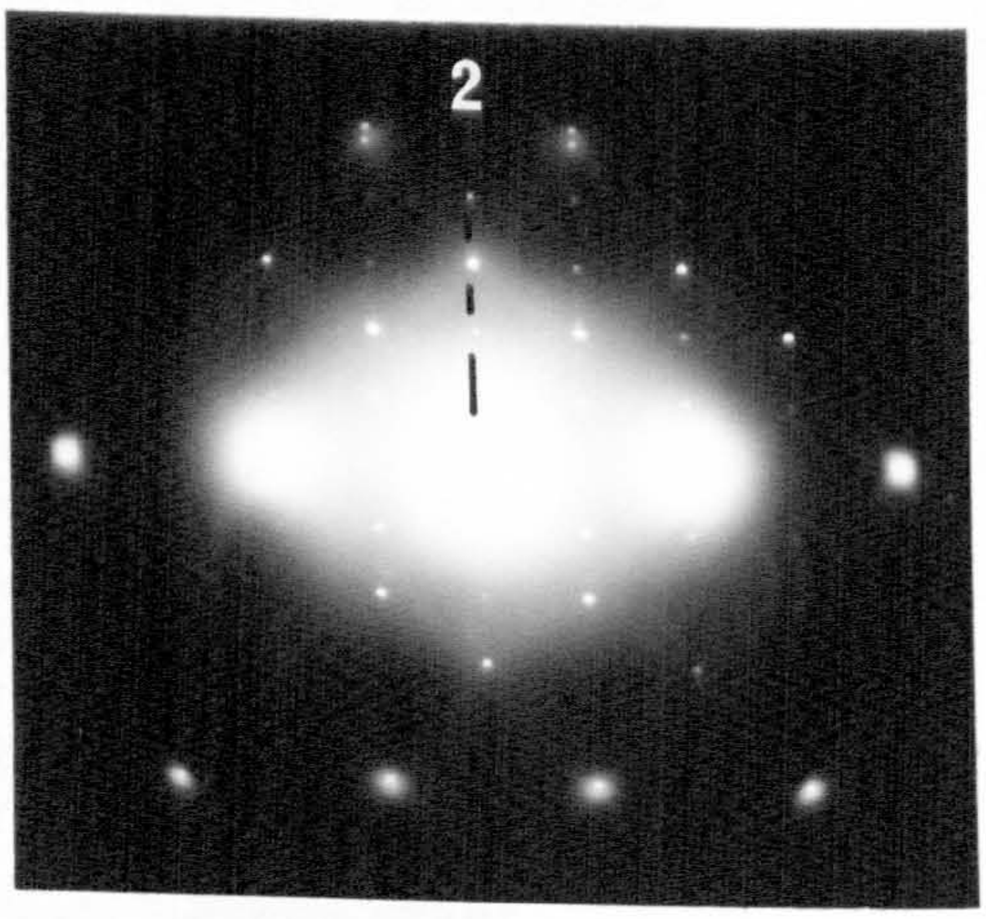

(b) (013)

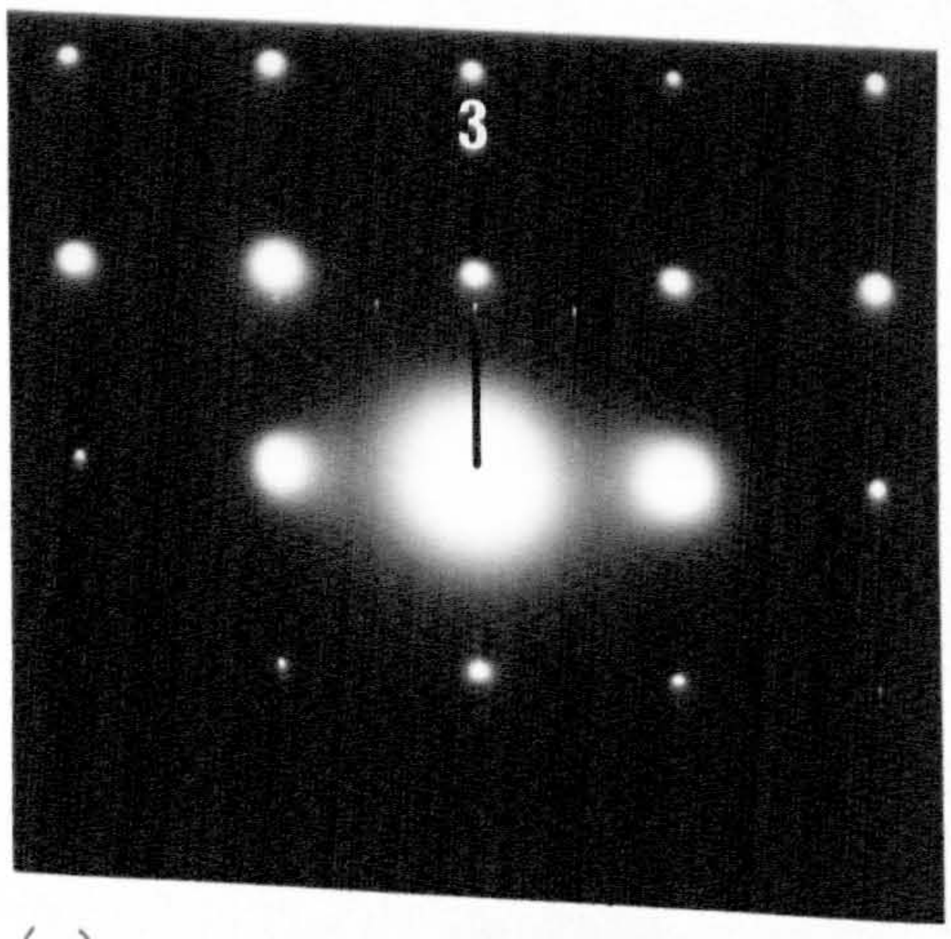

(c) (001)

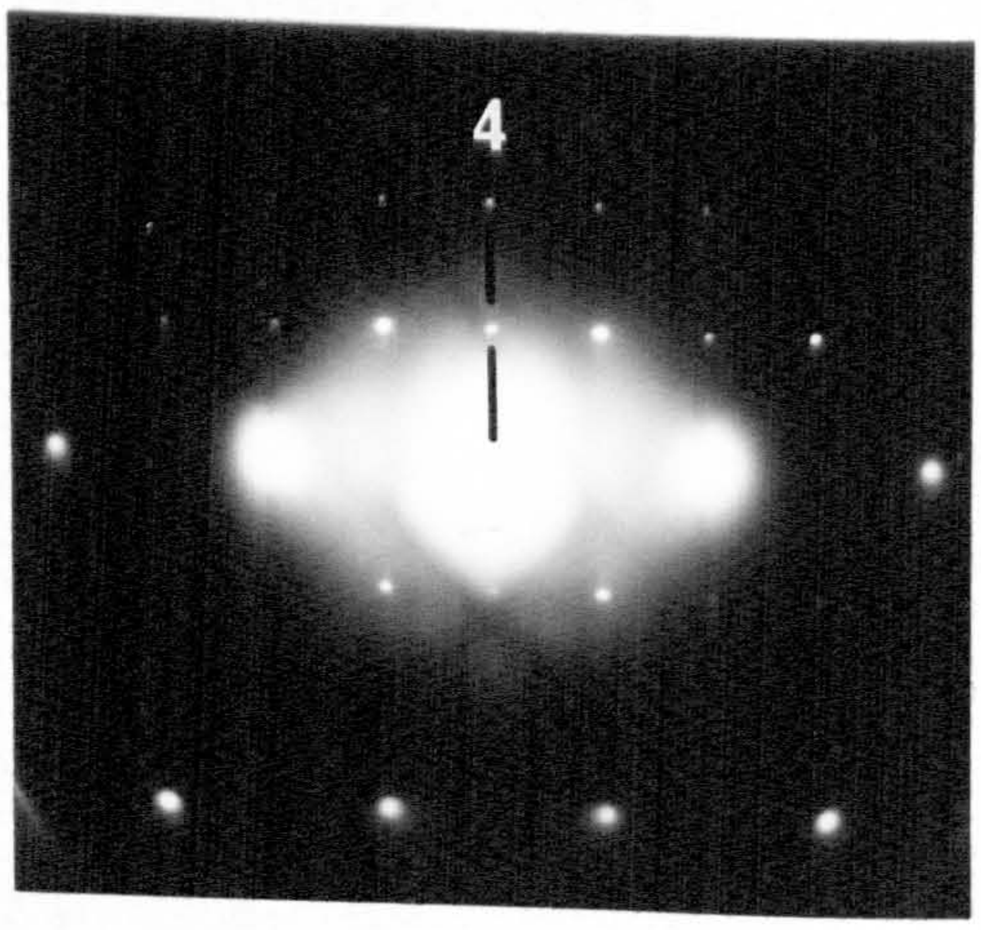

(d) (0$\bar{1}$3)

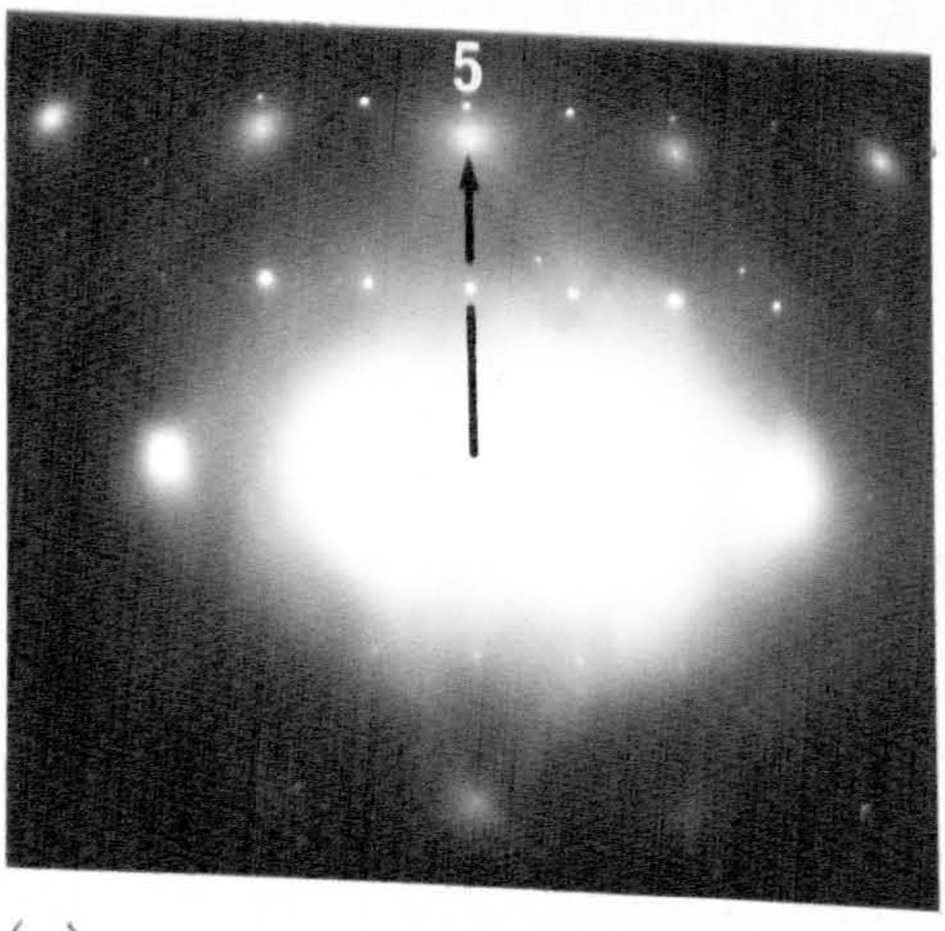

(e) near (0$\bar{1}$3)

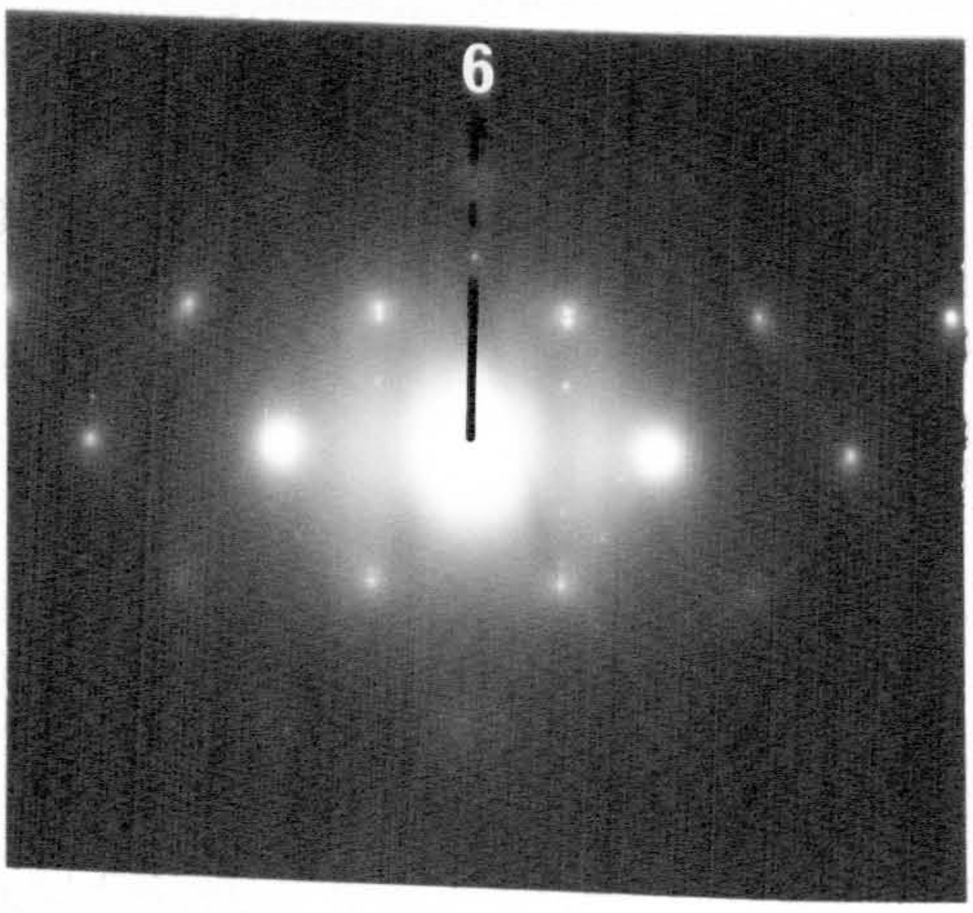

(f) near (0$\bar{1}$1)

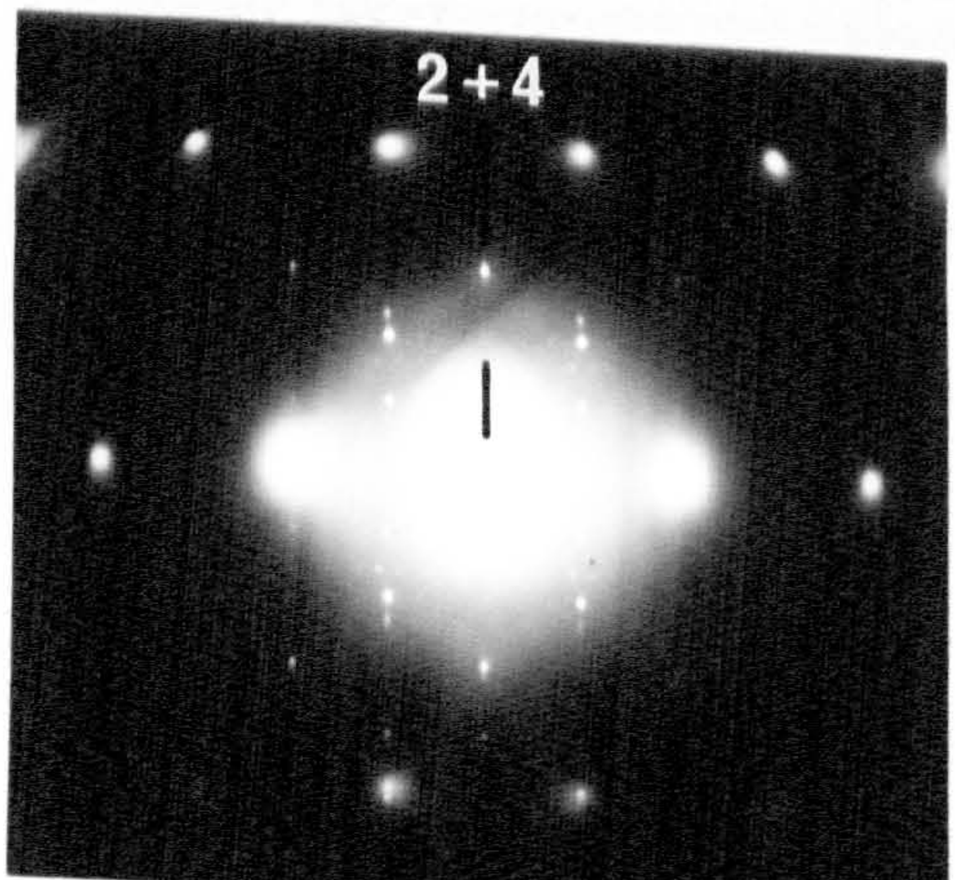

(g) (013)

Figure 3.8(a)-(f) Selected-area diffraction patterns from single needles along [100] matrix direction. The foil orientation and the line of spots corresponding to Figure 3.7 are given with each pattern.

Figure 3.8(g) This micrograph was obtained from an area containing two needles along [100] matrix (see text).

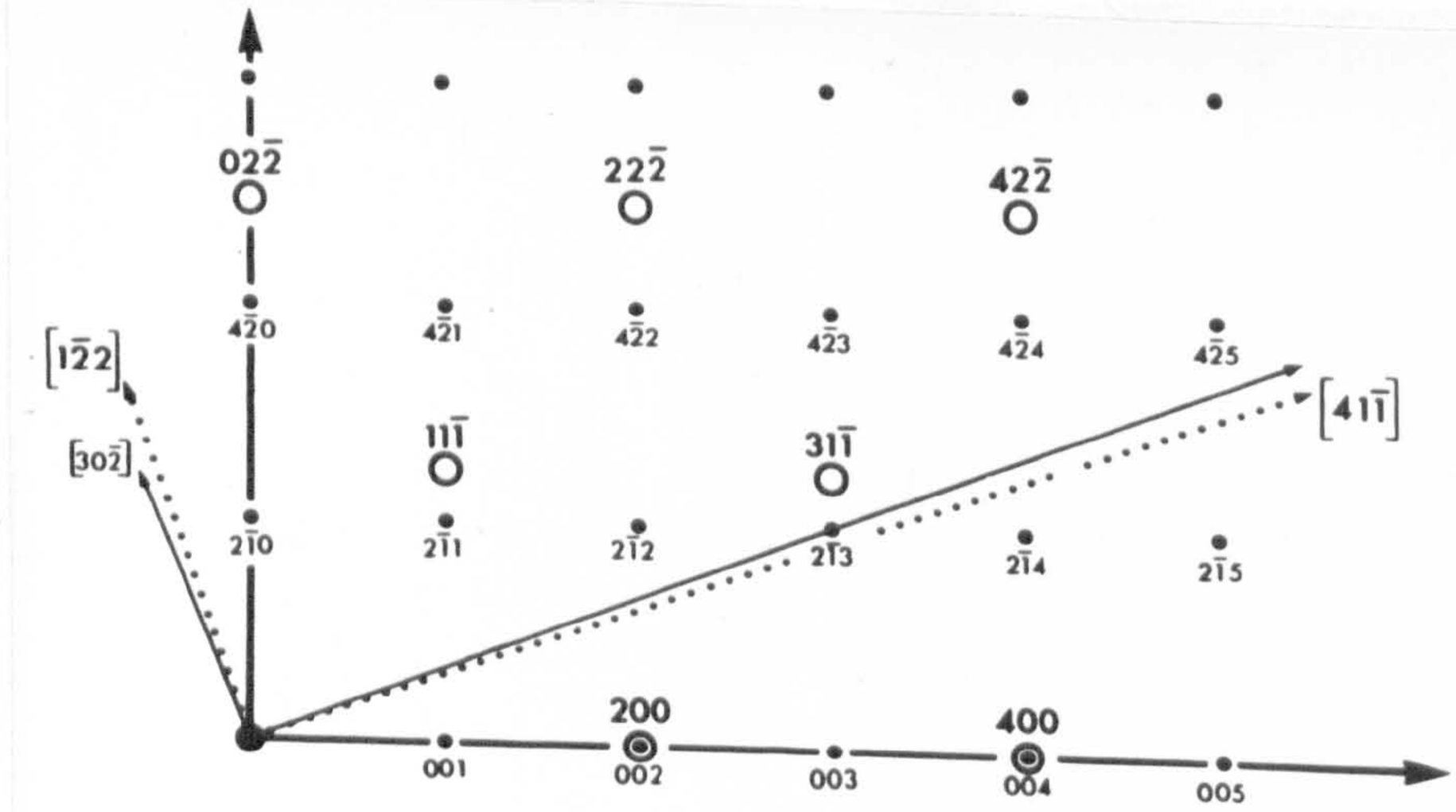

(a)

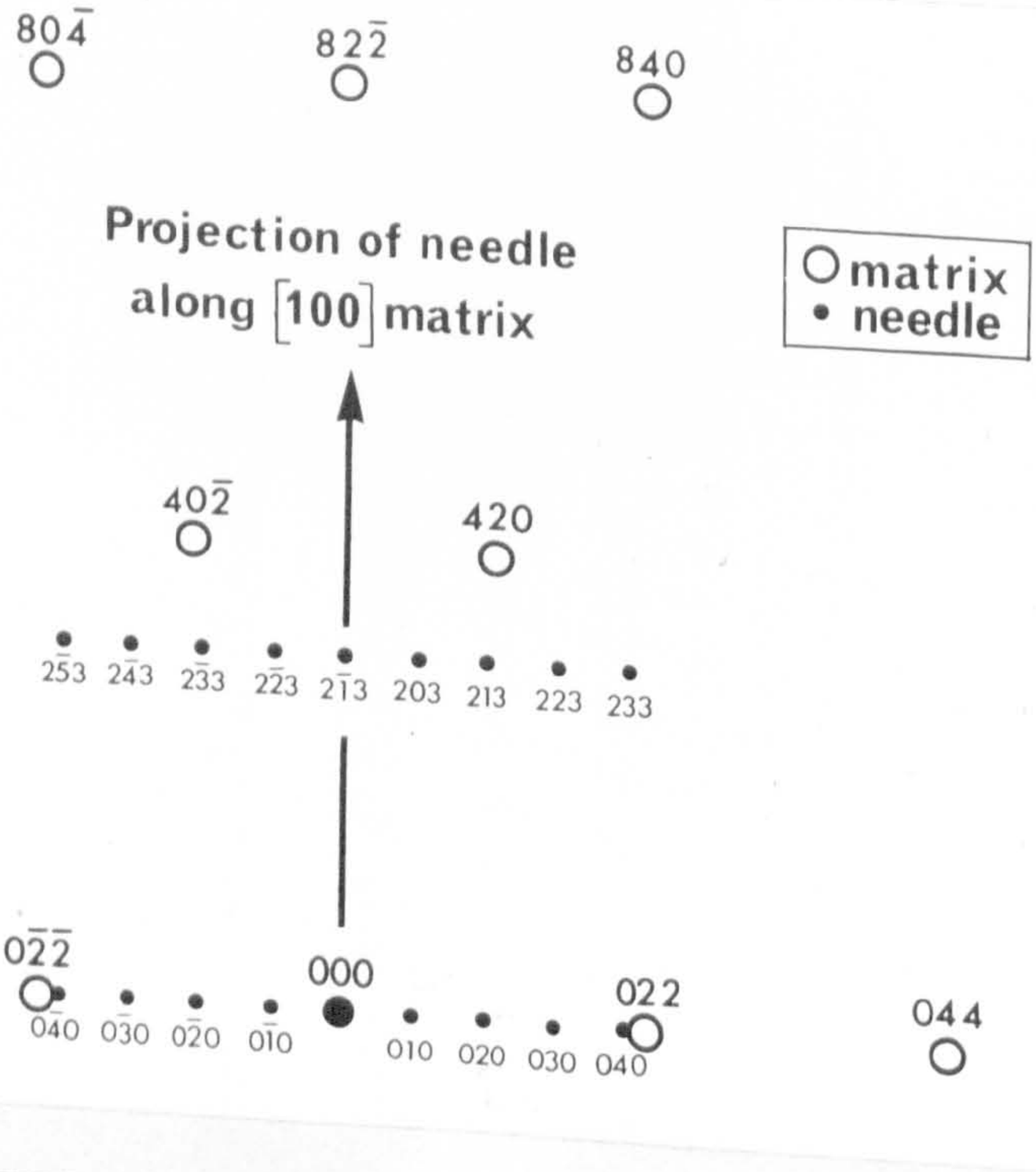

(b)

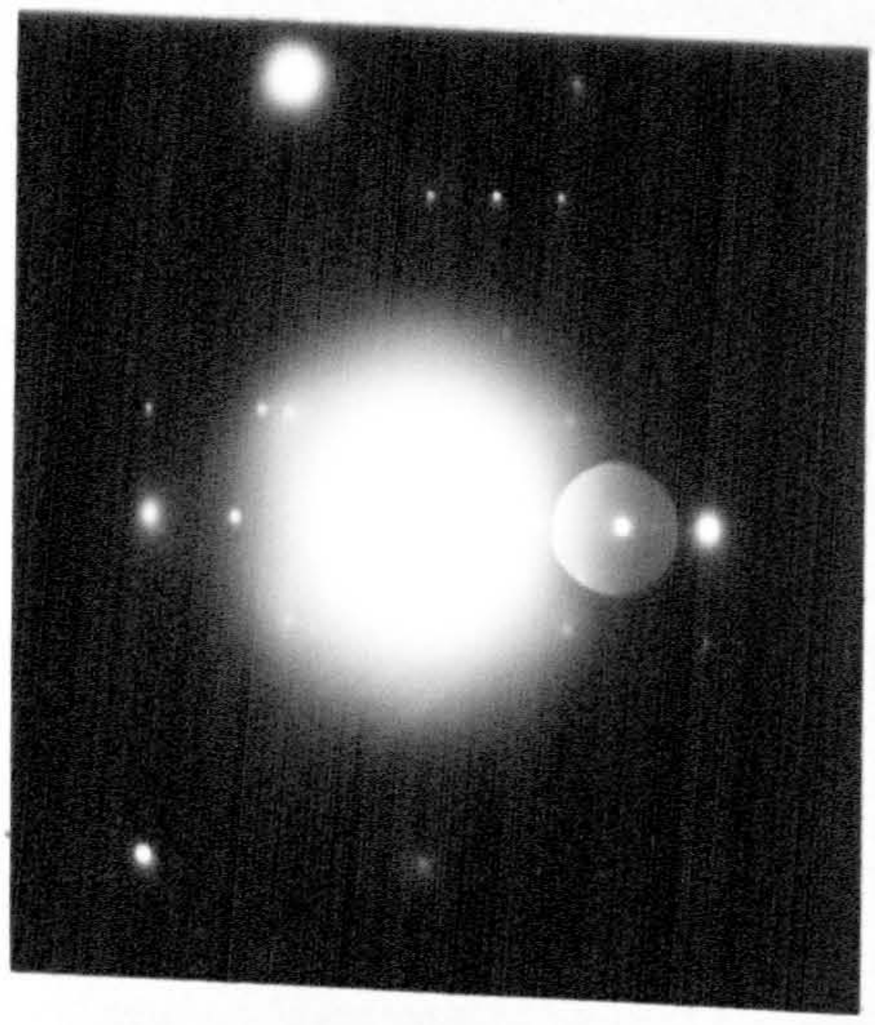

(c)

Figure 3.9 (a) is a diagram of the (011) matrix reciprocal lattice section and the corresponding reciprocal lattice section for a needle in orientation I (see Figure 3.8(a)). If the electron beam is parallel to the $[1\bar{2}2]$ matrix direction the predicted diffraction pattern is shown diagrammatically in (b), which should be compared with the actual pattern (c).

of a needle corresponding to orientation I above. As an example of the way in which Figure 3.6 was constructed part of it is redrawn in Figure 3.7 to illustrate the sections labelled (1) to (6), which refer to the diffraction patterns Figures 3.8(a) - (f), all obtained from single needles along $[100]$ matrix. The matrix orientation is given with each pattern. The numbered arrow on each pattern indicates the line of spots intersected by the corresponding arrow on Figure 3.7. A careful inspection of all the diffraction patterns shows that the array of precipitate reciprocal lattice spots represented by Figure 3.7 is repeated on every $\{100\}$ plane of the matrix and hence leads to the conclusion that the c-spacing of the precipitate unit cell is equal to the $\{100\}$ spacing of the matrix (i.e. c = 4.05 Å).

As orientations I and II are related by inversion of Figure 3.7 about the $[010]$ matrix axis, it will be seen that a selected-area diffraction pattern taken near to (013) matrix orientation from an area containing two or more needles may include both sections, labelled (2) and (4), simultaneously. Figure 3.8(g) is an example of such a pattern. This type of pattern is regarded as proof of the co-existence of both orientations I and II.

As an example of a diffraction pattern obtained from a needle along $[100]$ matrix which made an oblique angle with the electron beam, consider the case where the electron beam was parallel to the $[1\bar{2}2]$ matrix direction. The geometry of this situation is illustrated by Figure 3.9(a) from which it will be seen that the $(1\bar{2}2)$ reciprocal lattice section of the matrix is only rotated by $\sim 1\frac{1}{2}^{o}$ about the $[011]$ matrix axis from the $[30\bar{2}]$ zone of the precipitate. The diagram, Figure 3.9(b), shows the predicted diffraction pattern when the $[30\bar{2}]$ precipitate zone is superimposed upon the $(1\bar{2}2)$ reciprocal lattice plane

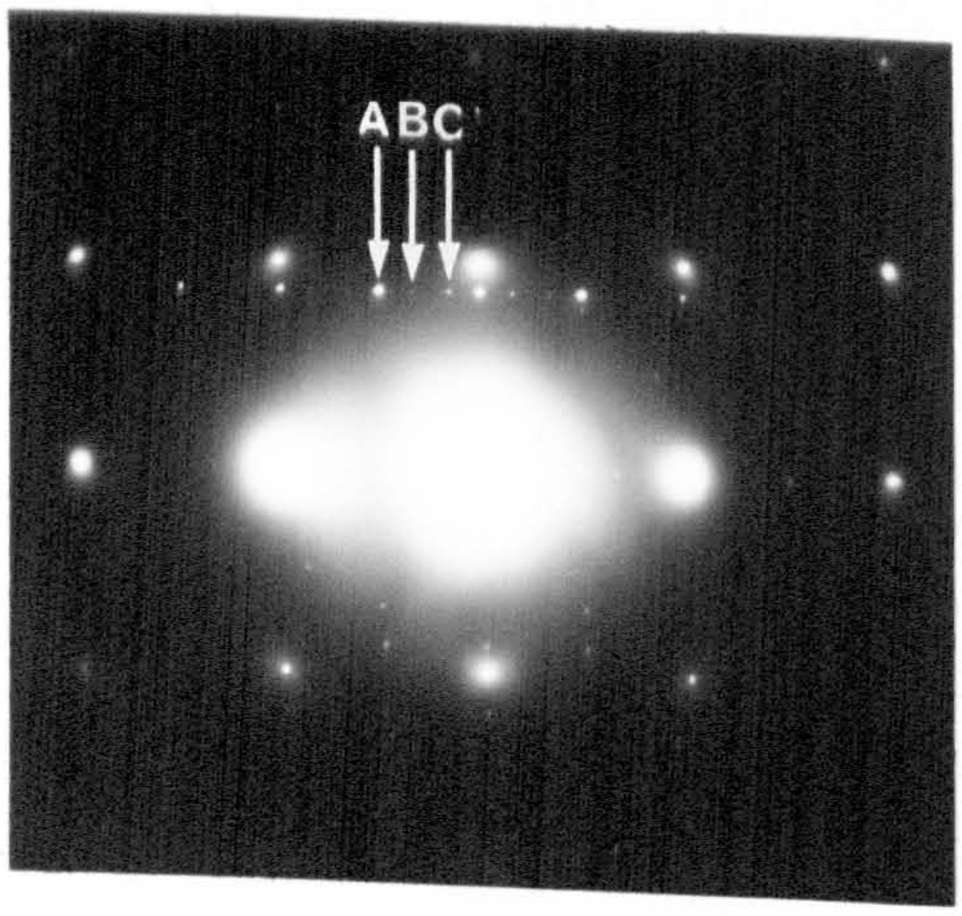

Figure 3.10(a) An electron diffraction pattern from the area shown in (b) and (c).

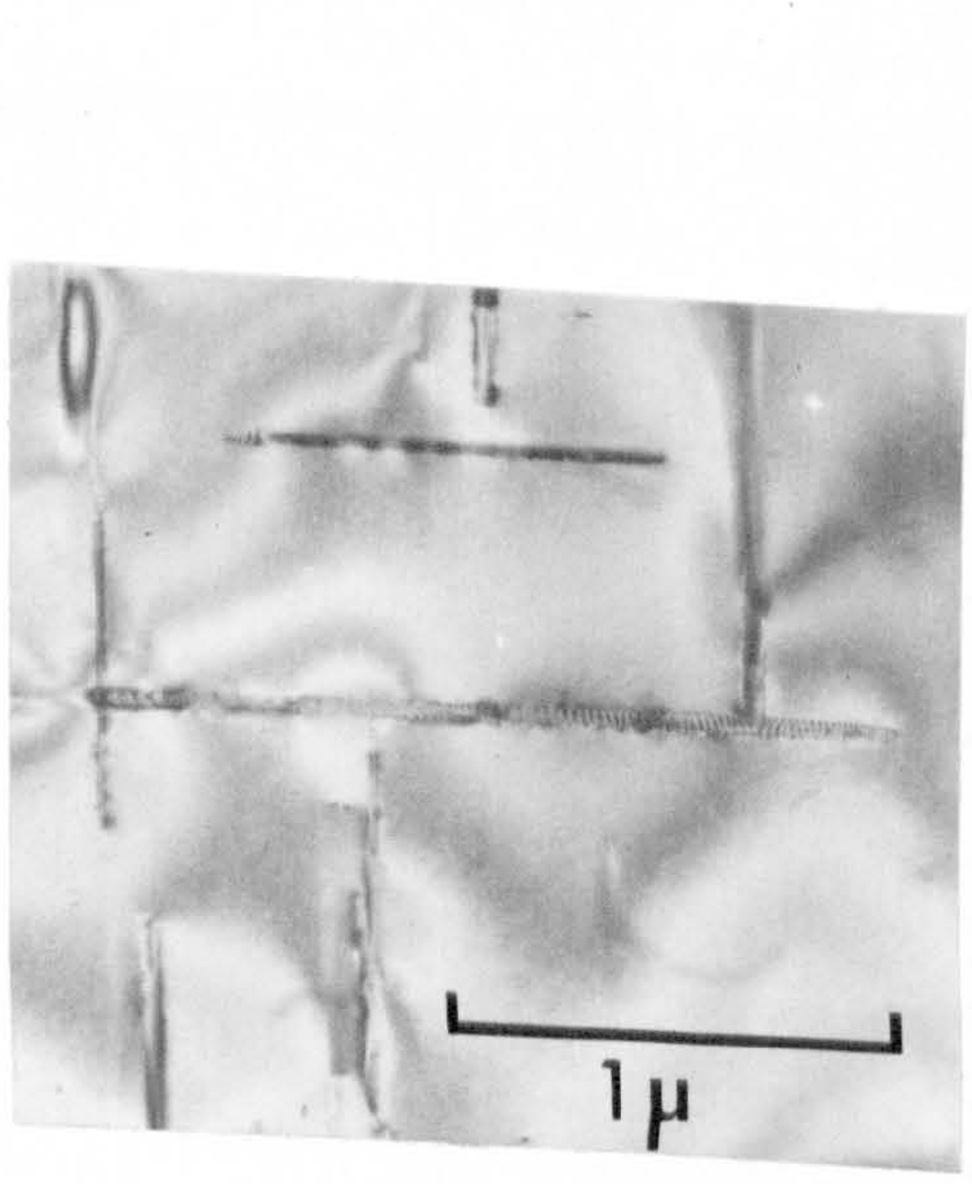

Figure 3.10(b) A bright field micrograph from a foil, close to (001) matrix orientation, illustrating the presence of dislocation loops around a large needle.

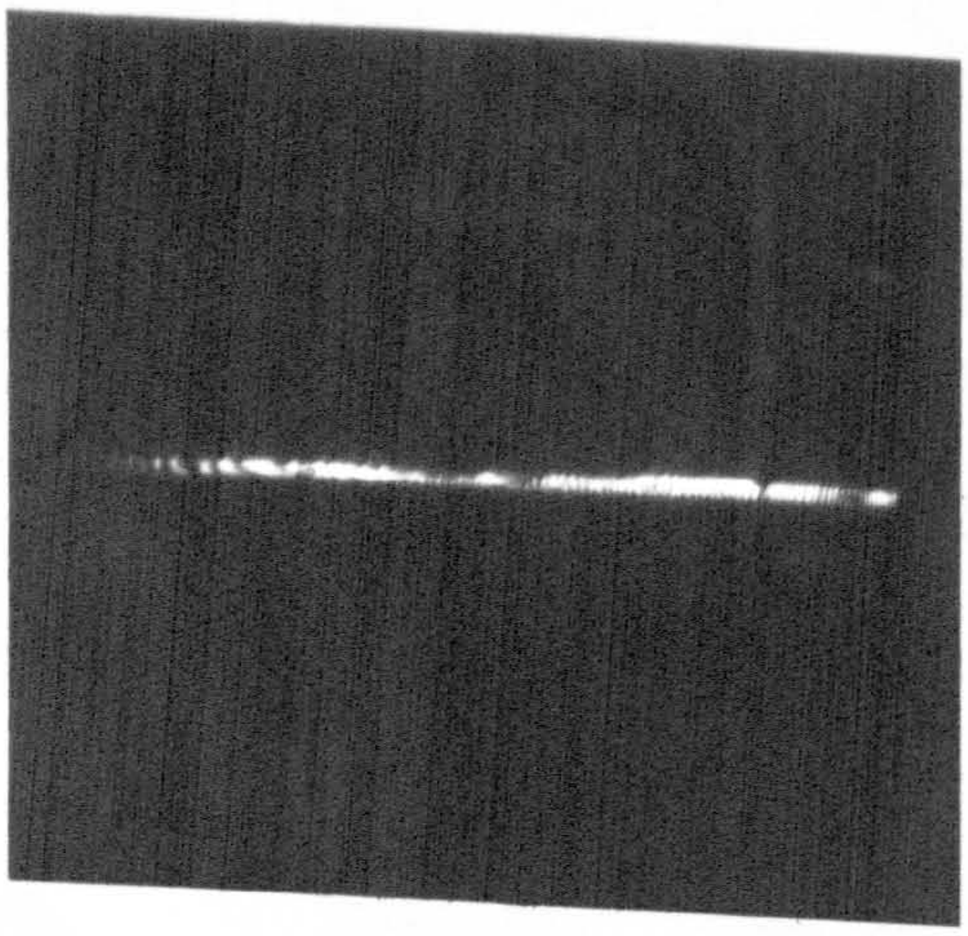

Figure 3.10(c) A micrograph of the dark field image produced by the precipitate spot labelled A.

of the matrix. This should be compared with Figure 3.9(c), which is an electron diffraction pattern close to this orientation. The agreement is good and provides additional evidence to support the proposed unit-cell.

It should be pointed out that some electron diffraction patterns have been obtained which contain extra faint spots parallel to the c-axis of the precipitate which would be consistent with a hexagonal unit cell with a = 7.05 Å and c = 12.15 Å, i.e. a unit cell three times longer along the c-axis but still coherent with the matrix along the needle length. Figure 3.10(a) is an example of this type of pattern from a foil close to (001) matrix orientation. Figure 3.10(b) is the bright field micrograph of the area from which the diffraction pattern was obtained and Figure 3.10(c) is the dark field image produced by the precipitate spot labelled A. If Figure 3.10(a) is compared with Figure 3.8(c) it will be seen that the extra spots exemplified by those labelled B and C in the former are missing in the latter. These extra spots were only visible on patterns obtained from larger needles. It is possible that they were present in the patterns obtained from smaller needles but were too weak to be detected. However, there is a certain amount of evidence which suggests that the appearance of the extra spots coincided with the formation of dislocation loops around the needle (see Figure 3.10(b)). The observation of these loops has been reported by Pashley and Rhodes[99] and discussed in detail by Weatherly[100] and Weatherly and Nicholson[101] who determined the mechanism for the loss of coherency of large needles in this alloy. Loss of coherency appears to occur by a series of complex climb mechanisms. The process is initiated when a matrix dislocation climbs to the needle and either lies along one interface of the needle or loops around it. This dislocation subsequently breaks down to form a series of loops with Burgers vectors of the type

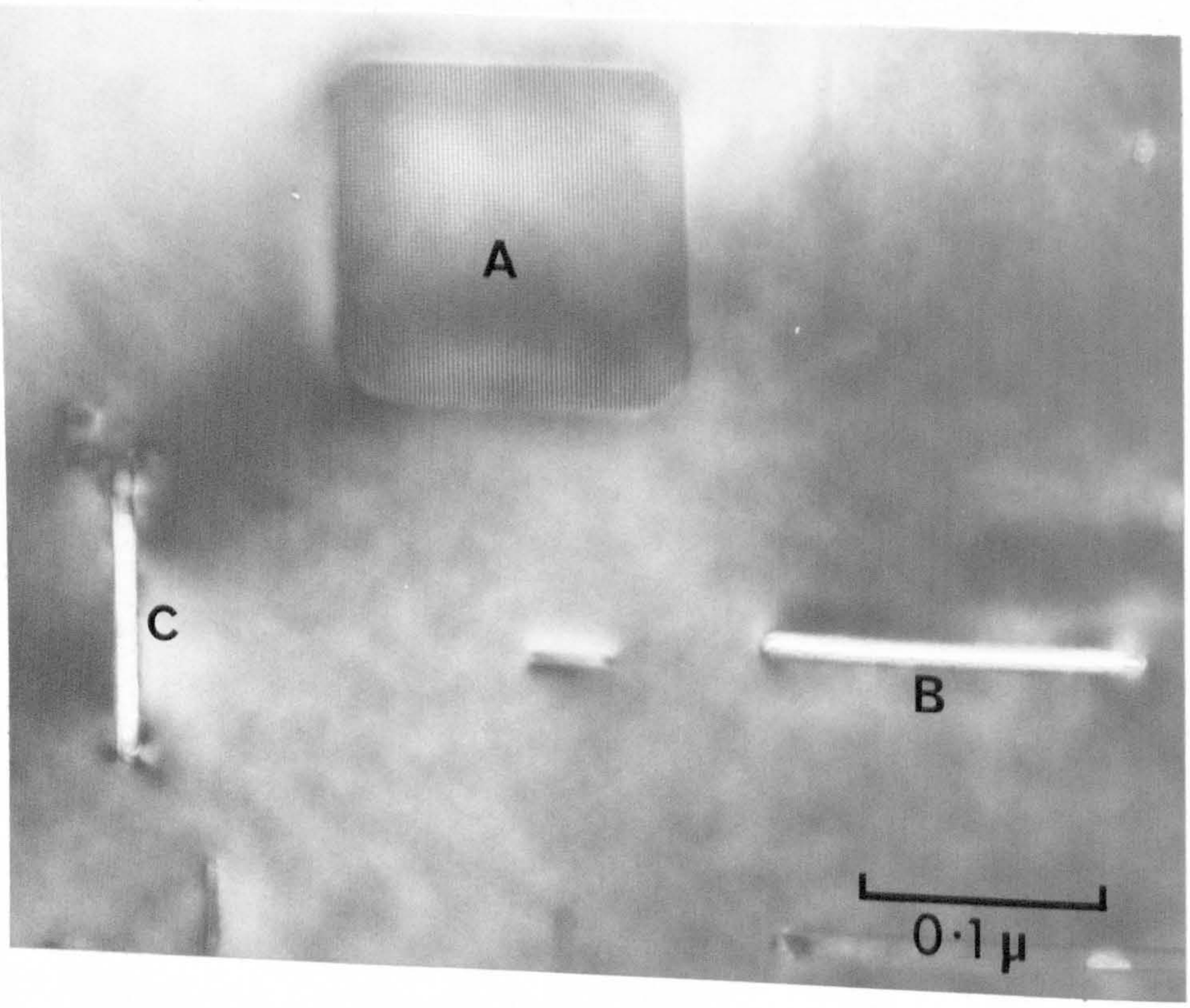

Figure 3.11(a) The precipitates labelled A, B and C are platelets of the equilibrium Mg_2Si phase contained in a foil in (001) matrix orientation.

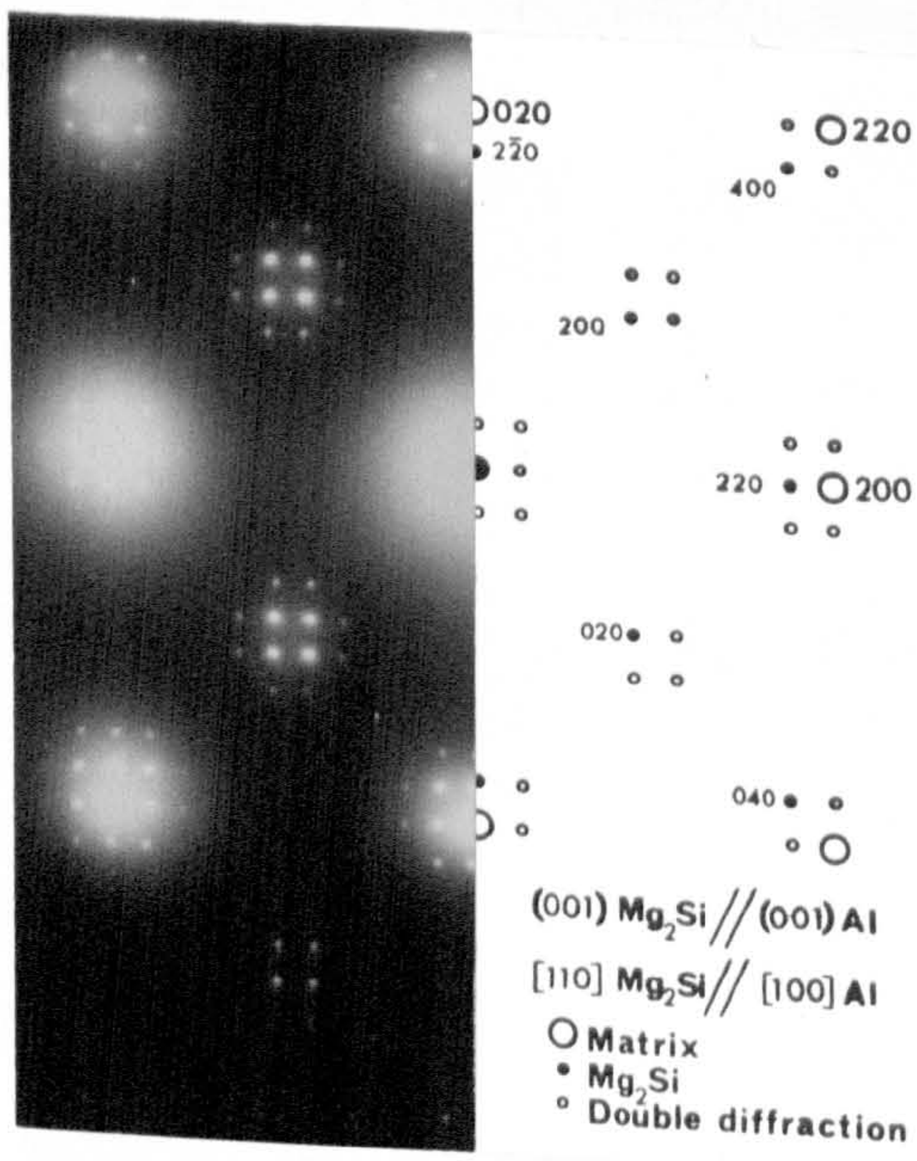

(b)

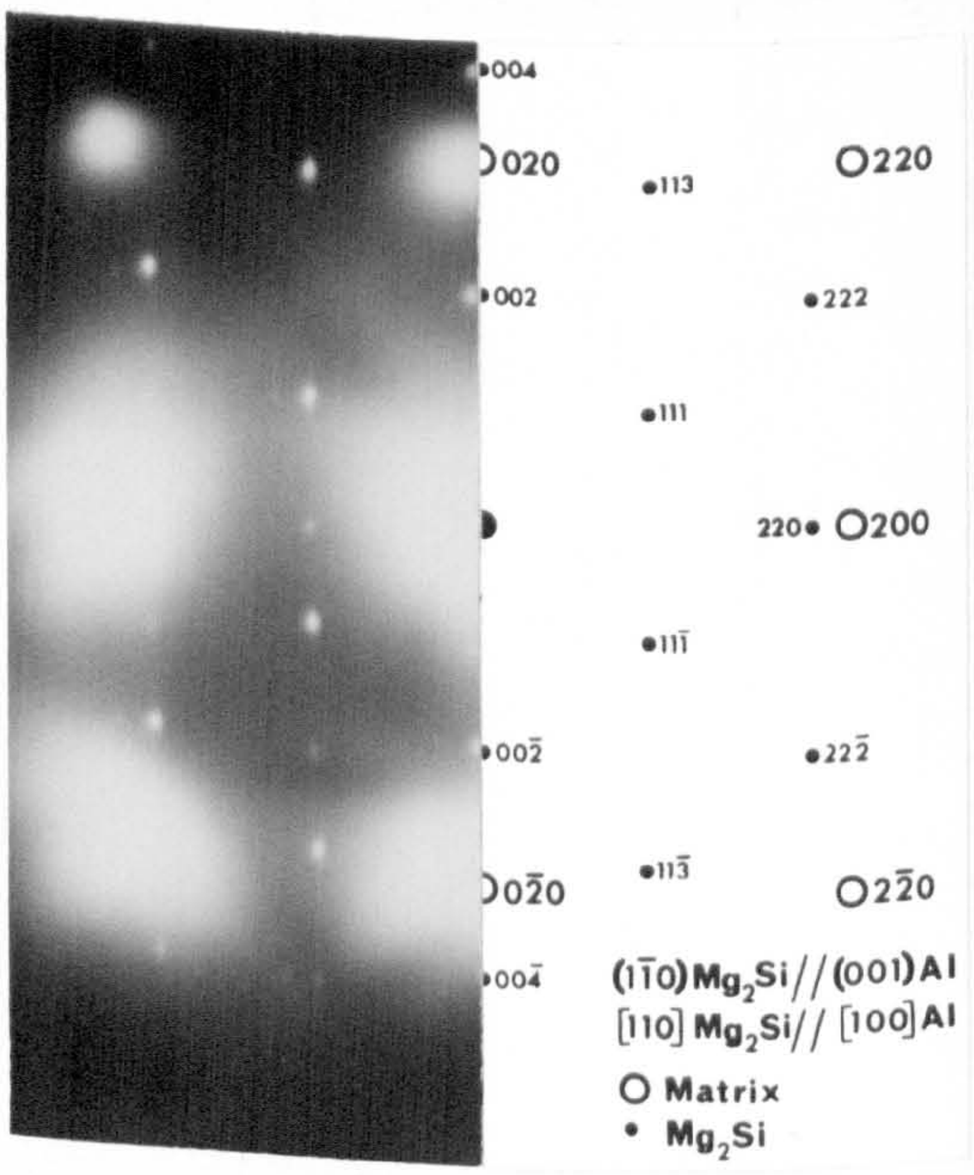

(c)

Figure 3.11(b) A selected-area diffraction pattern from a platelet of type A shown in (a); the moiré patterns of 20 Å spacing in platelet A, arise, through double diffraction, from the (020) matrix and the (2$\bar{2}$0) platelet reflections, and the (200) matrix and the (2$\bar{2}$0) platelet reflections, respectively.

(c) A selected-area diffraction pattern from a platelet of type B shown in (a).

$^{a}/2$ [110] which can then, at high ageing temperatures, glide and climb to their equilibrium configuration. It is possible that the relief of coherency strain with misfit dislocations enables a modification of the crystal structure of the needle to occur, which is revealed as extra spots on the diffraction pattern. A definite correlation between these two events was not, however, confirmed.

No information was obtained about the arrangement of atoms within the unit cell during this investigation, so it is not known if the proposed hexagonal structure represents a non-equilibrium form of Mg_2Si or if it may contain aluminium atoms as an integral part of the structure. Although some diffraction patterns showed structure factor effects (e.g. Figure 3.8(b) , where some precipitate reflections are brighter than others) these could not be interpreted because the scattering factors of Al, Mg and Si are all very similar.

In addition to large needles, many of the foils examined contained platelets of equilibrium Mg_2Si. These are illustrated, at high magnification, in Figure 3.11(a). Three orientations of platelet are visible, at A, B and C. The foil is in matrix cube orientation and the platelets have the following well-known orientation relationship with the matrix(88, 96):

$$(001)\ Mg_2Si \ // \ (001)\ \text{matrix}$$
$$[110]\ Mg_2Si \ // \ [100]\ \text{matrix}$$

No confusion can arise between needles and platelets of type A in this orientation but the images of platelets B and C are very similar to the larger needles. A diffraction pattern from a platelet of type A is illustrated by Figure 3.11(b) and for platelet of type B by Figure 3.11(c). Thus, platelets of types B and C can be distinguished from needles either

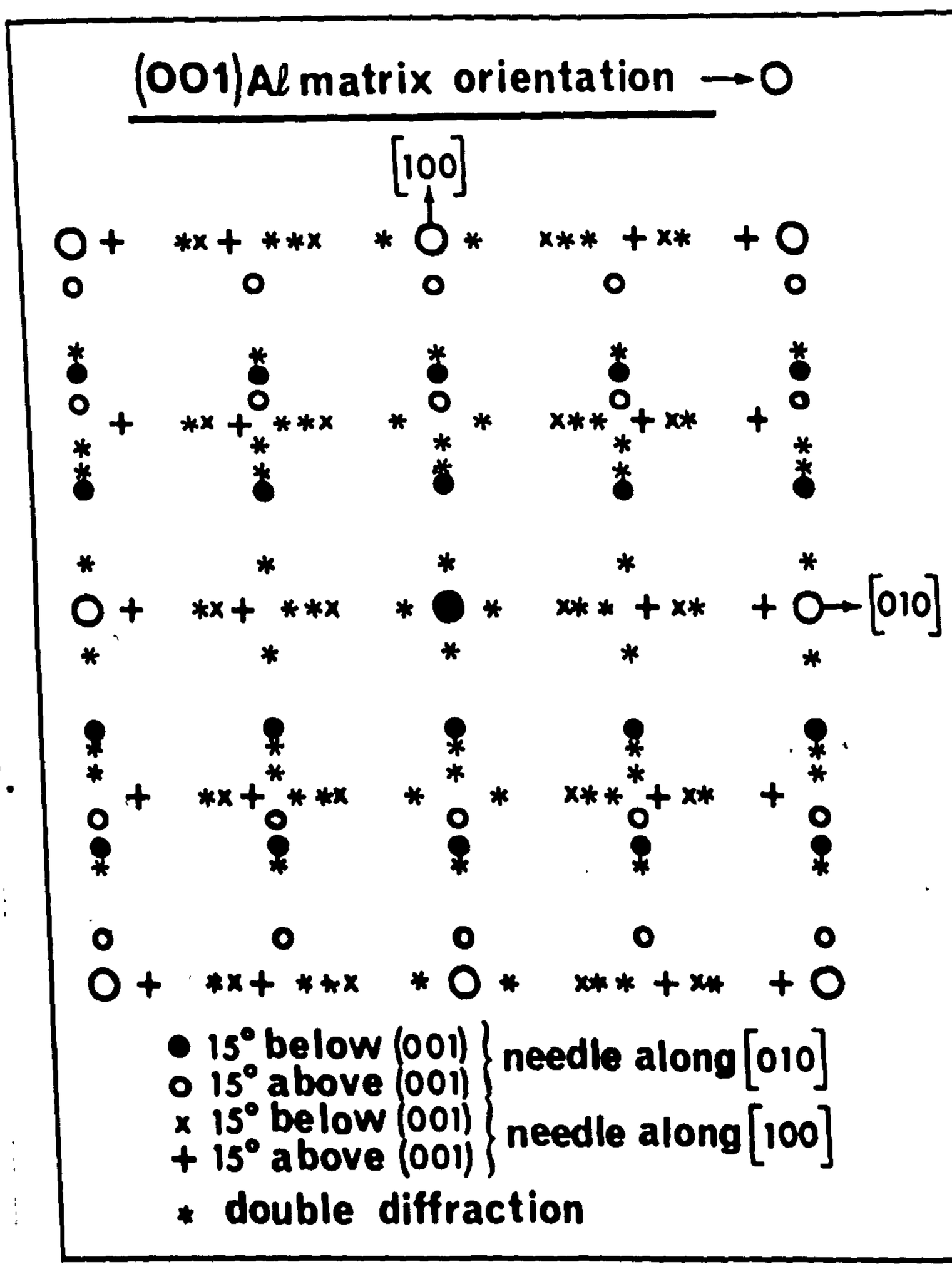

Figure 3.12 The predicted diffraction pattern from a foil, in (001) matrix orientation, which contains a large number of very small needles along the [010] and [100] matrix directions.

by electron diffraction or by tilting the foil.

Finally, we return to a discussion of Figure 3.4(b), that is the streaked diffraction pattern obtained from a large number of small needle-shaped zones. It will now be demonstrated that this pattern is consistent with the unit cell proposed above for the larger needles. In the case of very small needles the precipitate reciprocal lattice points are broadened into sheets of intensity through each point, perpendicular to the major axis of the needle (see Hirsch et al[85]). For a large number of very small needles the sheets may be continuous planes of intensity in reciprocal space with intensity modulations having maxima and minima related to the crystal structure of the needles normal to their major axis. Thus, the reciprocal lattice points along sections (2), (3) and (4) of Figure 3.6 will be projected onto the (001) plane of the matrix, and similarly for other reciprocal lattice points contained in planes parallel to this.

Figure 3.12 shows the diffraction pattern predicted for the (001) matrix orientation when small needles along $[100]$ and $[010]$ have the unit cell derived above. This should be compared with Figure 3.4(b) where it will be seen that the variation in intensity along the streaks is correctly predicted, which suggests that the crystal structure of the very small needle-shaped zones is very similar to that of the much larger needles. It is suggested that there is no discrete transformation from needle-shaped zones $\rightarrow$ β' precipitate in this alloy, the two differing only in size and degree of radial strain with possibly a slow change in internal ordering as the needle increases in size. The possibility exists, however, that the needles may undergo a structural modification when they loose coherency along their major axis and, if so, this will be a true metastable intermediate precipitate.

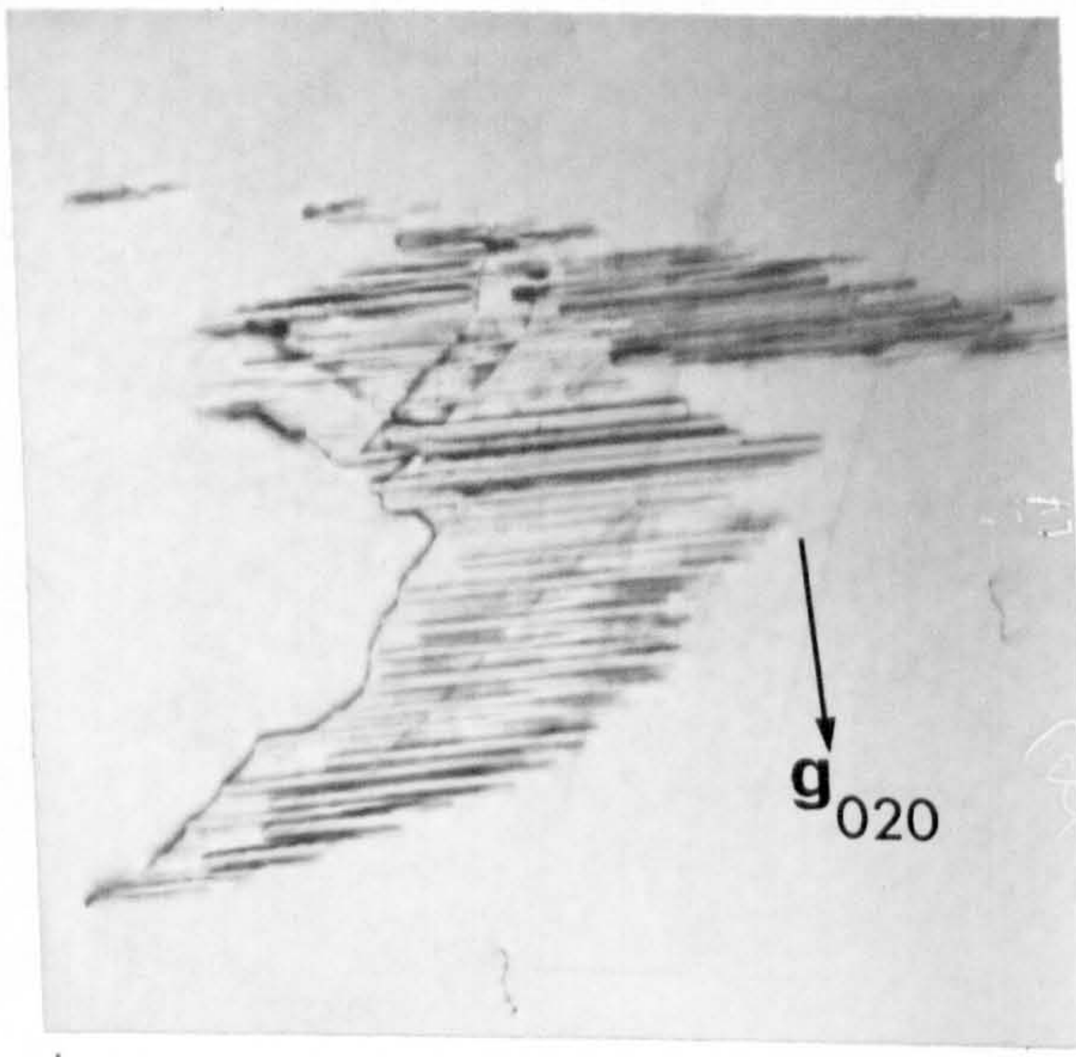

Figure 3.13(a) Needles along [100] matrix direction nucleated heterogeneously on a dislocation line. Foil orientation (001); matrix operating reflection (020).

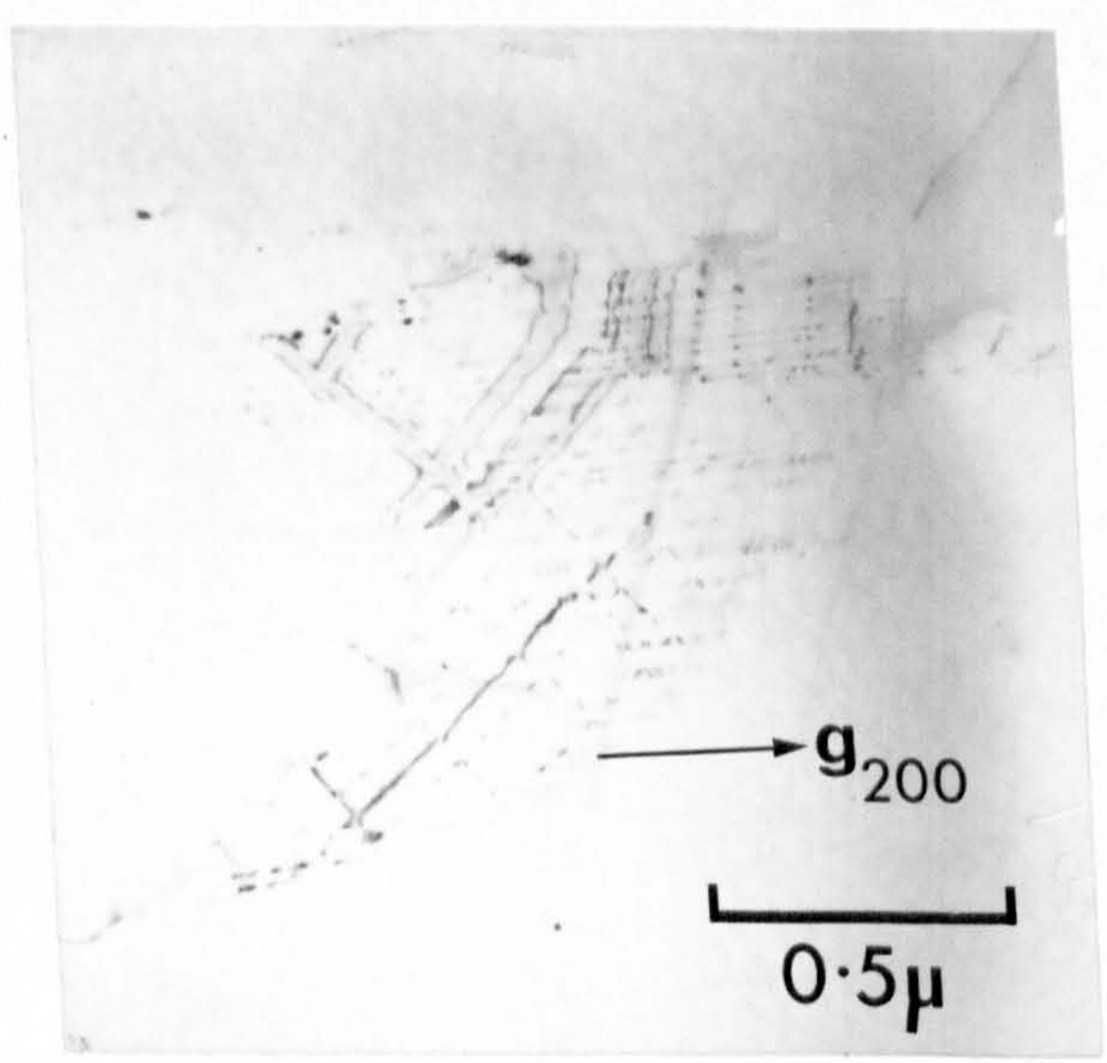

Figure 3.13(b) The same area as (a), but with matrix operating reflection (200).

The strain field associated with the needle-precipitates

The presence of a strain field in directions perpendicular to the major axis of the needle is revealed in the nature of the diffraction contrast observed by transmission electron microscopy[85,116-118]. The characteristic "tram-line" type of contrast is illustrated in Figure 3.4(a).

Thomas[97] has carried out contrast experiments in dark-field in two beam orientations which indicated that the strain field is of "interstitial" type i.e. the matrix surrounding a needle is compressed in directions perpendicular to the needle length. This conclusion is based on the theory of Ashby and Brown[117,118].

This cylindrical strain field is thought to be responsible for the preferential formation of needles on dislocation lines. There will be an interaction between the strain field of a needle and the strain field of the edge-component of the dislocation such that the misfit between the needle and the matrix may be partly relieved during the nucleation and early stages of growth of the needle. It is to be expected that for a dislocation with a given Burgers vector a certain needle orientation will be preferred if this affords the greatest relief of misfit: this is observed and is illustrated by Figure 3.13(a). The foil was in (001) matrix orientation with the needles parallel to the $[100]$ matrix direction. The operating reflection was (020) in this case and both the dislocation and the needles are in strong contrast. Figure 3.13(b) is the same area but with the (200) matrix reflection operating and it will be seen that the dislocation is invisible and the needles only just visible. It was therefore deduced (by application of the $\bar{g}.\bar{b}.= 0$ criterion[85]) that the Burgers vector of the dislocation was either $^{a}/_{2}\,[011]$ or $^{a}/_{2}\,[01\bar{1}]$ i.e. normal to the direction of the needles. For a given Burgers vector only

one set of needles satisfies this geometry, which is consistent with the observations. The needles will all tend to grow on one side of the dislocation, the side giving the greatest relief of misfit depending upon the sense of the Burgers vector.

The nucleation of needles on dislocations in this system is discussed again in Chapter 4.

3.3 PRECIPITATION IN Al - Zn ALLOYS

3.3.1 The ageing sequence

The initial decomposition of dilute Al-Zn alloys (up to ~ 30wt.% Zn) is characterised by the formation of small spherical regions within the matrix, G.P. zones, which are rich in zinc atoms and coherent with the matrix. They appear to be randomly distributed within the matrix in the sense that their sites of formation are not associated with any line or planar defects. They were discovered in 1943 by Guinier[102] during his early small-angle X-ray experiments on quenched alloys. The necessary conditions for the formation of G.P. zones in this alloy are discussed fully in Chapter 4 where it is demonstrated that they form readily, provided that the solute supersaturation is sufficiently high. Their rate of growth is considerably influenced by the vacancy supersaturation, as discussed in Chapter 1.

In an X-ray and metallographic study of alloys containing 12 and 25 wt.% Zn, Geisler et al[103] detected the presence of equilibrium precipitates of hexagonal zinc in the matrix with their basal planes parallel to (111) matrix planes. In this paper, published in 1943, they suggested that the equilibrium precipitate is preceded by a coherent, plate-like precipitate. This was not confirmed until 1960, when Garwood, Davies

along one of the <111> directions inside the zones which was accompanied by a rhombohedral deformation of their lattice and a change from a spherical to an ellipsoidal shape.

(3) Further growth led to a partial loss of coherency of the zones with the α-matrix, except in the {111} - habit planes, and to the development of a transition rhombohedral phase, the so-called α'_R - phase.

(4) On further ageing, the rhombohedral phase lost coherency in the (111) - habit plane, which led to a transformation to the non-coherent α' - phase.

(5) The β equilibrium precipitates (almost pure hexagonal zinc) were formed from the α' - phase by epitaxial growth of hexagonal zinc platelets with their basal planes parallel to the {111} planes of the α - matrix.

These authors explained the change of shape of G.P. zones from spherical to ellipsoidal by considering the factors affecting the value of the coherence strain associated with a zone as it increases in volume. It was assumed that, following the work of Gerold[40,41], the zinc concentration within the zones remained constant during zone growth. Since zinc atoms are smaller than aluminium atoms, the lattice constant within the zones is smaller than that of the surrounding impoverished matrix. They suggested that this leads to progressively increasing coherency strains during ageing. They interpreted their diffraction evidence as indicating that the spherical form of the zones changes first into the form of flat ellipsoids, with their minor axes directed parallel to one of the <111> - directions of the matrix. The (111) planes

become compressed owing to the anisotropic coherency strains which leads to a rhombohedral deformation of the lattice within the zones.

Simerska and Synecek communicated this mechanism to Gerold in 1964 and, as a result, he and his co-workers[108] studied carefully, by means of small-angle X-ray scattering, the shape changes occurring at room temperature during the growth of G.P. zones in alloys containing between 9 and 25 wt.%Zn. These authors confirmed the change from spherical to ellipsoidal shape and found that it occurred at room temperature when the zones exceeded a critical diameter of about 60 Å.

In a later paper, Merz and Gerold[109] studied the transformations occurring in an Al-9 wt.%Zn alloy, aged at room temperature, by means of electron microscopy and deduced that coherent ellipsoidal G.P. zones were the final state of precipitation at room temperature (further changes occurring at a negligible rate). According to these authors, a typical ellipsoidal G.P. zone is 100 to 150 Å in diameter in the (111) - plane and 30 to 50 Å in thickness, after several weeks ageing at room temperature. Whereas, for an Al-18.8wt.%Zn alloy aged at 130°C, the ellipsoidal G.P. zones were observed to grow to much larger sizes (e.g. with a diameter $>$ 1000 Å and a thickness of 100 to 200 Å) and these subsequently transformed to the partia l ly coherent α'_R - phase.

Carpenter and Garwood[111] have carried out a structural investigation of the α'_R - phase which they observed in an Al-22.5wt.%Zn alloy, isothermally aged at 200°C for a few hours. Their Debye-Scherrer X-ray patterns indicated that the α'_R - phase has a rhombohedral unit cell which may be thought of as a slightly distorted f.c.c. unit cell with a = 4.005 Å and α = 91° 6'. In terms of a hexagonal unit cell it has dimensions a = 2.859 Å and c = 6.804 Å ; $^c/_a$ = 2.38. Similar results were obtain by other workers[107,109,112,113] with the $^c/_a$ ratios

varying from about 2.34 up to 2.42.

Ciach[114] has critically compared all the experimentally determined values of $^{c}/_{a}$ and has attempted to correlate the small differences in measured values with differences in ageing temperature and alloy composition. He suggests that the contraction of the (111) interplanar spacing within the α'_R - phase is dependent upon their zinc content which, for a given ageing temperature, is defined by the zinc-rich boundary of the metastable α-α' miscibility gap as derived by Gerold[40,41]. Also, since the lattice parameter of the matrix decreases with increase in zinc content, the lattice misfit between the precipitate and the matrix decreases with increase in zinc content of the matrix. He was thus able to show that the degree of rhombohedral distortion depends on the lattice misfit between the α'_R precipitate and the matrix and that this in turn depends on the alloy composition and the ageing temperature. On this basis all the different values of $^{c}/_{a}$ were accounted for.

Carpenter and Garwood[111] discussed possible reasons why the unusual $\{111\}$ habit plane is adopted by the α' platelets (it is unusual since the normal habit plane of precipitates in f.c.c. metals is $\{100\}$, which has been attributed[9] to the fact that f.c.c. metals exhibit a minimum in Young's modulus (E) in $\langle 100 \rangle$ directions[31]). In the absence of experimental data, they based their discussion on the theoretical work of Leigh[115] and so calculated the values for E in various crystallographic directions. Their results are reproduced in Table 3.1.

Table 3.1

The calculated values of Young's Modulus in the crystallographic directions indicated

(Reproduced from Carpenter and Garwood[111])

Zinc concentration in wt.%	$E_{[UVW]}$ x 10^{11}dynes /cm^2		
	[100]	[111]	[110]
0	6.3	7.6	8.9
22.5	5.5	5.6	5.6
80	12.2	2.9	3.5

It will be seen that a solid solution containing 22.5% Zn is nearly isotropic, whereas an α'_R precipitate containing 80% Zn has a very large value of $E_{[100]}$. Their experimental evidence showed that the α'_R lattice is expanded along the $\langle 110 \rangle$ directions lying in the (111) plane of the platelet and contracted in the [111] direction perpendicular to this plane. They suggested that this combination of strain is such as to leave the three $\langle 100 \rangle$ directions, situated symmetrically with respect to the plane of the platelet, effectively undistorted and so deduced that the $\{111\}$ habit plane is adopted because it involves the least strain in the $\langle 100 \rangle$ precipitate directions of high E and that the elastic properties of the matrix are of only secondary importance.

They also considered possible reasons why spherical G.P. zones are formed at room temperature, whereas at elevated temperatures these rapidly develop into platelets. They proposed that the elastic coefficients of the precipitates are functions of precipitate size and ageing temperature. They deduced, again by using Leigh's[115] data, that

zinc-rich zones formed at room temperature are likely to be more isotropic in their elastic coefficients than those formed at high temperatures.

Thus, in summary, there is now strong evidence to support the following precipitation sequence in dilute Al-Zn alloys when aged at a temperature where G.P. zones are the initial decomposition product:

Spherical G.P. zones → ellipsoidal G.P. zones → platelets of partially coherent α'_R - rhombohedral phase → plates of incoherent f.c.c. α' - phase → equilibrium β precipitate (h.c.p. zinc-rich solid solution of equilibrium composition).

Electron microscopy of G.P. zones and α'_R - precipitates

The diffraction contrast effects associated with G.P. zones when examined by transmission electron microscopy are now well established[85,116-118] and can be of two types, "structure factor" contrast and "strain" contrast. Both types are important in the case of G.P. zones in Al-Zn alloys.

Structure factor contrast has been discussed in detail by Ashby and Brown[118] and arises when the solute atoms have an electron scattering factor which is significantly different from that of the solvent atoms. Thus, a unit cell rich in solute atoms will have an electron structure factor (F) different from that of a unit cell impoverished in solute atoms. Since F enters the equation for the extinction distance[85]

$$\xi_g = \frac{\pi V \theta_g}{F \lambda}$$

(where V is the volume of the unit cell, θ_g is the Bragg angle corresponding to the reflection $\bar{g}$ and λ is the electron wave length), the extinction distance in the matrix ξ_g^m is different from the

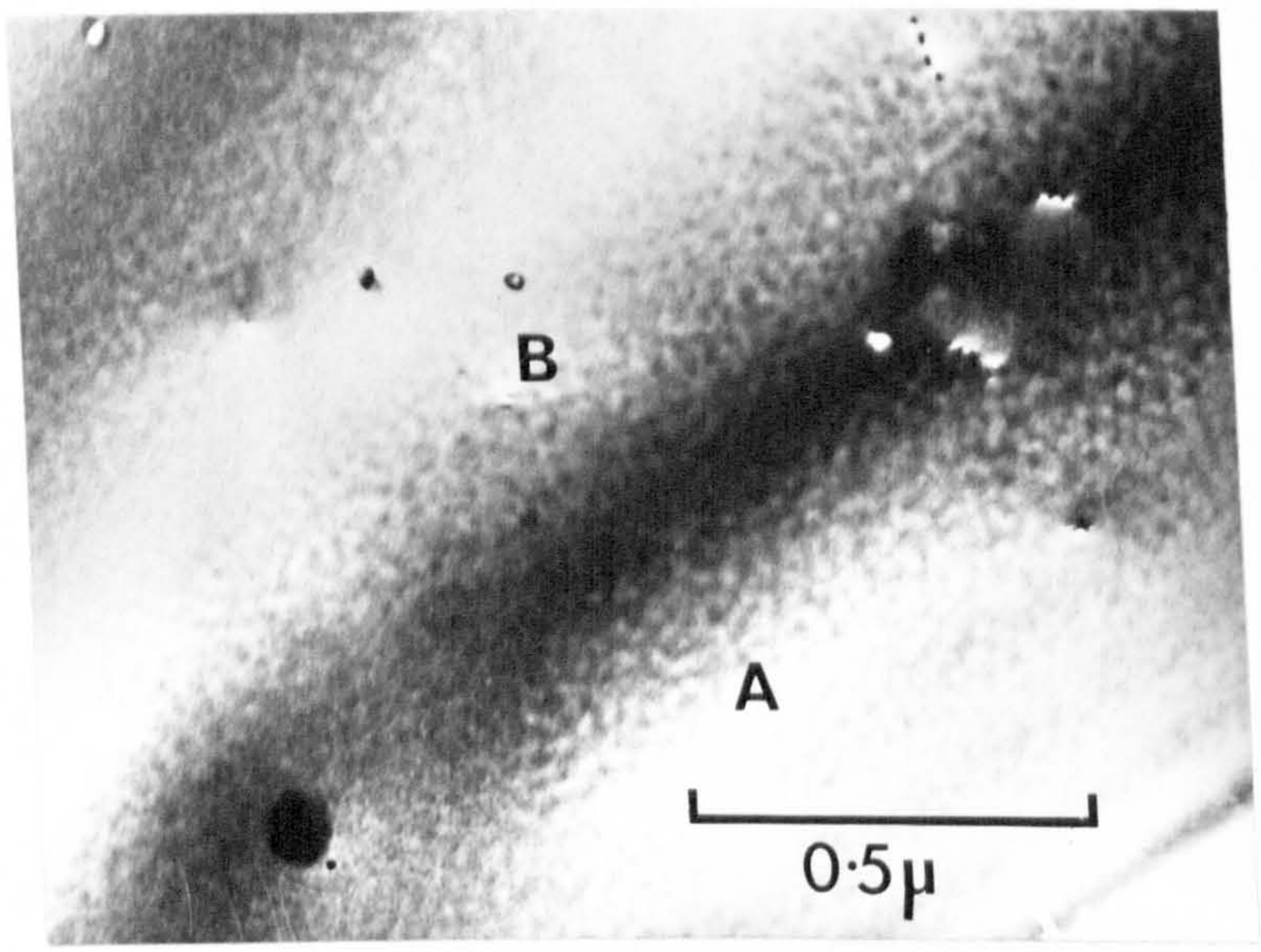

Figure 3.14(a) Al-10%Zn alloy, solution treated at 560°C, step-quenched via 100°C for 5 min. to 78°C and aged for 2 weeks. Foil orientation was close to (123) with $S_{11\bar{1}} = 0$. The G.P. zones on the two sides of the thickness contour are dark at A and light at B, as predicted by Ashby and Brown[118] for the case

$$\xi_g^z < \xi_g^m .$$

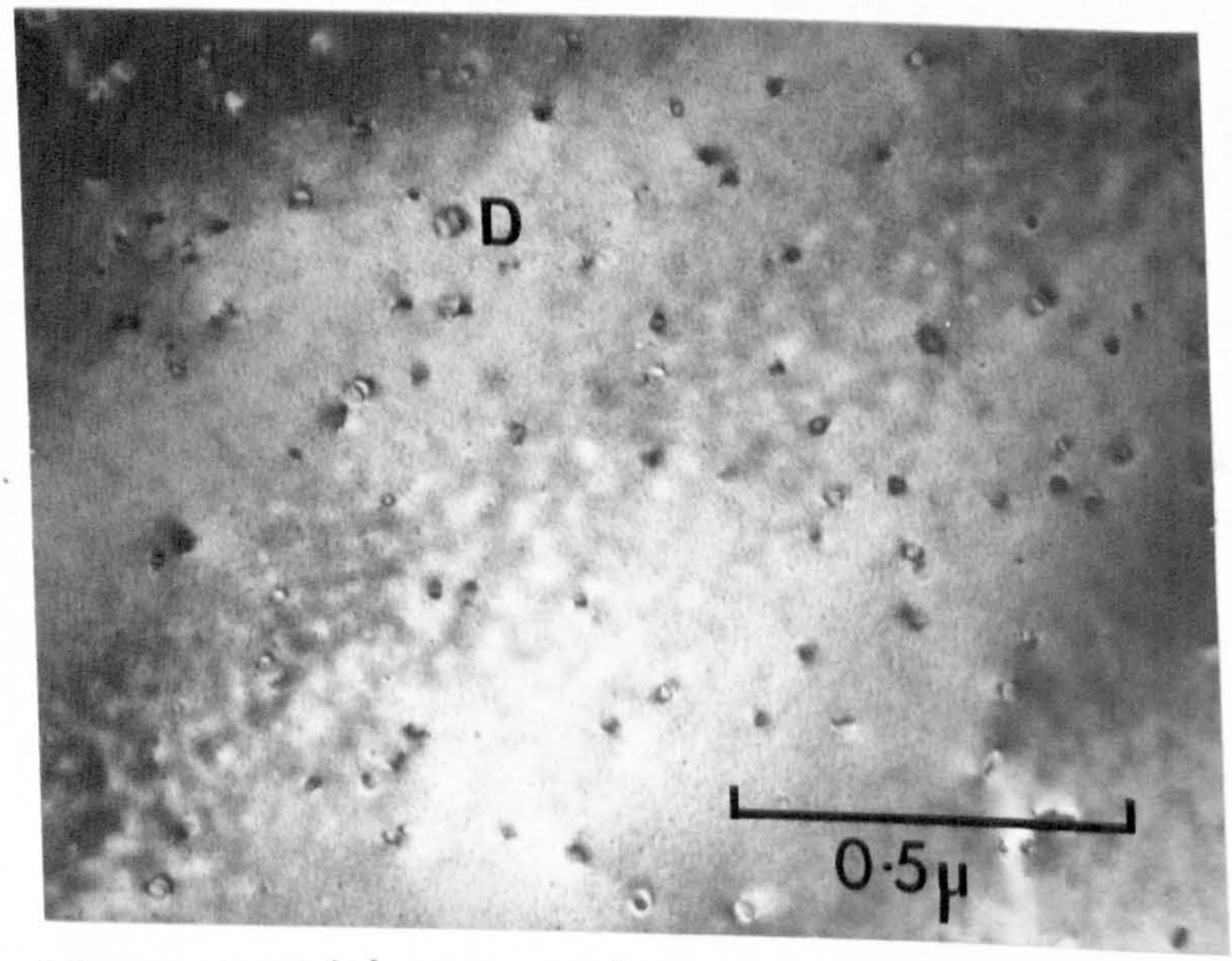

Figure 3.14(b) Al-10%Zn alloy, solution treated at 560°C and direct-quenched into oil at 55°C and aged for 2 weeks, illustrating good visibility of G.P. zones in a foil in (112) orientation with multiple reflections operating. The foil also contained a high density of prismatic dislocation loops, e.g. at D.

extinction distance in the G.P. zone ξ_g^z. It can be shown that[85,118] the effective thickness, t, of a foil, containing a G.P. zone of thickness Δt, is increased by an amount

$$\xi_g^m . \Delta t \left(\frac{1}{\xi_g^z} - \frac{1}{\xi_g^m} \right) \qquad (3.1)$$

if the foil is orientated exactly on the Bragg condition (i.e. the deviation parameter, $S_g = 0$). This gives rise to a maximum intensity change of

$$\Delta I = - \pi \Delta t \left(\frac{1}{\xi_g^z} - \frac{1}{\xi_g^m} \right) \sin \frac{2\pi t}{\xi_g^m} \qquad (3.2)$$

provided that $\Delta t << \xi_g^m$. Maximum visibility of the zones occurs when $t/\xi_g^m = 1/4, 3/4, 5/4$ etc. Their images are light for $t/\xi_g^m = 1/4, 5/4$, etc., and dark for $t/\xi_g^m = 3/4, 7/4$, etc., if $\xi_g^z < \xi_g^m$, which can be shown to be the case for G.P. zones in Al-Zn alloys (see Figure 3.14(a)).

Ashby and Brown[118] have emphasised that in a thin, non-absorbing crystal ($t < 3 \xi_g^m$), the change in intensity is independent of G.P. zone depth in the foil at $S_g = 0$. This is no longer true for $S_g \neq 0$. Therefore, it is always advantageous to orient the matrix so that $S_g = 0$. Since the intensity change (expression 3.2) is larger for small values of extinction distance, better contrast is obtained with low-order reflections. Rogulic[119] has demonstrated experimentally that G.P. zones in Al-Zn alloys give very good contrast in regions where low-order extinction contours cross. An example of this situation is shown in Figure 3.14(b), from a foil in (112) matrix orientation with multiple reflections operating. The zones in this

case were spherical and about 20 Å in diameter. Smaller zones were visible in other specimens, examined under similar conditions, and the smallest zone size detectable appeared to be limited by the resolution limit of the microscope ($\sim$ 10 Å).

Diffraction contrast from spherically symmetrical coherency strains has also been considered by Ashby and Brown[117]. They used the elastic model of a precipitate proposed by Mott and Nabarro[120] in which the precipitate is an isotropic misfitting sphere contained within an infinite isotropic matrix. The displacements are radial and are given by

$$\left.\begin{aligned} R &= \frac{\varepsilon r_0^3}{r^2}, \quad r \geq r_0 \\ R &= \varepsilon r, \quad r \leq r_0 \end{aligned}\right\} \qquad (3.4.)$$

at a distance r from the centre of the precipitate, where r_o is the precipitate radius and ε is the "constrained" strain. When the precipitate and matrix have equal shear moduli and when Poisson's ratio is $^1/_3$, the constrained strain is given by

$$\varepsilon = \frac{2}{9} \frac{\Delta V}{V} \qquad (3.5.)$$

where $\Delta V/V$ represents the fractional difference in atomic volume between precipitate and matrix material.

If this model is applied to the case of spherical G.P. zones in Al-Zn alloys a value of the constrained strain can be obtained. According to Merz and Gerold[109,110] the value of $\Delta V/V$ is $-$ 0.035 (the negative sign indicates that the atomic volume of the zone is less than that of the matrix). If this value of $\Delta V/V$ is substituted in equation (3.5)

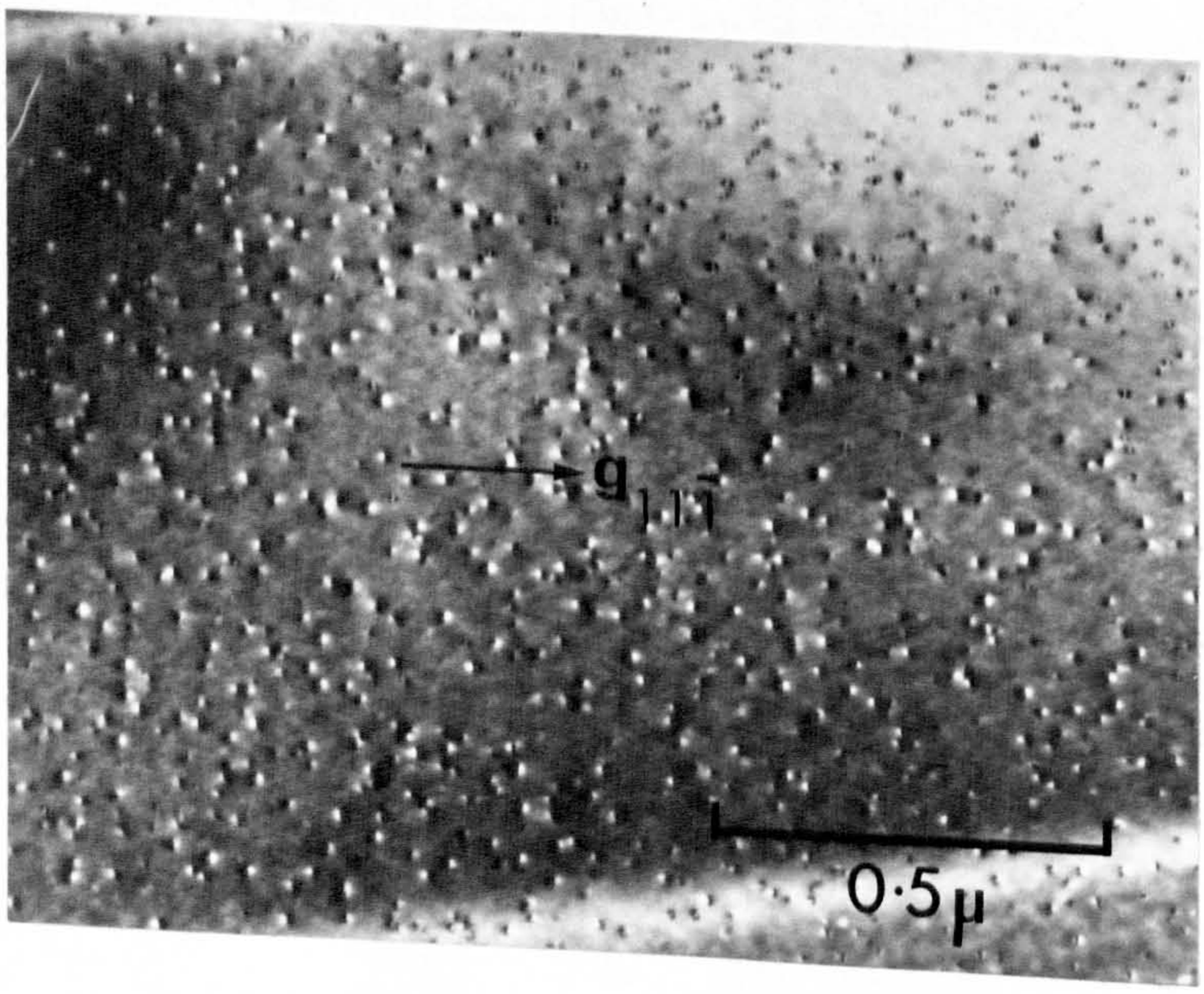

Figure 3.14(c) Al-17.5%Zn alloy, solution treated at 560°C, step-quenched via 180°C into water at 20°C and aged for 15 min. and then aged for 1 hr. at 160°C. Foil orientation (112). Large G.P. zones showing strain contrast.

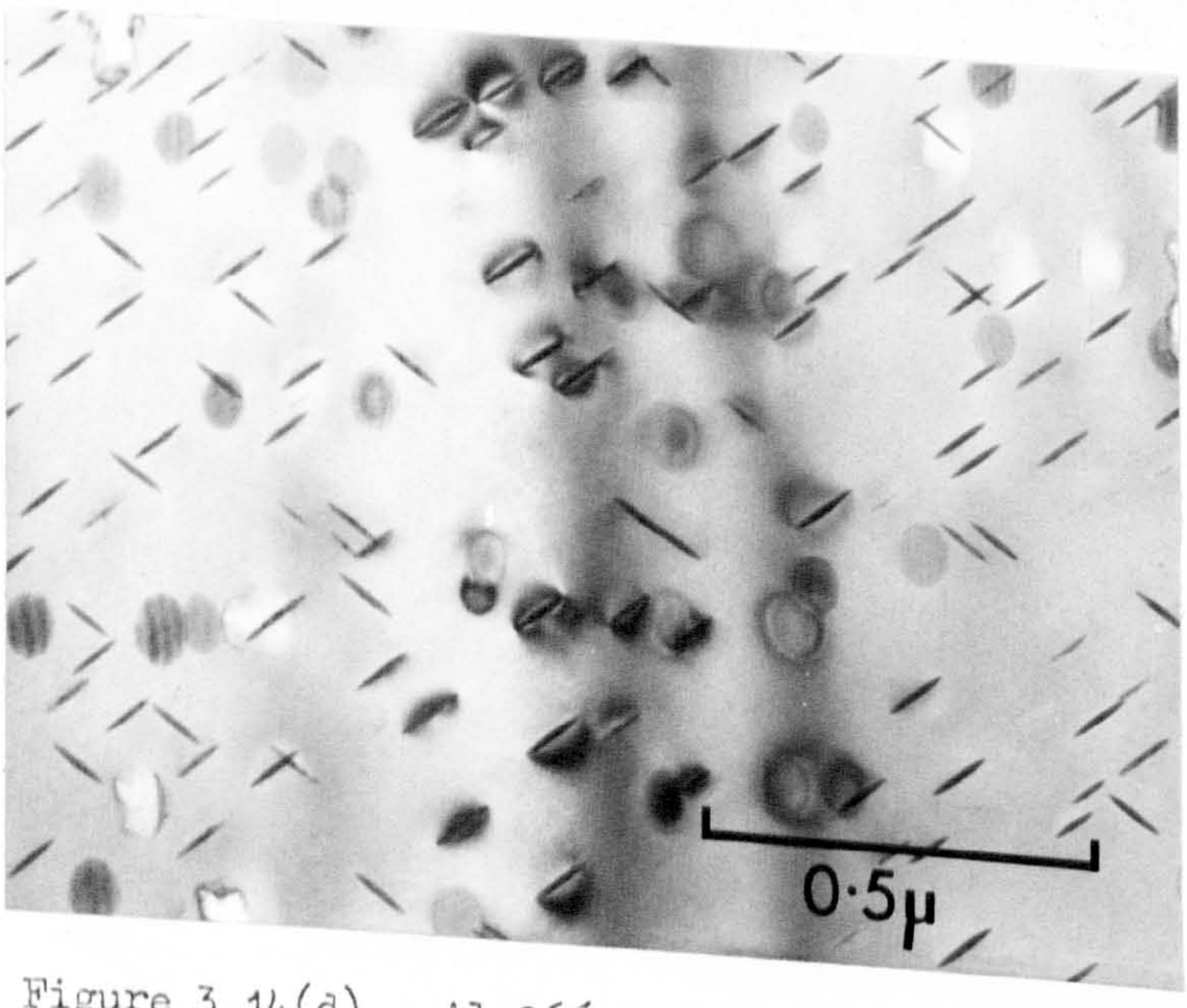

Figure 3.14(d) Al-26%Zn alloy, solution treated at 500°C, direct-quenched into Wood's metal at 213°C and aged for 15 mins., showing large plate-like precipitates. Foil orientation (110).

the value of ε so obtained is $-$ 0.0078 which should be treated as an approximate estimate since it is assumed that the shear moduli of zone and matrix are the same.

Ashby and Brown have used the dynamical theory of electron diffraction to study the way in which the diffraction contrast depends upon such factors as the magnitude of ε, the depth of the zone within the foil, the deviation from the Bragg condition, the absorption parameters and the order of operating reflection. In general, the contrast consists of two lobes of intensity separated by a "line of no contrast" which is perpendicular to the operating reflection (two-beam conditions are assumed). They derived a visibility criterion which can be used to estimate the smallest G.P. zone that can be detected by strain contrast. This requires that the image intensity must be 10% greater than that of the background intensity for a width larger than the G.P. zone diameter. From their results (reference 118, Figure 4) it is estimated that a spherical G.P. zone, with $\varepsilon = -0.0078$, will be invisible by strain contrast if it is smaller than about 80 $\mathring{A}$ in diameter. Since this diameter is approximately that at which the G.P. zone undergoes the shape change from spherical to ellipsoidal it seems likely that spherical G.P. zones will not be detected by means of strain contrast.

Figure 3.14(c) is a micrograph from a foil which contained larger G.P. zones than those visible in Figure 3.14(b). The operating reflection in this case was $(11\bar{1})$ and the typical "butterfly" contrast, characteristic of strain contrast, is clearly visible with the line of no contrast perpendicular to $[11\bar{1}]$. Similar strain contrast was observed by Merz and Gerold[109] and they demonstrated that the G.P. zones giving rise to the contrast were of the ellipsoidal type.

In samples of Al-26wt.%Zn, aged within the temperature range 190°C to 213°C, the G.P. zones were observed to grow rapidly into platelet-shaped particles of the α'_R - phase, with a $\{111\}$ habit. This is illustrated by Figure 3.14(d) for a case where the precipitates had grown to a relatively large size. The foil was in (110) matrix orientation, so that habit planes of two sets of the platelets are parallel to the electron beam direction and the other two sets are inclined at an angle. Displacement fringes[85] are visible in some of the inclined plates.

Heterogeneous precipitation

Thomas[121] has shown that a high density of prismatic dislocation loops and a lower density of helical dislocations may be formed in dilute Al-Zn alloys when they are quenched and then aged in the temperature range 20°C - 100°C. He found that loops are fewer in number but have larger diameters either when the quenching temperature is lowered or when the solute content is increased when quenching from the same temperature. The loops (see Figure 3.14(b)) are formed by the aggregation of vacancies and their collapse and shear to form loops of dislocation line[122,123]. The loop density is related to the quenched-in excess-vacancy concentration and loop-free regions were observed in the neighbourhood of grain boundaries (this point is discussed further in Chapter 6).

G.P. zones do not appear to be formed preferentially on dislocations. The probable reason for this is the extremely small misfit between a G.P. zone and the matrix and consequently it is almost as favourable, energetically, for the zone to form in the matrix.

Carpenter and Garwood[111] found that platelets of α'_R or α' phase precipitated on loops and helices in an Al-22.5%Zn alloy, aged at 200°C. Samples of this alloy aged at higher temperatures (but below the equilibrium solvus temperature) were found to have hexagonal zinc

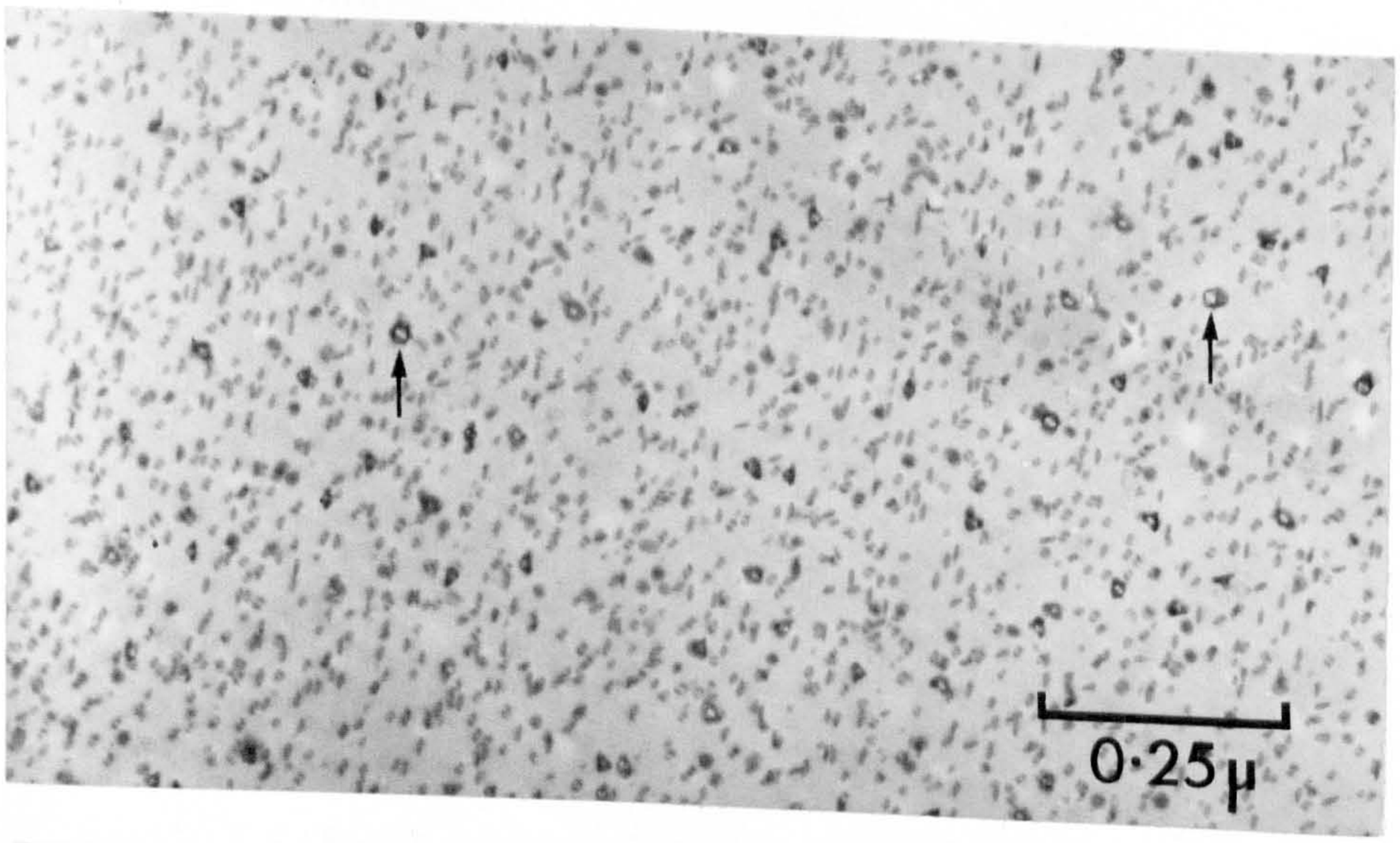

(a)

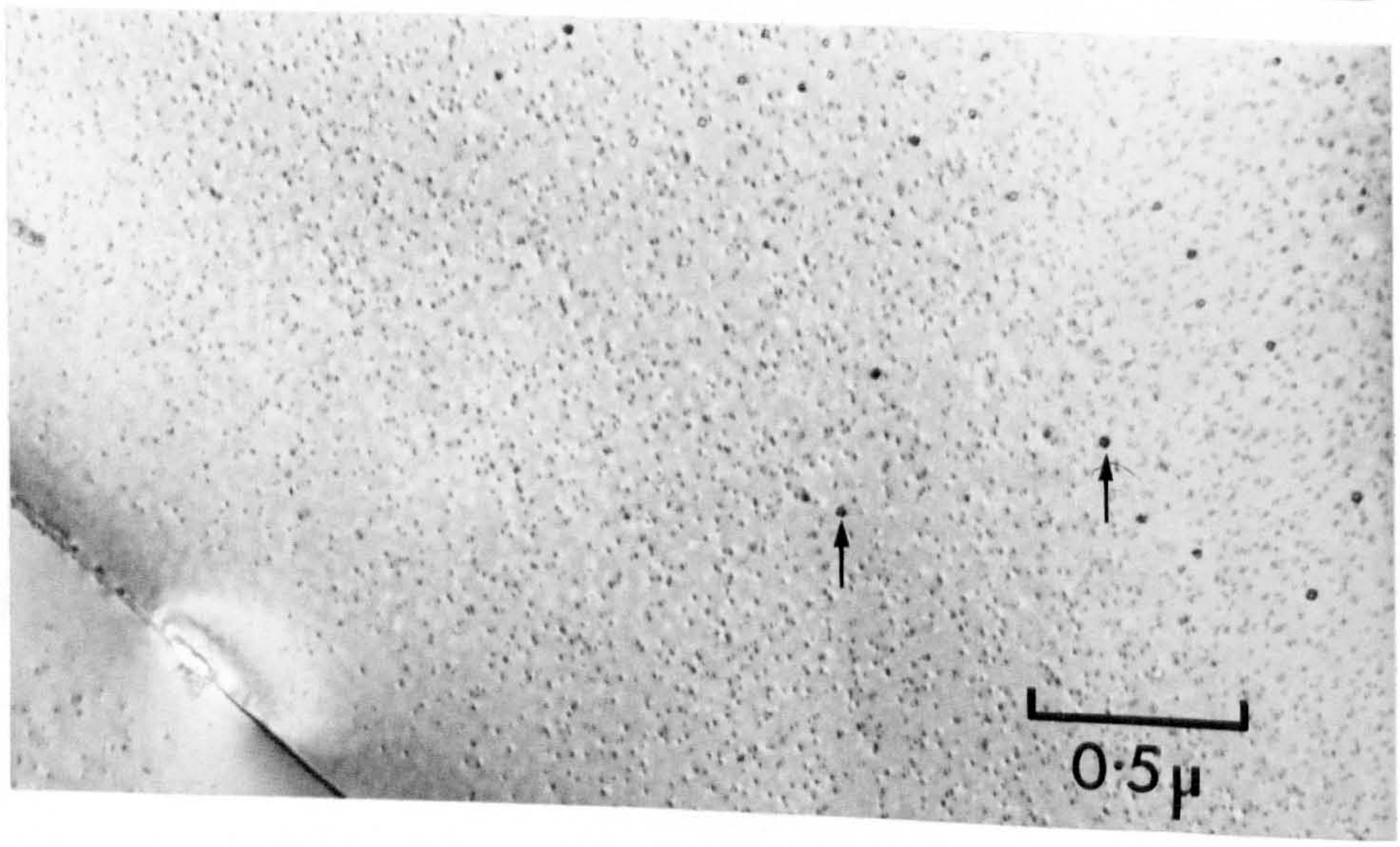

(b)

Figure 3.15 Al-17.5%Zn alloy, solution treated at 560°C, direct-quenched into Wood's metal at 160°C and aged for 1 hr., showing a mixture of Y-phase precipitates and ellipsoidal G.P. zones. (a) is a region in the centre of a grain boundary and (b) a region near to a grain boundary. Some of the Y-phase precipitates are arrowed.

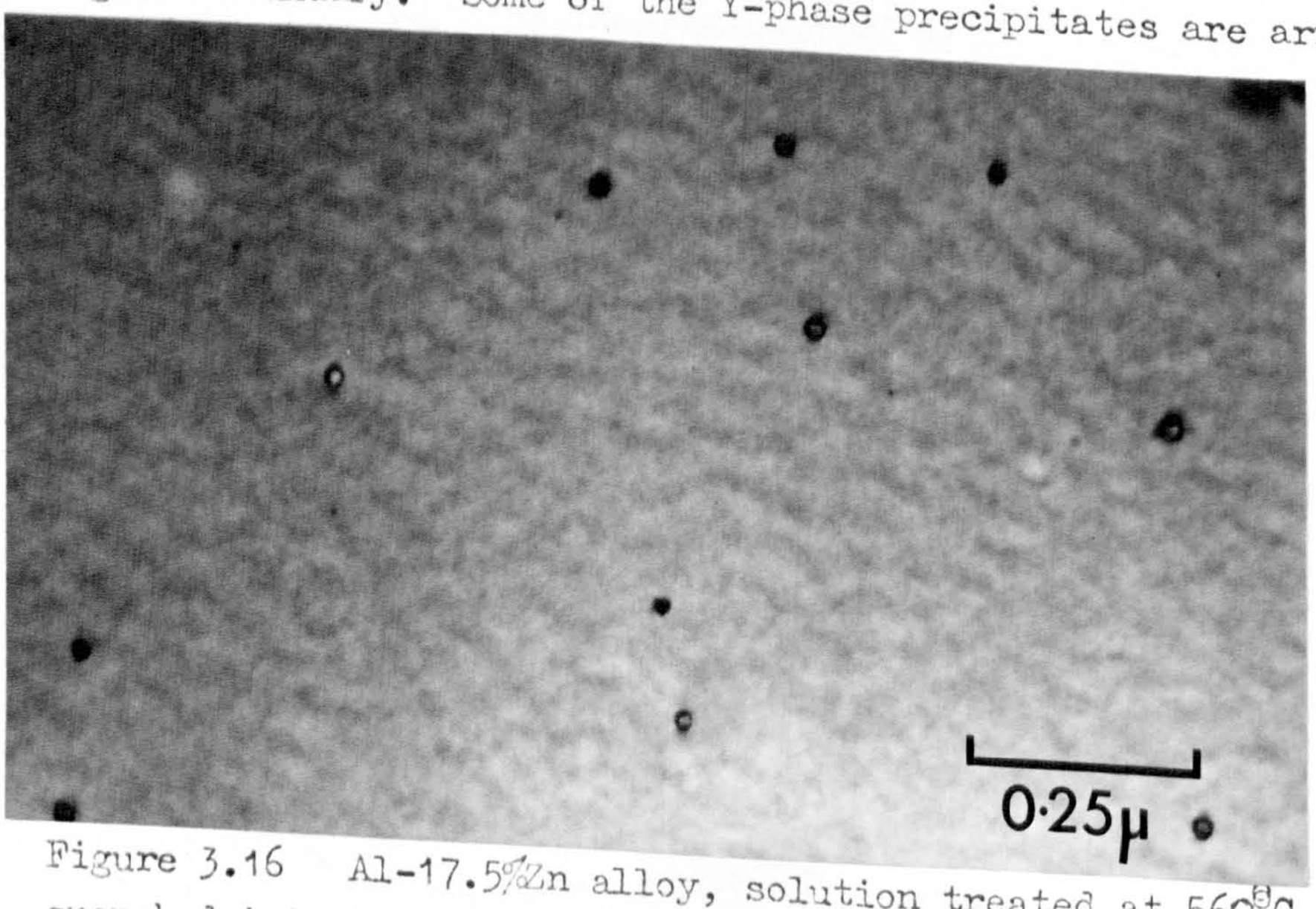

Figure 3.16 Al-17.5%Zn alloy, solution treated at 560°C, direct-quenched into Wood's metal at 180°C and aged for 20 min., showing only Y-phase precipitation.

particles on dislocations. Zinc precipitates were also formed at grain boundaries in all types of heat treatment, provided that the final ageing temperature was below the equilibrium solvus temperature.

3.3.2 Precipitation after rapid quenching: Y-phase precipitates

In Chapter 4 some experiments are described in which samples of Al-Zn alloy were directly quenched and aged in baths containing molten salt or Wood's metal. The object of using these two quenching media was to quench the samples rapidly and so retain a high supersaturation of vacancies. During these experiments a new type of precipitate was observed, which in the following is designated as Y-phase. The conditions under which the Y-phase precipitate was formed and its morphology and crystal structure are discussed below.

The factors influencing the formation of Y-phase precipitates

The ageing conditions required to form Y-phase precipitates were very stringent. They were observed in all three compositions of Al-Zn alloy examined, but only in samples directly quenched to a temperature close to the upper limiting temperature for G.P. zone formation (T'_c). In Chapter 4 it is shown that T'_c, for a direct quench into Wood's metal, is $97^{o}C \pm 4^{o}C$ for the Al-10%Zn alloy, $164^{o}C \pm 2^{o}C$ for the Al-17.5%Zn alloy and $213^{o}C \pm 2^{o}C$ for the Al-26% Zn alloy.

Figures 3.15(a) and (b) are electron micrographs from a foil of Al-17.5% Zn alloy which was directly quenched into Wood's metal at $160^{o}C$ and aged for 1 hour. Micrograph (a) is representative of the microstructure observed in the centre of the grains, which consisted of a mixture of Y-phase particles (some of which are arrowed) and ellipsoidal G.P.zones. In this case the foil orientation was (110) and the Y-phase particles had a diamond shape. Micrograph (b) shows the typical microstructure observed

in the neighbourhood of a grain boundary. The region free of G.P. zones either side of the grain boundary is characteristic of this type of heat treatment and is thought to be produced because of a depletion of vacancies in the vicinity of the grain boundary (this topic is discussed at length in Chapter 6). The important point here is that there is, in addition to a G.P. zone free region, a much wider region free of Y-phase precipitates either side of the grain boundary. This again is thought to be a consequence of the lower vacancy concentration in the vicinity of the grain boundary, and together with the fact that the Y-phase particles were only observed in rapidly quenched samples, strongly suggests that Y-phase precipitates can only nucleate in regions containing a very high vacancy concentration.

Y-phase precipitates were not observed in samples of Al-17.5%Zn aged at temperatures below 160°C. It is therefore concluded that Y-phase nucleation can only occur simultaneously with G.P. zone nucleation under conditions where the latter is difficult owing to insufficient solute and vacancy supersaturation. Y-phase precipitates were , however, observed in samples aged at 180°C, which is about 16°C above T_c' (see Figure 3.16). It is considered that this observation proves that Y-phase nucleation is independent of G.P. zone nucleation. Y-phase precipitates were also observed in samples directly quenched into molten salt, which shows that the Y-phase is in no way associated with the diffusion of Wood's metal into the sample during ageing.

There is a great similarity between the conditions required for the formation of Y-phase in this alloy and those required for the formation of X-phase in Al-Zn-Mg alloys[124,125,126], which also appears to form independently of G.P. zones. Thackery[126] has shown that the nucleation of X-phase in an Al-6%Zn-2% Mg alloy is sensitive to quench

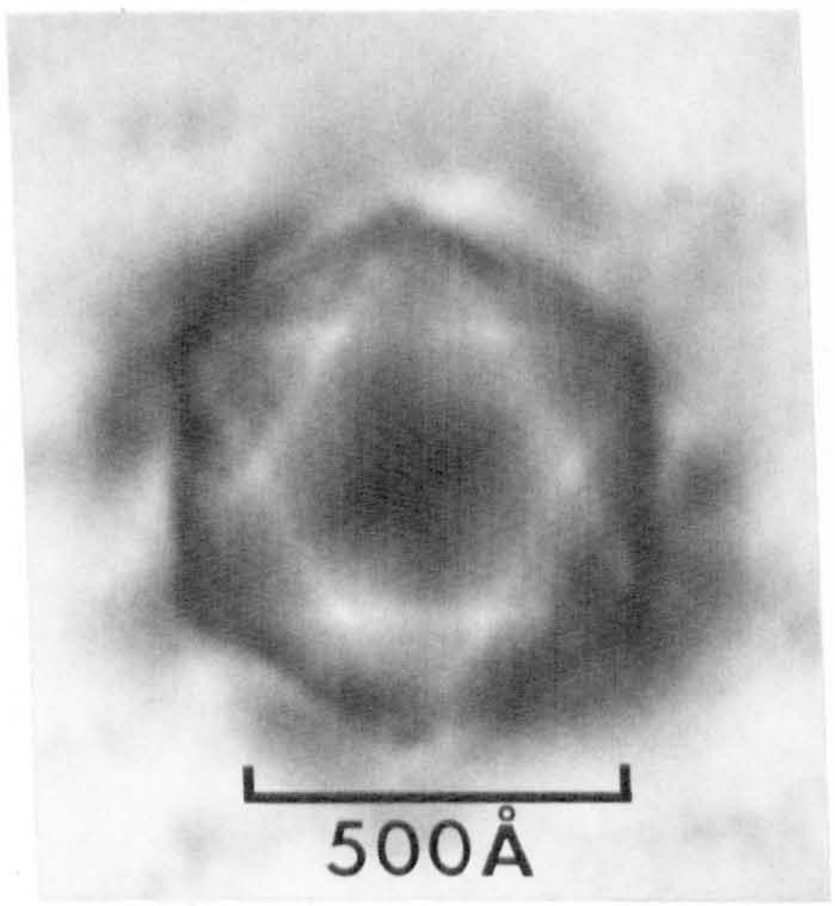

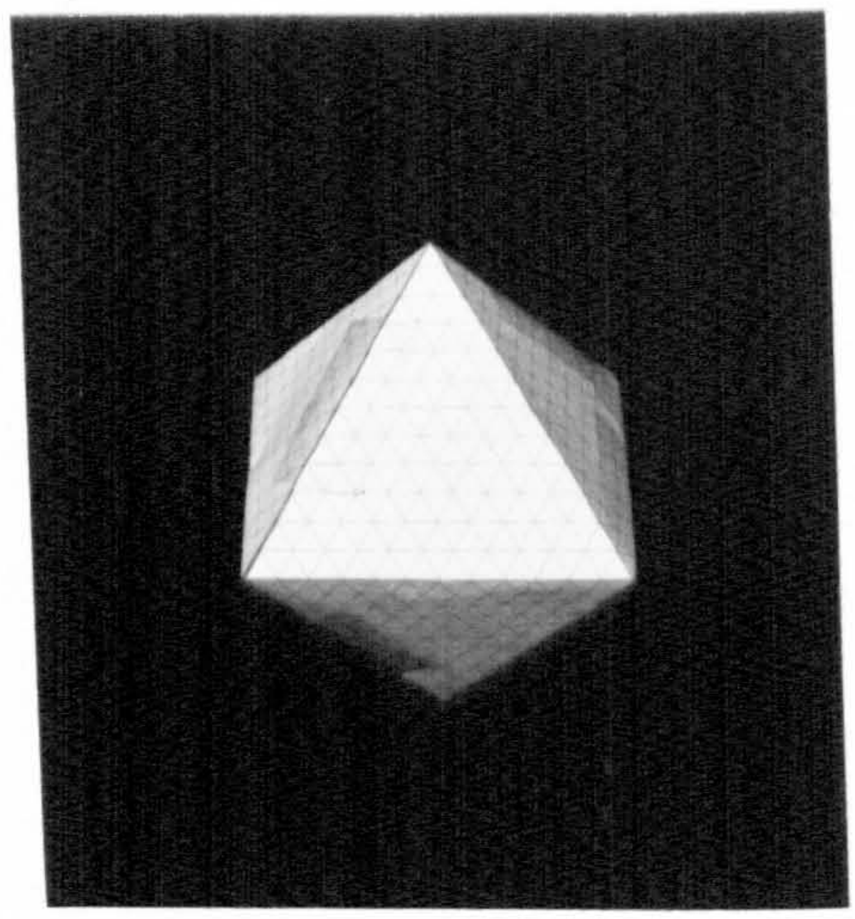

Figure 3.17(a) The micrograph, at left, is from an Al-26%Zn alloy, solution treated at 500°C, direct-quenched into salt at 207°C and aged for 5 min., showing a Y-phase particle in a foil in (111) orientation. Compare its outline with that of the octahedron, shown at right, which is oriented so that its faces are parallel to {111} planes.

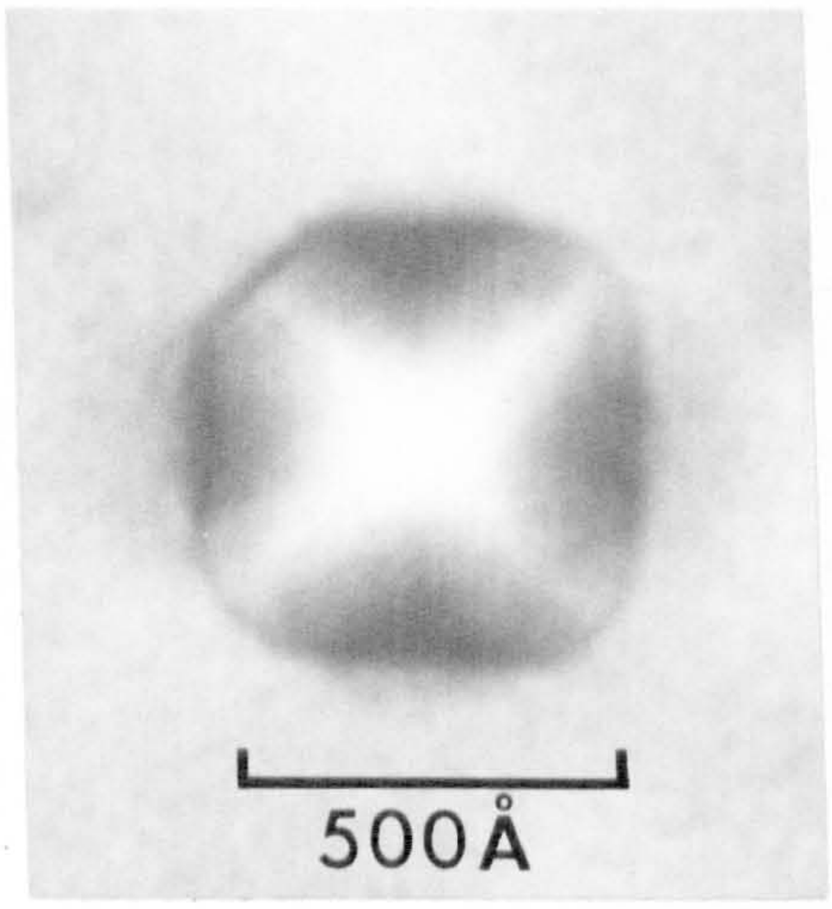

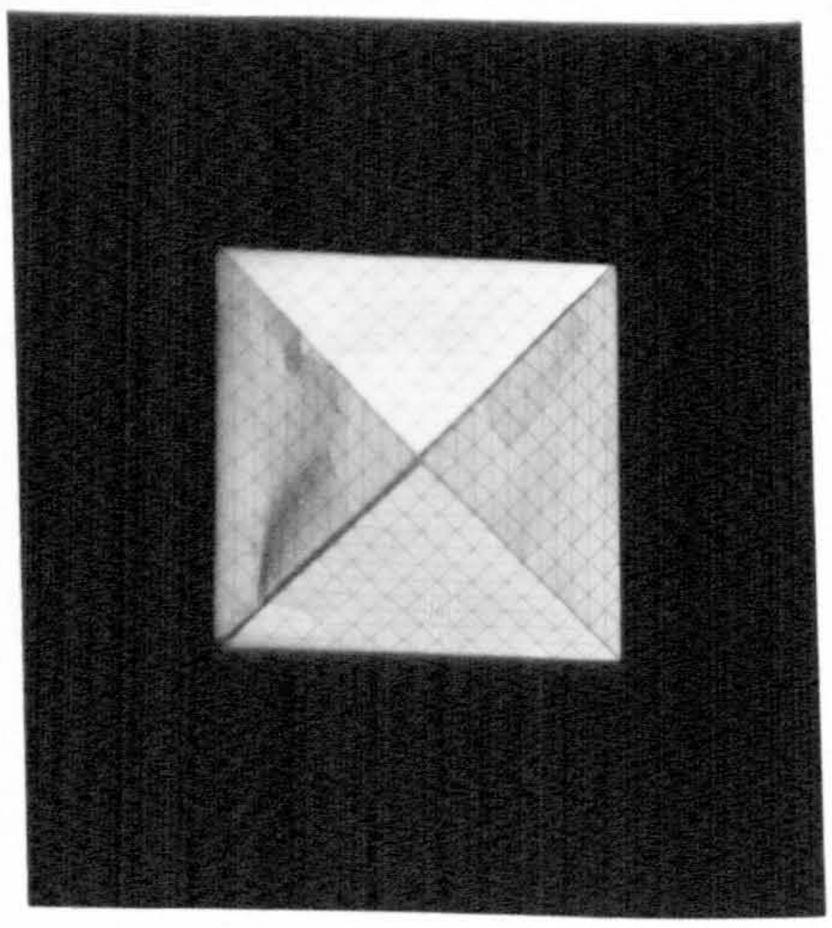

Figure 3.17(b) The micrograph, at left, shows a Y-phase particle in a foil in (100) orientation. Again, compare its outline with that of the octahedron, shown at right.

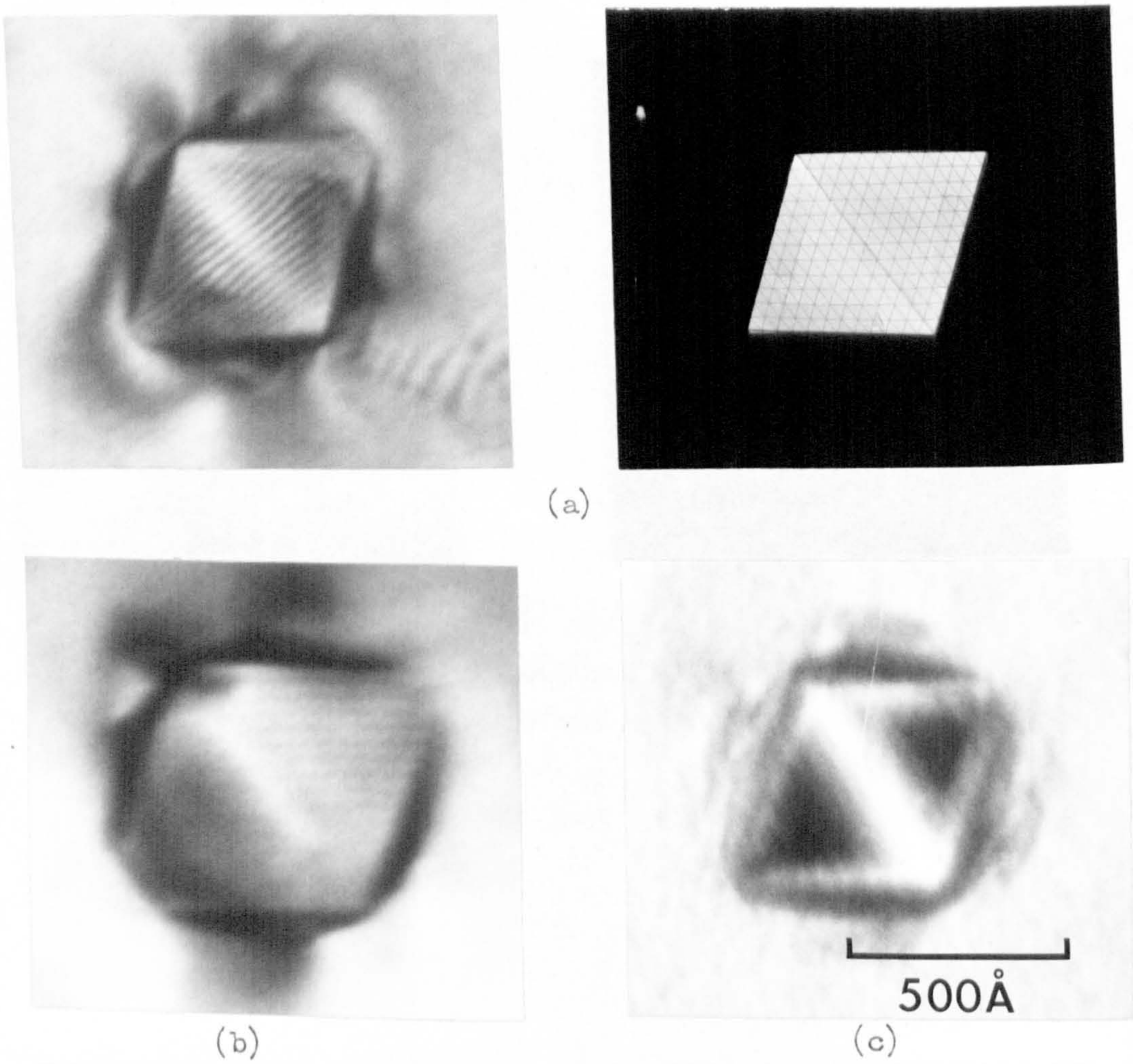

Figure 3.18 Y-phase particles in a foil in (110) orientation, with different matrix reflections operating. (a) at left, (022) matrix reflection operating and, at right, the octahedron in this orientation; (b) (111) matrix reflection operating; (c) (200) matrix reflection operating.

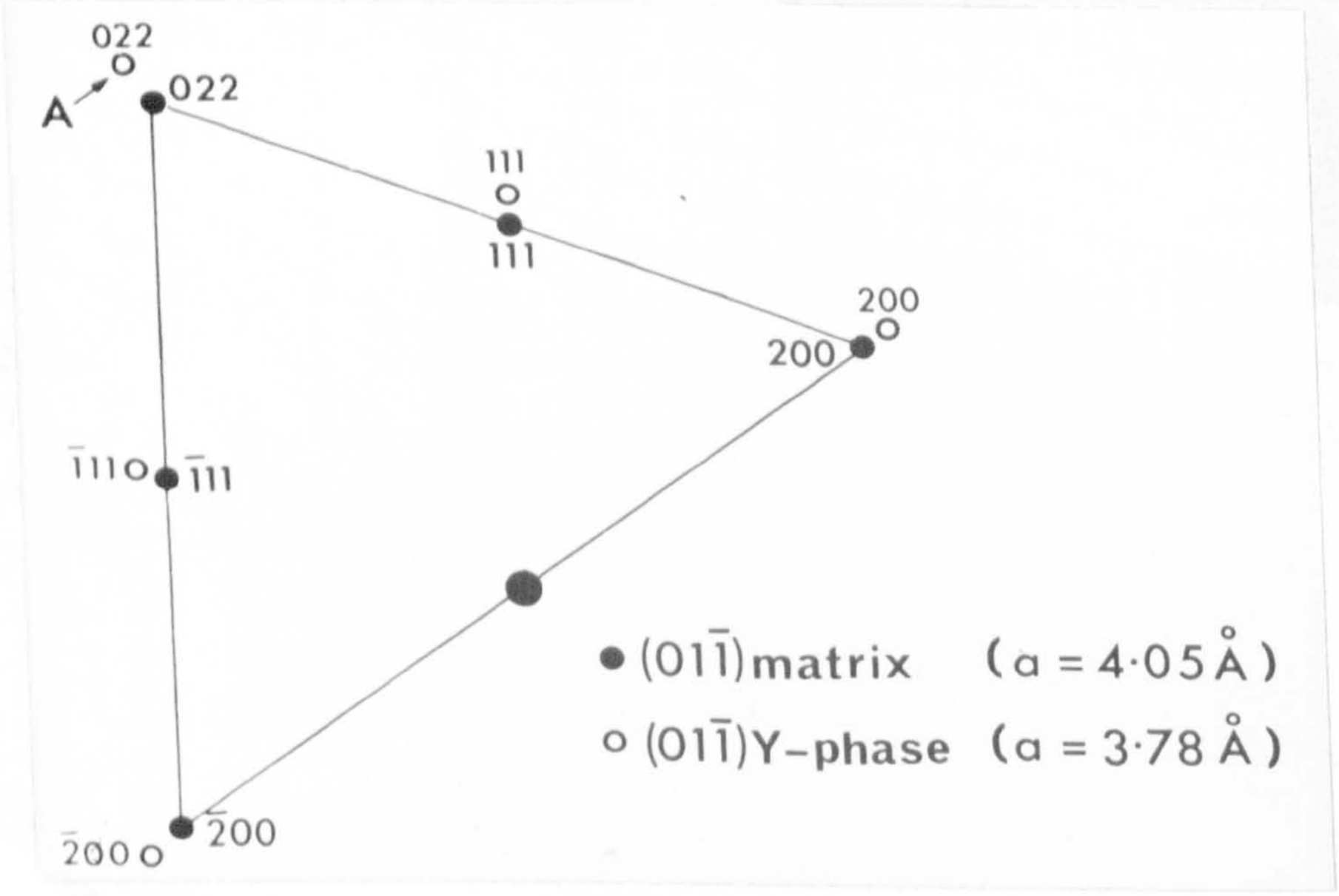

Figure 3.19 A diagram of the proposed (01$\bar{1}$) reciprocal lattice section of Y-phase superimposed upon the (01$\bar{1}$) reciprocal lattice section of the matrix.

rate; it was formed after a direct quench into Wood's metal at 165°C but not after a slower quench into oil at the same temperature. He suggested that X-phase may nucleate on small vacancy clusters. This could also be the case for Y-phase in Al-Zn alloys.

The morphology of Y-phase

Y-phase precipitates appear to have an octahedral shape with the faces of the octahedron parallel to the $\{111\}$ - planes of the matrix. This geometry was deduced by comparing electron microscope images of Y-phase particles in different matrix orientations with a three-dimensional paper model of an octahedron. The results are illustrated by Figures 3.17(a) and (b) and Figure 3.18(a) where it will be seen that the external shapes of the particles are the same as the projected out-lines of the model, which was orientated so that its faces remained parallel to $\{111\}$ planes of the matrix. Also, contrast effects within the images are clearly associated with changes in thickness of the particles (the moiré fringes are discussed in the next section).

The crystal structure of Y-phase

A complete structural determination of Y-phase was not achieved, although a certain amount of evidence suggested that the crystal structure of Y-phase is f.c.c. with a lattice parameter less than that of the matrix. The following is a brief description of the experimental results which were obtained.

The evidence in support of a f.c.c. unit cell was based upon the observation of moiré patterns associated with the precipitate. Figures 3.18(a),(b) and (c) are examples of moiré patterns in different Y-phase precipitates which were contained in a foil in $(01\bar{1})$ matrix orientation with different matrix reflections operating. Very weak precipitate spots

were sometimes observed just outside the operating reflections and these were consistent with the observed moiré patterns (double diffraction must, of course, be invoked to explain the observation of moiré fringes in bright field micrographs). It is proposed that the f.c.c. unit cell of Y-phase is oriented in parallel orientation with the f.c.c. unit cell of the matrix so that the reciprocal lattice section corresponding to a Y-phase precipitate contained in a foil in $(01\bar{1})$ orientation is as shown diagrammatically in Figure 3.19. The proposed Y-phase lattice parameter of 3.77 Å, as compared to 4.03 Å $^{(105)}$ for the matrix, was calculated from the observed moiré spacing of Figure 3.18(a) on the assumption that the precipitate reflection labelled A in Figure 3.19 could be indexed as (022). The observed moiré spacings of Figures 3.18(b) and (c) are compared with the calculated values in Table 3.2. The agreement is good.

Moiré patterns were also observed in Y-phase precipitates in other matrix orientations, for example in (100) orientation (Figure 3.17(b)) where a moiré of 21 Å spacing was resolved perpendicular to $[011]$. A moiré pattern of the same spacing was also observed in Y-phase particles contained in a foil in $(11\bar{1})$ orientation (Figure 3.17(a)). These are consistent with the proposed unit cell.

Table 3.2

Operating Reflections	Moiré spacings	
	Calculated	Observed
(022) matrix/(022) Y-phase Figure 3.18(a)	21 Å	21 Å
(111) matrix/(111) Y-phase Figure 3.18(b)	33 Å	35 Å
(200) matrix/(200) Y-phase Figure 3.18(c)	29 Å	28 Å

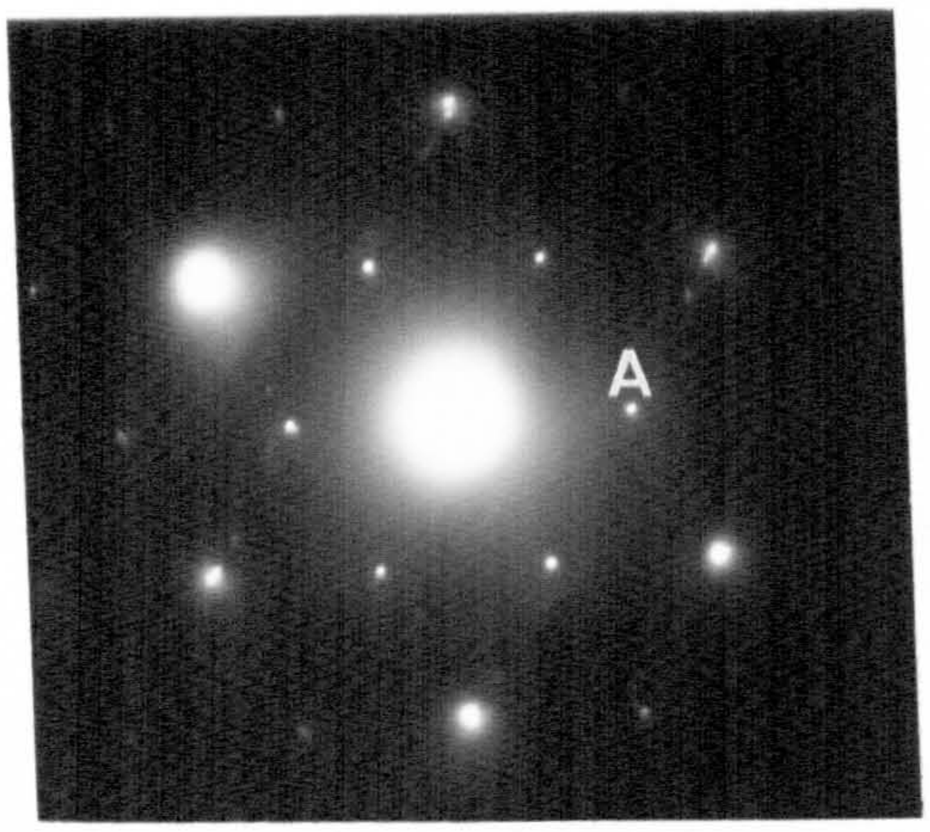

(a)

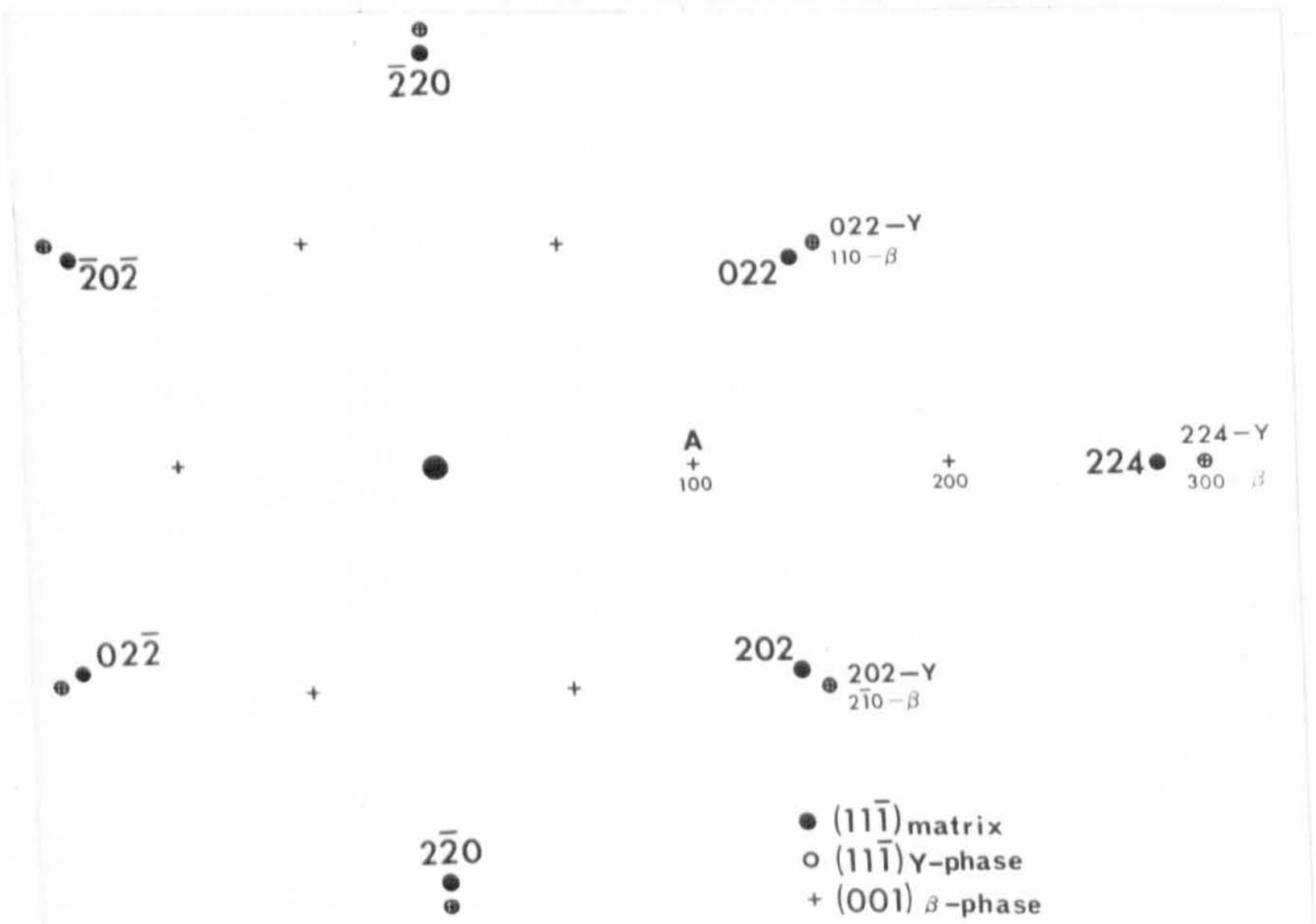

(b)

Figure 3.20(a) A selected-area diffraction pattern from a Y-phase particle in a foil in (11$\bar{1}$) orientation, showing extra spots of the type labelled A.

(b) This is an explanatory diagram of (a).

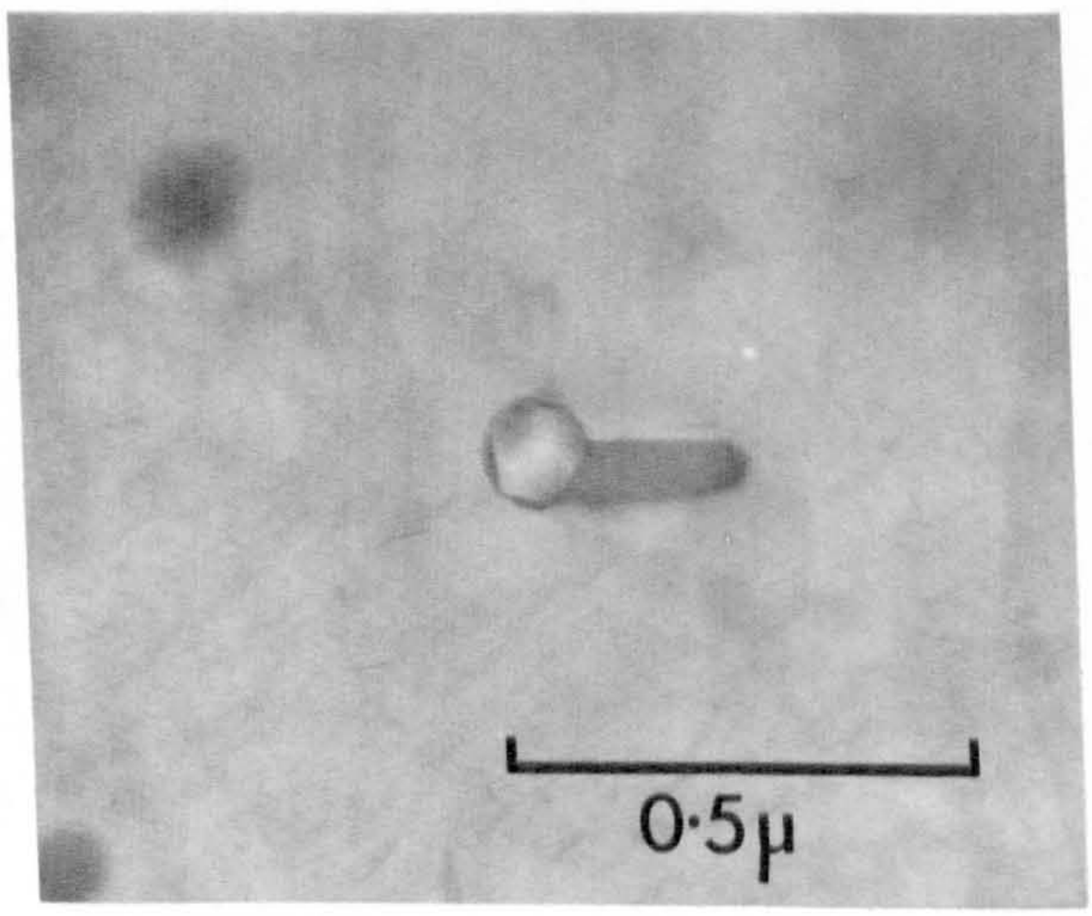

Figure 3.21 Al-26%Zn alloy, solution treated at 500°C, direct-quenched into Wood's metal at 210°C and aged for 10 min., showing a finger-like growth associated with a Y-phase precipitate.

Only a small number of electron diffraction patterns were obtained from Y-phase particles in $\{111\}$ matrix orientation but those that were, contained extra spots which could not be indexed as allowed reflections of the f.c.c. unit cell proposed above. One of these patterns is reproduced as Figure 3.20(a) and Figure 3.20(b) is an explanatory diagram of the pattern. Extra spots of the type labelled A indexed as $^1/3\ \{224\}$ on the basis of the f.c.c. unit cell.

A possible explanation of these extra spots is suggested by the observation that some of the larger Y-phase particles had associated with them a finger-like growth, as illustrated by Figure 3.21. It is believed that these growths were of the β equilibrium phase and that these were able to nucleate and grow epitaxially on one of the $\{111\}$ - faces of the Y-phase particle. It is proposed that the extra spots of the type labelled A in Figure 3.20(b) originate from a thin layer of β-phase precipitated at the $(11\bar{1})$ interface of the Y-phase particle. Spot A can then be indexed as (100) for a hexagonal unit cell with a = 2.67 Å, orientated so that (001) hex.// $(11\bar{1})$ matrix. This a-value is very close to that of hexagonal zinc, for which a = 2.66 Å.

In summary, the ageing sequence appears to be as follows :-

(i) After a rapid quench Y-phase particles nucleate in the matrix, possibly heterogeneously on vacancy clusters.

(ii) Y-phase particles then grow, with an octahedral shape and with the faces of the octahedron parallel to $\{111\}$ planes of the matrix. The crystal structure of Y-phase is f.c.c. with a = 3.77 Å. Its unit cell is in parallel orientation with the matrix.

(iii) Equilibrium zinc precipitates are formed by epitaxial growth of hexagonal zinc platelets on the $\{111\}$ interfaces between Y-phase and the matrix.

CHAPTER 4

THE UPPER LIMITING TEMPERATURE FOR G.P. ZONE FORMATION IN Al-Mg_2Si AND Al-Zn ALLOYS

4.1 INTRODUCTION

It is a well known fact that, for most aluminium-base age-hardening alloys, a considerable undercooling below the equilibrium solvus temperature is required before the supersaturated solid solution decomposes by the initial formation of G.P. zones. This is the case for the Al-Mg_2Si and Al-Zn alloys that were studied in this investigation. The object of the work described in this Chapter was to determine the "critical temperature", which represents the upper limiting temperature above which G.P. zones are not observed to form, and to determine the factors which control the value of this temperature.

In the case of the Al-Zn alloys, it is shown that G.P. zone formation can occur at a temperature that is above the corresponding coherent spinodal temperature for an alloy of given composition and it is therefore deduced that these G.P. zones are formed by a nucleation and growth process. The coherent spinodal is not known for the Al-Mg_2Si system, but it is assumed that G.P. zone formation at a low solute supersaturation in this system also occurs by a nucleation and growth process.

The experimental results, which are described in sections 4.3. and 4.4., show conclusively that, in addition to the degree of solute supersaturation, the other important factor which influences the value of the maximum temperature at which G.P. zones are observed to form is the degree of vacancy-supersaturation during the initial stages of

ageing. The higher the initial vacancy-supersaturation, the higher is the temperature at which G.P. zone nucleation is observed. This conclusion is obtained by comparing the resulting microstructure in samples which were either step-quenched or direct-quenched to the ageing temperature.

The results obtained with the Al-1.2%Mg_2Si alloy represent an extension of the results previously obtained with this alloy[81] in which a critical temperature T_c for homogeneous precipitation was determined which represented the maximum temperature at which observable G.P. zone formation occurred when an almost equilibrium vacancy concentration was present during the initial stages of ageing. (It was convenient to define T_c as the maximum temperature for which homogeneous G.P. zone formation is observed when only an equilibrium vacancy concentration is present during the nucleation period. The experimental values of critical temperature, as described below, then approach the defined value of T_c very closely). The value of T_c for this alloy was determined experimentally by the step-quenching technique and in section 4.3.1 it is shown that $T_c = 190^{\circ}C \pm 10^{\circ}C$.

By quenching samples rapidly, for example by quenching directly into molten salt, G.P. zone formation was observed[81] for ageing temperatures above T_c. The upper limiting temperature for G.P. zone formation in this case (T_c') was $\sim 35^{\circ}C$ higher than T_c. More recently direct-quenches into molten Wood's metal have been carried out for which an even higher value of T_c' was observed. These results are reported in detail in section 4.3.1.

G.P. zone formation also occurs heterogeneously on dislocation lines in the Al-1.2% Mg_2Si system and in section 4.3.2 it is shown that a "critical temperature" can also be associated with this reaction.

The type of experimental procedure described above has also been applied to samples of Al-Zn alloys and values of T_c and T_c' have been obtained (see section 4.4) for the three alloy compositions studied.

In section 4.5 an interpretation of the results is put forward, which is based on a qualitative nucleation model for G.P. zones, which considers some possible ways in which vacancies can aid nucleation. The relationship between the values of T_c, T_c' and $T_{G.P.}$ (the G.P. zone solvus temperature) is discussed.

4.2 EXPERIMENTAL TECHNIQUE

In all cases the samples were initially solution treated for a period of 1 hour. The value of T_s was normally well within the single phase region of the phase diagram, although a few samples of Al-1.2%Mg_2Si were deliberately solution treated at a low value of T_s which was within the two-phase region. The details of solution treatment are given with the experimental results in sections 4.3 and 4.4.

After solution treatment the samples were either direct-quenched or step-quenched to the ageing temperature, T_1. In section 1.4.1 it was seen that the equilibrium vacancy concentration of an alloy increases exponentially with temperature and that a non-equilibrium vacancy concentration can be retained immediately after a rapid direct-quench, in regions of a sample sufficiently distant from a vacancy sink. The more rapid the quench, the less is the time available for the excess-vacancies to decay to sinks during the quench and so the higher will be the initial quenched-in excess-vacancy concentration at the start of ageing (it is assumed that vacancy aggregation is negligible). In contrast to the rapid direct-quench, the step-quench was designed to reduce the excess-vacancy concentration to as low a value as possible during the initial stages of

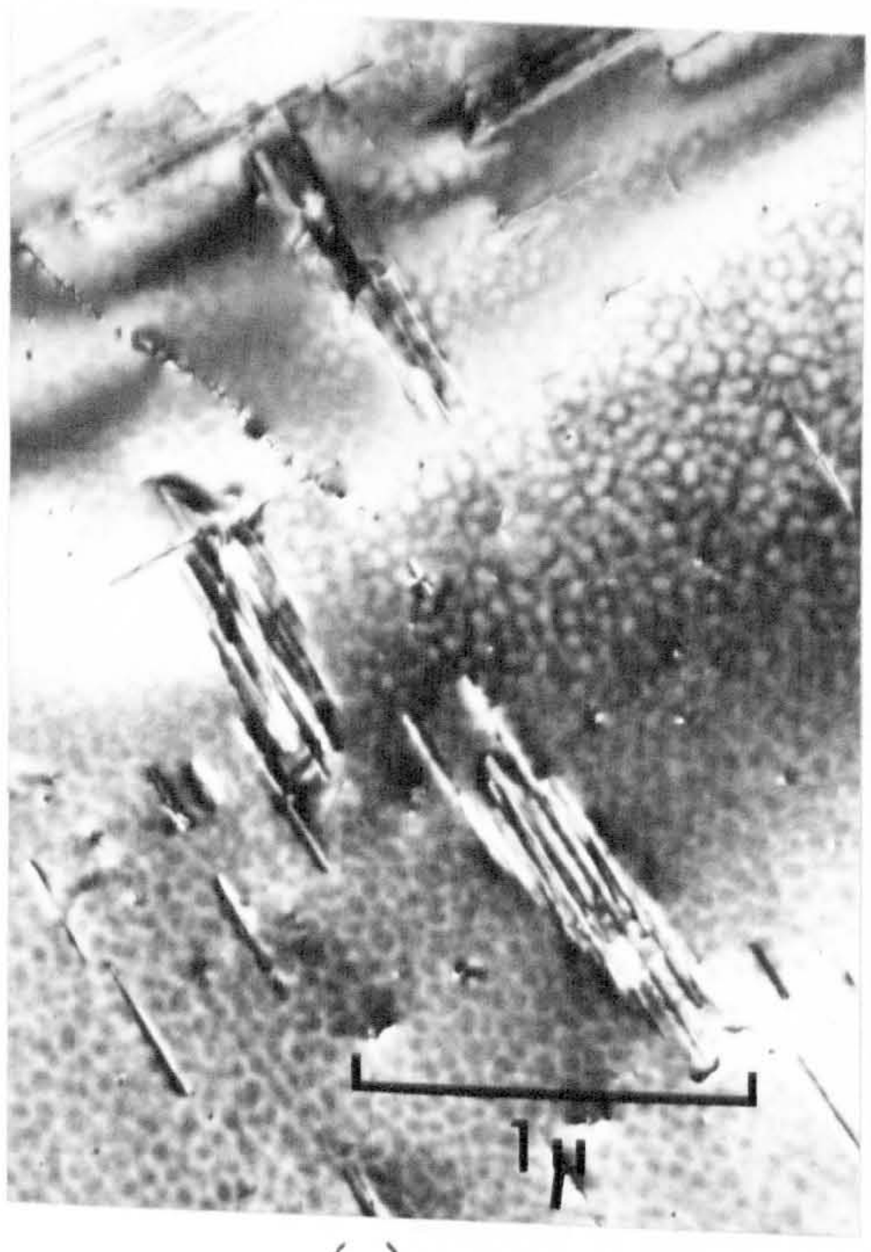

(a)

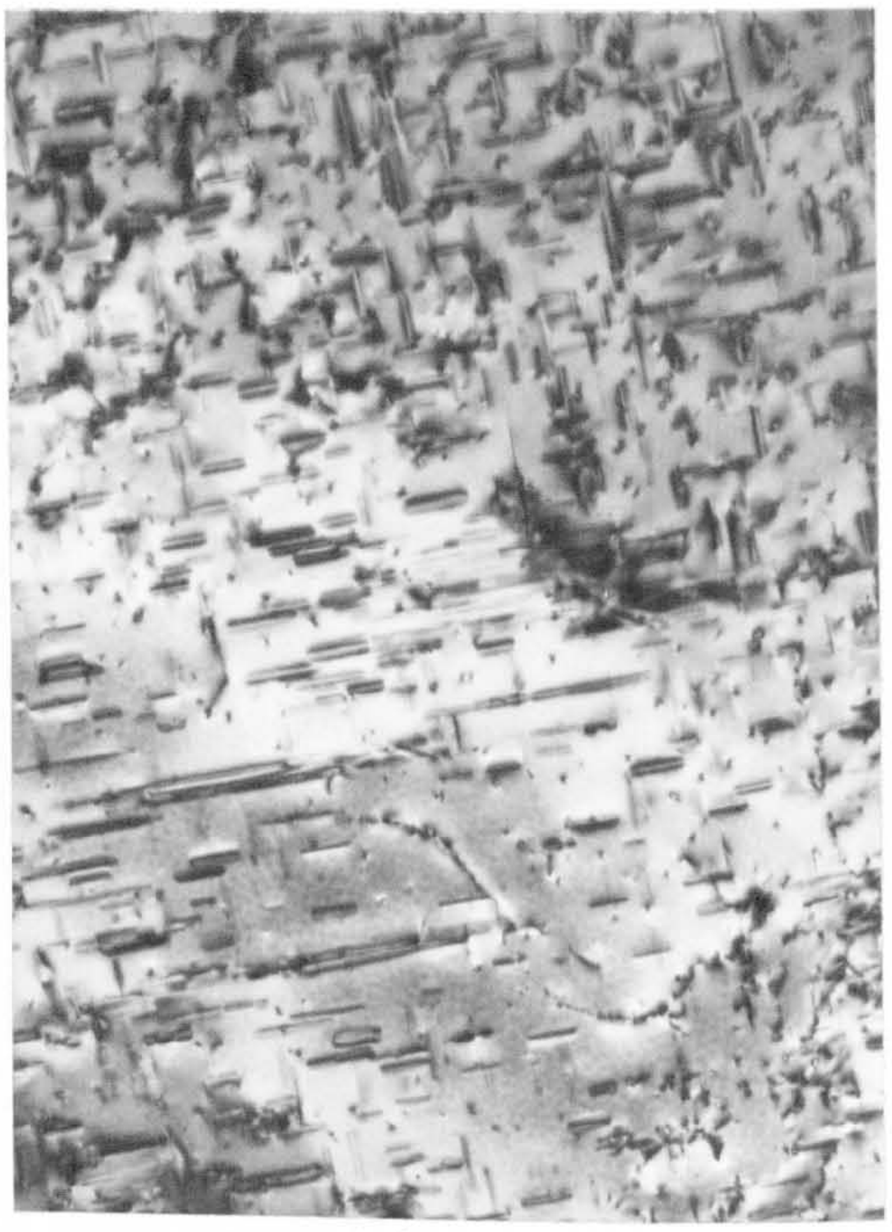

(b)

Figure 4.1 Al-1.2%Mg_2Si : (a) step-quenched from 560°C, via 250°C for 1 min., into oil at 200°C and aged for 3 hrs.; (b) direct quenched from 560°C into salt at 200°C and aged for $2\frac{1}{2}$ hrs.

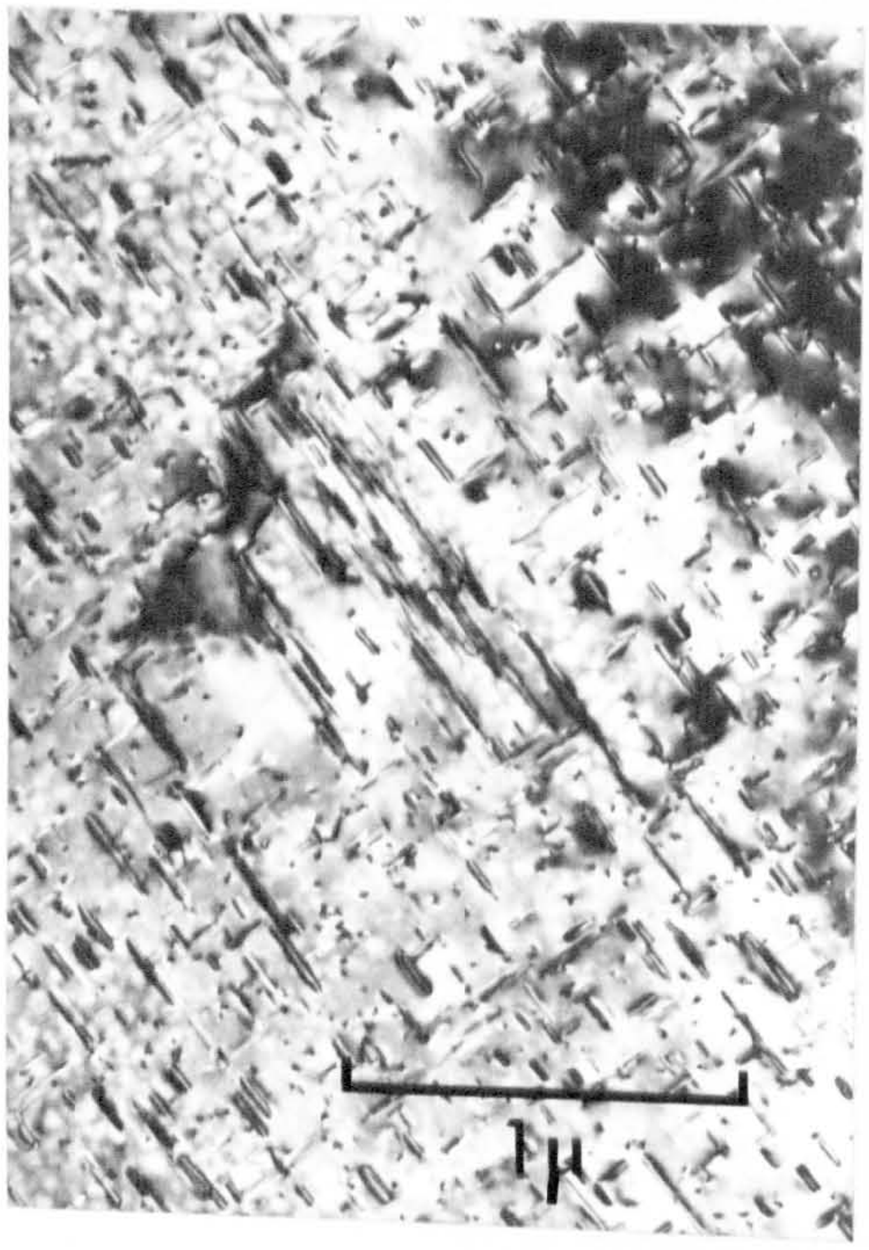

(a)

(b)

Figure 4.2 Al-1.2%Mg_2Si : (a) direct-quenched from 560°C into salt at 220°C and aged for $1\frac{1}{2}$ hrs.; (b) direct-quenched from 560°C into salt at 230°C and aged for $\frac{1}{2}$ hr..

ageing at T_1. The value of the temperature of interruption (T_Q) was adjusted so that no G.P. zones were nucleated at T_Q, although it was necessary for the temperature difference between T_Q and T_1 to be fairly small ($\sim 50^{o}C$, say) so that the initial excess-vacancy concentration on ageing at T_1 was reduced to a very low value. A standard time of 1 minute at T_Q was always used (longer times, especially for the Al-Mg_2Si alloy, caused excessive heterogeneous precipitation, for example on dislocations, and this reduced the matrix solute supersaturation).

It is emphasised that the results described in this chapter refer to regions of the matrix near to the centre of grains. The behaviour of the precipitation in the neighbourhood of grain boundaries, in the case of the Al-Zn alloys, is discussed separately in Chapter 6.

4.3 RESULTS FOR THE Al-1.2%Mg_2Si ALLOY

4.3.1 Random matrix precipitation

Consider, first of all, the samples which were solution treated at $560^{o}C$, so that all available solute was initially in solid solution at T_s. Samples which were step-quenched, via $250^{o}C$, to $160^{o}C$ and aged for 24 hours exhibited homogeneous precipitation which was similar to that illustrated by Figure 3.4(a), in which the sample was direct-quenched into oil at $160^{o}C$. Figure 4.1(a) illustrates the typical microstructures observed in a sample which was step-quenched, via $250^{o}C$, to $200^{o}C$. Practically all the needle-precipitates are clearly associated with "colonies" of needles which were nucleated on dislocation lines, so that this result illustrates that $T_c < 200^{o}C$. This, and other results, indicated that $T_c = 190^{o}C \pm 10^{o}C$.

Samples which were direct-quenched into molten salt at $200^{o}C$ (Figure 4.1(b)) and $220^{o}C$ (Figure 4.2(a)) contained copious homogeneous

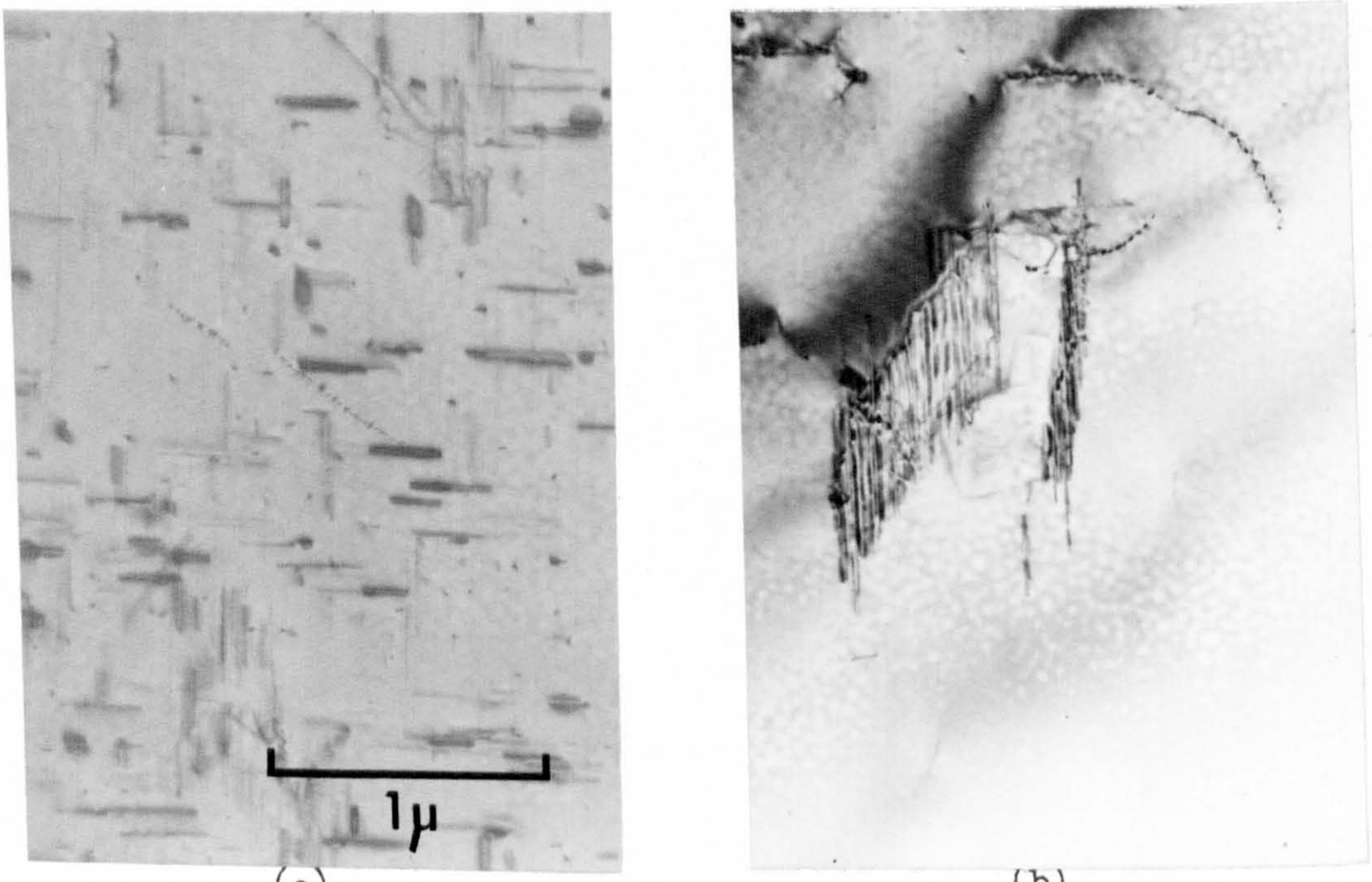

(a) (b)

Figure 4.3 Al-1.2%Mg_2Si : Direct-quenched from 560°C into Wood's metal at (a) 240°C and (b) 250°C and aged for 10 mins..

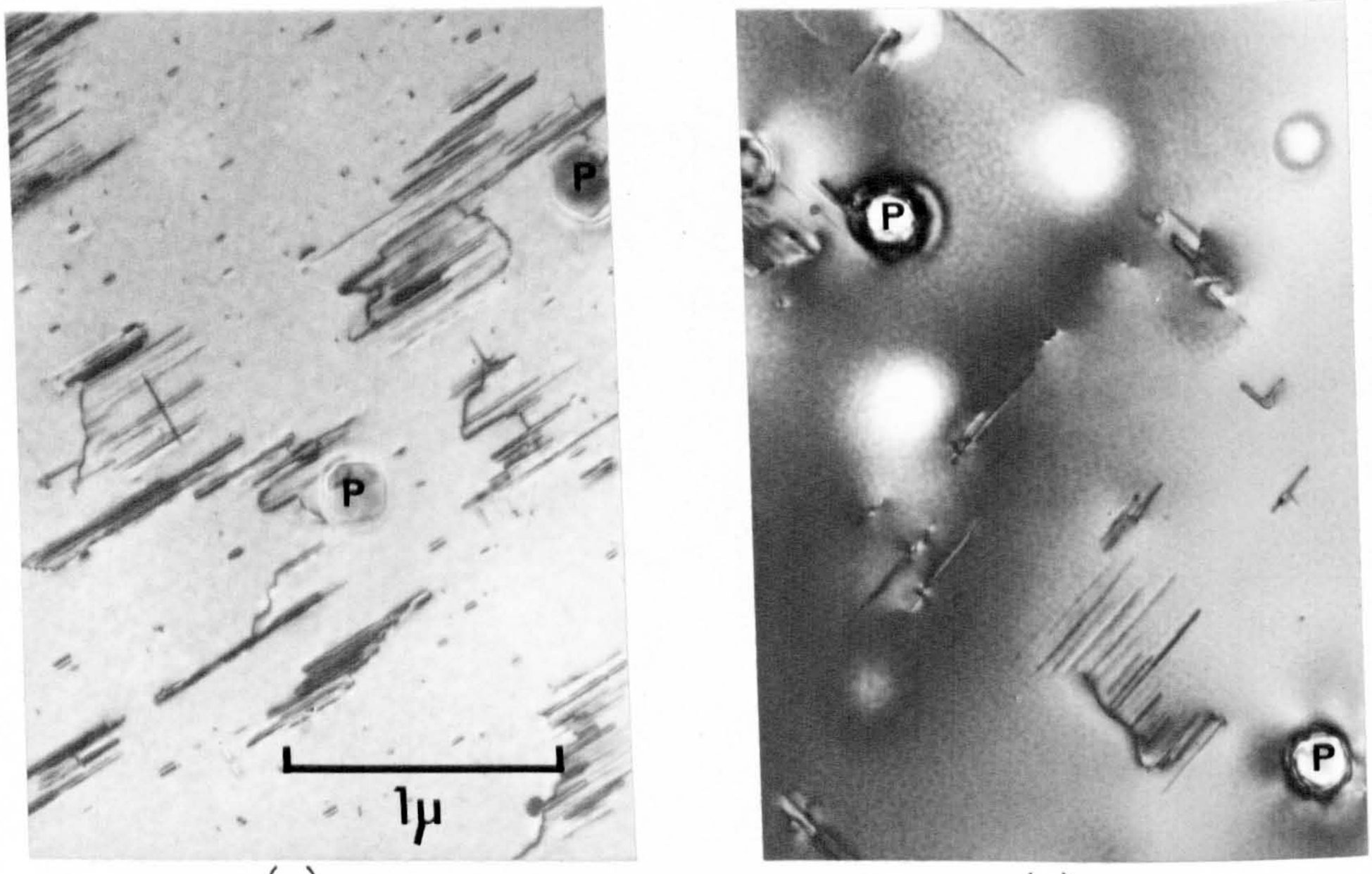

(a) (b)

Figure 4.4 Al-1.2%Mg_2Si : Direct-quenched from (a) 465°C and (b) 450°C into oil at 160°C and aged for 24 hrs.. Particles of Mg_2 Si are labelled P.

precipitates, but not at 230°C (Figure 4.2(b)). These results indicated that T_c' (salt) = 225°C ± 5°C. Similar experiments carried out with direct-quenches into Wood's metal indicated that T_c' (Wood's metal) = 245°C ± 5°C (see Figure 4.3(a) and (b)).

No detailed experimental work was carried out to determine the variation of either T_c or T_c' with changes in Mg_2Si content of the alloy, although some results were obtained which strongly suggest that T_c' (oil) decreases with decrease in Mg_2Si content of the alloy. Figures 4.4(a) and (b) illustrate the microstructure observed in samples of Al-1.2%Mg_2Si which were direct-quenched into oil at 160°C after solution treatment at 465°C and 450°C, respectively. Both of these values of T_s are below the equilibrium solvus temperature for the alloy (~ 540°C) and, as a consequence, large particles of Mg_2Si were precipitated during solution treatment (such as those labelled P). It seems reasonable to suppose that the matrix concentrations of Mg_2Si were reduced, during solution treatment, to the equilibrium values characteristic of T_s. From the phase diagram, Figure 3.1, these are 0.75% Mg_2Si and 0.83%Mg_2Si, respectively, at 450°C and 465°C. The absence of homogeneous precipitation in Figure 4.5(b) then indicates that T_c' (oil) < 160°C for an Al-0.75%Mg_2Si alloy direct-quenched from 450°C.

4.3.2 Dislocation-nucleated precipitation

A noticeable feature of Figures 4.2(b), 4.3(b) and 4.4(b) is the presence of precipitation on dislocations, even though homogeneous precipitation is absent in the matrix.

The object of this investigation was to see if a critical temperature can be associated with dislocation-nucleated precipitates in a similar way to that for homogeneous precipitates. The following

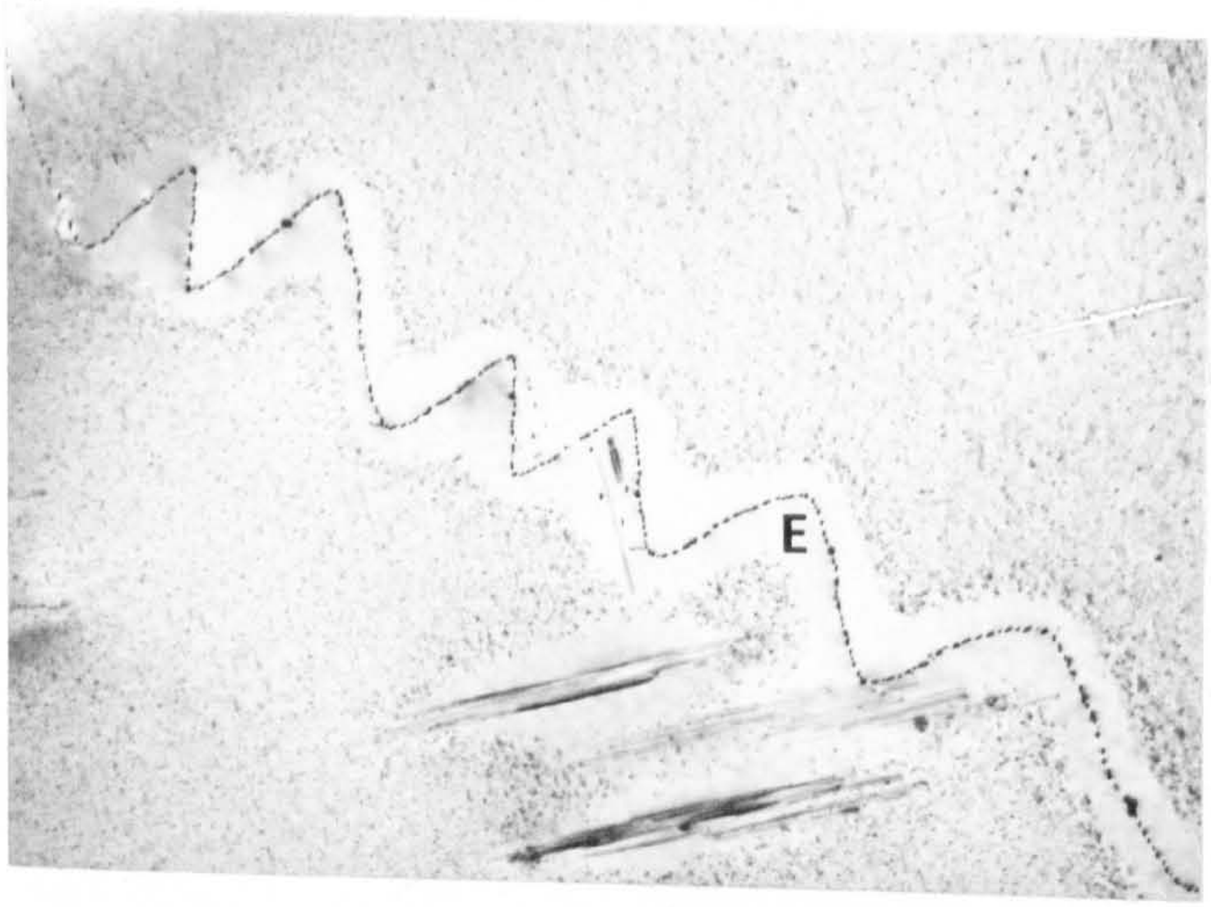

(a)

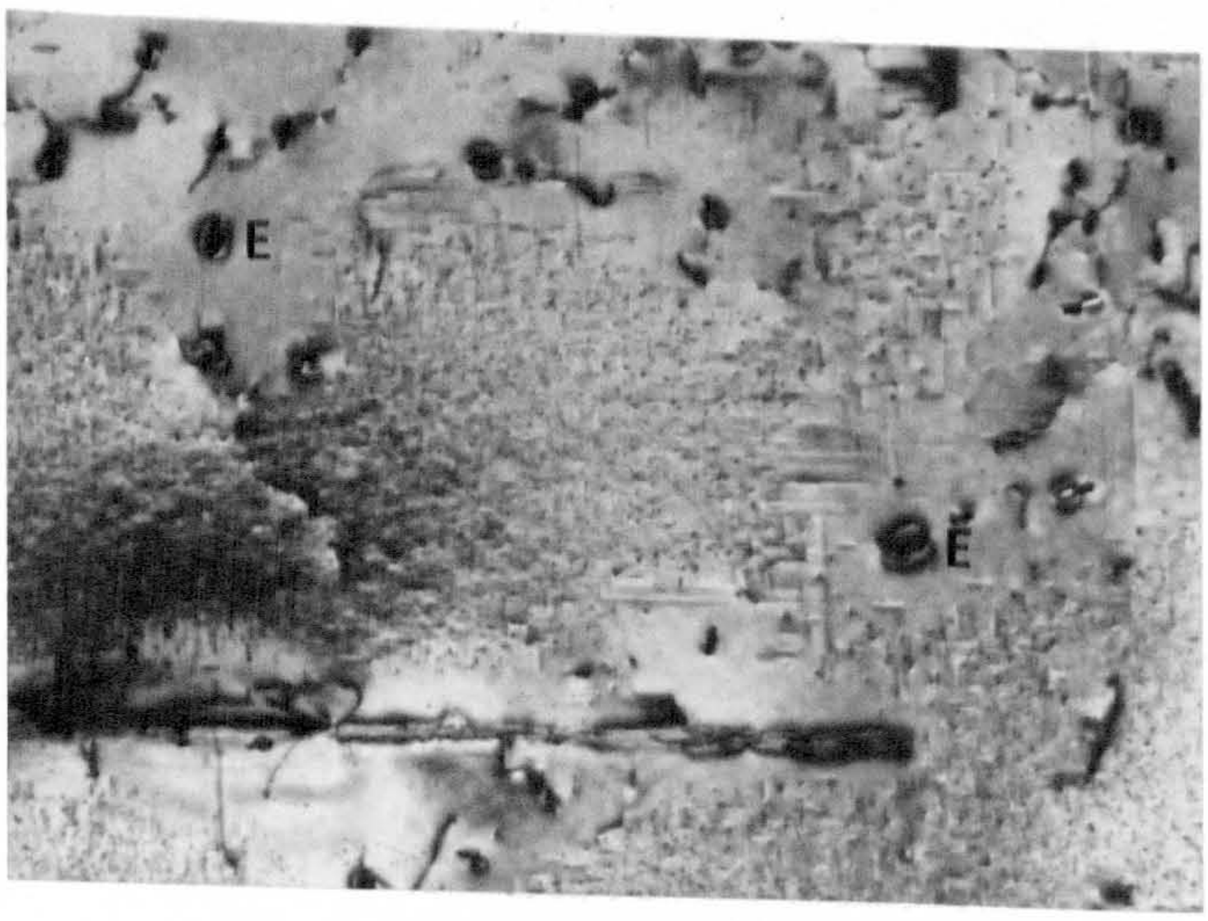

(b)

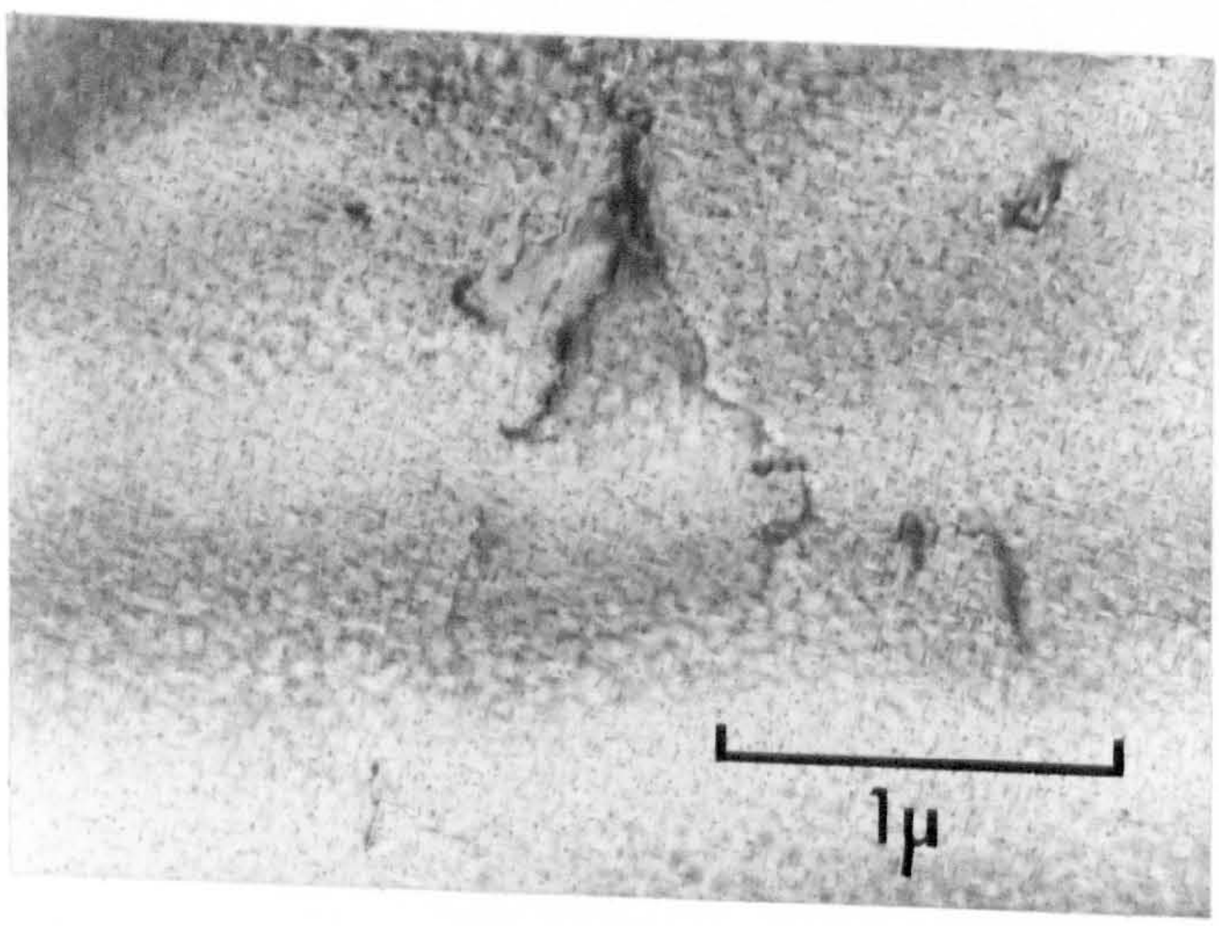

(c)

Figure 4.5 Al-1.2%Mg_2Si : Solution treated at 560°C and then (a) aged for 10 mins. at 250°C plus 6 months at 20°C plus 24 hrs. at 160°C, (b) aged 4 mins. at 320°C plus 2 months at 20°C plus 24 hrs. at 160°C, (c) aged 1½ mins. at 340°C plus 2 months at 20°C plus 24 hrs. at 160°C.

heat-treatment was studied:

(a) A sample was direct-quenched from 560°C into a salt bath held at some high temperature in the range 250°C to 340°C and aged for a few minutes;

(b) the sample was then quenched into water at room temperature and aged for several months before being aged at 160°C for 24 hours.

Only part (a) of this heat treatment was essential for the determination of the critical temperature above which dislocation-nucleated precipitates failed to form. The added information obtained by the inclusion of part (b), during which homogeneous precipitation was formed, is explained below. Figures 4.5(a), (b) and (c) illustrate the typical precipitation that was observed, in a region containing one or more matrix dislocations, in samples for which the ageing treatment was 250°C, 320°C and 340°C, respectively. These results indicated that large dislocation-nucleated needles were formed during the pre-treatments at 250°C and 320°C but not at 340°C, which leads to the conclusion that a critical temperature exists and that its value T_c' (dislocation) = 330°C $\pm$ 10°C.

The large needles labelled E are dislocation-nucleated needles which are viewed end-on. Those in Figure 4.5(a) all appear to have been nucleated on the same helical dislocation, which is either out of contrast or was removed during electro-polishing. In all three examples the fine matrix precipitation was produced during the treatment (b) (further examples of this type of heat treatment are discussed in Chapter 5). The regions free from matrix precipitation in Figure 4.5(a) and (b) are believed to be caused, predominantly, by local solute depletion which was produced during the rapid growth of the dislocation-nucleated needles (stage (a) of the heat-treatment). The absence of a wide precipitate-free region in the neighbourhood of the dislocation in

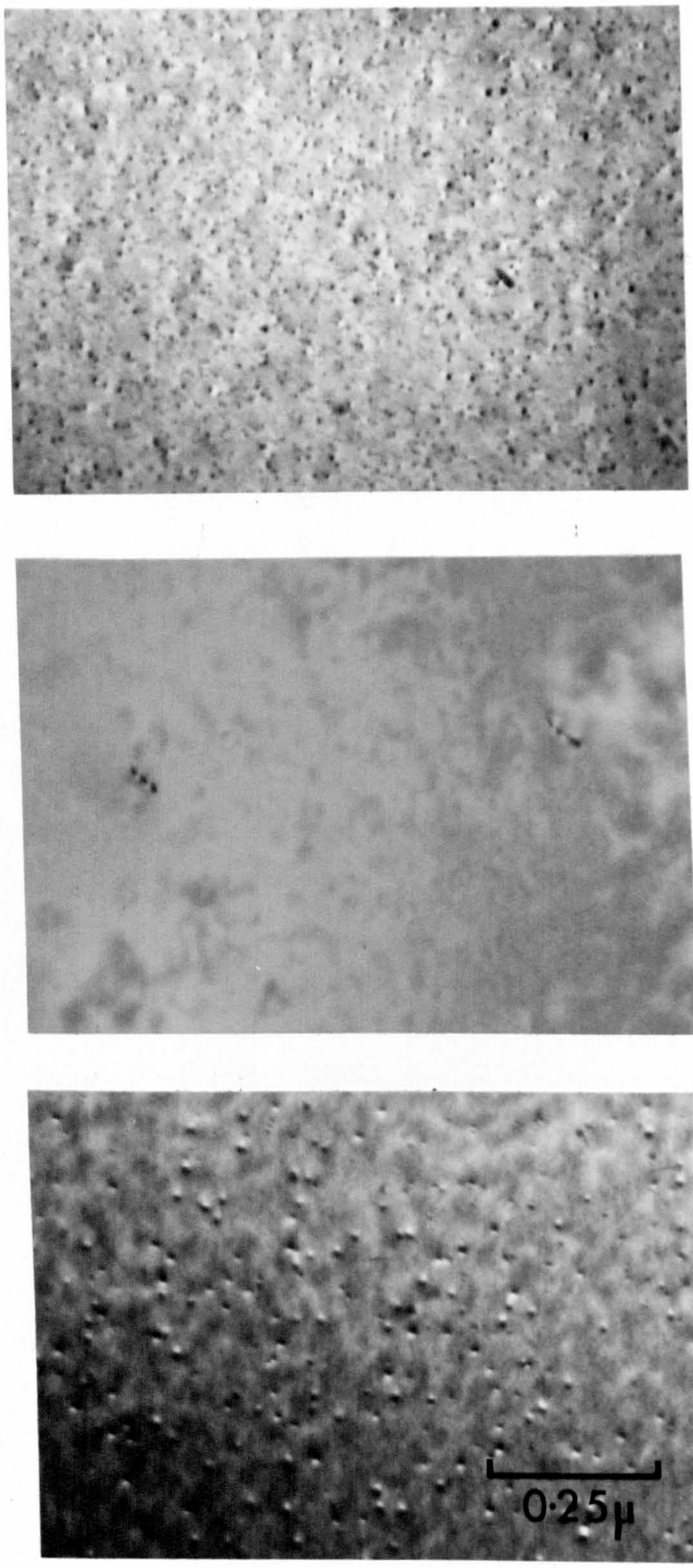

(a)

(b)

(c)

Figure 4.6 Al-17.5%Zn : Solution treated at 560°C and then (a) step-quenched, via 180°C for 1 min., into oil at 155°C and aged for 1 hr., (b) step-quenched, via 180°C for 1 min., into oil at 157°C and aged for 1 hr., (c) direct-quenched into oil at 160°C and aged for 1 hr..

Figure 4.5(c) is added evidence that 340°C is above T_c' (dislocation).

It is concluded that two similar, but fundamentally different, critical temperatures can be associated with a direct-quench into salt: T_c' = 225°C ± 5°C for homogeneous precipitation and T_c' (dislocation) = 330°C ± 10°C for dislocation-nucleated precipitation. The large difference between these two critical temperatures is considered in section 4.5.

4.4 RESULTS FOR THE Al-Zn ALLOYS

Samples from all three compositions of Al-Zn alloy were subjected to either the step-quench or the direct-quench procedure before being isothermally aged to see if G.P. zone formation had occurred at the chosen ageing temperature. From these experiments the values of T_c and T_c' were determined for each alloy composition.

Consider, as an example, the alloy of nominal composition Al-17.5%Zn. The experimental results obtained with samples which were step-quenched from 560°C, and via 180°C, into oil (Figures 4.6(a) and (b)) indicated that T_c = 156°C ± 2°C. The temperature of the ageing bath was carefully controlled to within ± 1°C of the desired ageing temperature during these experiments and the results were reproducible to within this experimental error. In contrast to this result, samples which were solution treated at 560°C and then direct-quenched and aged in oil at 160°C clearly contained G.P. zones (see Figure 4.6(c)), whereas, samples which were direct-quenched and aged in oil at 162°C did not: Thus, T_c' (oil) = 161°C ± 2°C. The highest temperature at which G.P. zone formation was observed in this alloy was obtained with a direct-quench into molten Wood's metal. Figures 4.7(a) and (b) indicate that T_c' (Wood's metal) = 164°C ± 2°C.

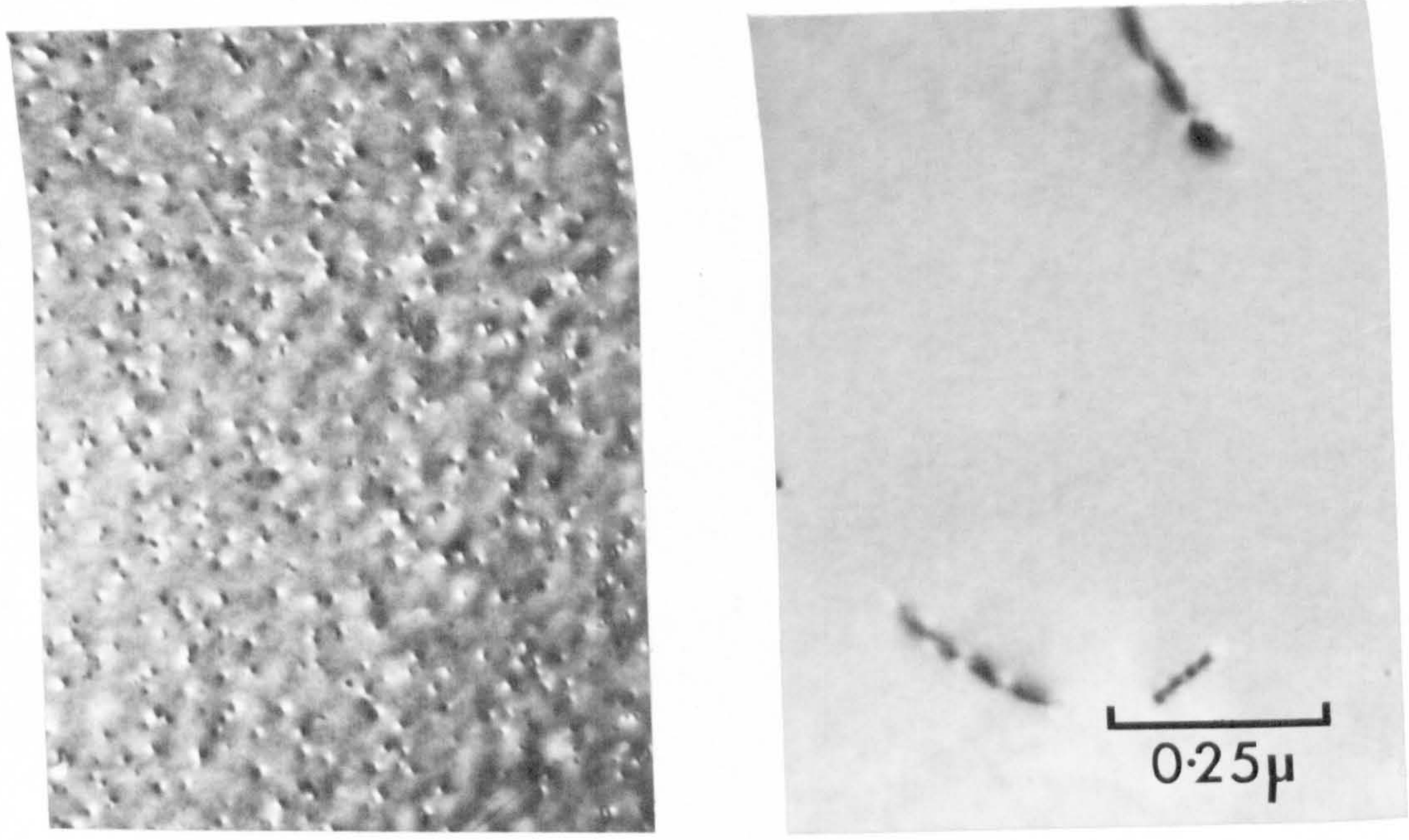

(a) (b)

Figure 4.7 Al-17.5%Zn : Solution treated at 560°C and then direct-quenched into Wood's metal at (a) 163°C and (b) 165°C and aged for 1 hr..

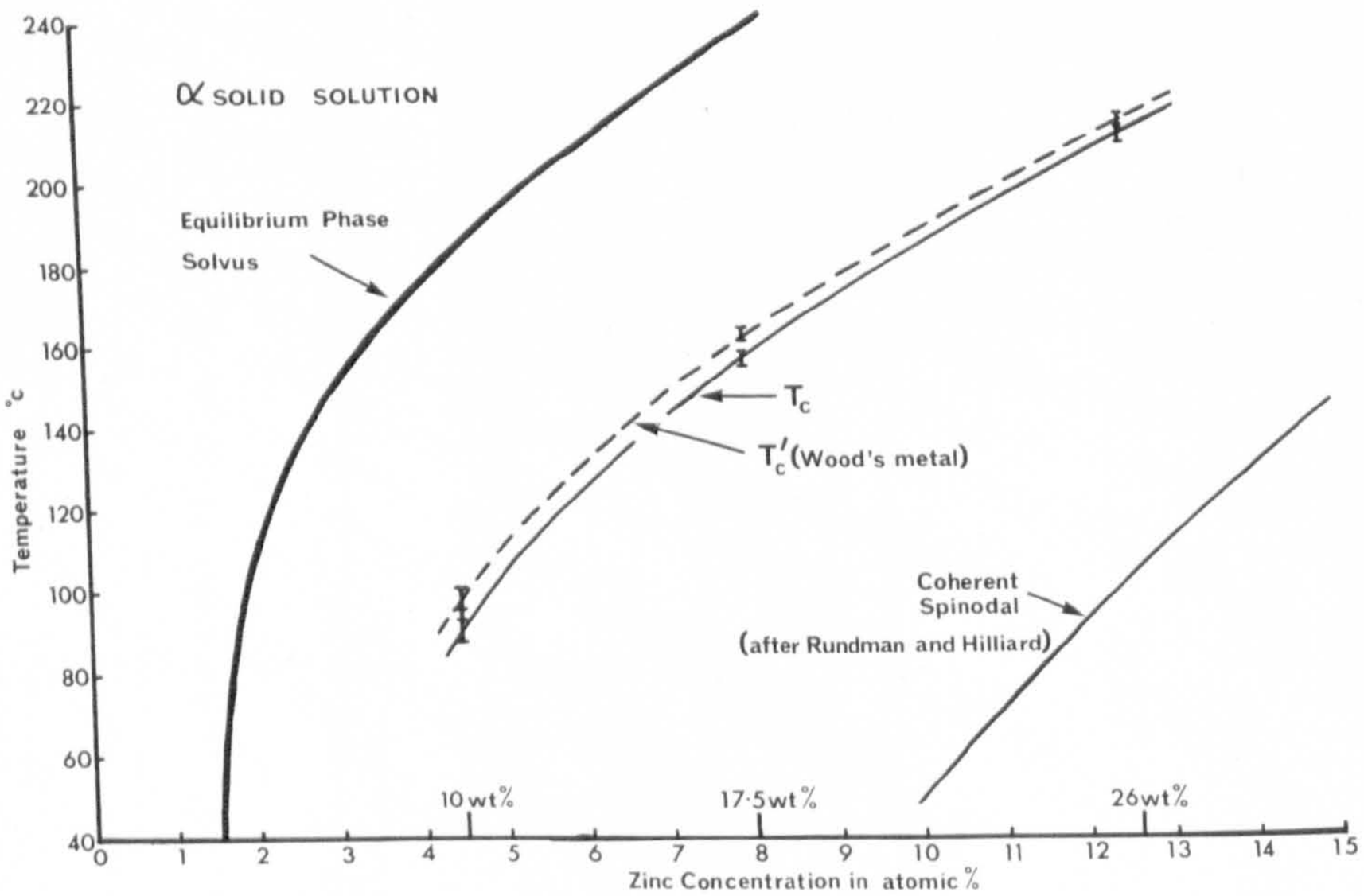

Figure 4.8 A diagram showing the experimentally determined T_c and T_c'(Wood's metal) curves for Al rich-Zn alloys. The coherent spinodal curve which was calculated by Rundman and Hilliard[127] is also shown.

Similar experiments were carried out with the Al-10%Zn and Al-26%Zn alloys for which T_s was 560°C and 500°C respectively. In the case of the Al-10%Zn alloy, an ageing time of about 1 week was required to be sure that the G.P. zones, if formed, were grown to a sufficient size to be positively detected by electron microscopy. The temperature control of the furnace over a period of 1 week was only to within $\pm$ 2°C, so the accuracy of the results in this case was not as good as for the Al-17.5%Zn alloy. For the Al-26%Zn alloy an ageing time of 10 minutes was sufficient to be able to easily detect whether or not G.P. zones had been formed. The results for these two alloy compositions were as follows :

(a) Al-10%Zn; T_c = 92°C $\pm$ 4°C; T'_c(Wood's metal) = 97°C $\pm$ 4°C

(b) Al-26%Zn; T_c = 210°C $\pm$ 2°C: T'_c (Wood's metal)= 213°C $\pm$ 2°C

The results for all three alloy compositions are plotted on the phase diagram in Figure 4.8 and what are considered to be reasonable curves have been drawn through the T_c and T'_c (Wood's metal) experimental points. Also plotted on this diagram is the coherent spinodal curve, as derived from theoretical considerations by Rundman and Hilliard[127]. It is to be noted that the coherent spinodal lies significantly below both the T_c and T'_c (Wood's metal) curves and this leads to the conclusion, mentioned earlier, that the G.P. zones that are formed at a temperature in the neighbourhood of T_c do so by a nucleation and growth process.

4.5 INTERPRETATION OF THE RESULTS

The results described above demonstrate the quench-rate dependence of the upper limiting temperature for G.P. zone formation. This effect was first discovered by Pashley, Jacobs and Vietz[81] during

an investigation of the two-step ageing behaviour of an Al-1.2%Mg_2Si alloy, which is discussed in Chapter 5. The variation in upper limiting temperature with quench-rate was interpreted in kinetic terms by considering the influence of the vacancy concentration on the nucleation kinetics of G.P. zones. As described in section 4.3, the effect is very large in the Al-1.2%Mg_2Si alloy, with a temperature difference of $55^{o}C \pm 15^{o}C$ between T_c and T_c' (Wood's metal) for homogeneous precipitation. In the case of the Al-Zn alloys, the effect is very much smaller, for example, with the Al-17.5%Zn alloy the difference between T_c and T_c' (Wood's metal) is only $8^{o}C \pm 4^{o}C$.

Similar step-quench and direct-quench experiments have been carried out recently by Lorimer and Nicholson[78,79] with Al-3.9%Cu and Al-4.5%Ge alloys and they also found a quench-rate dependence of the upper limiting temperature in these alloys. They interpreted their results by reference to the G.P. zone solvus temperature $T_{G.P.}$. The concept of a G.P. zone solvus was discussed briefly in section 1.3.4. Clearly, there is a need to inter-relate the temperatures T_c, T_c' and $T_{G.P.}$ and to examine the significance of these temperatures in relation to the experimentally determined values of upper limiting temperature. Also, there is a need to consider the possible ways in which vacancies can effect the nucleation of G.P. zones. These two important topics are discussed in the next section, in which a qualitative nucleation model is first derived and then used to discuss G.P. zone nucleation in Al-Mg_2-Si and Al-Zn alloys.

4.5.1 A nucleation model

Consider a binary alloy and let A represent the solvent atoms and B represent the solute atoms. The following assumptions are made initially :

(a) the atomic volumes of A and B atoms are identical, so that the unit cells of the G.P. zones and the matrix are identical apart from differences in chemical composition ;

(b) spherical G.P. zones are formed by a nucleation and growth process on ageing at a temperature T_1, provided that T_1 is low enough;

(c) the volume free energy per atom of the G.P. zone is independent of the G.P. zone radius r ;

(d) the interfacial energy (γ ergs/cm^2) between a G.P. zone and the matrix is also independent of r and T_1.

Consider the formation of embryo solute clusters by thermal fluctuations at a temperature T_1 which is in the neighbourhood of the upper limiting temperature for G.P. zone formation. Let the density of embryo clusters be sufficiently low so that there is a region between the clusters where the solute concentration is equal to the average solute content of the alloy at T_s. We wish to investigate the conditions under which these embryo clusters can become stabilized as G.P. zones.

For a solute cluster of critical radius (r = a) we may write the Gibbs-Thomson equation (equation 1.11) in the form

$$\log_e \frac{C_a^{T_1}}{C_\infty^{T_1}} = \frac{2\gamma\Omega}{akT_1} \qquad (4.1)$$

where the supersaturation i = $C_a^{T_1}/C_\infty^{T_1}$ ($C_a^{T_1}$ and $C_\infty^{T_1}$ are the solute concentrations in equilibrium with a cluster of radius a and ∞ , respectively). This equation expresses the fact that the supersaturation required to stabilize a very small cluster is higher than that required to stabilize a very large cluster. The necessary supersaturation to

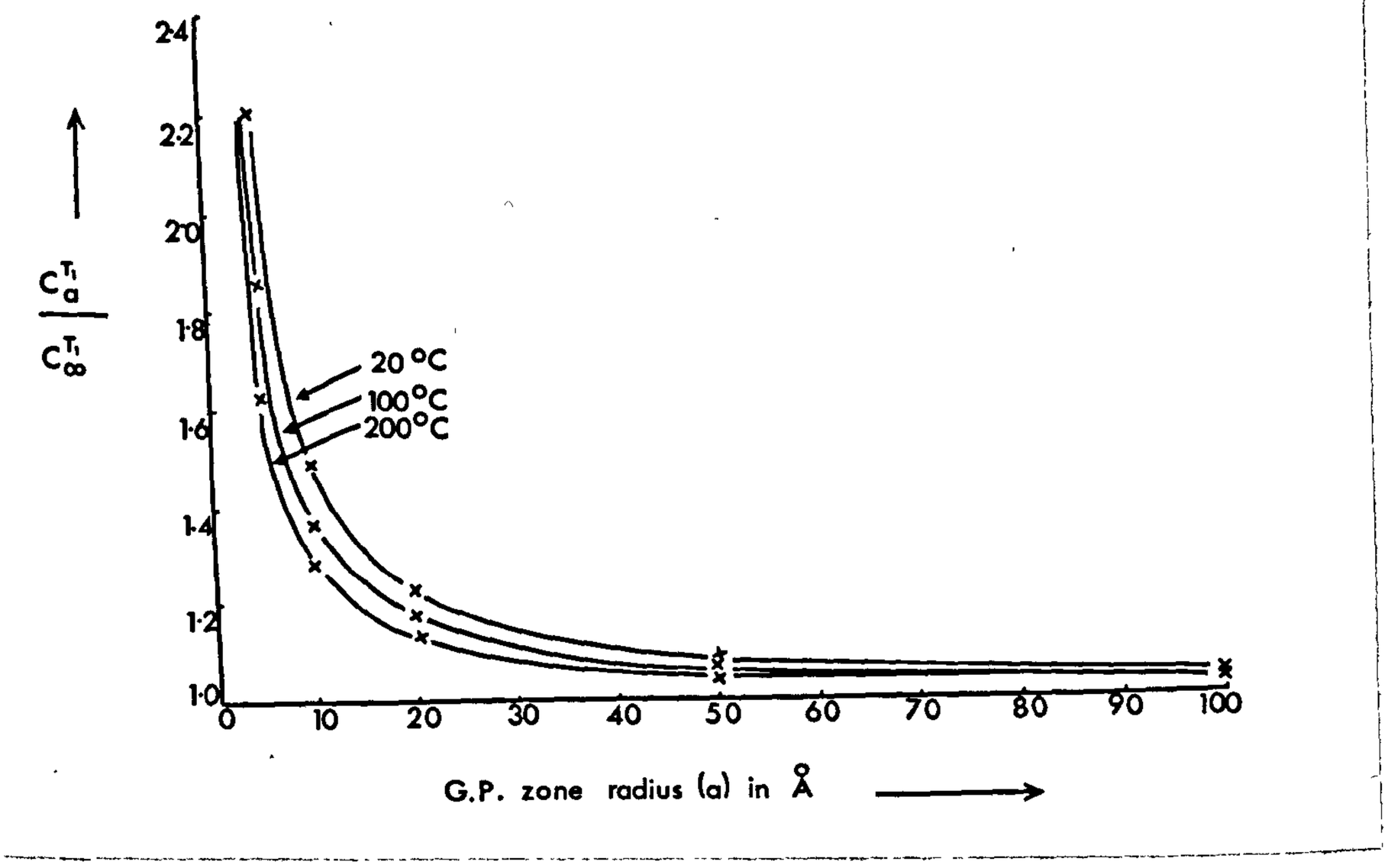

Figure 4.9 Solubility of small G.P. zones in a solid solution compared to the solubility of large G.P. zones (see text for further discussion).

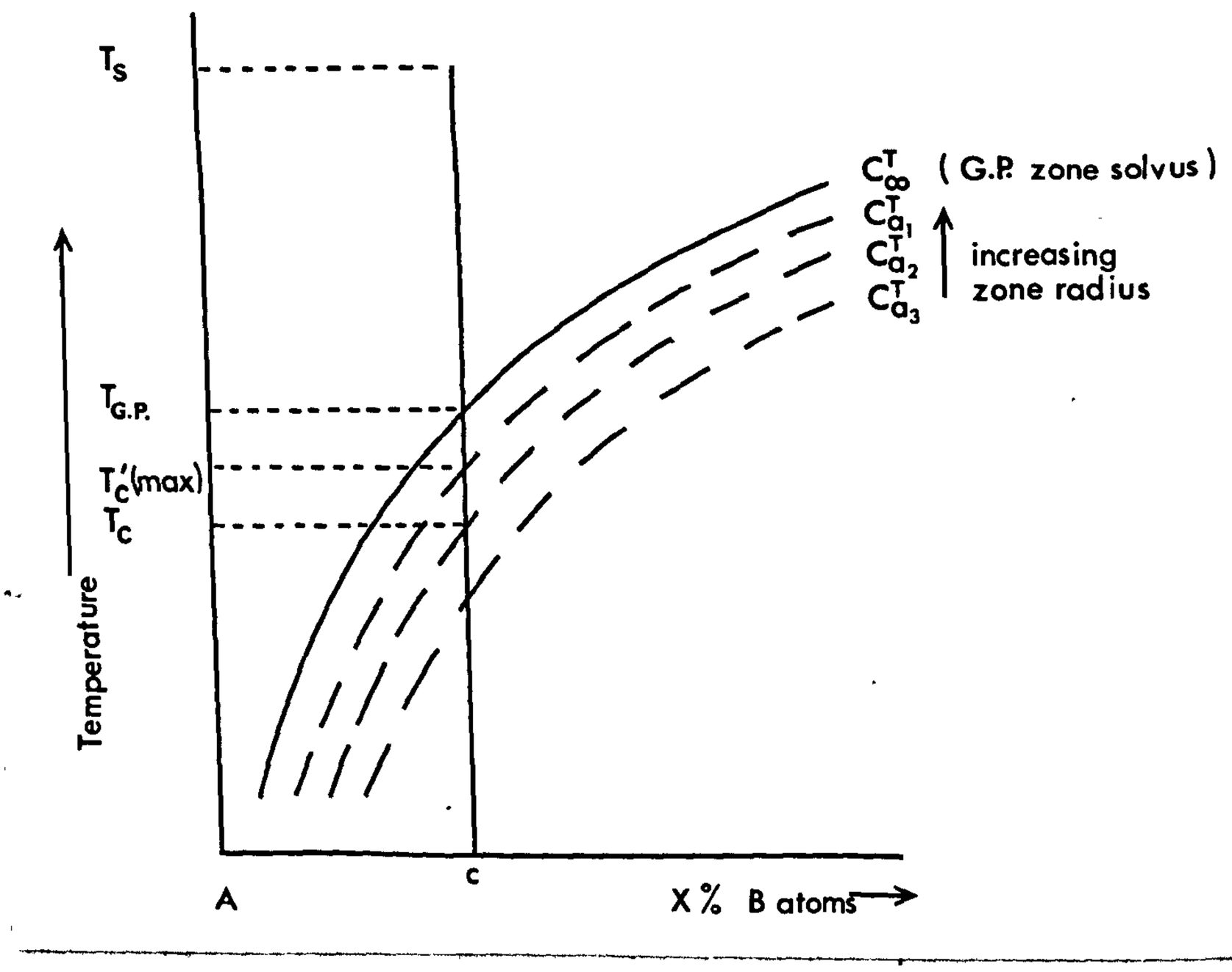

Figure 4.10 A diagram showing, schematically, the relationship between the stability curves for spherical G.P. zones of different sizes.

stabilize a cluster of any given radius is extremely sensitive to the value of the surface energy γ which, as discussed in section 1.3.4 is usually considered to be small for a coherent interface. According to Burke[33] the value of γ for a coherent interface is dependent upon the mismatch between the two lattices, with a lower limit being about 25 ergs/cm^2 and the maximum value about 200 ergs/cm^2. In the ideal case that we are considering the mismatch is zero (assumption (a)), so take as a reasonable example γ = 50 ergs/cm^2. If we consider the A atoms to be aluminium and take Ω = 1.6 x 10^{-23}cm^3, then the ratio $C_a^{T_1} / C_\infty^{T_1}$ can be calculated as a function of cluster radius (a) for any given temperature. As an illustration, let the temperatures be 20°C, 100°C and 200°C. The curves are then as shown in Figure 4.9, from which it will be seen that the effect of cluster size on stability is pronounced, in this case, only for clusters less than about 50 Å in radius, i.e.

$$C_a^T \simeq C_\infty^T \; ; \; (a > 50\text{Å}) \qquad (4.2)$$

for values of temperature T above 20°C. For larger values of γ, the effect will be significant for clusters of larger size.

The curve describing the variation of C_∞^T with alloy composition on the phase diagram is the G.P. zone solvus which was discussed in section 1.3.4 and shown schematically as the curve A'B' in Figure 1.5(b). On a similar diagram (Figure 4.10) we may also include stability curves for clusters of small size and, in the case considered here, those of radii less than 50 Å are particularly important. The curves labelled $C_{a_1}^T$, $C_{a_2}^T$ and $C_{a_3}^T$ on Figure 4.10 illustrate schematically the stability curves for clusters of radius $a_3 < a_2 < a_1 < 50$ Å.

Consider an alloy of composition c (Figure 4.10) which is step-quenched from T_s to T_1, where T_1 is below the G.P. zone solvus temperature $T_{G.P.}$. From the theory of section 1.3.2 and equations 1.14 and 1.23 we may write as the initial nucleation rate at T_1,

$$I(T_1) = A_2\left[\exp\left(\frac{-E_f}{kT_1}\right)\exp\left(\frac{-E_m}{kT_1}\right)\right]\left[\exp\left(-\frac{\Delta G_c}{kT_1}\right)\right] \qquad (4.3)$$

The nucleation rate is thus a product of a "kinetic factor" (the first square bracket on the right hand side), whose value is proportional to the solute diffusivity in the matrix, and a "thermodynamic factor" (the second square bracket on the right hand side) which involves the free energy barrier that a thermally activated solute cluster must overcome to become stabilized as a G.P. zone. The same equation has been considered by Lorimer and Nicholson[78] who correctly pointed out that an undercooling below $T_{G.P.}$ is necessary, for the nucleation rate to be high enough to produce observable G.P. zone formation. (When $T_1 = T_{G.P.}$, $r_c = \infty$ and $\Delta G_c = \infty$ (see equation 1.15), and the "thermodynamic factor" is zero; thus $I(T_{G.P.}) = 0$). Thus for $T_1 < T_{G.P.}$, the solute supersaturation, defined with respect to the G.P. zone solvus, provides the driving force for G.P. zone formation and the kinetics of this process are controlled by the value of the solute diffusivity in the matrix. After a step-quench to T_1 the value of the solute diffusivity is dependent upon the equilibrium vacancy concentration at T_1 (the small vacancy supersaturation produced on quenching from T_Q to T_1 is neglected). If it is supposed that the probability of forming a solute cluster at T_1 of radius larger than a_2 (see Figure 4.10) by a thermal fluctuation is negligible, then G.P. zone formation will be observed up to the critical temperature T_c, but not above this temperature. Clearly, the precise value of T_c will be dependent upon

a delicate balance between the "kinetic" and "thermodynamic" factors, which, respectively, increase and decrease exponentially with increase in the value of T_1.

Next, consider an ideal direct-quench from T_s to T_1 in which all excess vacancies are quenched-in. From the theory of section 1.4.2 and equation 1.25, the initial nucleation rate at T_1 is now given by

$$I(T_1) = A_2 \left[exp\left(-\frac{E_f}{kT_s}\right) exp\left(-\frac{E_m}{kT_1}\right)\right]\left[exp\left(-\frac{\Delta G_c}{kT_1}\right)\right] \qquad (4.4)$$

which differs from the initial nucleation rate after a step-quench to T_1 (see equation 4.3) since the quenched-in excess vacancy concentration increases the rate of diffusion in the solid solution by a factor

$$\frac{exp\,(-E_f/kT_s)}{exp\,(-E_f/kT_1)}.$$

The "kinetic" factor is increased in value, relative to that for the step-quench, and therefore the nucleation rate at T_1 is increased. It is suggested that, for $T_1 = T_c$, there is now an increased probability of forming a significant number of solute clusters of radius larger than a_2, and so G.P. zone formation will occur at an observable rate at this temperature and up to a temperature T_c' (maximum). For temperatures above T_c' (maximum) the probability of forming a solute cluster of radius greater than a_3 (see Figure 4.10) by a thermal fluctuation is negligible. In a real direct-quench the vacancy supersaturation at the start of ageing will be reduced owing to the migration of excess vacancies to sinks during the quench, but it is thought that the observed value of T_c' (Wood's metal) will approach the value of T_c' (maximum) fairly closely.

To this point the model is similar to that proposed by Lorimer and Nicholson[78], but it is now emphasized that it is believed that

without a detailed quantitative knowledge of the curves illustrated in Figure 4.10 and of the nucleation data, the magnitude of the temperature difference between T_c' (Wood's metal) and $T_{G.P.}$ cannot be estimated from the results of direct-quenching experiments.

Let us now consider the effect of relaxing some of the assumptions (a) - (d) so that the model can be applied to the Al-Zn and Al-Mg_2Si systems. The assumption of spherical G.P. zones is valid for the early stages of ageing in the Al-Zn system but not in the Al-Mg_2Si system when needle-shaped zones are thought to form. As pointed out by Pashley et al[81] it is possible that the small sized clusters in Al-Mg_2Si are equi-axed, and therefore approximately spherical, but even if the initial clusters are needle-shaped it seems likely that the curvature at either end of the needle (where growth and dissolution occurs predominantly) will decrease with increase in cluster size. So a similar effect of zone size on solubility is to be qualitatively expected.

As discussed in Chapter 3, the atomic volume of the spherical G.P. zones in Al-Zn alloys is slightly less than that of the matrix, so the clustering of Zn atoms in this system will introduce elastic strain into the cluster and also into the matrix surrounding the cluster. As also discussed in Chapter 3, there appears to be a significant cylindrical strain field associated with the needle-shaped zones in the Al-Mg_2Si system. Thus, it is necessary to relax assumption (a) and to consider the effect of a lattice strain on the nucleation of a G.P. zone.

Nabarro[128,129] has calculated that the total elastic strain energy per unit volume (E) of a coherent spherical nucleus of bulk modulus K in an isotropic elastic matrix of rigidity μ is

$$E = \frac{6\mu\delta^2}{1 + \frac{4\mu}{3K}} \qquad (4.5)$$

where δ is the misfit between the lattices. He also deduced that the elastic energy of a coherent nucleus can be reduced by no more than 20% if a shape other than spherical is assumed. Nabarro also considered the strain energy per unit volume of an incoherent spheroidal nucleus and derived the following expression for the case where all the strain is accommodated in the matrix:

$$E = 6\mu\delta^2 f\left(\frac{c}{a}\right) \qquad (4.6)$$

where a, a and c are the semi-axes of the spheroid and $f(\frac{c}{a})$ is a function of the shape of the spheroid. The strain energy is a maximum for a spherical nucleus and can be reduced if a shape other than spherical is assumed.

The strain energy is always positive, irrespective of the sign of δ, and this introduces an additional free energy nucleation barrier, so that the free energy change on forming a cluster of volume V is now given by

$$\Delta G = (\Delta G_V + E)V + \gamma A \qquad (4.7)$$

where A is the interfacial area. Nucleation is impossible unless $(\Delta G_V + E) < 0$. For a spherical cluster, maximization of equation 4.7 yields a critical radius

$$r_c = -\frac{2\gamma}{\Delta G_V + E} \qquad (4.8)$$

Thus, an increase in strain energy density will increase the critical nucleus size and a higher solute supersaturation is required for nucleation to occur. The upper limiting temperature for G.P. zone formation will thus be depressed in systems where the lattice strain is large.

Baker, Brandon and Nutting[130], Embury and Nicholson[76,131] and Taylor[132] have suggested that, in a case where the cluster is in a state of compression (an "interstitial" type precipitate), the elastic strain energy may be relieved partially by the incorporation of vacancies within the cluster. This will lead to a decrease in the critical nucleus size. It is suggested that this effect might make itself particularly apparent for nucleation in the neighbourhood of the critical temperature T_c. After a rapid direct-quench a large number of vacancies are available to become incorporated within the embyro cluster (compared to after a step-quench) and the associated strain relief will enable vacancy assisted nucleation to occur at temperatures which are higher than T_c.

It has also been suggested, by Hart[68], that vacancies which become incorporated within a cluster may act as an additional "chemical" constituent of the cluster and, perhaps, thereby lower its volume free energy, which would decrease the critical nucleus size at a given temperature. It is thought that this effect might be particularly important if the incorporated vacancies allow the solute and solvent atoms within the cluster to become ordered, if an ordered lattice has a lower volume free energy than a disordered lattice.

If, by the incorporation of vacancies within a solute cluster, the strain energy density and/or the volume free energy of the cluster are decreased this is a direct result of a modification to the structure of the solute cluster. It is suggested that such a modification in structure will effect the value of $T_{G.P.}$, which will be correspondingly increased since a solute cluster of given size will now be stable at a high temperature.

4.5.2 Application of the model to the Al-Zn and Al-Mg_2Si alloys

Three different mechanisms by which vacancies can aid G.P. zone nucleation have been discussed above:

(1) a purely "kinetic" effect, in which excess-vacancies can increase the probability of nucleation by increasing the solute diffusivity;

(2) an elastic strain relieving effect, in which vacancies become incorporated within an "interstitial" type of solute cluster and reduce the critical nucleus size;

(3) a "chemical" effect, in which a vacancy becomes a "chemical" constituent of the cluster and reduces its volume free energy.

It is informative to consider which of these possible mechanisms may be operative in the two types of alloy which have been studied.

Consider the Al-Zn alloy first. The atomic volume of the coherent G.P. zones in this system is known to be slightly less than that of the matrix (see Chapter 3), so the zones are of "vacancy" type and this would appear to preclude mechanism(2). The evidence in support of vacancy trapping by G.P. zones in this system put forward by Cohen et al[133] has been questioned by Carpenter[134]. This point is considered again in Chapter 7 where the results obtained by the author are interpreted in favour of the ideas of Carpenter. It is therefore believed that there is little conclusive evidence to confirm that vacancy trapping occurs to any significant extent. It is therefore concluded that the major effect of vacancies on the nucleation of G.P. zones in this system is derived from mechanism (1). The small observed difference between T_c and T_c' (Wood's metal) would seem to indicate that the vacancy concentration only has a secondary influence on the nucleation kinetics in this system, the major factor being the solute supersaturation. The slightly smaller difference

between T_c and T_c' (Wood's metal) for the 26%Zn alloy as compared to the 17.5%Zn alloy is also consistent with mechanism (1), for the higher is the absolute value of T_c, the higher is the associated equilibrium vacancy concentration, and thus the lower is the vacancy supersaturation that can be quenched-in by a direct-quench.

Now consider the Al-1.2%Mg_2Si alloy. Let us first recall what is known about the coherency of the needle-shaped zones in this system. In Chapter 3 it was shown that the zones are coherent with the matrix along their major axis (they appear to have almost the same periodicity as the matrix along this direction). In directions normal to the needle-axis the zones are believed to take on an arrangement that is different from the matrix. Such zones are only partially coherent and are therefore fundamentally different from the completely coherent G.P. zones of the Al-Zn system. The evidence of Thomas[97] indicates that the strain field in directions normal to the needle-axis is "interstitial" in character. The evidence of Lutts[90], which was reviewed in Chapter 3, and the marked "slow reaction"observed with this alloy (see Chapter 1) can be understood if it is considered that vacancies become incorporated within the needle-shaped zones and in so-doing help to relieve the cylindrical strain associated with the cluster. If this is so, then mechanism (2) above could play an important role in aiding the nucleation of the needle-shaped zones. Mechanism (3) may play a part as well if the atomic arrangement of solute and solvent atoms within the zones is important. In addition, mechanism (1) could make a significant contribution towards aiding the nucleation, so it is possible that all three mechanisms may operate simultaneously. Which of the mechanisms plays the dominant role cannot, with the present knowledge, be ascertained in a quantitative way.

It is relevant at this point, however, to consider the marked

catalyzing effect of matrix dislocations on the nucleation of the needle-shaped zones in the Al-Mg_2Si system. The theory of heterogeneous nucleation on dislocations has been considered by Nicholson[135] and Cahn[136], who have shown that the regions of tensile and compressive strain associated with the edge-component of a dislocation can have a catalyzing effect on the nucleation. In the case of a coherent or partially coherent precipitate the most favourable region for heterogeneous nucleation will be that region of the dislocation's strain field that affords greatest relief of the misfit. In the case of the needles in Al-Mg_2Si, the misfit is normal to the needle-axis and, as was seen in Chapter 3, only one of the three possible sets of needles are nucleated on any given dislocation line. The experimental observation that needles can be nucleated on dislocations at much higher temperatures than homogeneously in the matrix again suggests that lattice strain is responsible for depressing the critical temperature T_c to a low value, i.e. a high solute supersaturation, calculated with respect to the equilibrium solvus, is required for homogeneous nucleation to occur. After a direct-quench, when excess-vacancies are available to relieve partially the lattice strain, homogeneous nucleation may occur at a significantly lower solute supersaturation, which would account for the relatively large difference between T_c and T_c' (Wood's metal). The fact that dislocation-nucleated needles can be formed at a temperature above T_c' (Wood's metal) can be explained if a dislocation is more efficient at relieving lattice-strain around a needle than the incorporation of vacancies within the needle.

Matrix dislocations do not appear to catalyze G.P. zone formation in the Al-Zn system. As mentioned in Chapter 3, the probable reason for this is that the misfit between a G.P. zone and the matrix in this alloy system is extremely small, so there is little to be gained

energetically by preferential nucleation on a dislocation.

The practical significance of the parameters T_c, T_c' and $T_{G.P.}$ will become evident in the following chapters, particularly in relation to two-step ageing treatments. The theoretical significance of the parameters T_c, T_c' and $T_{G.P.}$ is discussed critically in Chapter 8.

CHAPTER 5

TWO-STEP AGEING BEHAVIOUR OF AN Al-1.2%Mg_2Si ALLOY

5.1 INTRODUCTION

The commercial potentiality of aluminium-base alloys which contain an addition of Mg_2Si as the major age-hardening constituent has been recognised for several years. This has led to a number of detailed investigations of the age-hardening behaviour of the ternary Al-Mg_2Si alloys[80,81,137-144]. Much of the experimental work has been concerned with heat treatments that are similar to those used commercially, in which a sample is first solution treated, then quenched to room temperature and subsequently artificially aged in the temperature range 160°C to 175°C for a period of about 24 hours. These studies have revealed an important phenomenon, known as "the delayed-ageing effect" which occurs if the alloy is stored at room temperature for a few hours between quenching and artificial ageing. A sample that is artificially aged immediately after quenching is found to have a final level of tensile properties which is superior to that of a sample which is stored at room temperature for a few hours before ageing. Unfortunately, a period of delay is usually inevitable in commercial processing and, since it is desirable to exploit the full potential strength of this alloy, it is important to understand this phenomenon and to find ways of overcoming it.

Nock[137] showed that the tensile strength of a quenched Al-1.5%Mg_2Si alloy increases fairly rapidly at room temperature during the first few hours of ageing but thereafter the rate of increase is considerably slower. He showed, however, that the strength is still increasing at a measurable rate even after 10 years of ageing. This result is consistent with more recent resistometric observations by

Panseri and Federighi[66] who detected an initial "fast reaction" at room temperature which is followed, after about 4 hours, by a "slow reaction". A correlation between the amount of low temperature ageing and the onset of the delayed-ageing effect was established by Renouard and Meillat[139] who showed that by storing samples at a low temperature (0°C or - 20°C) the natural ageing was even slower than that at room temperature and, as a consequence, a longer safe delay time was then available before inferior properties were produced after artificial ageing. They also showed that a short artificial pre-ageing treatment, if carried out immediately after quenching could reduce (and, with the appropriate pre-treatment, eliminate) the loss of final tensile properties in samples which were subsequently stored at room temperature for a week before being artificially aged.

Fortin made two interesting observations.[141] Firstly, he showed that the deleterious effect of delay on samples of a commercial Al-1.45%Mg_2Si alloy was confined to solution treatment with $T_s > 480°C$ and that for temperatures below this value the delay period could actually be beneficial, although the final mechanical properties produced by the latter treatment were too low in value to be of practical importance. Secondly,[142] he showed that, with normal solution treatment, the detrimental effect of room temperature delay can be obviated if the sample is subjected to a short ($<$ 3 min) high temperature (240°C - 400°C) anneal between storage and artificial ageing.

Recently, Pashley, Rhodes and Sendorek[80] have studied the delayed-ageing behaviour of a high purity Al-1.2%Mg_2Si alloy in considerable detail and their results confirmed many of the earlier observations. They also showed that an addition of 0.24%Cu to the alloy slows down the rate of natural ageing and thereby increases the safe delay time before the onset of loss of properties due to storage. These workers carried

out, in addition, an electron metallographic investigation with thin foils of the same alloy. The significant result of this work was a correlation between the solute clustering that occurred during natural ageing (this was not detected by electron microscopy but was inferred from the observed increase in tensile properties) and the precipitation which formed during artificial ageing. The final size and distribution of needle-shaped precipitates (see Chapter 3), as observed by electron microscopy, in a sample that had been stored at room temperature for a sufficient length of time to induce inferior tensile properties were appreciably coarser than in a sample which was immediately aged (a quantitative assessment of this result was obtained by determining the distribution in needle-lengths as a function of delay time). A tentative explanation of this coarsening behaviour was put forward in which it was proposed that the reduction in matrix solute supersaturation associated with the clustering of solute atoms at room temperature has a deleterious effect on the stability of solute clusters at the beginning of artificial ageing. This approach recognised that, in this case, the final precipitation is developed by a two-step ageing treatment in which the alloy is firstly aged at room temperature and then subsequently aged at an elevated temperature.

In order to explore the consequences of this approach further, an investigation was undertaken by Pashley, Jacobs and Vietz[81] into the basic processes affecting a wide range of different two-step ageing treatments of an Al-1.2%Mg_2Si alloy. The results of these experiments were then used to develop a model which could qualitatively account for the observed response of the alloy to any chosen type of two-step ageing treatment.

The purpose of this chapter is to discuss some of the more

important aspects of this model for two-step ageing and to amplify some of the ideas contained in it. The chief extension of the model involves the incorporation of the G.P. zone solvus temperature as one of the parameters which must be considered during a two-step ageing treatment. The concept of a critical temperature T_c, as defined in Chapter 4, is still retained and shown to be the most useful parameter for aiding the interpretation of the response of the alloy to a two-step ageing treatment.

The model is described in section 5.2 and then illustrated by a few selected results in sections 5.3 and 5.4.

5.2 THE MODEL FOR TWO-STEP AGEING

In this section a summary is given of the salient points which were considered in the model for two-step ageing, as proposed by Pashley, Jacobs and Vietz[81]. In many cases the same results are derived by an alternative approach, which is based on the ideas outlined in section 4.5.1.

The aim of the model was to describe the basic factors which control the precipitation of solute clusters during a two-step ageing-treatment. A simple binary alloy was considered in which spherical, strain-free, clusters are formed during isothermal ageing at T_1 ($< T_c$). One of the important results obtained by the model was a stability criterion which defined the necessary conditions under which solute clusters, formed during a pre-treatment at T_1, would continue to grow if the ageing temperature was suddenly raised to T_2. This behaviour was described as "seeding" clusters at T_1 for growth at T_2. It is emphasized that the seeded clusters at T_2 were considered to be identical, in all respects apart from size, to those formed at T_1. This stability criterion will now be derived with the aid of a stability curve of the type introduced in Chapter 4.

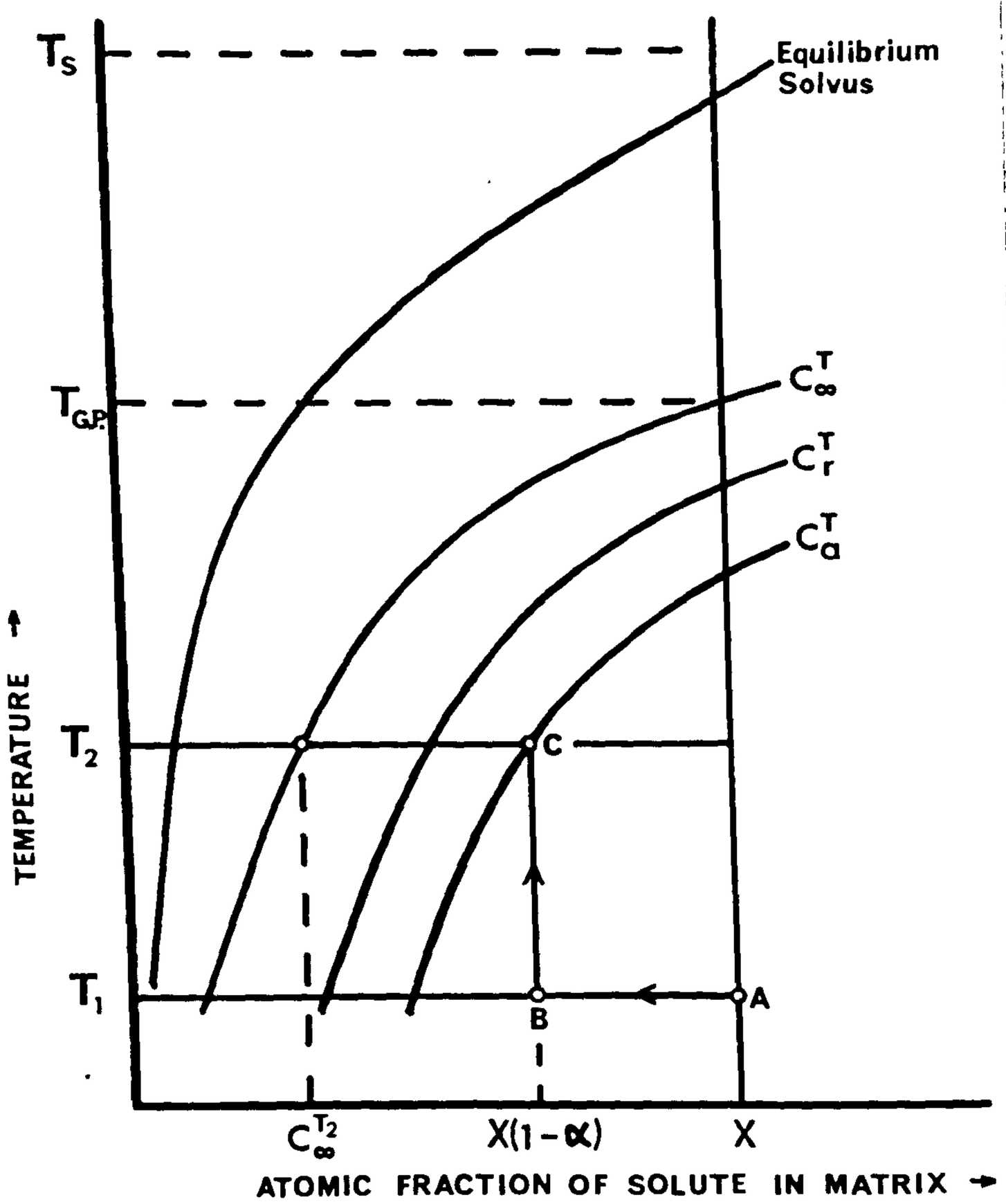

Figure 5.1 The general form of the stability curves for G.P. zones. The curve labelled C_∞^T is the G.P. zone solvus. The stability curves for small sized zones, of radius r and a (r > a), are labelled C_r^T and C_a^T, respectively.

Consider Figure 5.1. Let X be the atomic fraction of solute atoms distributed at random within the alloy at the solution treatment temperature T_s. If the alloy is now rapidly quenched from T_s to T_1 ($< T_c$) then we may represent the fully supersaturated alloy by the point A in Figure 5.1. During a subsequent isothermal pre-treatment at T_1 let a fraction α of the solute atoms precipitate in the form of clusters. The solute concentration in the matrix after this pre-treatment will be reduced to $X(1 - \alpha)$ (point B on the diagram) and we assume that this is uniformly distributed between the clusters. If the alloy is now up-quenched to T_2 (point C on the diagram) we have to decide whether or not the clusters formed at T_1 will remain stable. To do this, we first of all note that the remaining matrix solute supersaturation (i_R) at T_2 is given by*

$$i_R = \frac{X(1-\alpha)}{C_\infty^{T_2}} \qquad (5.1)$$

where $C_\infty^{T_2}$ is the solute concentration in equilibrium with a cluster of infinite radius at T_2. Next, suppose that the point C lies, as shown, on the stability curve C_a^T for a solute cluster of radius a. This tells us that, after the pre-treatment described above, a cluster of radius a will be in equilibrium at T_2, since, according to the Gibbs-Thomson equation (see section 4.5.1),

$$a \log_e i_R = \frac{2\gamma\Omega}{kT_2} = K \qquad (5.2)$$

where K is a temperature dependent constant (it is assumed that γ and Ω are independent of cluster size). For a cluster of radius r, which is larger that a, the corresponding stability curve C_r^T will be above C_a^T

* The nomenclature of Pashley et al[81] is changed to be consistent with that of this dissertation.

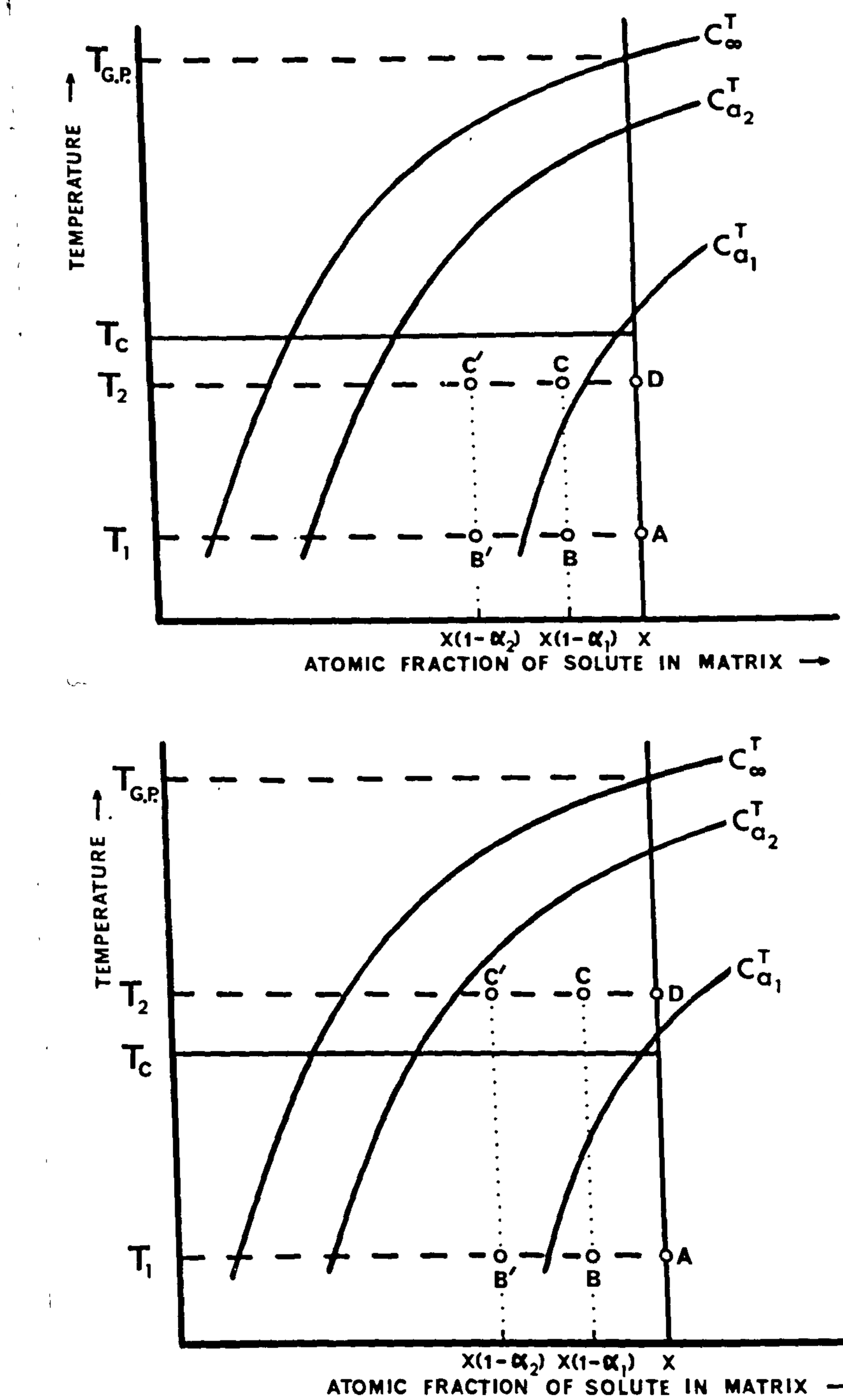

(a)

(b)

Figure 5.2 The general form of the stability curves for G.P. zones for the two cases when (a) $T_2 < T_c$ and (b) $T_2 > T_c$.

(see section 4.5.1). Thus, for a cluster of radius r, immediately after the up-quench to T_2 (point C on the diagram), we may write

$$r \cdot \log_e i_R > K \qquad (5.3)$$

Clearly, a cluster of radius r will be stable at T_2 and capable of further growth since the point C lies below the C_r^T stability curve. So equation 5.3 represents the criterion for stability such that the clusters formed at T_1 will continue to grow at T_2. This is the important stability condition that was derived, by a slightly different method, by Pashley, Jacobs and Vietz[81]. The implications of this result are now discussed for two different types of two-step ageing treatment.

After any given ageing time at T_1 let there be a distribution in cluster sizes whose radii range between maximum and minimum values of r_{max} and r_{min}.

Case (1) $T_2 < T_c$.

The situation is illustrated, schematically, by Figure 5.2(a). Consider, first of all, a short pre-ageing treatment at T_1 in which a fraction, α_1 of solute atoms is precipitated in the form of solute clusters. At the end of this pre-treatment let $r_{max} = a_1$. If the alloy is now up-quenched from T_1 to T_2 (B $\rightarrow$ C on the diagram) we can use the approach developed above to decide if the clusters will remain stable at T_2. Since the point C is shown above the stability curve labelled $C_{a_1}^T$ it follows that in this case even the maximum sized clusters are unstable at T_2 and thus all clusters will be initially unstable and will start to dissolve. However, since $T_2 < T_c$, all the clusters need not necessarily dissolve completely. Some of the smaller size clusters will, indeed,

completely dissolve and so feed-back solute atoms into the matrix. We may represent this process schematically on the diagram by imagining that the matrix solute concentration moves progressively along the line C → D. The increase in solute supersaturation provided by this process may eventually be sufficient to re-stabilize some of the larger clusters. The number re-stabilized will depend upon the relative rates of dissolution of clusters of different sizes and the initial size distribution. However, since the remaining solute supersaturation never attains the higher value expected after a direct-quench to T_2, the number of clusters that is re-stabilized and grown at T_2 after a short pre-treatment at T_1 is expected to be less than that nucleated and grown by direct-ageing at T_2. This is an important result and will be discussed again later.

Next, consider a longer pre-treatment at T_1 in which a larger fraction α_2 of solute atoms is precipitated in clusters. At the end of this pre-treatment let $r_{min} = a_2$. If the alloy is now up-quenched from T_1 to T_2 (B' → C' on the diagram) we again have to consider if these clusters remain stable. In the situation shown on the diagram the point C' is below the $C^T_{a_2}$ stability curve. We deduce from this that the minimum sized clusters, of radius a_2, will be stable at T_2 and therefore all clusters will remain stable. So this represents a case where all clusters can be seeded for growth at T_2.

Case (2) $T_2 > T_c$

The situation is described by Figure 5.2(b). Consider the same short pre-treatment at T_1, as in case (1). Again, let $r_{max} = a_1$ at point B. If the alloy is now up-quenched from T_1 to T_2 (B → C on the diagram) then the point C, as illustrated, is above the $C^T_{a_1}$ stability curve. Thus all clusters are initially unstable at T_2 and in this case they will

completely dissolve since a cluster of radius a_1 is even unstable at point D, i.e. under conditions of full supersaturation.

Next, consider the longer pre-treatment at T_1. Again, let $r_{min} = a_2$ at point B'. If the alloy is now up-quenched to T_2 (point C' on the diagram) then all clusters will continue to grow at T_2 since, as illustrated, the point C' lies below the stability curve $C^T_{a_2}$ for clusters of the minimum radius.

Clearly, the behaviour of an alloy is critically dependent upon the value of T_2 and whether it is above or below T_c. Inspection of Figure 5.2(b) shows that clusters can never be seeded for growth above $T_{G.P.}$, where $T_{G.P.}$ is the G.P. zone solvus temperature for the full matrix solute concentration of the alloy. Thus, the behaviour discussed in case (2) is limited to $T_c < T_2 < T_{G.P.}$.

Another important factor concerns the development of solute clusters during pre-treatment at T_1. Pashley et al[81] examined the situation where cluster development at T_1 takes place by following distinct but overlapping stages; (1) a nucleation stage during which the number of clusters increases with time; (2) a second stage during which the density of clusters (N) remains almost constant and cluster growth is accompanied by a corresponding decrease in the matrix solute concentration; (3) a final stage, which begins as the solute concentration in the matrix approaches the value in equilibrium with a very large cluster, during which the density of solute clusters decreases (Ostwald ripening). Stage (2) was assumed to be the most important stage for the types of pre-treatment that we[81] considered. The reasonable assumption was adopted that the lower the value of T_1 the higher will be the value of N. Thus, for a given pre-treatment in which a fraction α of solute is precipitated, the cluster sizes will be smaller for a low value of T_1 compared to that

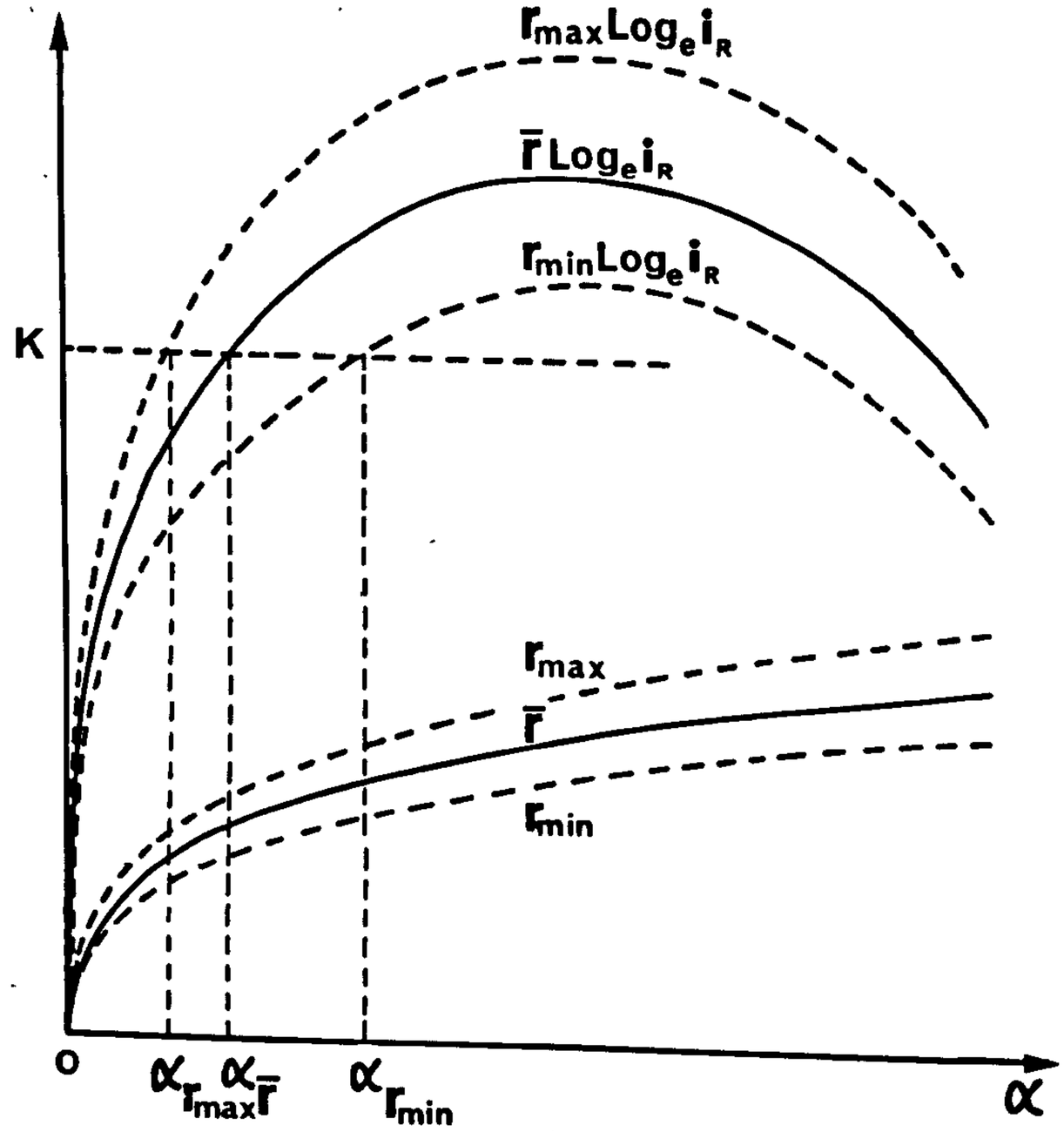

(a)

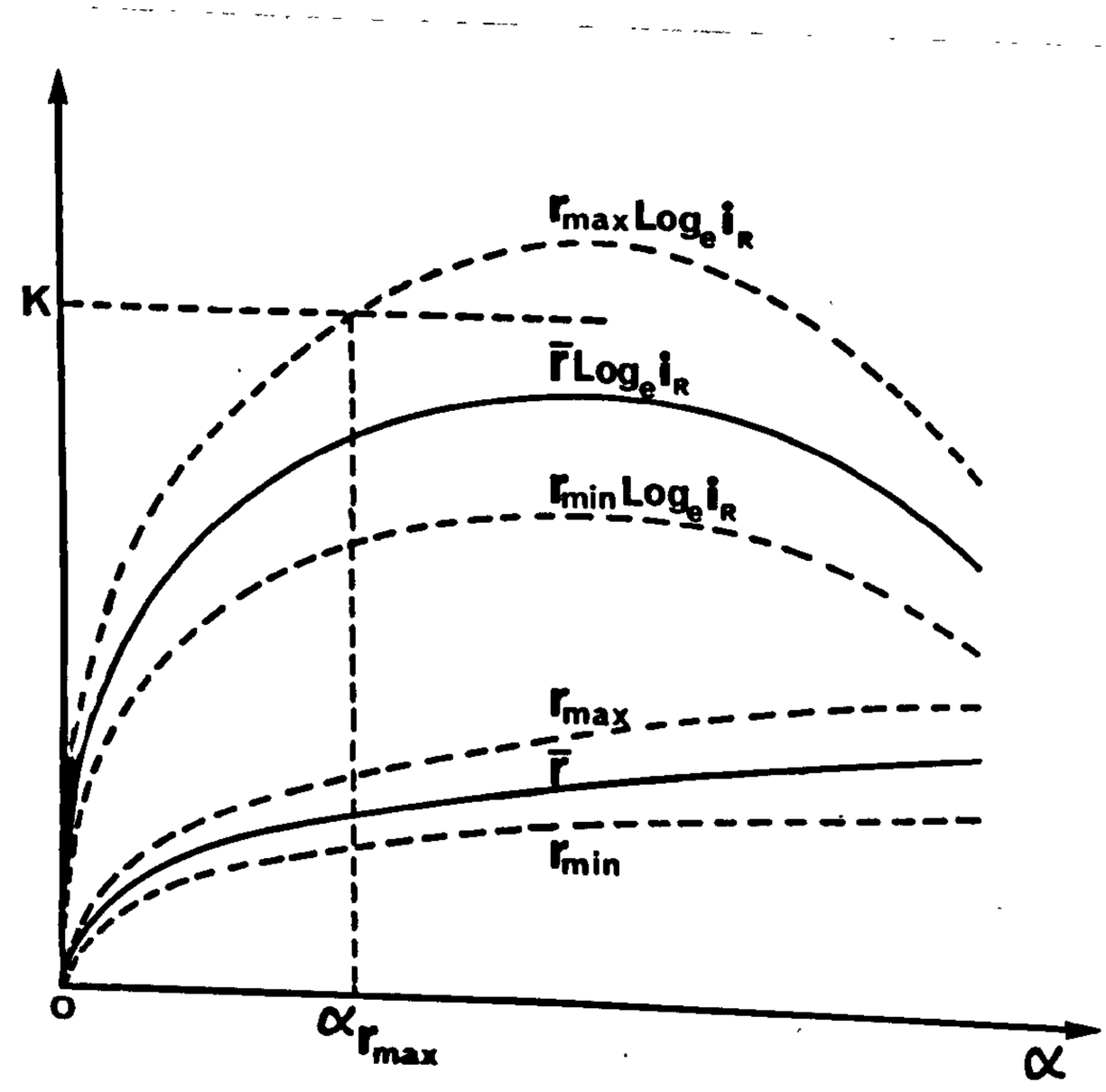

(b)

Figure 5.3 The general variation of the stability criterion with changes in the fraction α of solute atoms precipitated, when the sizes of clusters are distributed between r_{min} and r_{max} ; (a) all clusters can be stabilized at T_2 and (b) only a small proportion of clusters can be stabilized at T_2.

for a high value of T_1. The number of clusters that can be seeded at T_2 is thus critically dependent upon the value of T_1. Pashley et al[81] considered two important cases and we illustrated our arguments by two stability curves, which are reproduced here as Figures 5.3(a) and (b).

Figure 5.3(a) illustrates a case where a sufficiently long pre-treatment at T_1 is capable of stabilizing all of the clusters at T_2. The diagram is drawn for a high value of T_1 and the lower three curves illustrate, schematically, the cluster development during ageing at T_1, ($\bar{r}$ is the cluster of average size). The upper three curves show the variation of $r \log_e i_R$ for $r = r_{max}$, $\bar{r}$, r_{min}, respectively. The horizontal dashed-line represents the stability constant K of equation 5.3. Application of the stability criterion shows that clusters of maximum size (r_{max}) are the first to be stabilized and, as α increases from $\alpha_{r_{max}}$ towards $\alpha_{r_{min}}$, progressively more clusters become stabilized until all are stabilized for $\alpha > \alpha_{r_{min}}$.

Figure 5.3(b) illustrates the behaviour expected for a lower value of T_1, where the cluster density is higher. No clusters are seeded for growth until a fraction $\alpha_{r_{max}}$ of solute has been precipitated. Longer pre-treatments lead to a slight increase in the number of clusters seeded but, in the situation illustrated, the optimum pre-treatment is only capable of stabilizing a small proportion of the clusters. This result led Pashley et al[81] to define the temperature $(T_1)_{min}$ as that value of T_1, for a given value of T_2, above which it is possible to stabilize a large proportion of the clusters formed at T_1. It was realized that this definition was not rigorous, but the concept is useful as a means of classifying the observed response of an alloy to different two-step ageing treatments.

Two important modes of behaviour may now be distinguished,

depending upon whether T_2 is above or below T_c. Each mode may be sub-divided, depending upon whether T_1 is above or below the appropriate value of $(T_1)_{min}$.

Mode (1) : $T_2 < T_c$

(a) Since $T_2 < T_c$, clusters can be nucleated and grown during ageing after a direct-quench to T_2.

(b) If a sufficiently long pre-treatment is given at T_1 then clusters can be seeded for growth at T_2. If $T_1 > (T_1)_{min}$, then the appropriate pre-treatment is capable of seeding all clusters for growth at T_2. If $T_1 < (T_1)_{min}$, then only a proportion of the clusters can be seeded, however, the number seeded may still be significantly higher than that normally produced by direct-quenching to T_2.

(c) For a pre-treatment at T_1 such that $\alpha < \alpha_{r_{max}}$ (see Figures 5.3(a) and (b)), no clusters will remain stable initially when the temperature is raised to T_2. For very short pre-treatments, a large proportion of the smaller solute clusters formed at T_1 will completely dissolve and so the matrix solute supersaturation will be raised to a value which is only slightly less than that produced by a direct-quench to T_2. Re-stabilization of some of the remaining large clusters will occur and some fresh nucleation may take place as a result of thermally activated solute fluctuations. Since these two processes take place under the condition of almost full matrix solute supersaturation, the density of growing clusters at T_2 will be similar to that normally produced after a direct-quench to T_2.

For a slightly longer pre-treatment some re-stabilization of

the larger clusters, which are initially unstable at T_2 may occur in the manner described in case (1), above. This re-stabilization will occur under the condition of a reduced solute supersaturation, so that the size and distribution of precipitates at the completion of the two-step ageing treatment is expected to be coarser than that observed after either a direct-quench to T_2 or a quench to T_1 followed by immediate ageing at T_2.

Mode (2) : $T_c < T_2 < T_{G.P.}$

(a) Solute clusters can be formed after a direct-quench to a temperature between T_c and T_c', where the value of T_c' depends upon the quenching medium used (see Chapter 4).

(b) A short pre-treatment at T_1, such that $\alpha < \alpha_{r_{max}}$ (see Figures 5.3(a) and (b)) is insufficient to seed clusters for growth at T_2 and all clusters will dissolve.

(c) If $T_1 > (T_1)_{min}$, a suitably long pre-treatment at T_1 will be sufficient to seed all clusters for growth at T_2. For $T_c < T_2 < T_c'$, the final precipitation will be on a finer-scale than that produced by a direct-quench to T_2. For T_c' (maximum) $< T_2 < T_{G.P.}$, clusters will be stabilized for growth at T_2, whereas none can be nucleated by direct-quenching to T_2.

(d) If $T_1 < (T_1)_{min}$, only a small proportion of the clusters formed at T_1 can be seeded for growth at T_2.

These two modes of behaviour are clearly predicted by the model and in the next section they are illustrated by experimental results obtained by two-step ageing experiments which were carried out[81] with an Al-1.2%Mg_2Si alloy. The excellent qualitative agreement between the predictions of the model and the experimental results is considered as a

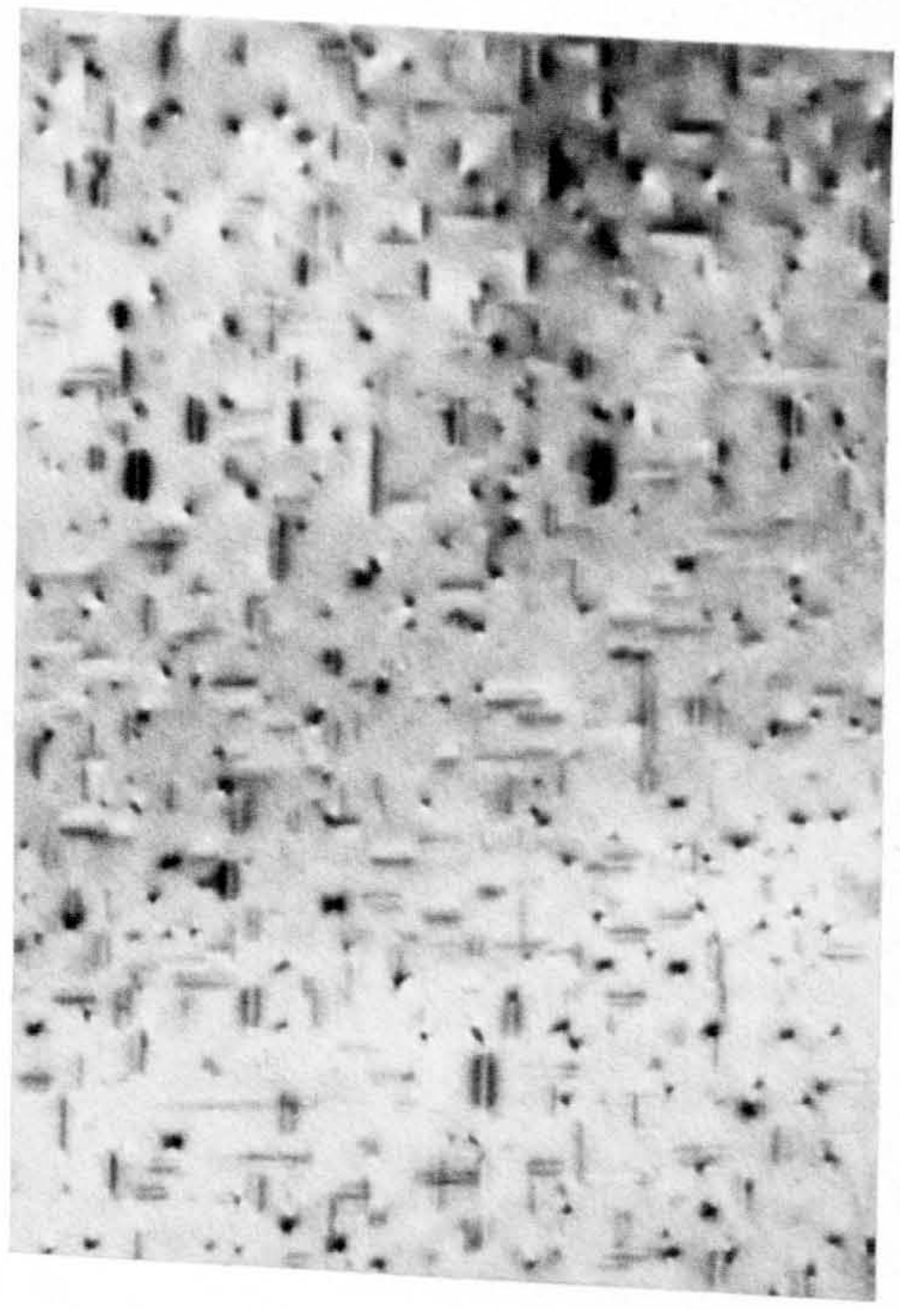

(a)

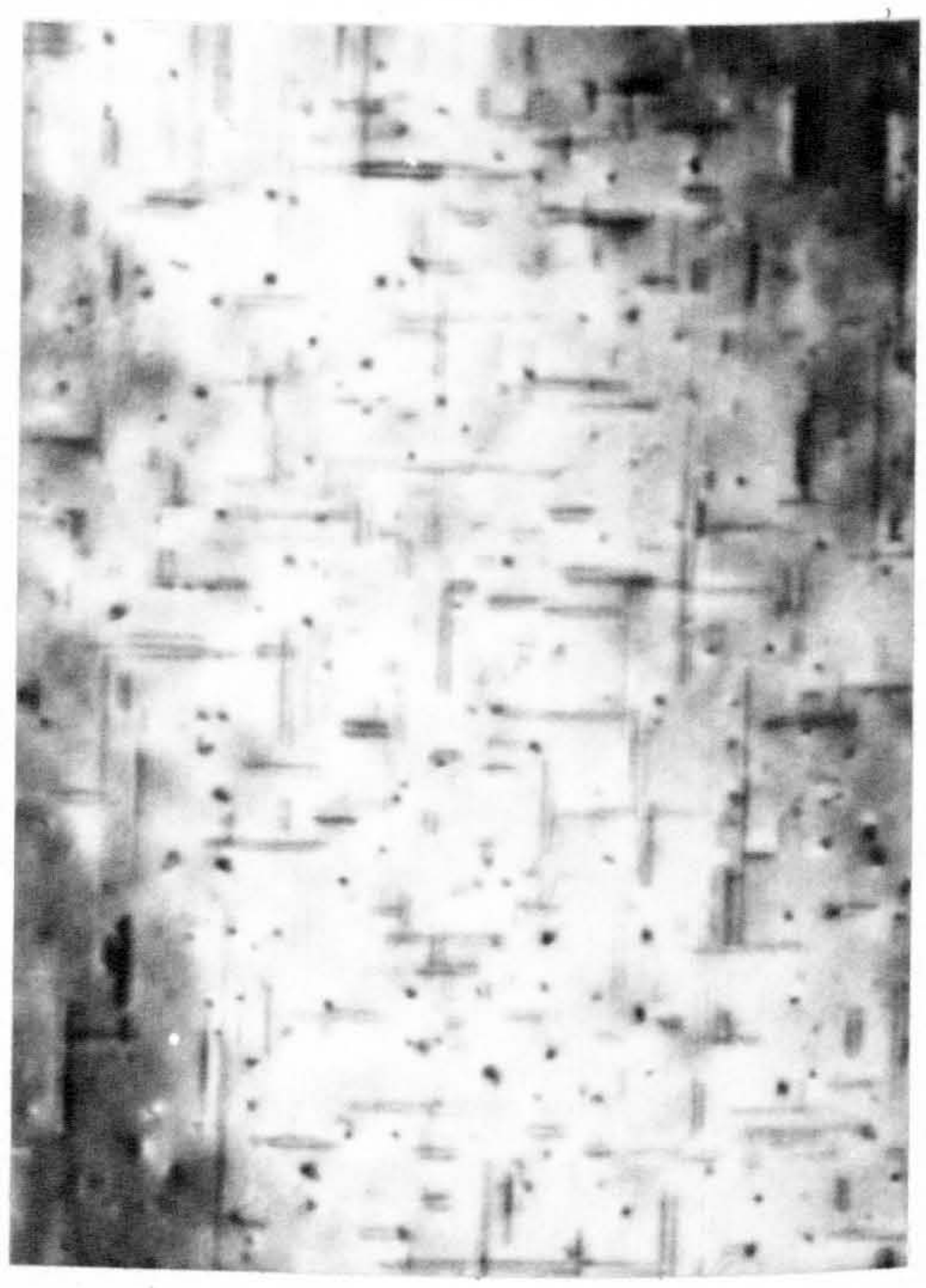

(b)

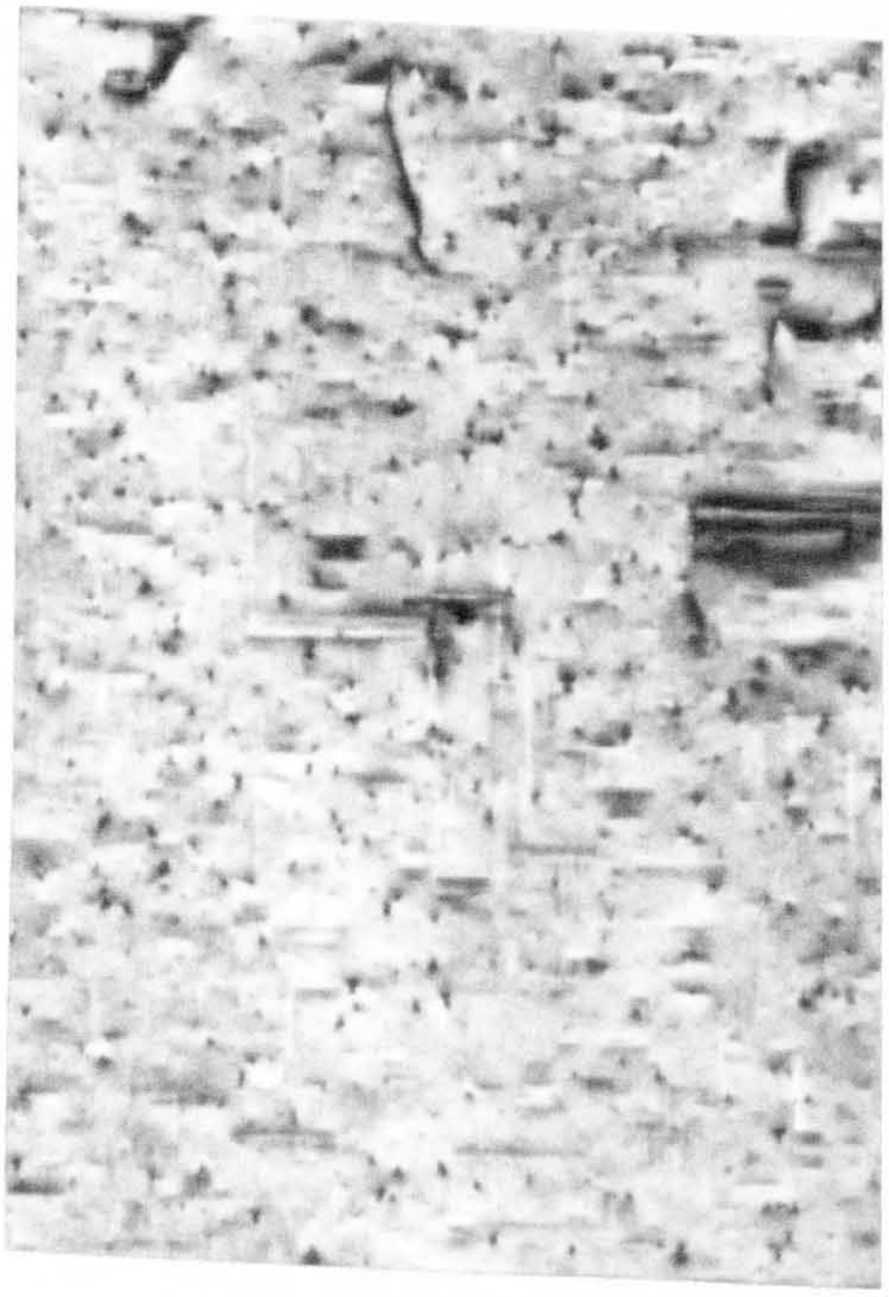

(c)

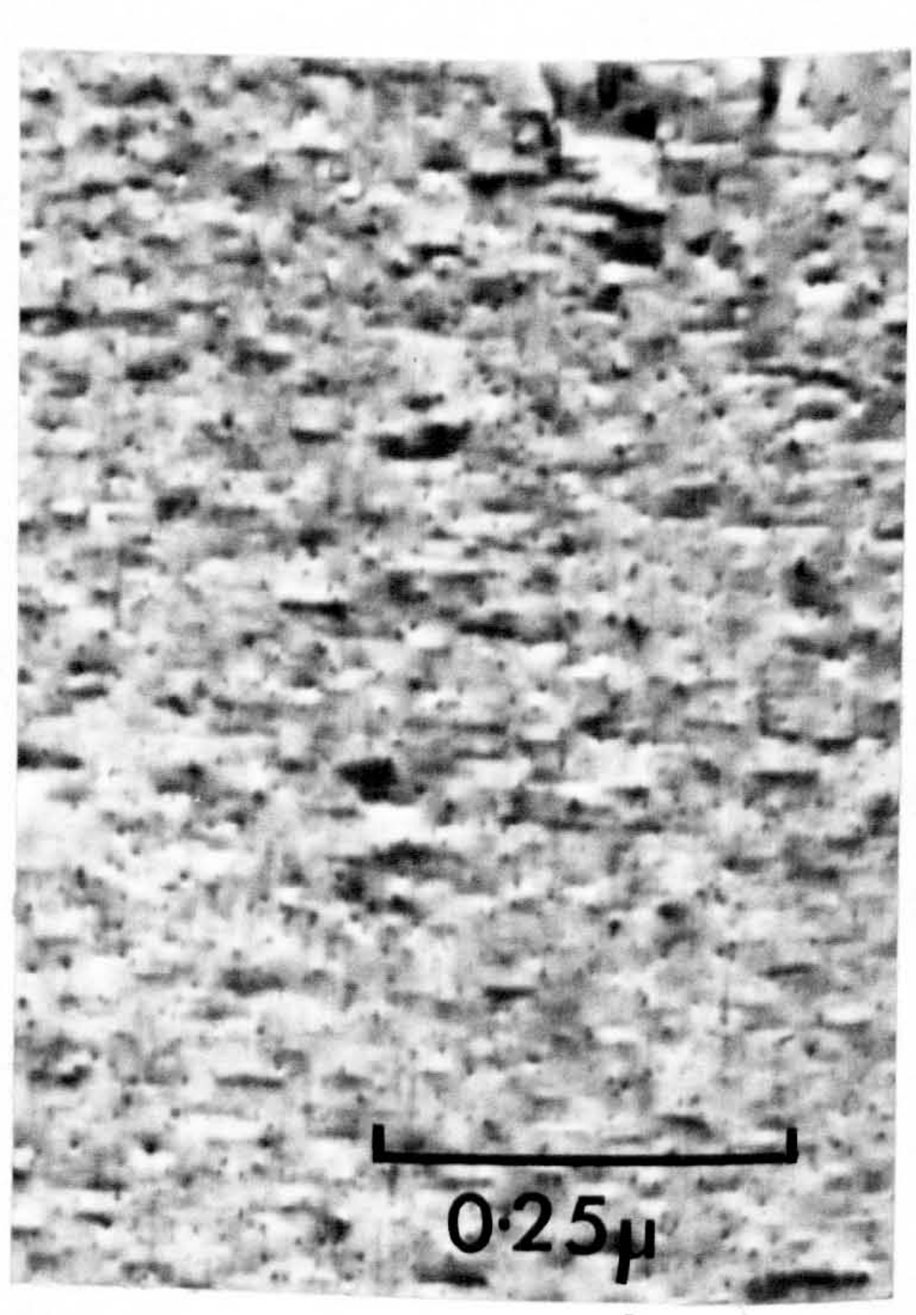

(d)

Figure 5.4 Al-1.2%Mg_2Si : The effect of pre-treatment at room temperature on the subsequent ageing of the alloy for 24 hours at 160°C. (a) a few seconds at room temperature; (b) 3 hours at room temperature; (c) 10 weeks at room temperature; (d) $2\frac{1}{2}$ years at room temperature.

good justification for the model. Clearly, a quantitative approach should attempt to take into account the fact that the solute clusters in Al-Mg_2Si alloys are needle-shaped and give rise to lattice strain. Further discussion of this point is postponed until Chapter 8.

5.3 EXPERIMENTAL RESULTS

Throughout the following description of the experimental observations obtained with an Al-1.2%Mg_2Si alloy[81] the following results, which were established in Chapter 4, should be borne in mind; (1) T_c = 190°C ± 10°C and (2) T_c' (Wood's metal) = 245°C ± 5°C.

Mode (1) : $T_2 < T_c$

For the example chosen to illustrate this mode the value of T_1 was room temperature and T_2 was 160°C. This is the "conventional" two-step ageing treatment that was investigated by Pashley, Rhodes and Sendorek[80] in which a coarsening of the final precipitate microstructure was observed in samples that were delayed at room temperature for a few hours between quenching (T_s = 560°C; quench into iced cold water) and ageing at 160°C for 24 hours. This behaviour is illustrated by Figures 5.4(a) and (b). Figure 5.4(a) shows the typical microstructure observed in a sample that was quenched into water at 20°C and then immediately up-quenched to 160°C and aged for 24 hours. The size and distribution of precipitates is very similar to that normally produced in a sample that is direct-quenched into oil at 160°C and aged for 24 hours (cf. Figure 3.4.(a)). Figure 5.4.(b) shows the coarsening of the final precipitate microstructure exhibited by a sample that was delayed at room temperature for 3 hours before being aged at 160°C.

According to the model described above, prolonged storage at

room temperature should induce appreciable seeding of clusters for growth at 160°C. That this is the case is illustrated by Figures 5.4(c) and (d). Pashley et al[81] showed that a sample stored at room temperature for 10 weeks exhibited fine-scale precipitation after subsequent treatment at 160°C (Figure 5.4(c)). However, since this precipitate microstructure is no finer than that produced in a sample which was direct-quenched to 120°C and aged to peak hardness (two weeks of ageing[143]) we[81] deduced that probably only a small proportion of the clusters grown at room temperature had been seeded for growth at 160°C. We[81] therefore suggested that room temperature is below $(T_1)_{min}$ for the case where the alloy is subsequently aged at 160°C. Lorimer[79] has correctly pointed out that, since solute clustering at room temperature occurs at a detectable rate[66] over a period of many years, a storage time which is considerably longer than 10 weeks may be required to ensure that the maximum proportion of clusters are seeded for growth at 160°C. Recently, a sample that was stored at room temperature for $2\frac{1}{2}$ years before ageing at 160°C for 24 hours was examined and its final microstructure is illustrated by Figure 5.4(d). The density (i.e. no./unit vol.) of seeded clusters is only slightly higher than was produced by the pre-treatment of 10 weeks at room temperature. Unfortunately, no precipitation was detected by electron microscopy in a sample that was only aged for $2\frac{1}{2}$ years at room temperature, so the density of clusters formed during natural ageing is still unknown. However, since this large increase in storage time does not appear to have significantly increased the density of clusters seeded at 160°C, the suggestion of Pashley et al[81], that $(T_1)_{min} > 20°C$, seems to be reasonably justified.

Since the coarsening of the final microstructure associated with a few hours delay between quenching and ageing has a detrimental effect

on the final tensile properties of the alloy it would be anticipated that the marked refining of the microstructure, associated with several months delay before ageing, might lead to a recovery of the tensile properties. It is therefore interesting to note that Nock[137] observed a recovery of the tensile strength with his alloy, to a level obtained by immediate ageing at 160°C, after storage for 6 months.

Finally, it should be mentioned that Pashley et al[81] carried out a second type of two-step ageing treatment which can be classified under mode (1). This involved pre-treatment for various times at 120°C followed by ageing for 24 hours at 160°C. In this case a short (15 minutes) pre-treatment at 120°C produced a marked coarsening of the final precipitate microstructure compared to that produced in a sample which was direct-quenched to 160°C and aged for 24 hours. For longer ($\geqslant$ 30 minutes) pre-treatments at 120°C, fine-scale precipitation was produced which was characteristic of that normally formed in a sample which was direct-quenched and aged at 120°C for 2 weeks. It was therefore concluded that a pre-treatment of 30 minutes at 120°C was sufficient to seed all clusters for growth at 160°C, i.e. 120°C $> (T_1)_{min}$ for subsequent ageing at 160°C. This is the type of behaviour predicted by the graph of Figure 5.3(a).

Mode (2) : $T_c < T_2 < T_{G.P.}$

Three different two-step ageing treatments were studied[81], with the following values for T_1 and T_2 :

(a) T_1 = 160°C, T_2 = 200°C

(b) T_1 = 160°C, T_2 = 250°C

(c) T_1 = Room temperature, T_2 = 250°C.

The results obtained with heat-treatments (a) and (b) will be described first and these will be followed by the results of heat-treatment (c).

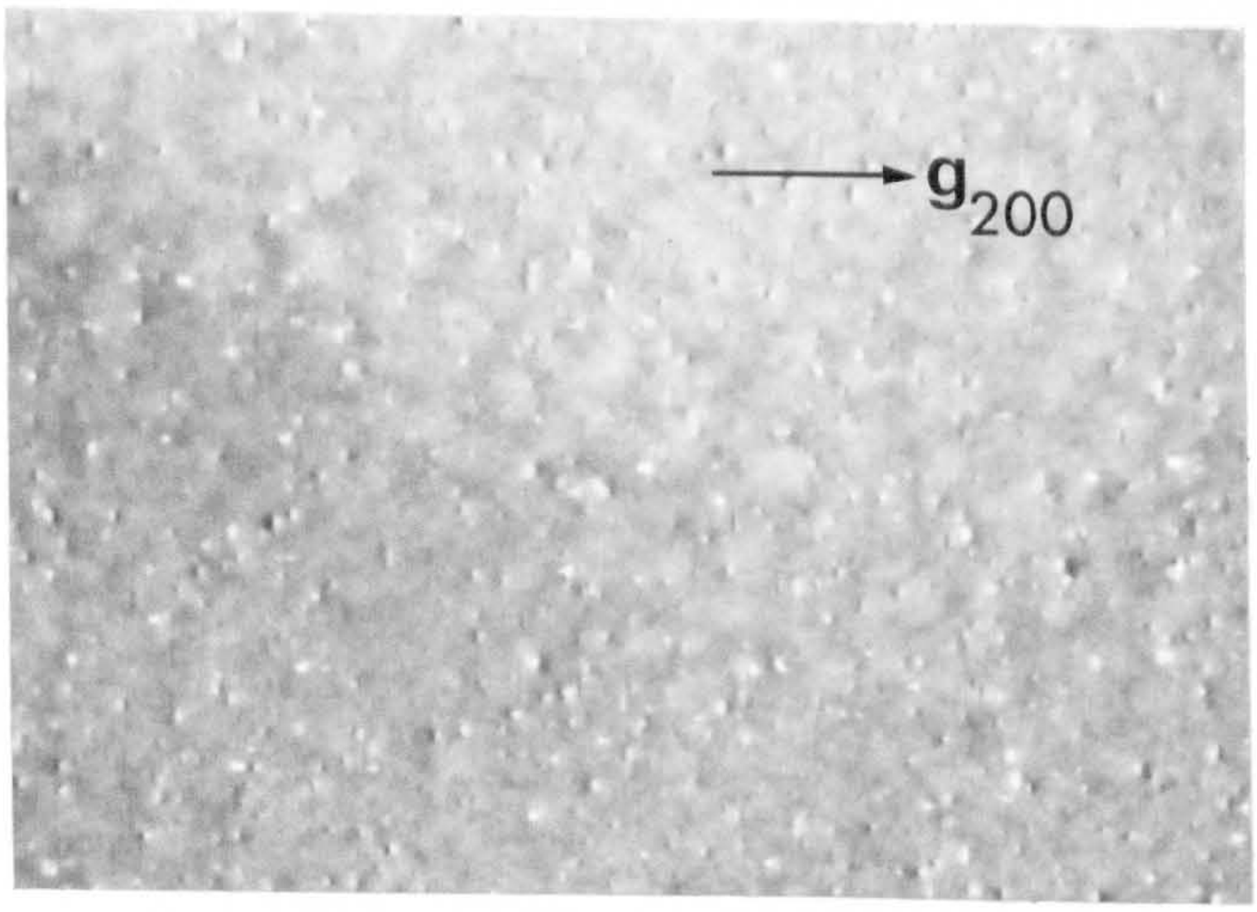

(a)

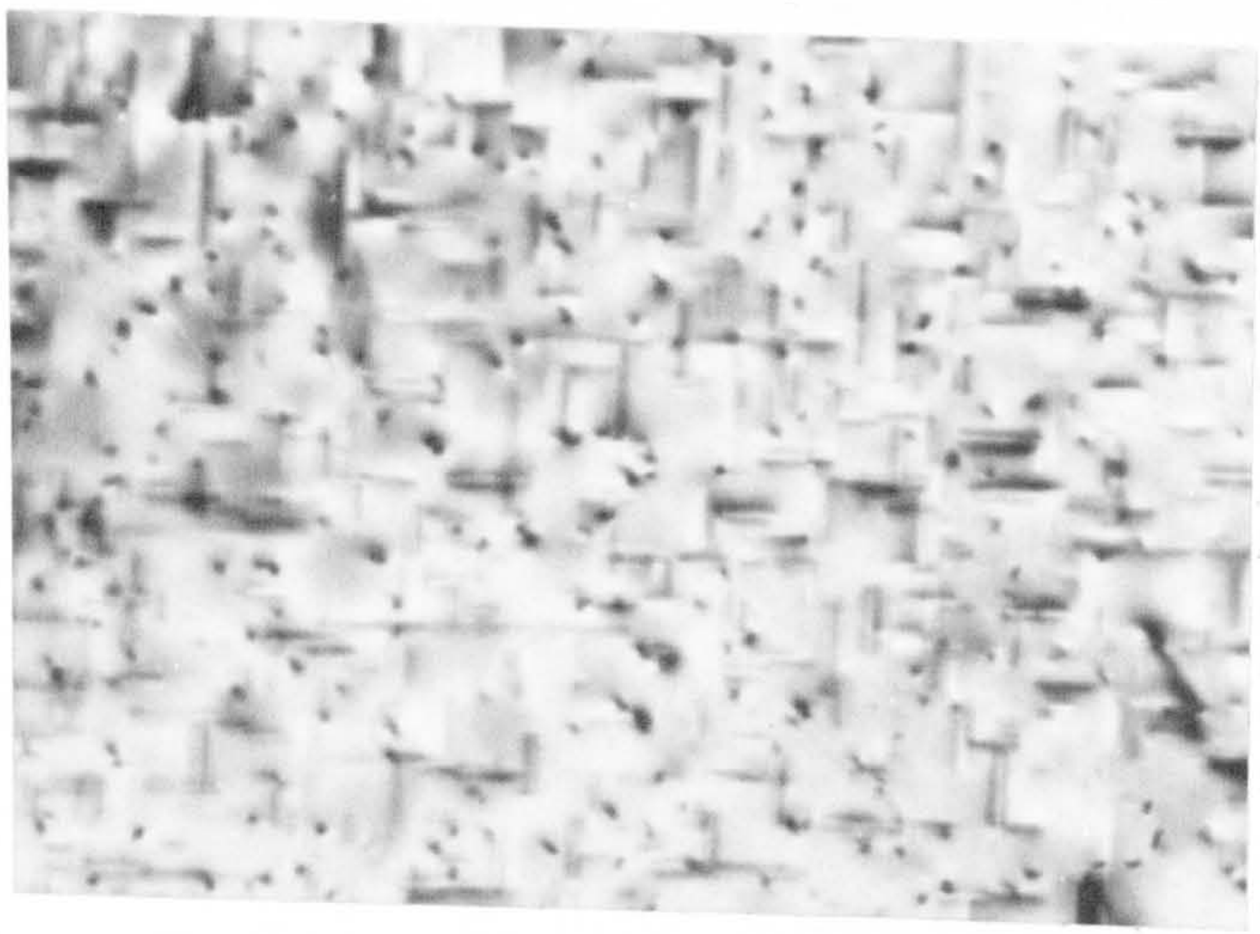

(b)

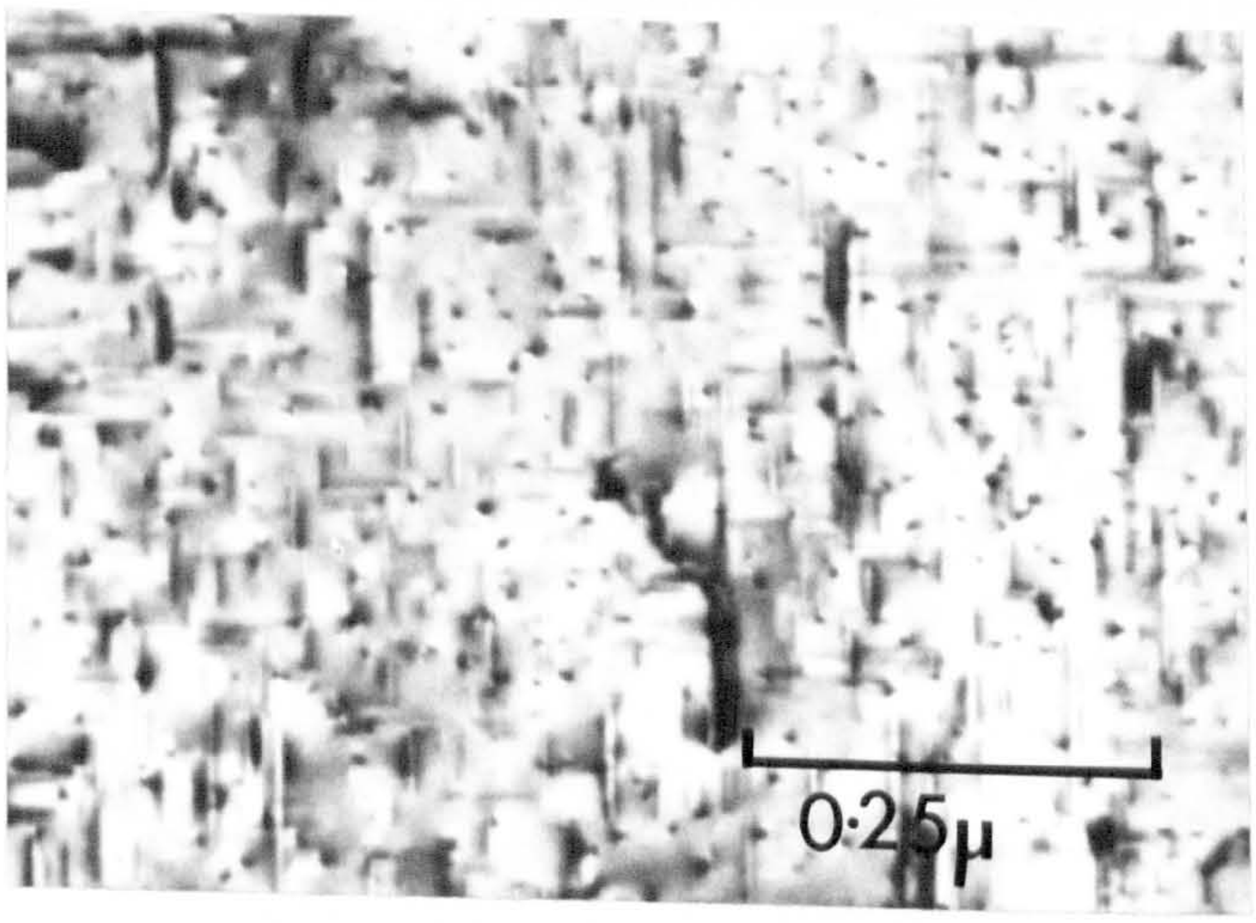

(c)

Figure 5.5 Al-1.2%Mg_2Si : (a) Direct-quenched into oil at 160°C and aged for 1 hour (tilted dark-field micrograph with (200) reflection); (b) pre-treated as (a) plus $2\frac{1}{2}$ hours at 200°C; (c) pre-treated as (a) plus 10 minutes at 250°C.

For the heat-treatments (a) and (b) the pre-treatments at 160°C were carried out for either $\frac{1}{2}$ hour or 1 hour. Attempts to detect homogeneous precipitation in a sample aged for only $\frac{1}{2}$ hour at 160°C were unsuccessful. Recently, however, needle-precipitates were detected by careful electron microscopy in a sample aged for 1 hour at 160°C (see Figure 5.5.(a)). The needles were very small and < 100 Å in length.

For heat-treatment (a) the value of T_2 (200°C) is above T_c but considerably below T_c' (Wood's metal). We have already seen that a fairly high density of needle-precipitates can be obtained with a direct-quench into molten salt at 200°C and ageing for $2\frac{1}{2}$ hours (see Figure 4.1(b)). A sample that was pre-treated for $\frac{1}{2}$ hour at 160°C before being subsequently aged at 200°C for $2\frac{1}{2}$ hours exhibited a very similar microstructure. A more interesting result was obtained with a sample that was pre-aged for 1 hour at 160°C before the second treatment at 200°C (Figure 5.5(b)). In this case the final microstructure was similar to that normally produced by a single ageing treatment at 160°C for 24 hours and finer than that produced by a direct-quench into salt at 200°C. It was concluded that a pre-treatment of 1 hour at 160°C is sufficient to seed a very large proportion of the clusters for growth at 200°C.

For heat treatment (b) the value of T_2 was 250°C, which is just above T_c' (Wood's metal). Pre-ageing for $\frac{1}{2}$ hour at 160°C resulted in only a few clusters being stabilized for growth at 250°C. Pre-ageing for 1 hour at 160°C resulted in a final microstructure at 250°C (Figure 5.5(c)) which was again similar to that produced by a single ageing treatment at 160°C for 24 hours. This observation that clusters can be seeded for growth at 250°C is important since it indicates, according to the model, that $T_{G.P.} > 250°C$.

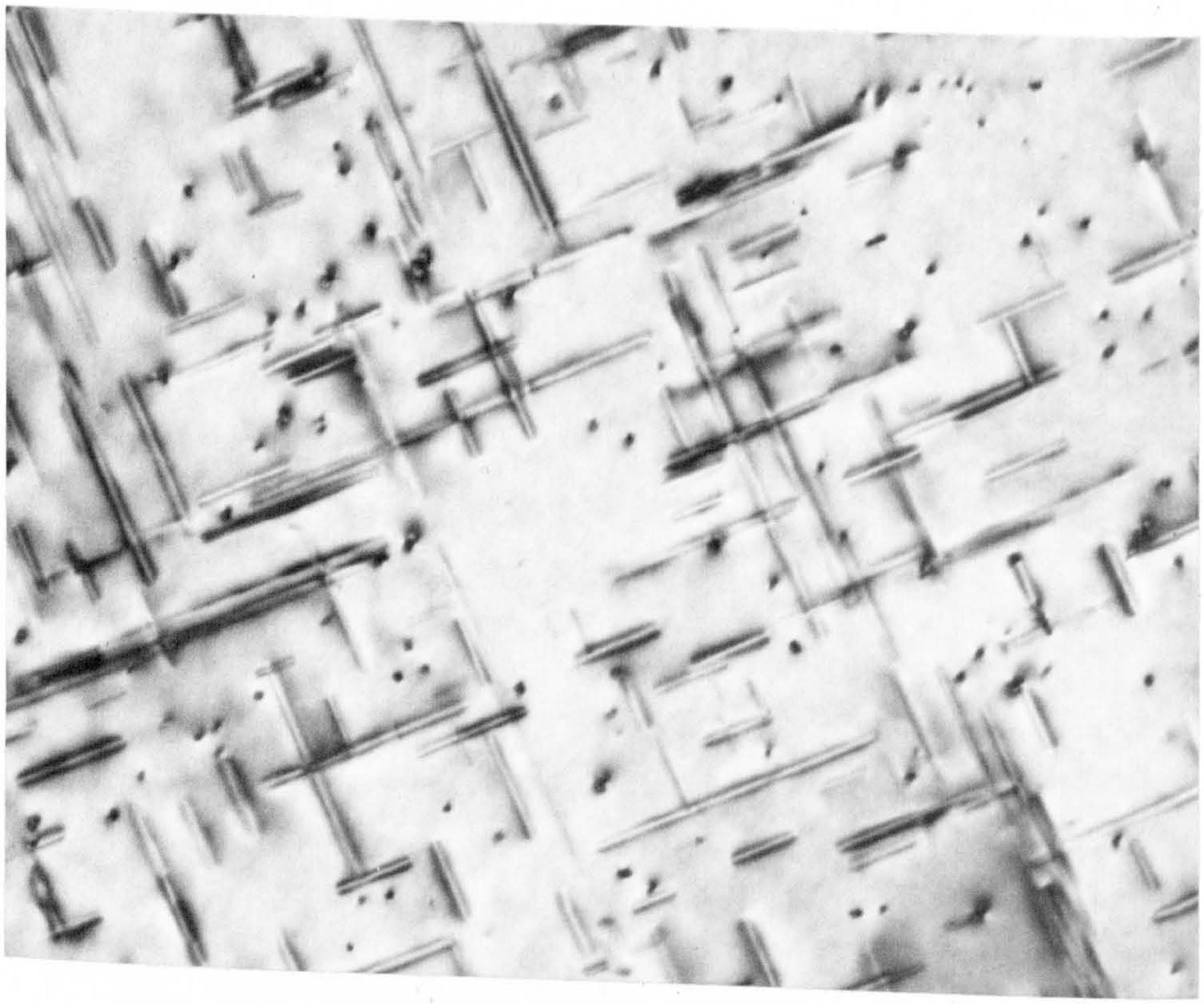

(a)

(b)

Figure 5.6 Al-1.2%Mg_2Si : The effect of pre-treatment at room temperature on subsequent ageing for 10 minutes at 250°C. (a) 10 weeks at room temperature; (b) $2\frac{1}{2}$ years at room temperature.

Finally, let us consider heat treatment (c). A pre-treatment at room temperature for one week was insufficient to produce any seeding at 250°C., but some seeding did occur with three weeks pre-ageing. A slightly higher density of needles was seeded after pre-ageing for 10 weeks (Figure 5.6(a)), but the precipitation was very coarse. Recently a sample was examined which had been stored at room temperature for $2\frac{1}{2}$ years before being aged at 250°C for 10 minutes. The homogeneous precipitation in this case (see Figure 5.6(b)) was finer than that produced by only 10 weeks pre-ageing (cf. Figure 5.6(a)) but still slightly coarser than that produced by a direct-quench and ageing treatment at 160°C for 24 hours. Thus it is deduced that, even after $2\frac{1}{2}$ years storage, only a small proportion of the clusters become seeded for growth at 250°C.

5.4 SOME ADDITIONAL EXPERIMENTAL RESULTS

It was stated in the introduction to this chapter that Fortin (141,142) has obtained two interesting results; (1) that if solution treatment is carried out at a temperature $T_s < 480°C$, then room temperature storage before ageing at 160°C can be beneficial, and (2) that with normal solution treatment the detrimental effect of room temperature delay can be obviated if the sample is subjected to a short high temperature anneal between storage and artificial ageing. The aim of the work described in this section was to determine the effect on microstructure of these two types of heat treatment and so to derive an explanation, in terms of the model[81] for two-step ageing, for the observed behaviour.

(1) The consequence of using a low value of solution treatment temperature

The experiments were carried out[81] with samples of the Al-1.2%Mg_2Si alloy and the value of T_s used was 450°C. In Chapter 4 it was seen that large particles of Mg_2Si were precipitated in a sample that

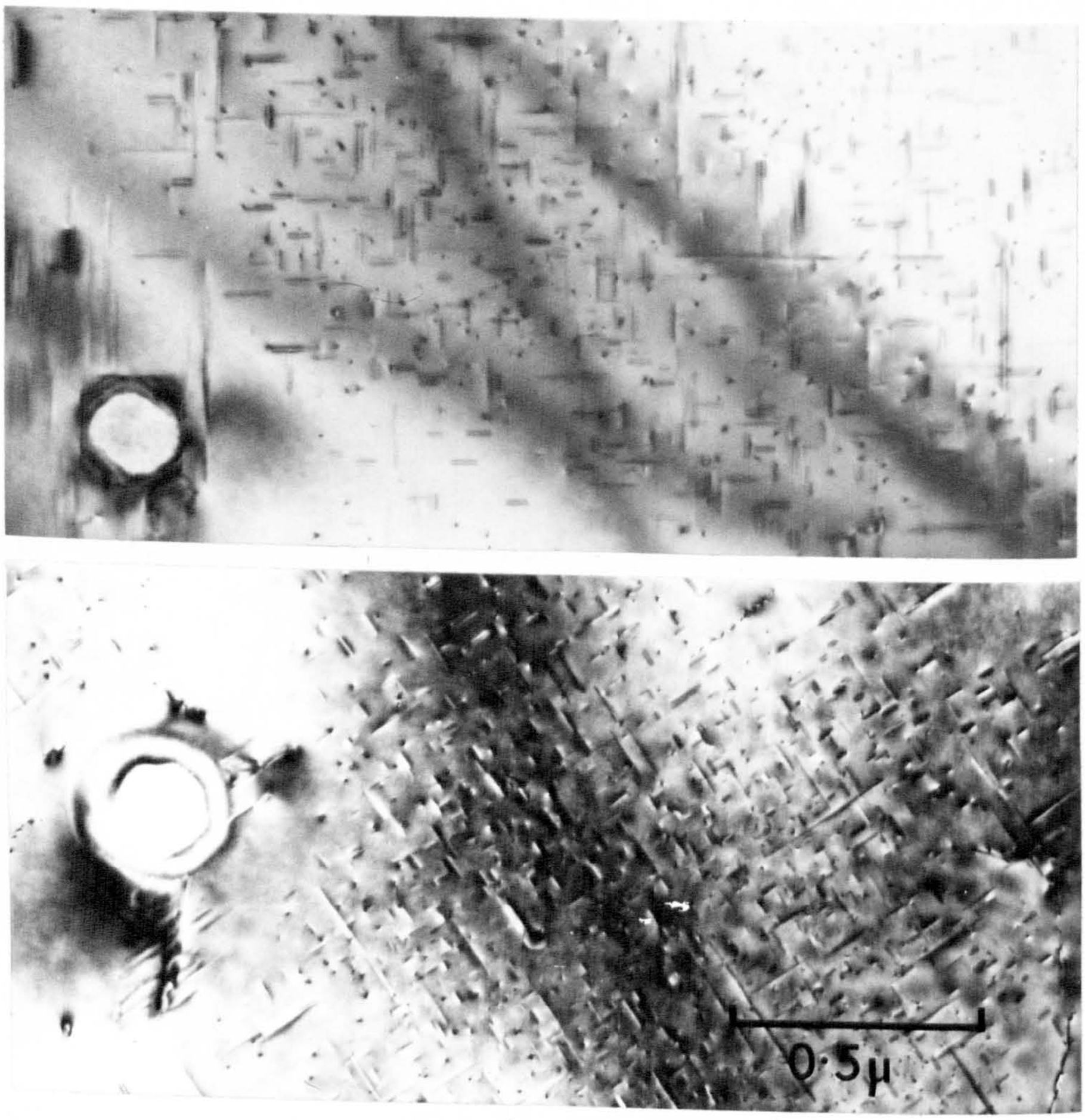

Figure 5.7 Al-1.2%Mg_2Si : The effect of pre-treatment at room temperature on subsequent ageing for 24 hours at 160°C when a low solution treatment temperature of 450°C is used. (a) 1 week at room temperature; (b) 6 months at room temperature.

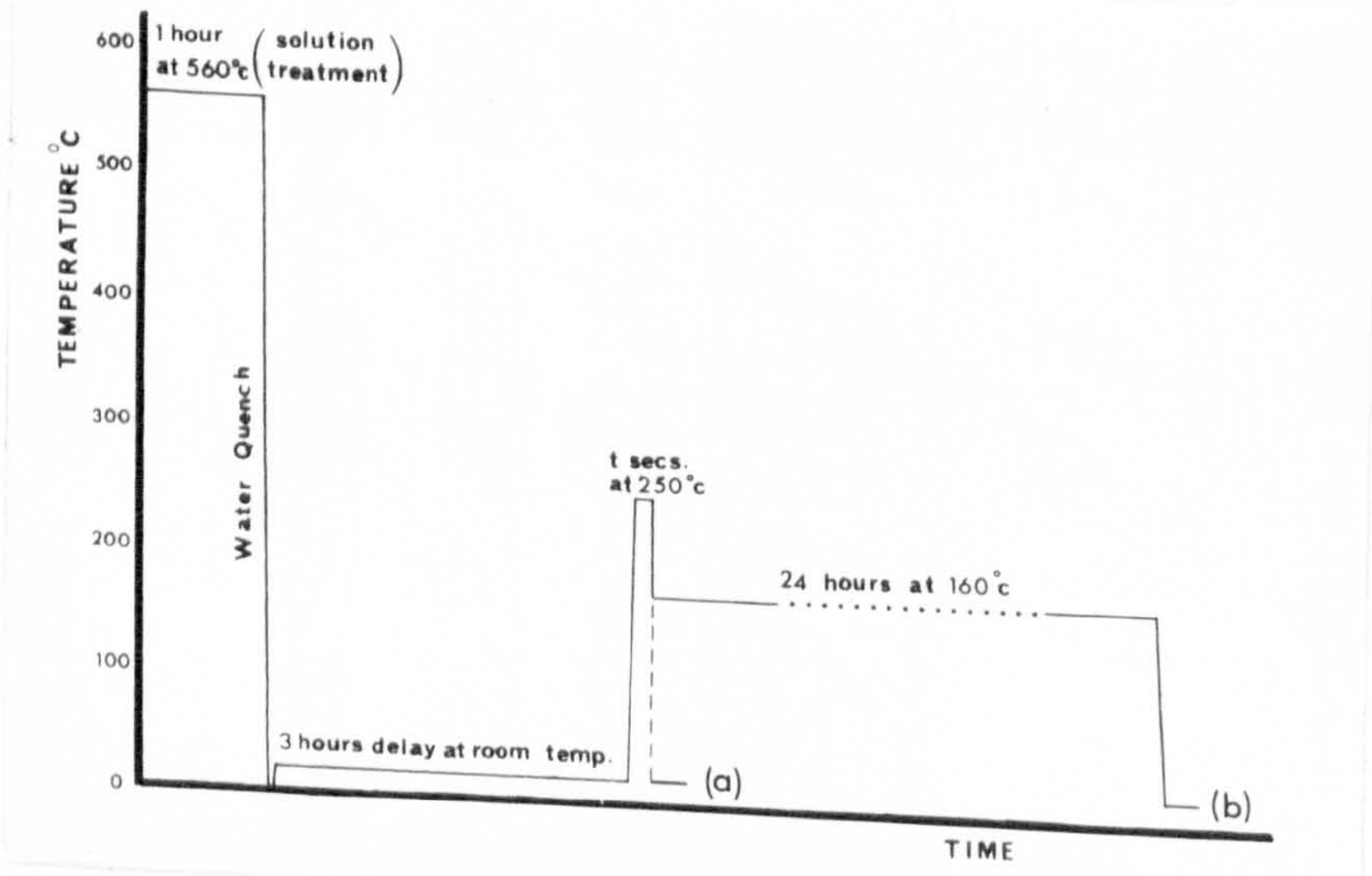

Figure 5.8 A schematic diagram illustrating the heat treatment used for re-dissolving the solute clusters formed during storage for 3 hours at room temperature.

was solution treated for 1 hour at 450°C (see Figure 4.4(b)) and it was believed that the matrix solute concentration was reduced in value to that in equilibrium at 450°C (0.75%Mg_2Si). As a consequence of this reduction in available matrix solute concentration the value of T_c was lowered to below 160°C. Thus, if a sample is aged with T_s = 450°C, T_1 = room temperature, and T_2 = 160°C then this two-step ageing treatment is an example of mode (2) of section 5.2, since $T_c < T_2$. According to the model for two-step ageing, homogeneous precipitation will not grow during ageing at 160°C unless it is seeded during the pre-treatment at room temperature. Progressively longer pre-treatments should increase the density of seeded clusters. This was the behaviour that was observed (see Figures 5.7(a) and (b)), but even after storage for 6 months the final precipitation was still coarse when compared to that formed in a sample which is solution treated at 560°C, direct-quenched to 160°C and then aged at 160°C for 24 hours. The coarseness of the precipitation is consistent with the low level of tensile properties observed by Fortin after this type of heat treatment.

(2) <u>The effect of an intermediate anneal</u>

The type of experimental heat treatment that was investigated is illustrated diagrammatically by Figure 5.8. All samples were given a pre-treatment at room temperature for 3 hours after solution treatment at 560°C. The final ageing treatment was always carried out at 160°C for 24 hours. The time of intermediate treatment at 250°C ranged between 30 seconds and 10 minutes, and samples were examined either (a) immediately after the intermediate treatment or (b) at the completion of the final treatment at 160°C.

Figure 5.9(a) illustrates the typical microstructure of a sample

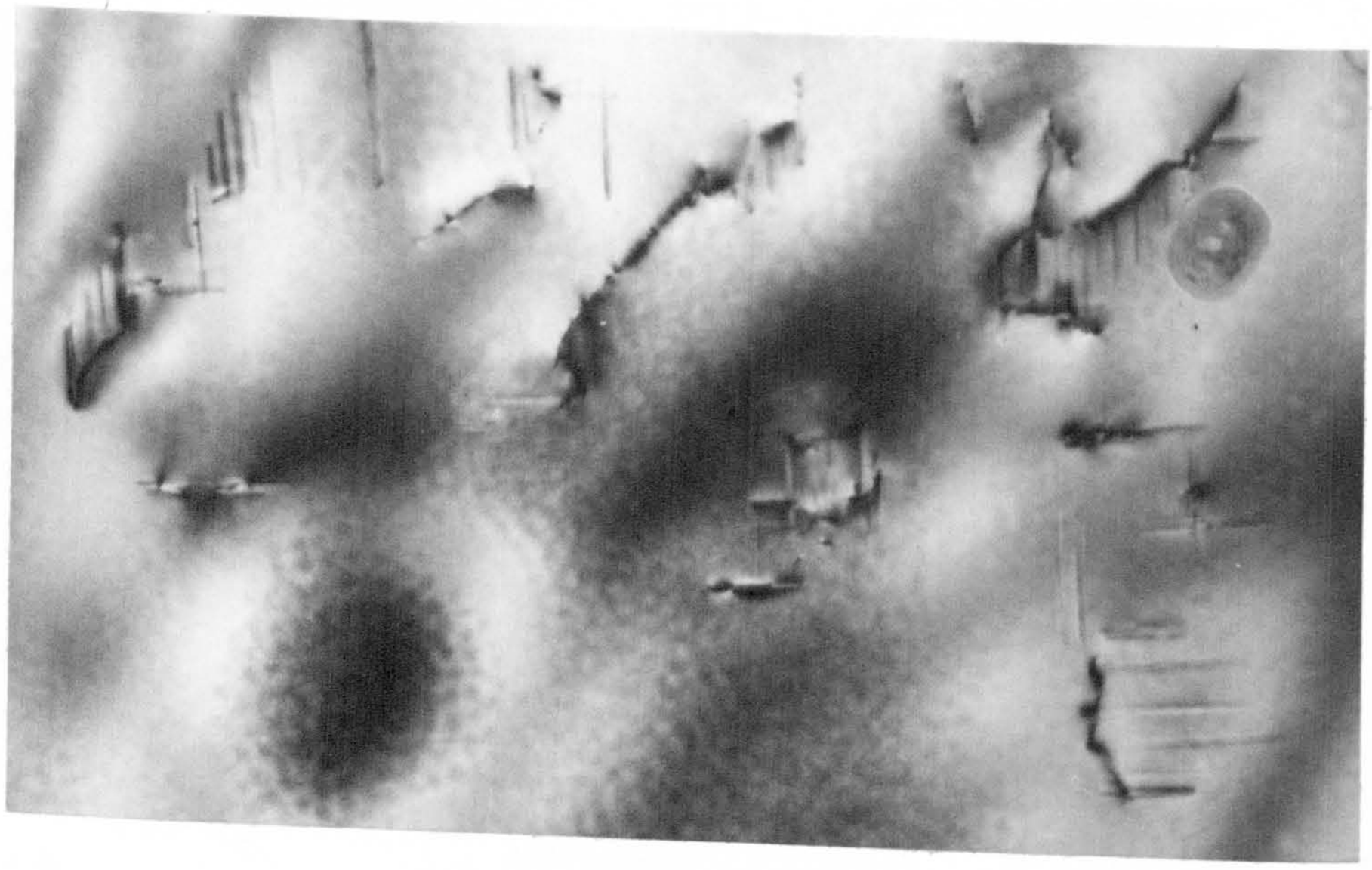

(a)

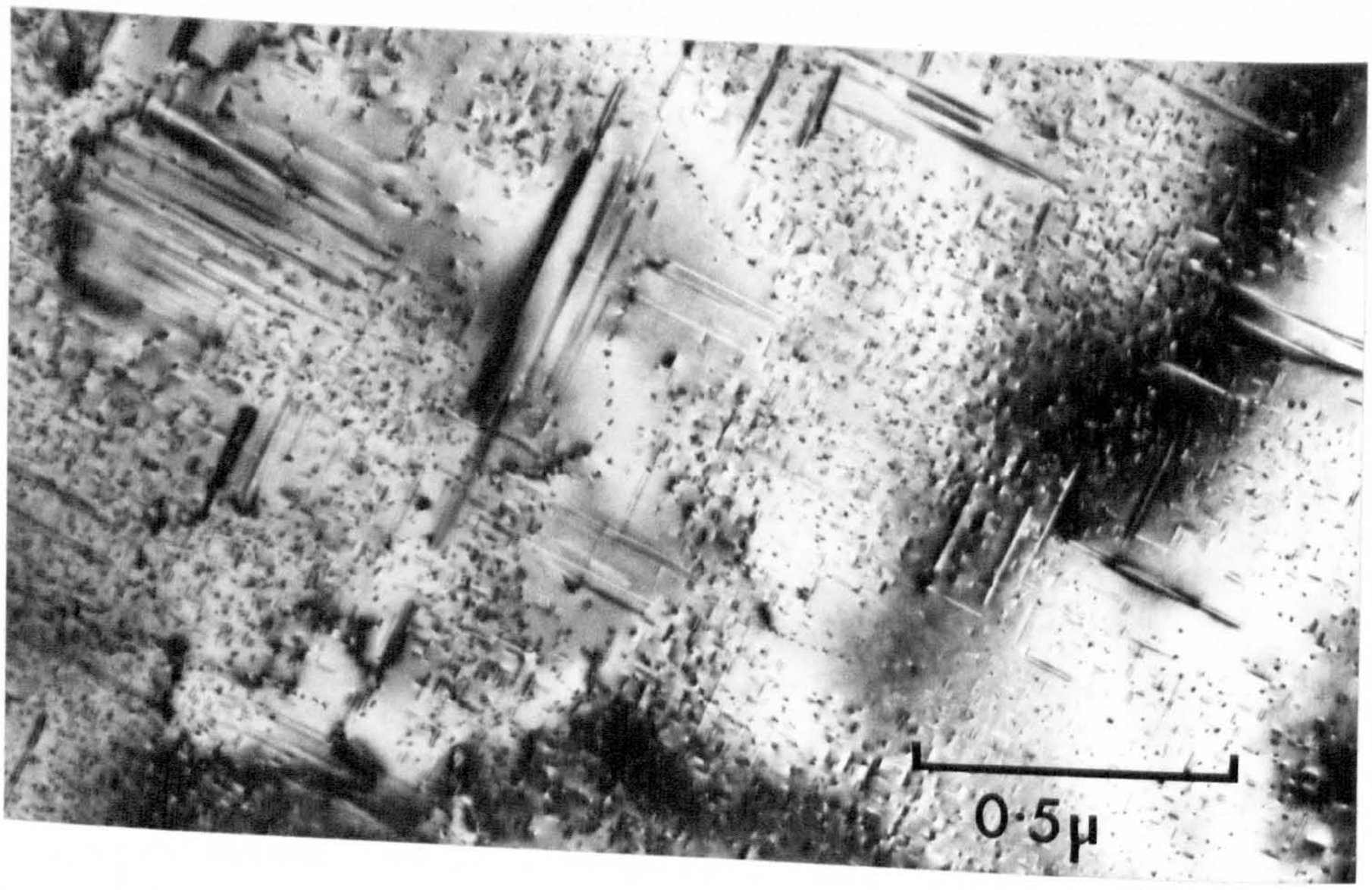

(b)

Figure 5.9 Al-1.2%Mg_2Si : The effect of heat treatment illustrated by Figure 5.8 on the precipitate microstructure. (a) 90 seconds at 250°C without any further ageing; (b) as for (a) plus 24 hours at 160°C.

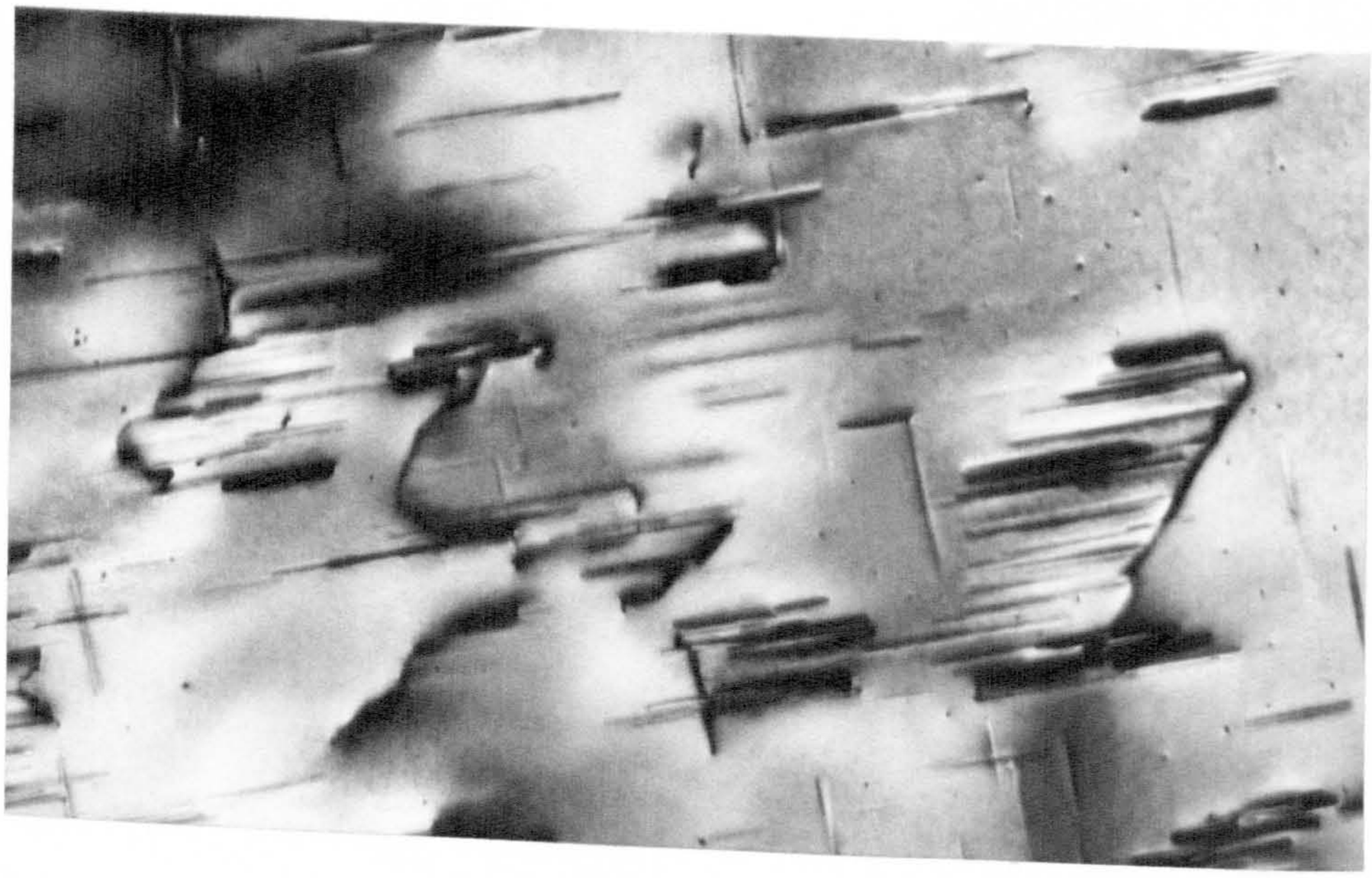

(c)

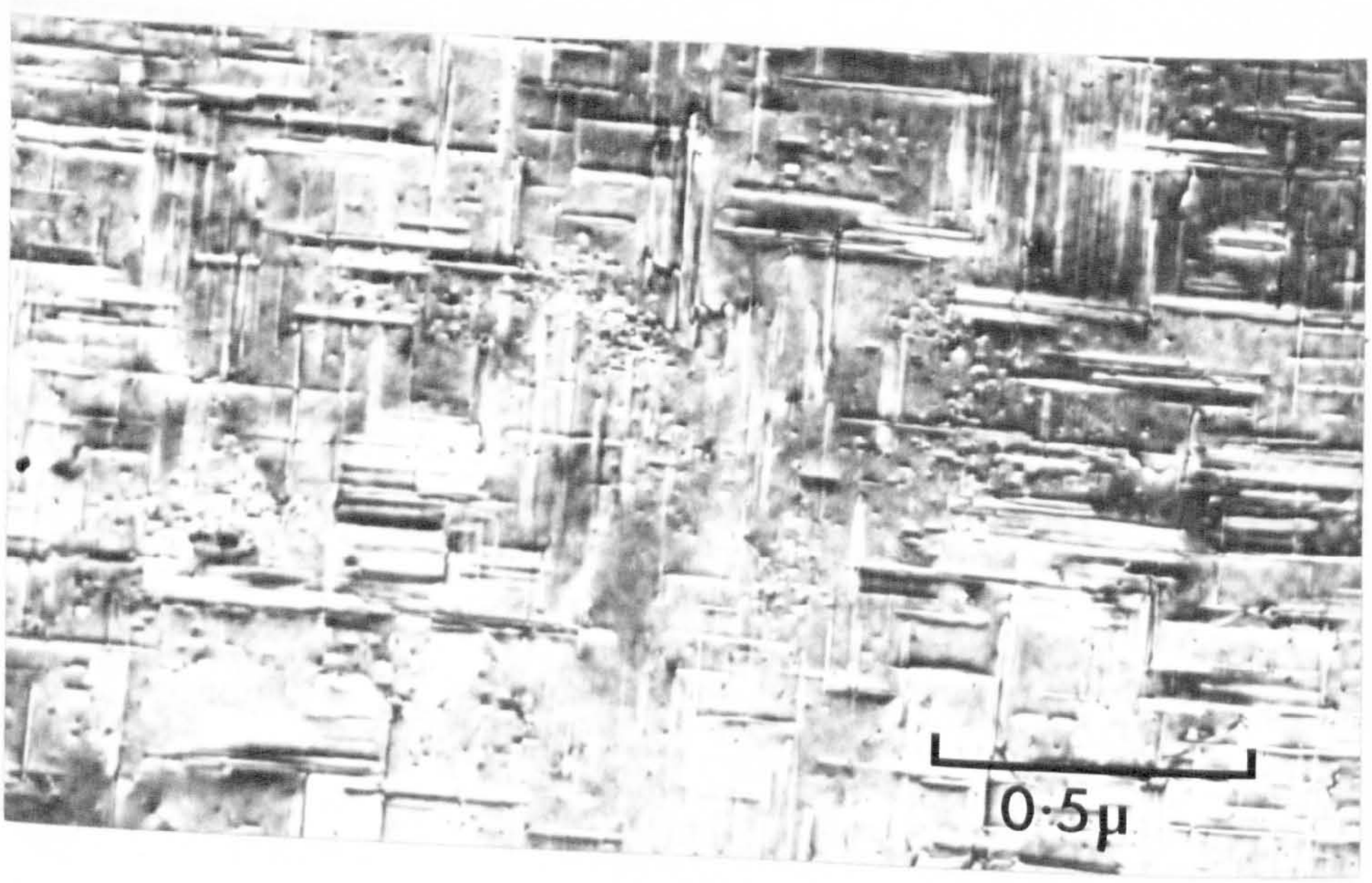

(d)

Figure 5.9 Al-1.2%Mg_2Si : The effect of the heat treatment illustrated by Figure 5.8 on the precipitate microstructure. (c) 3 minutes at 250°C without any further ageing; (d) as for (c) plus 24 hours at 160°C.

examined after 90 seconds at 250°C. No homogeneous precipitation could be detected but marked heterogeneous precipitation was present on the dislocations. Since a period of pre-ageing at room temperature of longer than one week is required to seed any clusters for growth at 250°C (see section 5.3) it is believed that all clusters formed by storage for 3 hours are completely dissolved by this intermediate anneal at 250°C. This will return the matrix to a fully supersaturated state, apart from regions in the neighbourhood of the heterogeneous precipitation which will be locally depleted in solute atoms. Thus, if a sample was aged at 160°C after the anneal at 250°C (Figure 5.9(b)), fine-scale homogeneous precipitation was produced in regions where the solute supersaturation was high. The precipitate-free zones surrounding the heterogeneous precipitates were believed to be caused by the local solute-depletion mentioned above.

If the intermediate treatment at 250°C was extended to 3 minutes then much larger dislocation-nucleated precipitates were formed (Figure 5.9(c)). It is thought that this produced wide-spread solute-depletion throughout the matrix so that, for a sample subsequently aged at 160°C, the solute supersaturation was insufficient to nucleate homogeneous precipitation throughout most of the matrix (Figure 5.9(d)). With an intermediate anneal at 250°C for 10 minutes the solute depletion was so extensive that no homogeneous precipitation occurred on ageing at 160°C.

Thus, it is believed that the effect of the intermediate treatment is to dissolve the solute clusters which are grown during the storage period. This returns the alloy to a fully supersaturated state except in regions surrounding the large dislocation-nucleated precipitates. Fortin's heat treatment will overcome the detrimental effect of room temperature delay provided that the intermediate treatment is controlled so that excessive heterogeneous precipitation is not formed.

5.5 CONCLUSIONS

The model for two-step ageing, as proposed by Pashley, Jacobs and Vietz[81], has been outlined and shown to be consistent with concepts discussed in Chapter 4. The model predicts two distinct modes of behaviour, depending upon whether T_2 is above or below T_c, and these two modes have been illustrated by experimental results obtained with an Al-1.2%Mg_2Si alloy. There is good qualitative agreement between the predictions of the model and the experimental results. Since the solute clusters in Al-Mg_2Si are thought to be needle-shaped and to give rise to lattice strain there is clearly a need to consider how the model, in which it is assumed that the clusters are spherical and strain-free, must be modified. Further discussion of these points is postponed until Chapter 8.

CHAPTER 6

THE FACTORS AFFECTING THE WIDTH OF PRECIPITATE-FREE ZONES IN Al-Zn ALLOYS

6.1 INTRODUCTION

Precipitate-free zones (p.f.z's) are commonly observed in the neighbourhood of grain boundaries and sometimes around certain types of heterogeneity within the grains (e.g. matrix dislocations) of aluminium-base precipitation-hardened alloys. During the last few years considerable attention has been paid to these p.f.z.'s, particularly those associated with grain boundaries, since relatively minor changes in heat treatment conditions, in certain circumstances, can alter the width of the p.f.z's and so modify the mechanical properties of the alloy[9, 132, 135, 145-152].

The precipitation within the grains may consist of G.P. zones, intermediate precipitates or equilibrium precipitates (or a mixture of two or more of these different types of precipitate) depending upon the heat treatment given to the alloy.

Various theories have been put forward to explain the origin of grain boundary p.f.z's. In an early theory, due to Geisler[145], the formation of grain boundary p.f.z's was attributed to local solute-depletion, caused by the rapid growth of grain boundary precipitates. In a later investigation, Rosenbaum and Turnbull[153] observed wide p.f.z's at grain boundaries in samples of Al-lat.%Si which were cooled to room temperature before being subsequently aged at 200°C when the equilibrium Si solid solution was precipitated. They found that the p.f.z. that was established on ageing at 200°C increased in width with decrease in cooling rate to room temperature, e.g. it was ~ 0.5μ wide after a water quench but ~ 10μ wide after an air cool. These observations led them to

attribute the p.f.z. to vacancy-depletion near to the grain boundary, caused by the diffusion of vacancies to the grain boundary sink during the cooling to room temperature. They suggested that the precipitates were nucleated heterogeneously on dislocation loops formed by the collapse of vacancy clusters[122] and that in the neighbourhood of a grain boundary, where the vacancy-supersaturation was insufficient for loops to form, a loop-free zone was produced[123], and no precipitates were nucleated in this region. Since a slower cool to room temperature would give rise to a wider region of vacancy-depletion, and hence a wider loop-free zone, the observed increase in p.f.z. width with decrease in cooling rate was explained. Saulnier[154] cast doubt on this interpretation by showing that dislocation loops are unstable in this alloy at 200°C and Kelly and Nicholson[9] have suggested an alternative explanation whereby small vacancy clusters provide the heterogeneous nucleation sites.

Taylor[132] and Embury and Nicholson[76] further developed the idea of vacancy-depletion near to a grain boundary as the major cause of the grain boundary p.f.z. for the special case of homogeneous precipitation in an Al-Zn-Mg alloy. They postulated that a certain critical concentration of vacancies is required for G.P. zone nucleation to occur in this system. Vacancies were considered to be an essential constituent of the G.P. zone nucleus, thereby aiding the nucleation by either or both of the mechanisms listed as (2) and (3) in section 4.5.2. According to their model, G.P. zones may fail to form near to a grain boundary because the local vacancy concentration is less than the critical value required for nucleation.

Lorimer and Nicholson[77,78,79] have re-interpreted and extended the results of Embury and Nicholson[76] by considering the effect of a reduced vacancy concentration, in the vicinity of a grain boundary, on the

kinetics of nucleation and growth of G.P. zones in a sample which is quenched to an ageing temperature $T_1 < T_{G.P.}$. According to their interpretation, only zones formed during the treatment at T_1 which exceed a certain critical size can act as nuclei for the intermediate η' precipitates that are observed to form, under certain conditions, during a second ageing treatment at a temperature $T_2 > T_{G.P.}$, (a similar hypothesis has been put forward by Holl[149,150]). By invoking the concept of a vacancy concentration profile adjacent to a grain boundary they deduced that, after a given ageing time at T_1, the mean size of G.P. zones will be smaller near to a grain boundary than further away in the matrix since the reduced vacancy concentration lowers the solute diffusivity and hence lowers the growth rate of the G.P. zones. Upon ageing at $T_2 > T_{G.P.}$, the zones close to the grain boundary may have grown insufficiently to exceed the critical size and therefore will dissolve and give rise to a p.f.z.. A more detailed account of this model is given in Chapter 8.

Cornish and Day[155,156] have also examined the effect of a wide range of heat treatments on the precipitation in the neighbourhood of grain boundaries in an Al-Zn-Mg alloy. They attributed the p.f.z's that were observed after some heat treatments primarily to solute-depletion and after other heat treatments primarily to vacancy-depletion.

Thus, both solute-depletion and vacancy-depletion have been invoked to explain the origin of grain boundary p.f.z's. In many cases, similar arguments can explain the p.f.z's that are sometimes observed around matrix dislocations or large heterogeneous precipitates produced during some prior heat treatment. The object of the experimental work described in this Chapter was to determine which of these two mechanisms (i.e. vacancy-depletion or solute-depletion) provides the major factor controlling the width of the p.f.z's which were observed, under certain

conditions, in the Al-10%Zn, 17.5%Zn and 26%Zn alloys. The majority of the work was carried out with the alloy of nominal composition of Al-17.5%Zn and all experimental results discussed here refer to this alloy. Similar heat treatments were carried out on the other two alloys and in all cases similar, although less extensive, results were obtained. Most of the work was concerned with grain boundary p.f.z's and this is reported in detail in section 6.2. A brief account of these studies has been published[82].

6.2 GRAIN BOUNDARY PRECIPITATE-FREE ZONES IN AN Al-17.5%Zn ALLOY

We have already seen, in Chapter 4, that G.P. zones were formed in the Al-17.5%Zn alloy if it was given a suitable heat treatment. In this section the discussion is confined to the factors affecting the precipitation of G.P. zones in the neighbourhood of grain boundaries.

Pronounced p.f.z's were observed in samples which were either (1) direct-quenched to the ageing temperature or (2) given a two-step ageing treatment. In the majority of cases the grain boundary was located midway between the edges of the p.f.z. and it is this type of p.f.z. that is discussed in sections 6.2.1 and 6.2.2 where, respectively, the p.f.z's formed by direct-quenching and two-step ageing are considered. Occasionally, particularly after prolonged ageing, p.f.z's were observed that were asymmetrical with respect to the grain boundary. These are discussed separately in section 6.2.3.

In both section 6.2.1 and section 6.2.2 the account of the experimental results is preceded by a theoretical model which can qualitatively explain the observed behaviour. The models are based on the concepts and ideas already outlined in Chapters 4 and 5 and contain considerations of the factors affecting the nucleation, growth and stability of spherical, strain-free G.P. zones. It is therefore believed that these

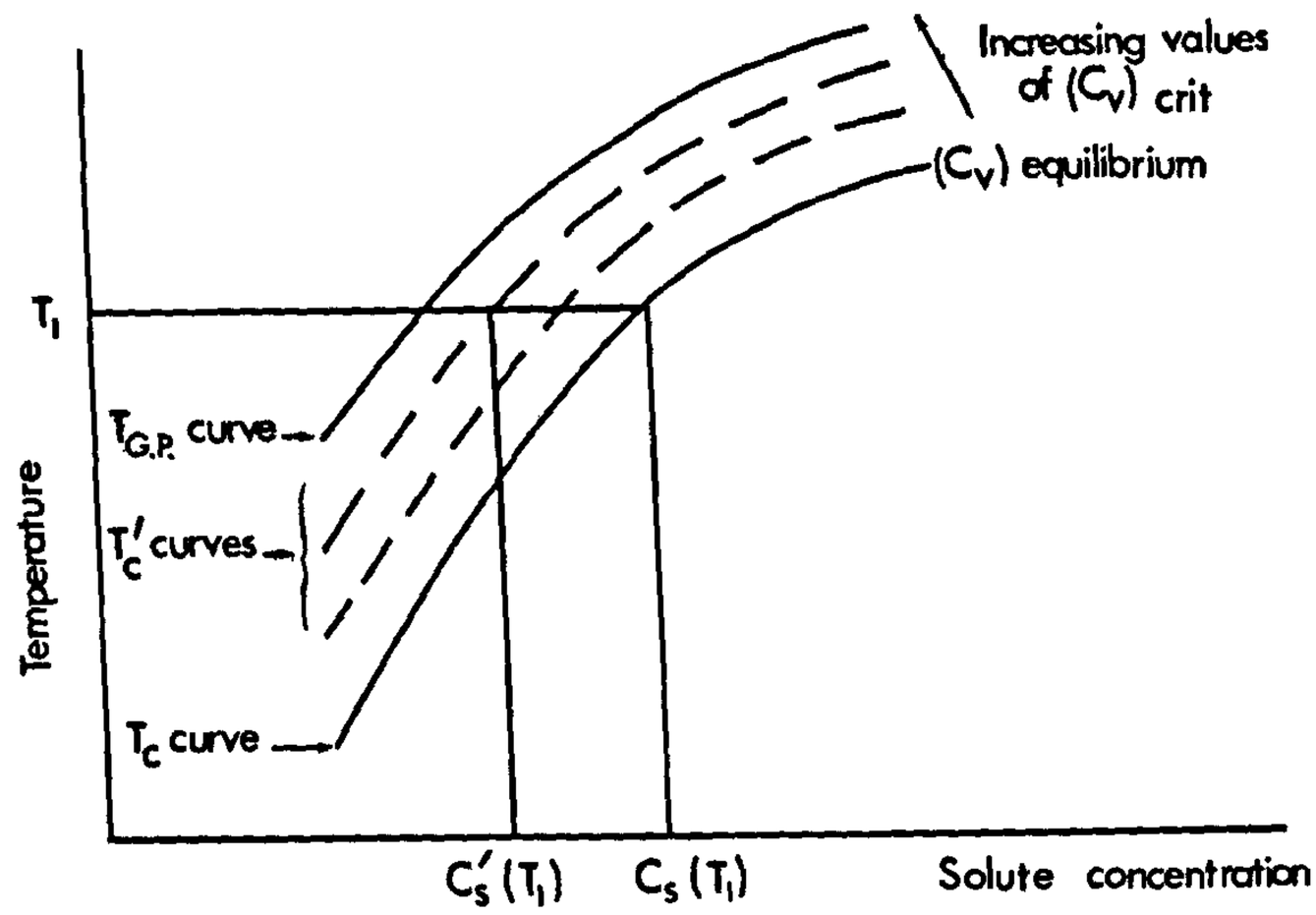

Figure 6.1 A schematic diagram showing the variation of T_c, T_c' and $T_{G.P.}$ with solute concentration.

models are reasonably applicable to the Al-Zn system for which it is known (see Chapter 3) that the small G.P. zones are spherical in shape and only slightly strained.

6.2.1 Precipitate-free zones produced by direct-quenching to the ageing temperature

Theoretical model

The concept of a critical temperature (T_c), as defined in Chapter 4, is of fundamental importance in the interpretation of the factors controlling the width of p.f.z's produced by direct-quenching. In the following discussion we will need to know how the value of T_c varies with alloy composition and this is provided by Figure 4.8 which shows that a lower value of T_c is associated with a reduced solute concentration. The other fact that we will need to use, which has already been established in section 4.4, is that G.P. zone nucleation can occur at an observable rate above T_c (but below $T_{G.P.}$) provided that sufficient excess vacancies are available to aid the nucleation. The experimental observation that T_c' (Wood's metal) is higher than T_c' (oil) (see section 4.4) is considered as confirmation that a higher excess-vacancy concentration is quenched-in by a rapid quench into Wood's metal than by a slower quench into oil. From this result it is then reasonable to postulate that G.P. zone formation will occur up to a temperature T_c' provided that the quenched-in excess-vacancy concentration exceeds a certain critical value $(C_v)_{crit}$. The family of curves labelled T_c' in Figure 6.1 represents schematically the situation for different values of $(C_v)_{crit}$. The factors controlling the width of p.f.z's formed by direct-quenching to the ageing temperature can now be deduced by direct application of the concepts summarized by this diagram.

The arguments are clarified by initially making the assumption that, immediately after a direct-quench to an ageing temperature T_1, the solute concentration is uniform throughout the matrix and, in particular, no solute-depletion has occurred in the vicinity of grain boundaries. This is the ideal situation considered in case (1), below. This assumption is relaxed in case (2).

Case (1) : No solute depletion during the quench

Consider the excess-vacancy concentration in the vicinity of a grain boundary immediately after the quench to T_1. During the quench the excess-vacancies in the matrix immediately adjacent to the grain boundary can migrate to the boundary and become annihilated, whereas those further away from the boundary will be retained in the matrix. An excess-vacancy concentration gradient will be set-up and its profile will depend upon the value of T_Q (the quenching temperature) and the quench-rate from T_Q to T_1. Immediately adjacent to the grain boundary the vacancy concentration tends towards that value which is in equilibrium at T_1.

The excess-vacancy concentration gradient will be set-up during the quench irrespective of whether T_1 is above or below T_c. However, in the absence of solute-depletion, G.P. zone nucleation will occur right up to a grain boundary if $T_1 < T_c$ (this follows from the definition of T_c, see Chapter 4) and no p.f.z. will be formed on ageing at T_1. So we now confine the discussion to the situation when $T_1 > T_c$.

$T_1 > T_c$

G.P. zone nucleation will only occur in regions of the matrix where the local excess-vacancy concentration, immediately after the quench, exceeds the critical value $(C_v)_{crit}$ discussed above. Consider the situation in the neighbourhood of a grain boundary for three different, but

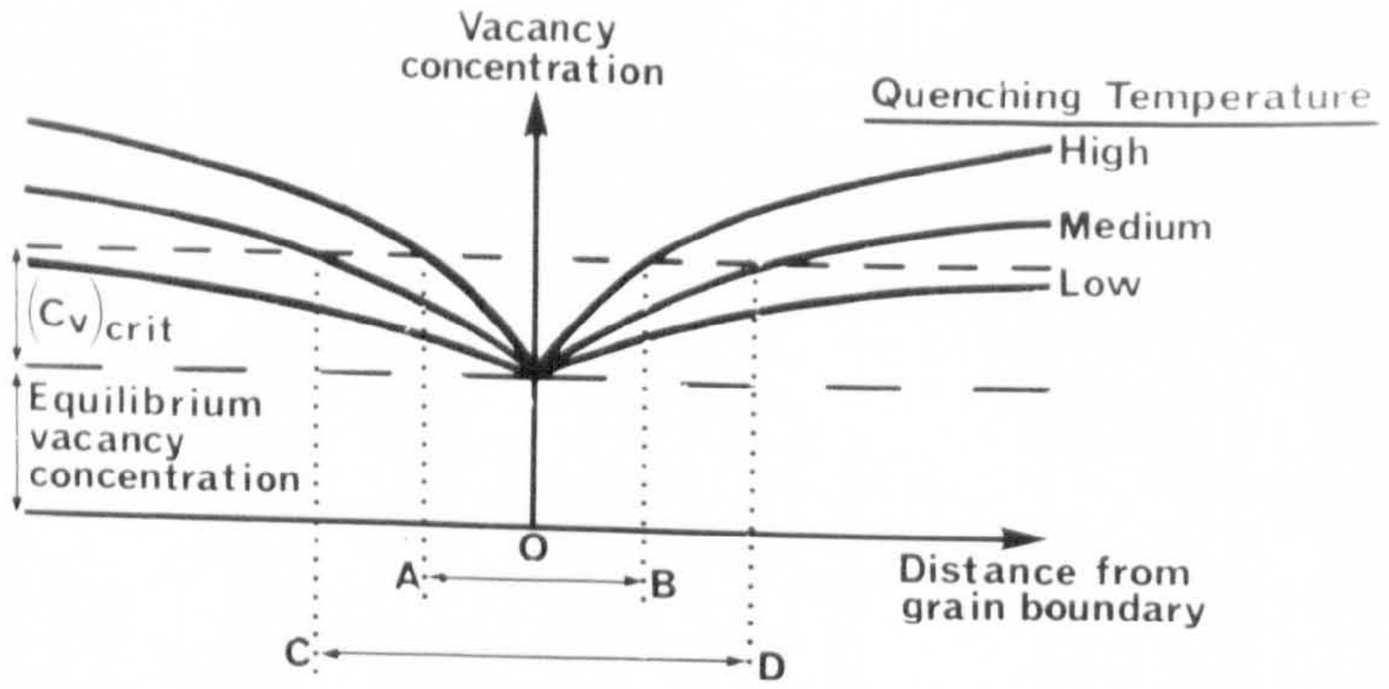

Figure 6.2 Al-17.5%Zn : The effect of vacancy-depletion near to a grain boundary on G.P. zone formation during ageing at 160°C. (a) a schematic diagram illustrating the excess-vacancy profiles expected near to a grain boundary for a high, medium and low value of quenching temperature. (b), (c) and (d) are micrographs illustrating the precipitate-free zones established after quenching from (a) 475°C, (b) 370°C and (c) 300°C.

similar-sized, samples after a direct-quench into oil at T_1 from a quenching temperature T_Q. Figure 6.2(a) illustrates, schematically, on the same diagram, the three different excess-vacancy profiles that would be expected for a high, medium and low value of T_Q. The appropriate value of $(C_v)_{crit}$ is also indicated schematically on the diagram. G.P. zone formation will not occur in the sample quenched to T_1 from the high quenching temperature within the region defined by A-B on the diagram since between A and B the actual excess-vacancy concentration is less than $(C_v)_{crit}$: A-B thus defines the p.f.z. in this case. Similarly, the wider region denoted by C-D defines the p.f.z. in the sample quenched from the medium value of T_Q. The excess-vacancy profile corresponding to the quench from the low value of T_Q illustrates the case where the excess-vacancy concentration never exceeds $(C_v)_{crit}$, even at a large distance from the grain boundary. No G.P. zone formation will occur in the sample in this case.

Case (2) : Solute depletion during the quench

We now consider the case where the solute concentration is reduced in the vicinity of a grain boundary during the quench because either (1) preferential segregation of solute atoms occurs at the grain boundary during the quench to T_1 and so locally depletes the matrix, or (2) grain boundary precipitates are nucleated and grown during the quench and the matrix adjacent to the grain boundary provides solute atoms for these precipitates. In either case a solute concentration gradient will be established similar to that illustrated by Figure 6.3(a).

First of all let us examine the simplest situation when, immediately after the quench, there is a uniform, equilibrium, vacancy concentration throughout the grains. In order to decide whether or not G.P. zone formation can occur within the region of solute-depletion we

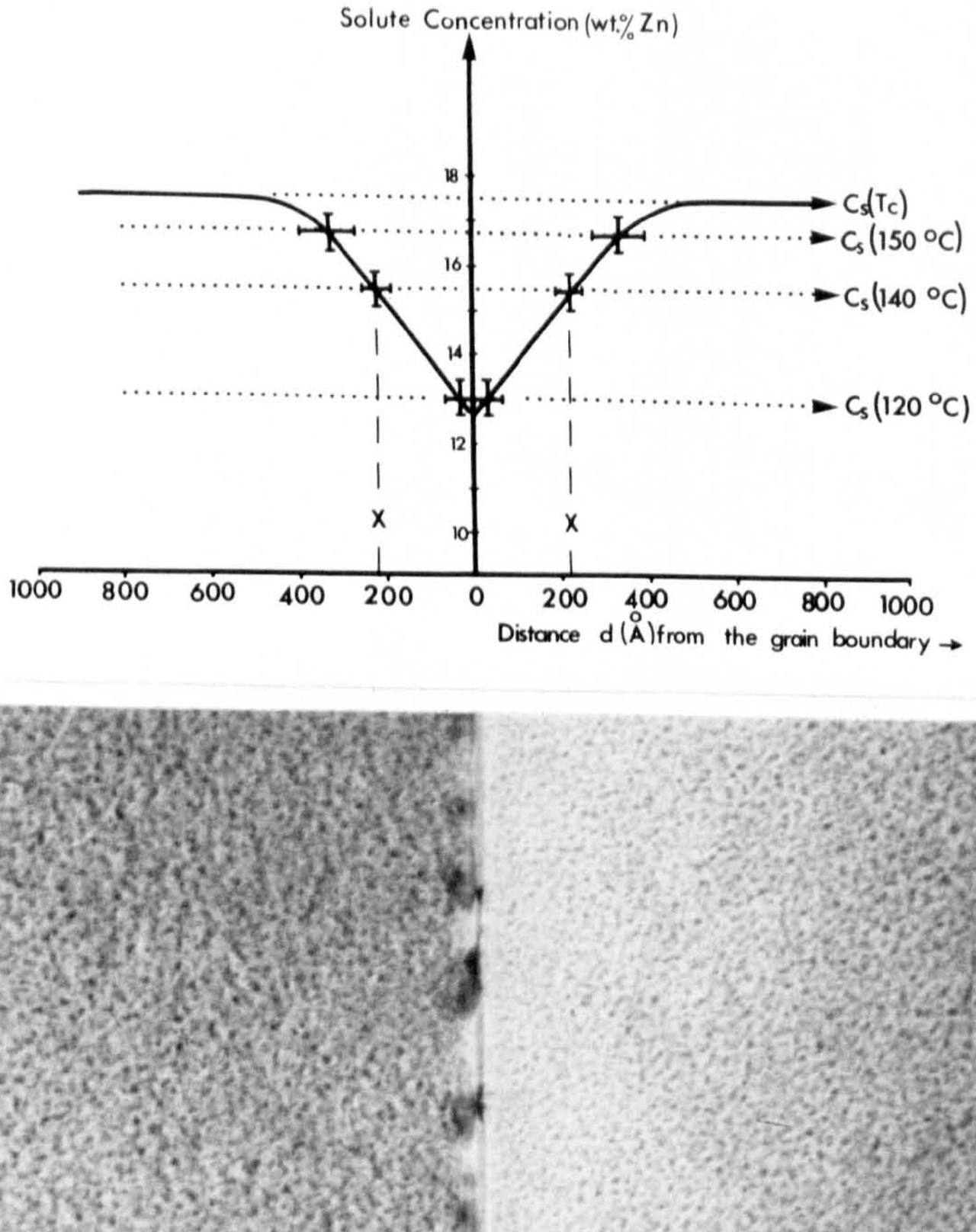

(a)

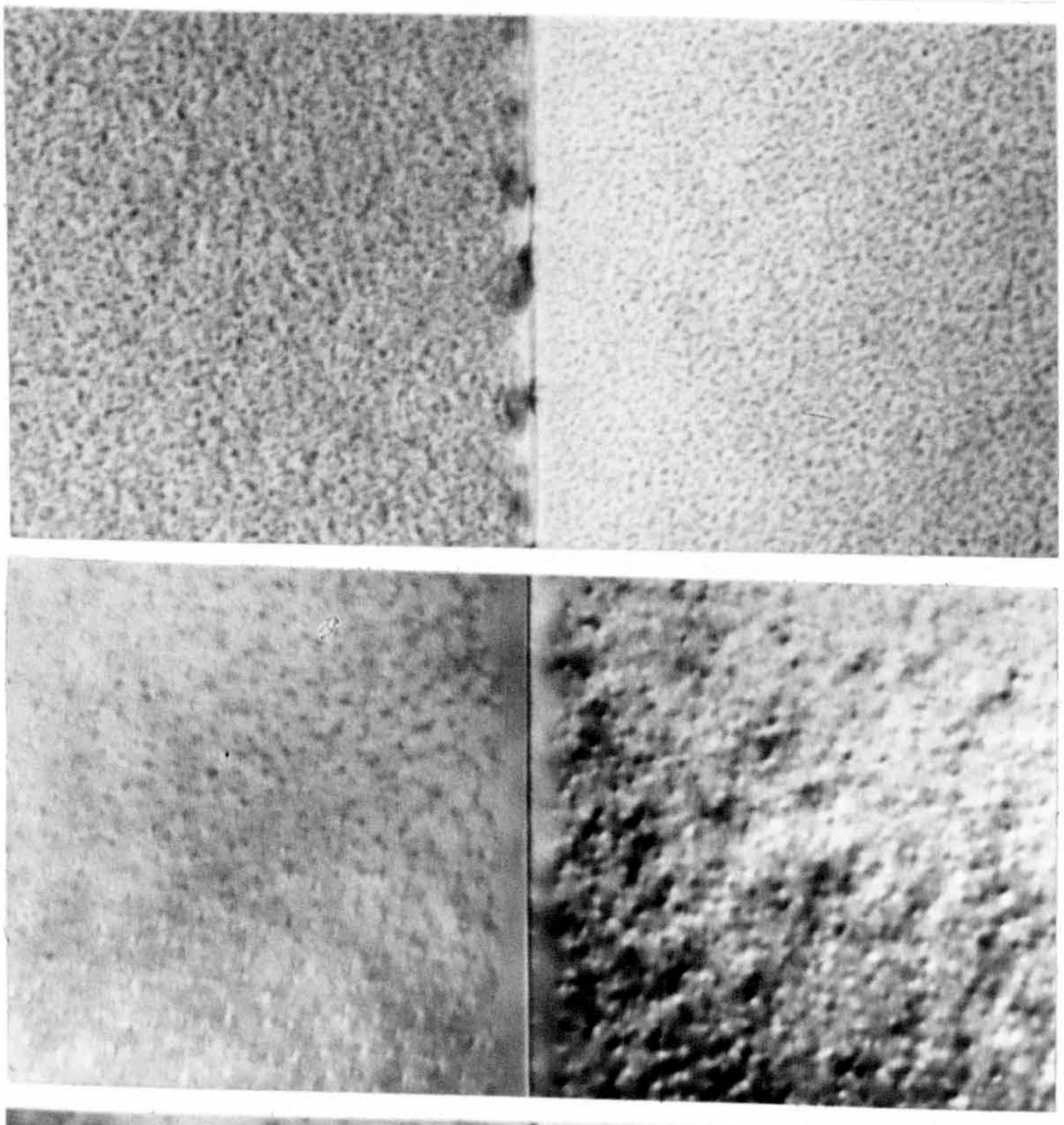

(b)

(c)

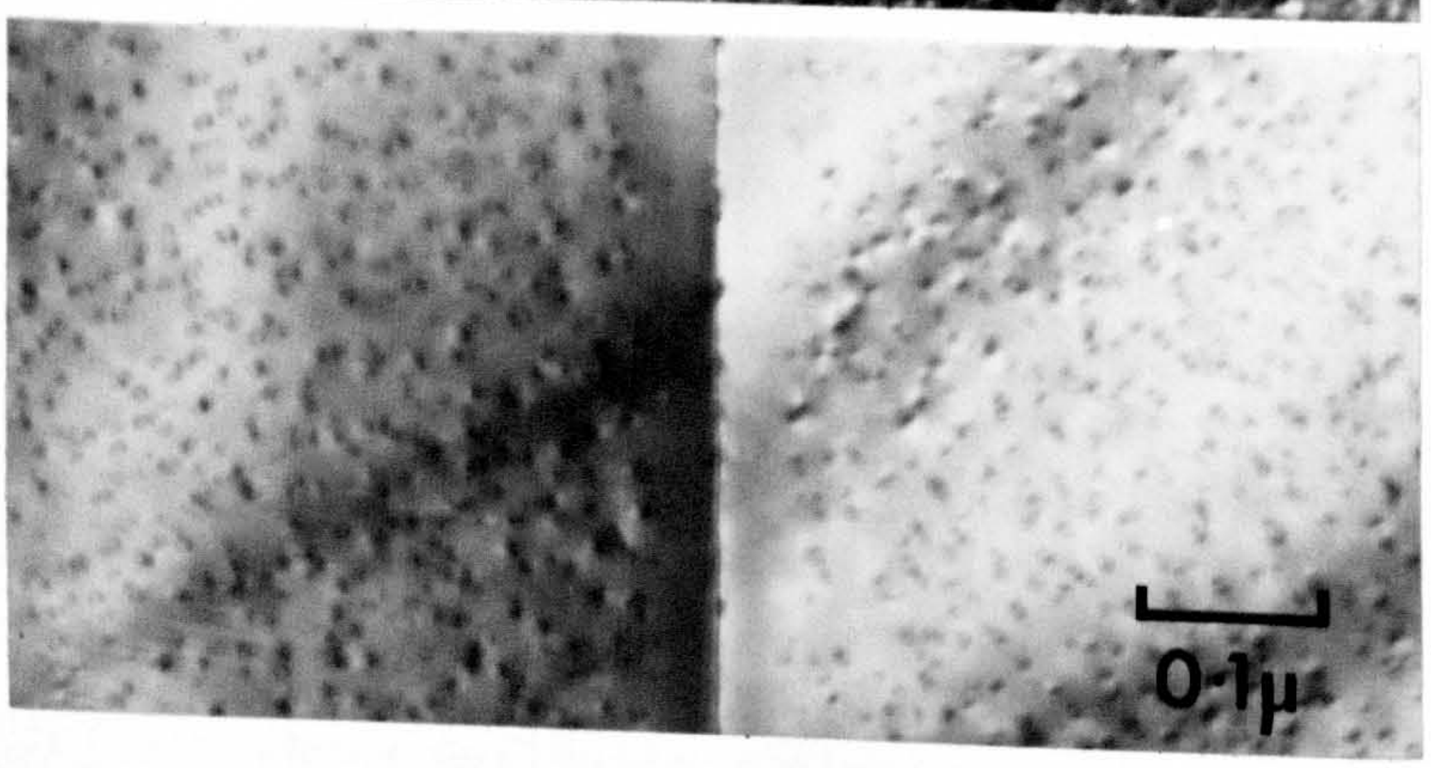

(d)

Figure 6.3 Al-17.5%Zn : The effect of solute-depletion near to a grain boundary on G.P. zone formation. (a) the solute concentration profile (see text for further discussion). (b), (c) and (d) are micrographs illustrating the precipitation after a direct-quench into oil at (b) 120°C, aged for 2 hours, (c) 140°, aged for 2 hours and (d) 150°C, aged for 1½ hours.

refer to the T_c curve of Figure 6.1 from which it will be seen that the solute concentration must exceed a certain critical value $C_s(T_1)$ for nucleation to occur at T_1 (i.e. $T_c = T_1$ for an alloy of solute concentration $C_s(T_1)$). Thus, if an alloy of composition which exceeds $C_s(T_1)$ at T_s is quenched to T_1 then G.P. zone formation will occur in regions of the matrix where the full solute concentration is retained but will not occur in the neighbourhood of a grain boundary within a region where the local solute concentration is reduced to a value less than $C_s(T_1)$. If the local solute concentration is less than $C_s(T_1)$ within a distance $\pm$ w/2 of the grain boundary then a p.f.z. of width w will be formed on ageing at T_1.

Figure 6.3(a) is in fact drawn for the special case of the Al-17.5%Zn alloy, which will be discussed in more detail shortly. However, in order to illustrate the argument given above, consider ageing this alloy at $T_1 = 140^oC$. If the solute concentration profile shown in this diagram is set-up during the quench to T_1 then a p.f.z. of width X-X will be formed on ageing at 140^oC since the local solute concentration is $< C_s(140^oC)$ within this region.

The situation described above essentially refers to the situation where the alloy is step-quenched to the ageing temperature, since the assumption of a uniform, equilibrium, vacancy concentration at T_1 is believed to be approximately valid in that case. For a direct-quench to T_1 account must be taken of the associated excess-vacancy profile in the vicinity of the grain boundary. Under these conditions a modified value of critical solute concentration $C_s'(T_1)$, which is less than $C_s(T_1)$, must be used (see Figure 6.1). The precise value of $C_s'(T_1)$ will depend upon the local excess-vacancy concentration and will thus vary with distance from the grain boundary.

Summary of the model

The model shows how either vacancy-depletion or solute-depletion

may give rise to a p.f.z. at a grain boundary. In many cases both types of depletion will be present simultaneously at the beginning of ageing at T_1. Thus, when $T_1 > T_c$, the presence of solute-depletion in addition to vacancy-depletion may modify the widths of the p.f.z's discussed in case (1) above. Similarly, as discussed in case (2), vacancy-depletion in addition to solute-depletion may modify the widths of the p.f.z's for ageing at $T_1 < T_c$. Nevertheless, two points are worth emphasizing :

(1) the presence of p.f.z's on ageing at a temperature $T_1 > T_c$ indicates that, in regions where precipitation has occurred, the local excess-vacancy concentration exceeds the critical value $(C_v)_{crit}$ and that the p.f.z's are formed predominantly because of the depletion of excess-vacancies ;

(2) no p.f.z's would appear on ageing at a temperature $T_1 < T_c$ unless solute-depletion occurs.

Finally, it should be pointed out that, according to this model, the width of a p.f.z. is controlled solely by the extent of the region of solute-depletion (and/or vacancy-depletion) and the inhibiting affect that this has on the local nucleation of G.P. zones. Once the p.f.z. has been established it is assumed to undergo no significant change in width during subsequent isothermal ageing.

Experimental results

These results were obtained with the alloy of nominal composition Al-17.5%Zn. During the electron microscopic examination of the heat treated samples full use was made of the specimen tilting facility of the microscope so that the grain boundary under observation could be oriented, as near as possible, parallel to the electron beam. The selected-area electron diffraction technique was used to determine the orientation of the

grains either side of the grain boundary in order that their relative misorientation could be measured.

It is convenient to separate the results into two groups, depending upon whether the ageing temperature (T_1) was above or below the critical temperature $T_c = 156^oC \pm 2^oC$ (see Chapter 4).

Group (1) : $T_1 > T_c$

Consider, first of all, samples which were direct-quenched into an oil bath held at 160^oC, which was $\sim 4^oC$ above T_c and $\sim 1^oC$ below T_c' (oil) (see Chapter 4). The samples were initially solution treated for 1 hour at 560^oC and then quenched into a salt bath held at either 475^oC, 370^oC or 300^oC and annealed at that temperature for 1 minute to allow the majority of the excess-vacancies to anneal out. The samples were then quenched from T_Q (the quenching temperature) into the oil at 160^oC and aged for 1 hour.

Figures 6.2(b), (c) and (d) illustrate the typical p.f.z's observed on quenching from 475^oC, 370^oC and 300^oC, respectively. The narrowest p.f.z. was observed in the sample quenched from 475^oC and was $\sim 1\mu$ in width. A much wider p.f.z. was formed in the sample quenched from 370^oC and was $\sim 3.5\mu$ in width. This pair of results is consistent with Figure 6.2(a) if 475^oC and 370^oC are made to correspond to the high and medium values of quenching temperature. The sample quenched from 300^oC contained no G.P. zones after ageing for 1 hour at 160^oC, which is the situation predicted by Figure 6.2(a) for the excess-vacancy profile which corresponds to the low quenching temperature. Thus, the variation of p.f.z. width with quenching temperature, as predicted by the model and summarized by Figure 6.2(a), is in qualitative agreement with these experimental results.

A noticeable feature of both Figure 6.2(b) and (c) is that the edge of the p.f.z. is not well defined since there is a gradual decrease in the density of G.P. zones rather than a sharp cut-off. This sort of behaviour is to be expected if the density of G.P. zones formed is dependent upon the excess-vacancy concentration, i.e. in a region where the excess-vacancy concentration is only slightly higher than $(C_v)_{crit}$ only a few zones are formed, whereas further away from the grain boundary, where the excess-vacancy concentration is much higher than $(C_v)_{crit}$, a much higher density of zones is formed. This effect makes it difficult to determine the width of the p.f.z. accurately. The same effect was observed in samples that were direct-quenched into Wood's metal at 160°C and aged for 1 hour for which, with the same values of T_Q, the p.f.z.'s appeared to be very similar to those illustrated by Figures 6.2(b) and (c).

The precipitation in the neighbourhood of a grain boundary in a sample that was direct-quenched from 560°C into Wood's metal at 160°C has already been described in Chapter 3 and illustrated by Figure 3.15(b). In Chapter 3 the discussion concentrated on the observation that the Y-phase -free zone ($\sim 2.5\mu$ wide) was much wider than the G.P. zone-free zone ($\sim 0.4\mu$). This observation is completely consistent with the model if the critical excess-vacancy concentration required to nucleate a Y-phase precipitate is higher than that required to nucleate a G.P. zone. However, the mechanism by which the excess-vacancies aid the nucleation may be different in the two cases. As discussed in Chapter 3, it is possible that the Y-phase precipitates are nucleated heterogeneously on small vacancy clusters, whereas, as discussed in Chapter 4, it is thought that the role of excess-vacancies in G.P. zone formation (in this system) is to increase the kinetics of homogeneous nucleation.

Most of the grain boundaries that were examined in this group of results were of the high-angle type[157] although a few low-angle tilt boundaries[157] were examined for which the rotation between grains was $\geqslant 5^{o}$. No variation of p.f.z. width with angular misorientation of the boundaries was detected. No very low-angle boundaries were examined but it is pertinent that Unwin, Lorimer and Nicholson[158] found that all boundaries, in alloys of Al-Zn-Mg and Al-Cu, except those with a misorientation $\lesssim 2^{o}$, acted as ideal sinks for vacancies. It would appear that a similar condition holds for an Al-17.5%Zn alloy.

Group (2) : $T_1 < T_c$

Much narrower p.f.z's were observed in samples which were direct-quenched and aged at a temperature in the range $120^{o}C$ - $150^{o}C$. Figures 6.3(b), (c) and (d) illustrate the typical p.f.z's observed in aged samples which were direct-quenched from $560^{o}C$ into an oil bath held at $120^{o}C$, $140^{o}C$ and $150^{o}C$, respectively. Almost identical results were obtained with samples direct-quenched into Wood's metal and aged at the same three temperatures. At least three different grain boundaries were examined for each type of quench (i.e. oil or Wood's metal) and for each ageing temperature and the results can be summarized as follows:

(a) with $T_1 = 120^{o}C$, the p.f.z. width was 60 Å $\pm$ 60 Å ;

(b) with $T_1 = 140^{o}C$, the p.f.z. width was 440 Å $\pm$ 60 Å ;

(c) with $T_1 = 150^{o}C$, the p.f.z. width was 660 Å $\pm$ 120 Å.

According to the model (case (2) above) these p.f.z's are produced predominantly because of solute-depletion in the vicinity of the grain boundary immediately after the quench. If it is assumed that the small differences in ageing temperature had little effect on the amount of solute-depletion which occurred during the quench from $560^{o}C$, so that a

similar solute concentration profile was established during the quench for all samples, we may use the theory developed by the model to deduce the shape of the solute concentration profile.

First of all it is noted that even the widest p.f.z. (i.e. that produced by ageing at 150°C) is less than 25% of the width of the p.f.z. formed in a sample which was direct-quenched into Wood's metal at 160°C (as described above). This suggests that the excess-vacancy concentration immediately after the quench within a distance of about 2000 Å from the grain boundary is too low to have a major effect on the nucleation rate of G.P. zones. It is therefore believed that, to a good approximation, the effect of excess-vacancies may be ignored, so that only solute depletion effects need be considered. This approximation allows the critical solute concentrations for ageing at the three different values of T_1 that were investigated, to be calculated directly from the T_c curve of Figure 4.8. If allowance is made for a $\pm$ 1°C experimental error in the control of the value of T_1 and a $\pm$ 2°C experimental error in the determination of the T_c curve then the critical solute concentrations are as follows :

(a) C_s (120°C $\pm$ 1°C) = 13.0 $\pm$ 0.4 wt.%Zn;

(b) C_s (140°C $\pm$ 1°C) = 15.4 $\pm$ 0.4 wt.%Zn;

(c) C_s (150°C $\pm$ 1°C) = 16.7 $\pm$ 0.4 wt.%Zn.

With the knowledge of these critical solute concentrations and the corresponding experimentally determined p.f.z. widths the solute concentration profile in the neighbourhood of a grain boundary can be constructed, as shown in Figure 6.3(a). In view of the assumption made in deriving this result and the experimental errors involved, this curve is only approximate but it illustrates the degree of solute-depletion required to produce p.f.z's under these ageing conditions.

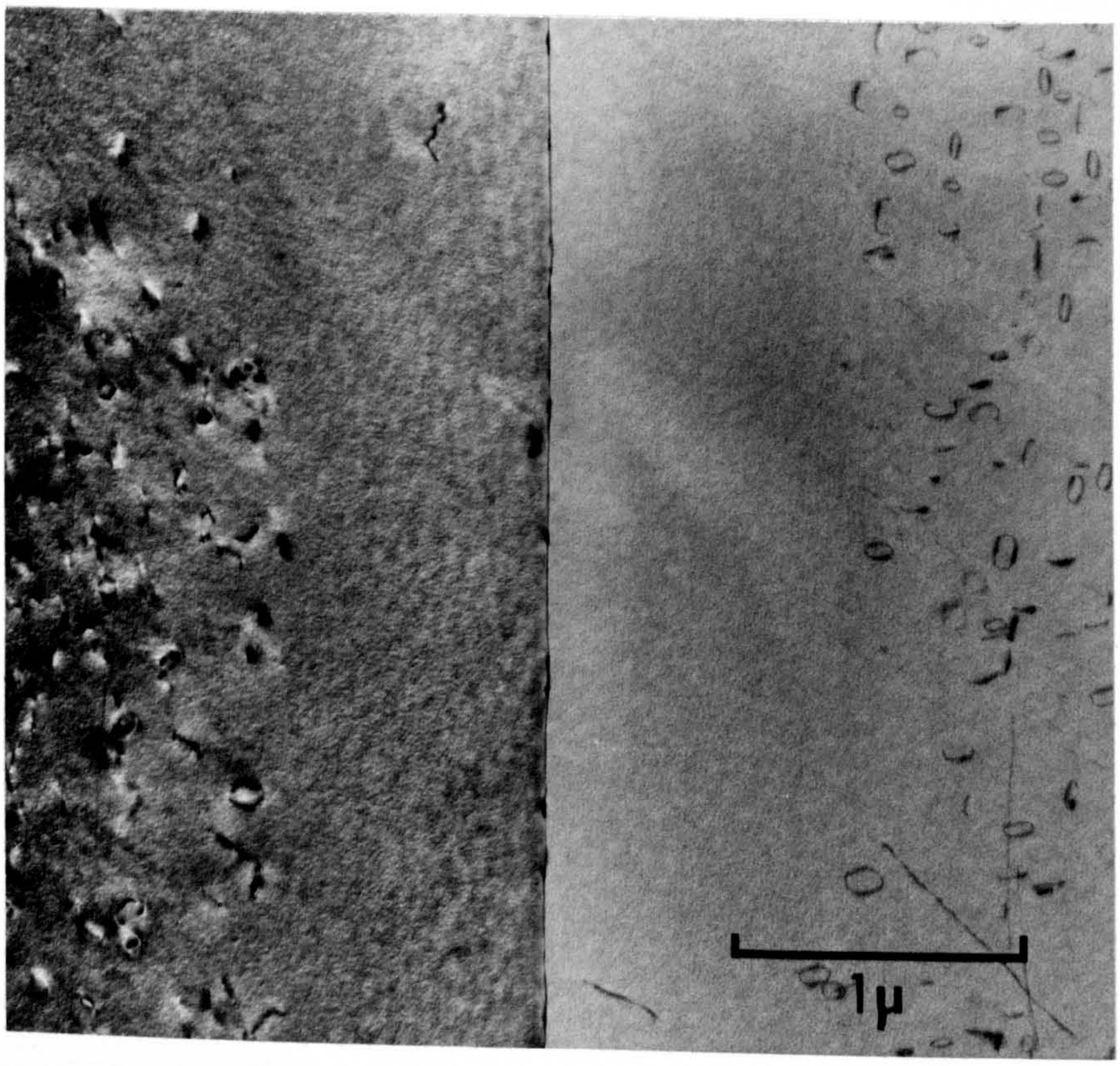

Figure 6.4 Al-17.5%Zn : A micrograph showing a wide loop-free zone in a sample direct-quenched into Wood's metal at 120°C and aged for 2 hours.

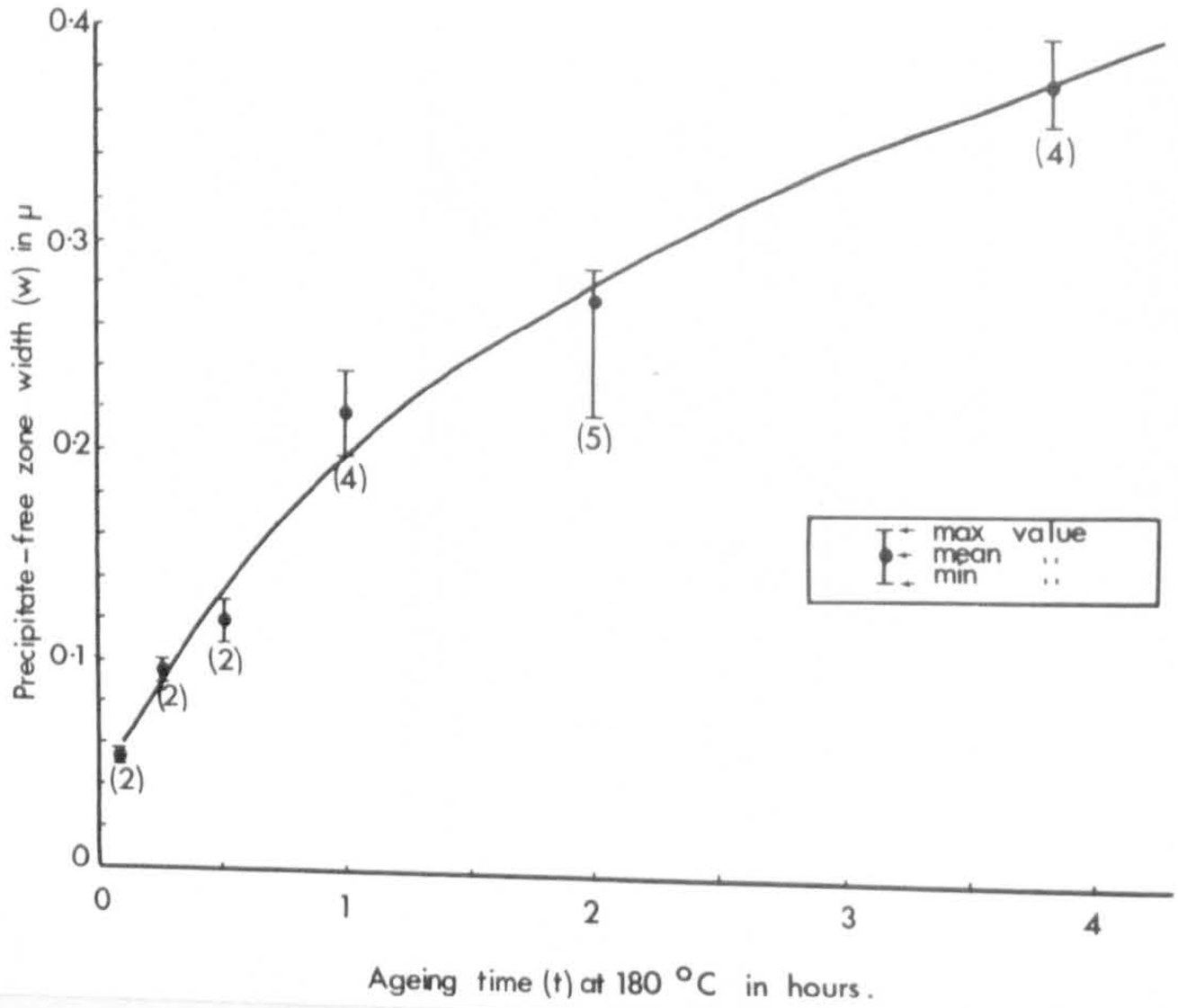

Figure 6.5 (a) Al-17.5%Zn : The effect of pre-ageing time at 180°C on the width of precipitate-free zones established after subsequent ageing at 140°C for 2 hours. The number adjacent to each experimental point is the number of different grain boundaries that were examined.

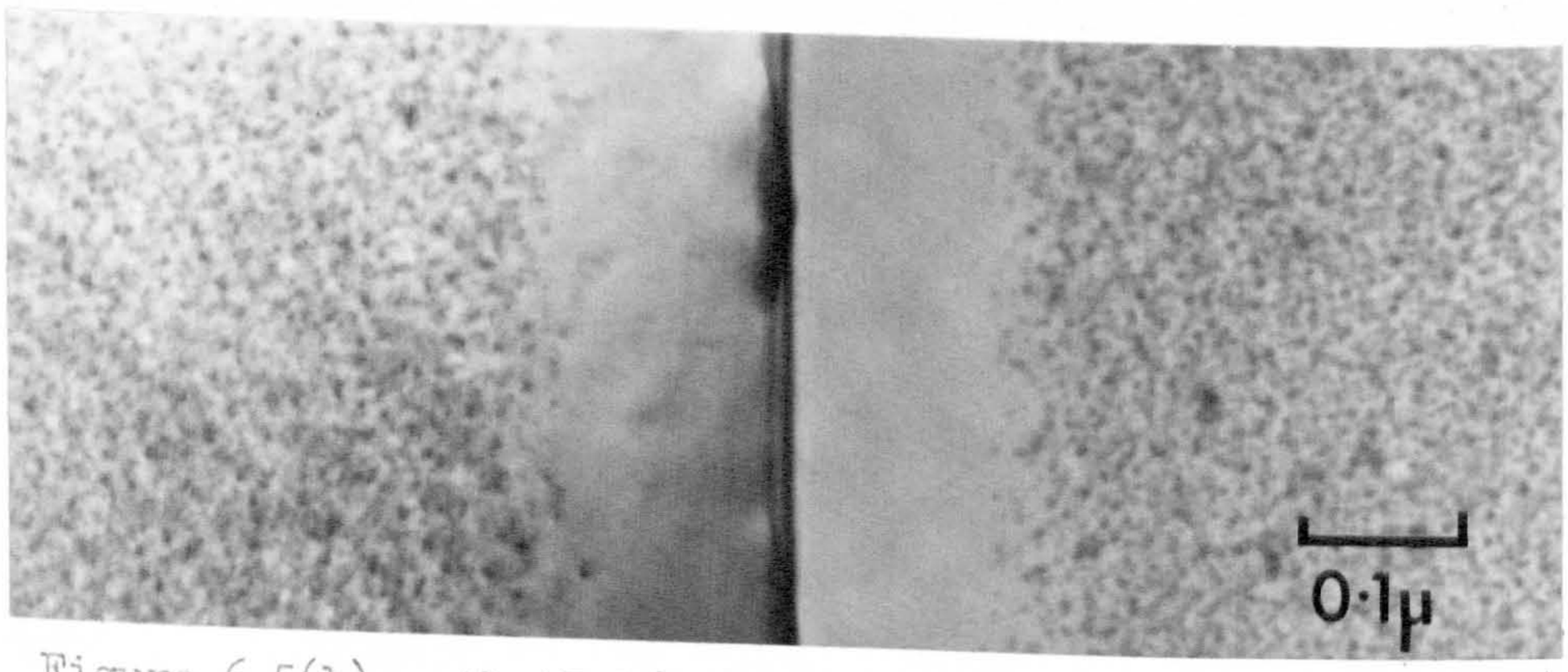

Figure 6.5(b) Al-17.5%Zn : The wide precipitate-free zone established after holding the sample at 180°C for 2 hours before a subsequent ageing treatment at 140°C for 2 hours.

All the grain boundaries that were examined were of the high-angle type and no variation of p.f.z. width with misorientation was detected.

A characteristic feature of the samples which were direct-quenched and aged in Wood's metal at 120°C was a high density of dislocation loops well within the grains and a wide loop-free zone adjacent to all grain boundaries. This is illustrated by Figure 6.4. No stacking fault fringes were observed in any of the loops, so it was concluded that the loops were of the prismatic type[122,123], which is consistent with the observations of Thomas[121]. The observation of a loop-free-zone ($\sim 2\mu$ wide in Figure 6.4) may be considered as indirect evidence of the presence of an excess-vacancy profile in the neighbourhood of the grain boundary during and immediately after the quench, by the following reasoning[121,123]; the formation of dislocation loops requires a high vacancy supersaturation and, because of the vacancy-depletion near to grain boundaries, the vacancy supersaturation is too low for loops to form within a certain distance of the grain boundary.

Much wider p.f.z's were observed in samples that were step-quenched, via a long holding treatment at 180°C, into oil at 140°C. It was found that the width of the p.f.z's increased with increase in holding time at 180°C, as shown by Figure 6.5(a). The wide p.f.z. established at 140°C after a holding treatment of 2 hours at 180°C is illustrated by Figure 6.5(b). It is believed that the width of these p.f.z's was controlled solely by the degree of solute-depletion which occurred during the holding at 180°C, since it is thought that the vacancy concentration would have rapidly decayed to the equilibrium value at this temperature. As the holding time at 180°C was increased a progressively wider region of solute-depletion was formed so that progressively wider p.f.z's were established during subsequent ageing at 140°C. An analysis of the results is given in the Appendix

where it is shown that the rate of solute-depletion can be explained in terms of the diffusion of Zn atoms to the grain boundary at the equilibrium rate.

All the grain boundaries that were examined in this group of experiments were of the high-angle type. Cornish and Day[155,156] have carried out similar step-quenching experiments with an Al-Zn-Mg alloy and they also found that progressively wider p.f.z's were established near to high-angle grain boundaries in different samples which were progressively held for a longer time at a temperature above T_c before being subsequently aged at a temperature below T_c. They also explained their results in terms of solute-depletion and deduced that the diffusion of solute atoms to the grain boundary during the holding treatment occurred at approximately the equilibrium rate, except for during an initial transient period immediately after the quench to the holding temperature when the rate of diffusion was probably increased by a quenched-in excess-vacancy concentration. They also obtained the interesting result that, although the p.f.z's associated with high-angle boundaries were all uniform in width, the p.f.z's associated with low-angle boundaries were of variable width if a high value of holding temperature was used. This observation was attributed to the large separation between grain boundary precipitates, when they were formed at a high temperature, so that their individual regions of solute-depletion did not overlap, and to the absence of a high diffusivity path (as usually provided by a high-angle boundary[10]) connecting these particles.

6.2.2 Precipitate-free zones produced by two-step ageing

Theoretical model

Consider a two-step ageing treatment in which a sample is

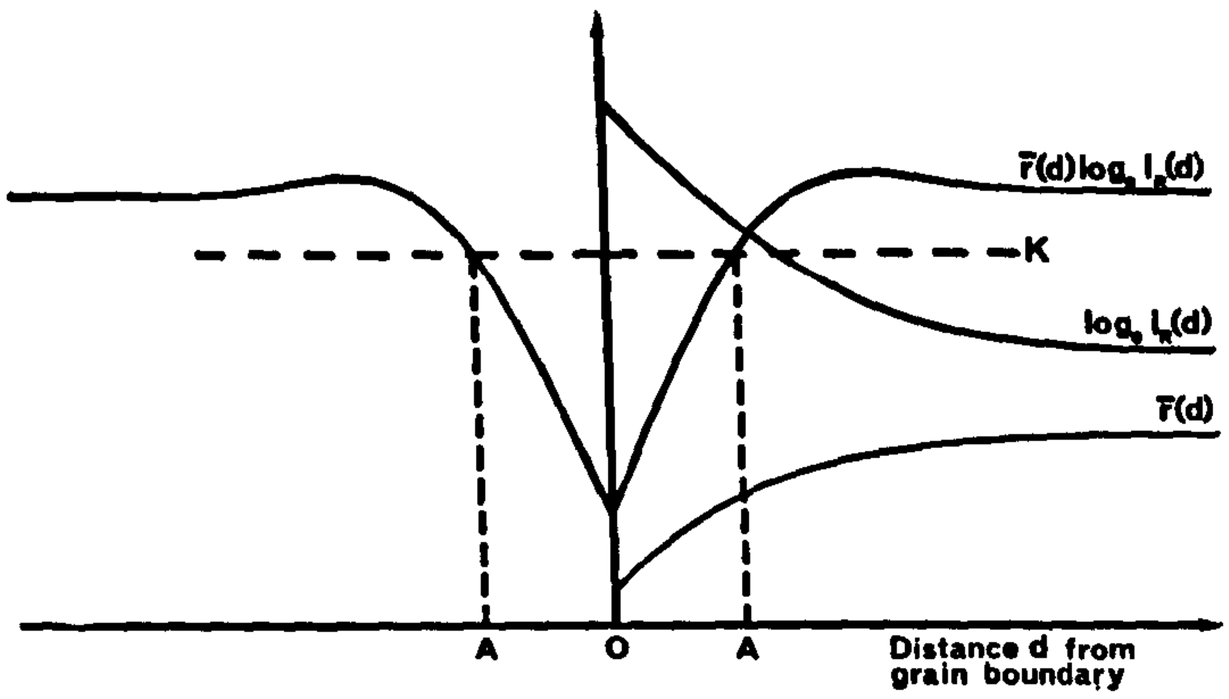

Figure 6.6(a) The general form of the stability function $\bar{r}(d)\ \log_e i_R(d)$ in the vicinity of a grain boundary at T_2. A-A defines the region within which the G.P. zones grown at T_1 will be unstable at T_2.

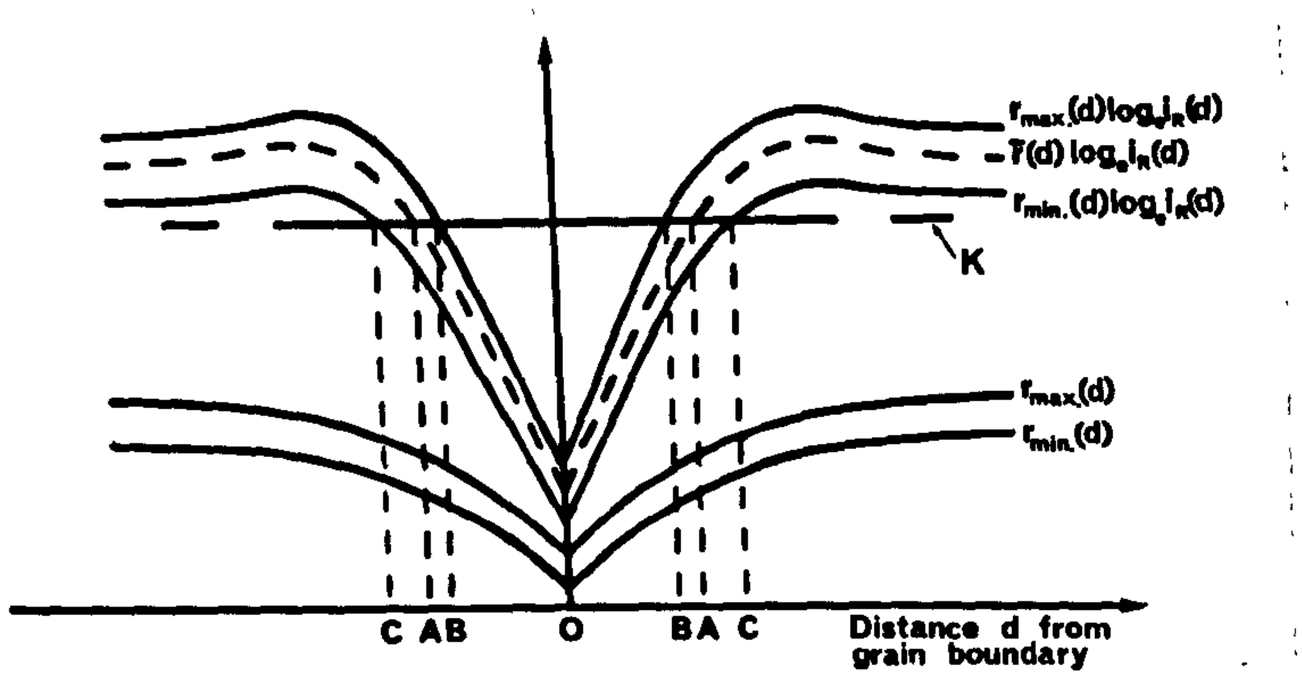

Figure 6.6(b) The form of the stability function at T_2 when the sizes of G.P. zones are distributed between r_{min} and r_{max}.

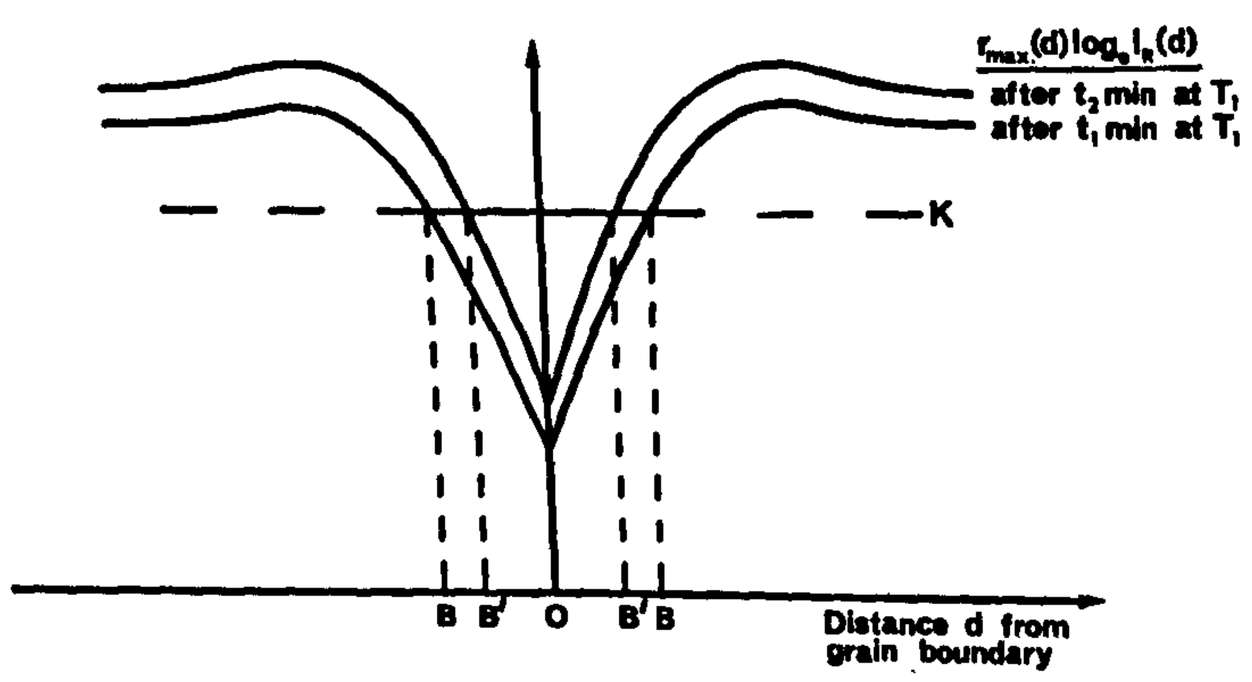

Figure 6.6(c) Comparison of the stability function curves at T_2, for the maximum-sized G.P. zones, after times t_1 and t_2 ($t_1 < t_2$) at T_1.

initially quenched to a temperature T_1 (below T_c), aged for a time t_1, and then subsequently aged at a higher temperature T_2 (which may be either above or below T_c). Let us examine the situation where $T_1 \ll T_c$ so that G.P. zone nucleation occurs at T_1 throughout the grains and right up to the grain boundary (see section 6.2.1 above). Immediately after a direct-quench to T_1 an excess-vacancy concentration gradient will be established adjacent to all grain boundaries and within these regions of excess-vacancy-depletion the growth rate of the G.P. zones will be lower than in the grain interiors. For the case of spherical G.P. zones, the radius of the average-sized G.P. zone, $\bar{r}$ (d), will vary with distance d from a grain boundary after an ageing time t_1 at T_1 in the manner illustrated schematically in Figure 6.6(a). During the ageing time t_1 the density of G.P. zones (N) in the neighbourhood of a grain boundary is assumed to remain constant (the validity of this assumption is discussed in Chapter 8) and the remaining solute concentration is assumed to be distributed uniformly between the zones. If the temperature of the alloy is now increased to T_2 then, in principle, the variation with distance d from the grain boundary of the remaining solute supersaturation in the matrix, $i_R(d)$, can be determined. According to the model for two-step ageing that was outlined in Chapter 5, the G.P. zones will only remain stable and continue to grow in regions of the matrix where

$$\bar{r}\,(d)\,\log_e i_R(d) \;>\; K \qquad (6.1)$$

The general form of the stability function $\bar{r}$ (d) $\log_e i_R(d)$ in the neighbourhood of a grain boundary is shown schematically on Figure 6.6(a) and the stability constant K is indicated by the horizontal broken line. G.P. zones within the region defined by A-A on this diagram will be

initially unstable at T_2 and will start to dissolve, whereas zones outside this region will be seeded for growth at T_2.

The model is now extended to include the situation where G.P. zones at T_1, at a distance d from a grain boundary after a time t_1, have a distribution in sizes ranging between the maximum and minimum values $r_{max}(d)$ and $r_{min}(d)$, as illustrated schematically by Figure 6.6(b), which is drawn for the case where $T_1 > T_1(min)$ - see Chapter 5. The functions $r_{max}(d)\ \log_e i_R(d)$ and $r_{min}(d)\ \log_e i_R(d)$ now determine the stability of the maximum-sized and minimum-sized G.P. zones, respectively. Thus, the maximum-sized G.P. zones are initially unstable at T_2 within the region defined by B-B in Figure 6.6(b), whereas the minimum-sized G.P. zones are initially unstable within the wider region defined by C-C. Between the two regions B-C, either side of the boundary, there will be a gradation in the number of G.P. zones that are seeded for growth at T_2 from zero at B to N at C, and the width of B-C will depend upon the size distribution of G.P. zones.

Next, consider the situation after a longer period of ageing (t_2) at T_1. During the time $t_1 \rightarrow t_2$ the G.P. zones will grow in size so that the general form of the $r_{max}(d)\ \log_e i_R(d)$ curves after up-quenching to T_2, after the periods t_1 and t_2 at T_1, will be as illustrated by Figure 6.6(c), from which it may be deduced that the region within which no seeding occurs is reduced from B-B to B'-B' for the increased period of ageing at T_1.

The ideas developed above can now be used as a basis for predicting the types of p.f.z. that can be formed at T_2 and two cases may be distinguished.

Case (1) : $T_2 > T_c$

Since $T_2 > T_c$ then G.P. zones will only grow at T_2 if they have been seeded for growth at T_1. Clearly, if $T_2 > T_{G.P.}$ then it is impossible

for G.P. zones to be seeded for growth at T_2 (see Chapter 5). If $T_c < T_2 < T_{G.P.}$ then the situation will be as illustrated by Figure 6.6(c) where B-B and B'-B' define the widths of the p.f.z's that will be established on ageing at T_2 after pre-ageing times of t_1 and t_2 at T_1, respectively. Progressively narrower p.f.z's will be established at T_2 as the pre-ageing time at T_1 is progressively increased. If T_1 is only slightly below T_c, so that a solute-depleted p.f.z. is established during ageing at T_1, it follows that G.P. zones cannot be formed within this region during ageing at T_2 even for a very long pre-treatment at T_1. Even if $T_1 \ll T_c$, so that solute-depletion during the quench does not inhibit G.P. zone formation adjacent to the grain boundary at T_1 (see section 6.2.1 above), the solute-depletion will modify the condition for seeding at T_2 so that it is more difficult for seeding to occur and a p.f.z. may be formed even with a very long pre-treatment.

Case (2) : $T_2 < T_c$

If $T_2 < T_c$ then B-B and B'-B' of Figure 6.6(c) still define regions within which G.P. zones are not seeded for growth at T_2. Within B-B or B'-B' the G.P. zones will initially be unstable at T_2 and will start to dissolve, but restabilization of some of the larger G.P. zones may occur in the manner already described in Chapter 5. Thus, after the final ageing treatment at T_2 a lower density of G.P. zones is expected within B-B or B'-B' than outside these regions. No true p.f.z. will be formed unless, because of solute-depletion, the effective critical temperature in a narrow region either side of the grain boundary is reduced to a value below T_2 so that, in this region, the situation becomes as described in case (1) above, and a narrow p.f.z. will be formed.

Experimental results

Two-step ageing studies were carried out on samples of Al-17.5%Zn

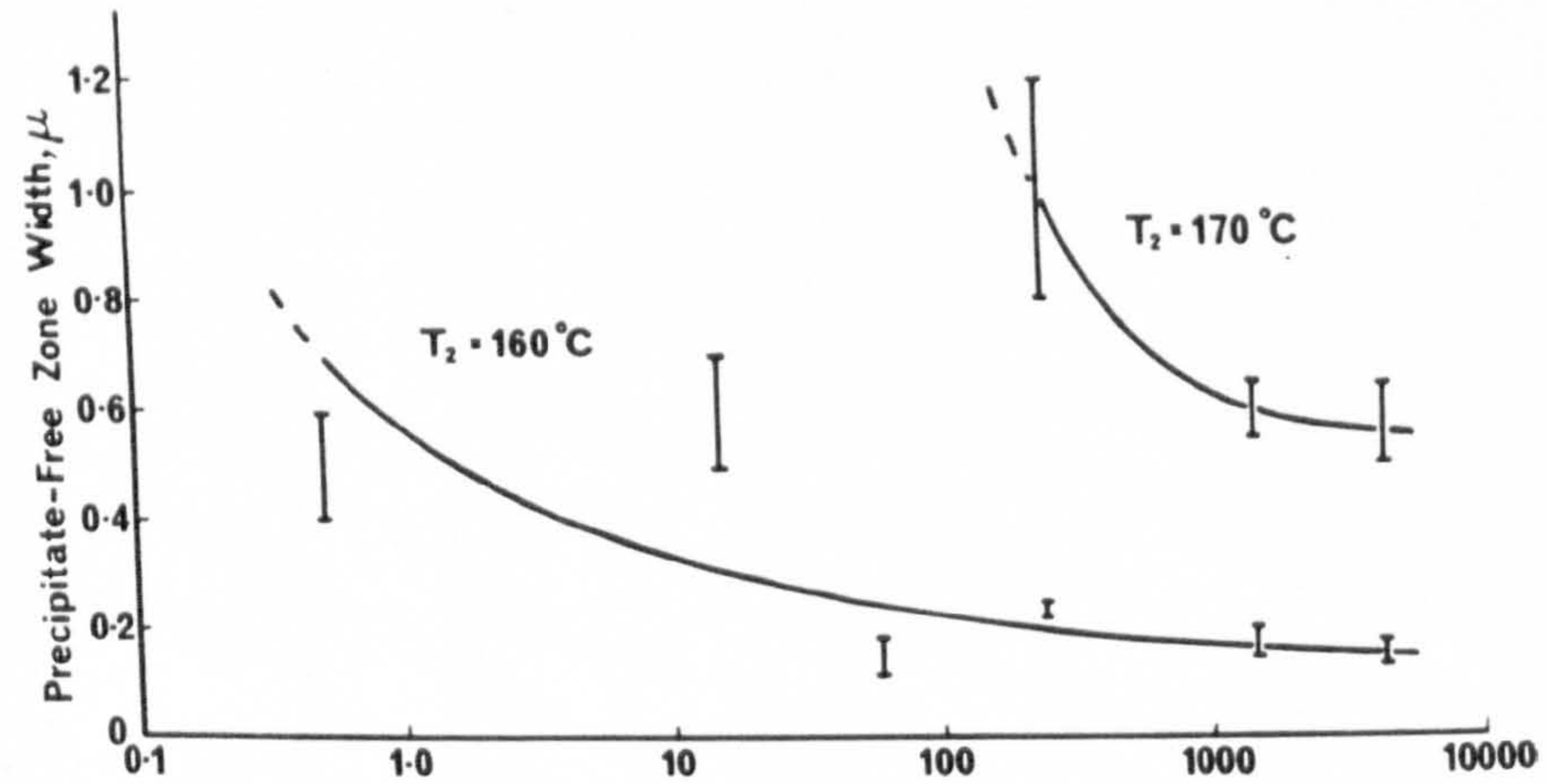

Figure 6.7 The effect of pre-treatment time at room temperature on the width of precipitate-free zones established after subsequent ageing at either 160°C for 1 hour or 170°C for 20 minutes.

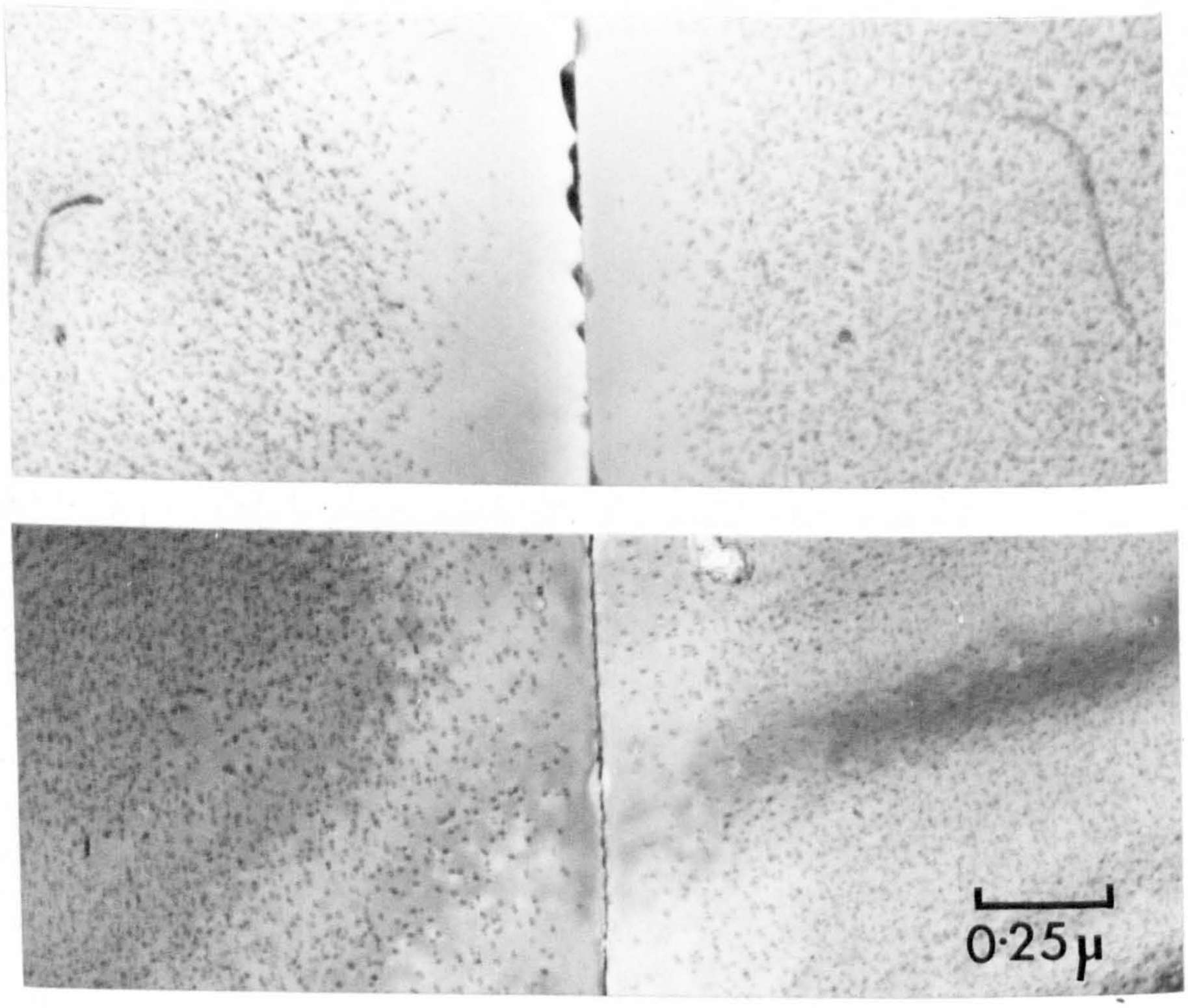

Figure 6.8 Al-17.5%Zn : The nature of the precipitation near to a grain boundary in a sample which was direct-quenched into water at room temperature and aged for $\frac{1}{2}$ minute before being subsequently aged at (a) 160°C for 1 hour and (b) 150°C for $1\frac{1}{2}$ hours.

which were solution treated at 560°C, direct-quenched into water at room temperature, aged for times ranging between $\frac{1}{2}$ minute and 3 days, and then subsequently aged with T_2 at either 150°C, 160°C, 170°C or 180°C. The reader is reminded that for this alloy composition, $T_c = 156°C \pm 2°C$ (see Chapter 4).

Case (1) : $T_2 > T_c$

Samples which were pre-aged at room temperature for short times exhibited wide p.f.z's after subsequent ageing at both 160°C and 170°C, whereas those pre-aged for longer times exhibited narrow p.f.z's. The experimentally observed variation of p.f.z. width as a function of pre-ageing time at room temperature is plotted in Figure 6.7 for T_2 at 160°C and 170°C. All thegrain boundaries examined were of the high-angle type. No G.P. zones were observed in samples that were pre-aged at room temperature for up to 1 hour and then subsequently aged at 170°C. Also, no G.P. zones were observed in samples which were pre-aged at room temperature for up to 3 days before being subsequently aged at 180°C. These results are discussed again in Chapter 7.

Figure 6.8(a) illustrates a typical p.f.z. obtained by pre-ageing a sample for $\frac{1}{2}$ minute at room temperature before ageing at 160°C. The gradation in G.P. zone density at the edge of the p.f.z., as predicted by the model, is visible on this micrograph.

G.P. zones could easily be detected in a sample that was direct-quenched into water at room temperature and aged for 3 days. The nature of the precipitation in the neighbourhood of a grain boundary after this treatment is illustrated by Figure 6.9(a). The G.P. zones are clearly much smaller near to the grain boundary. The narrow p.f.z. which was established in a sample that was pre-aged at room temperature for 3 days

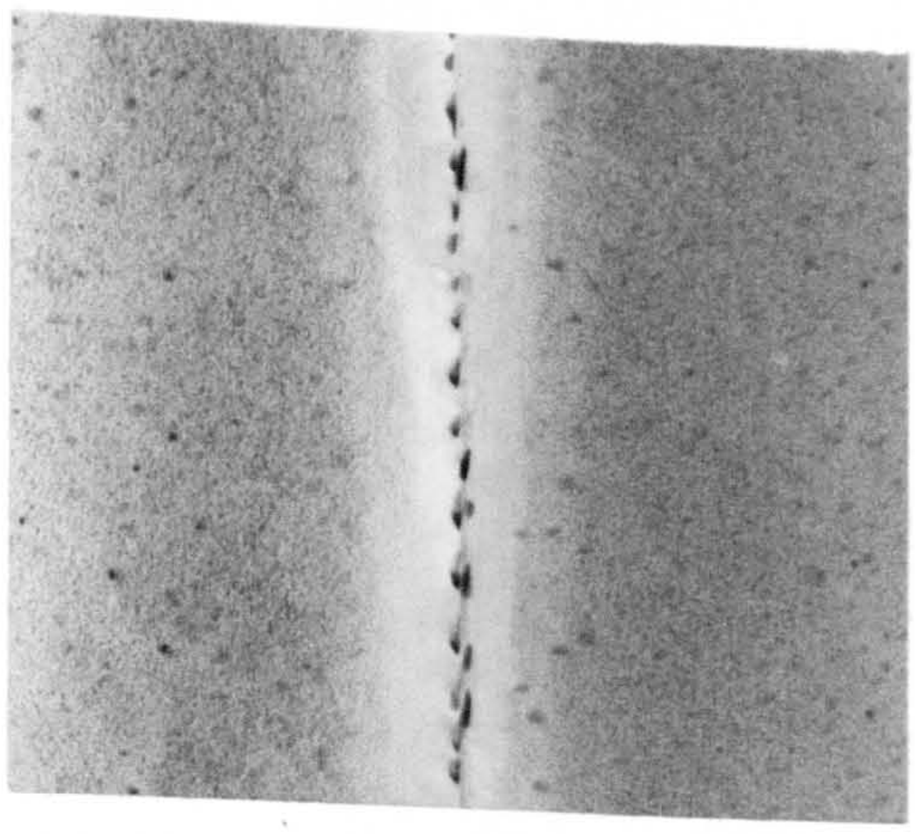

(a)

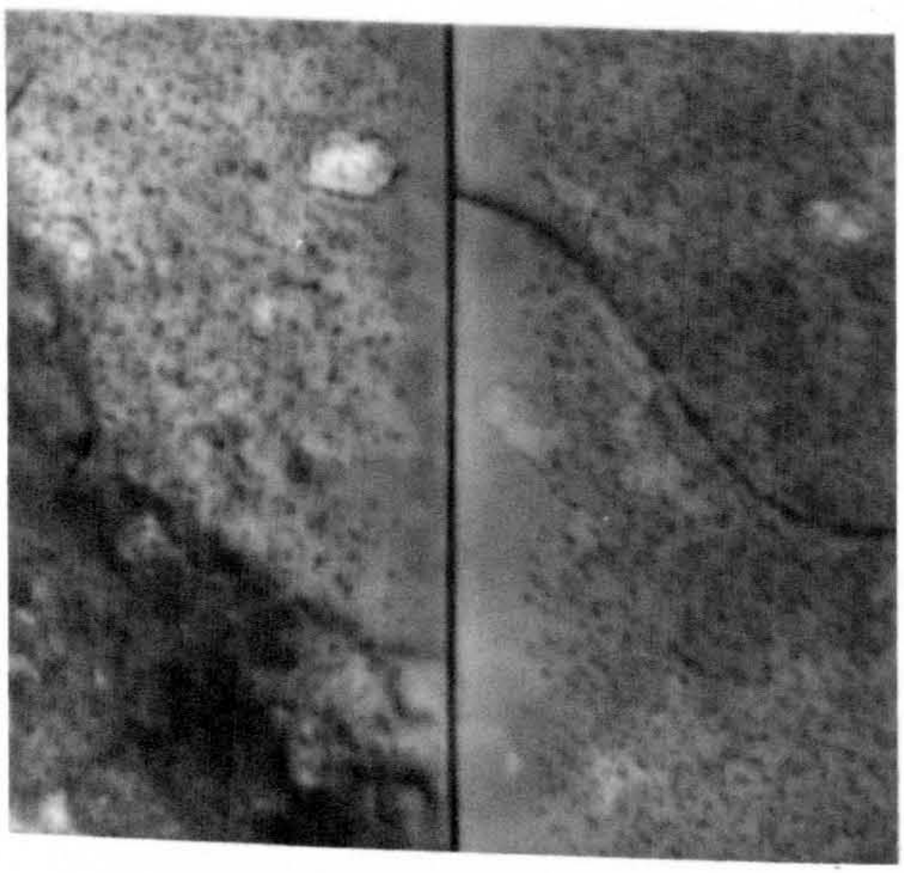

(b)

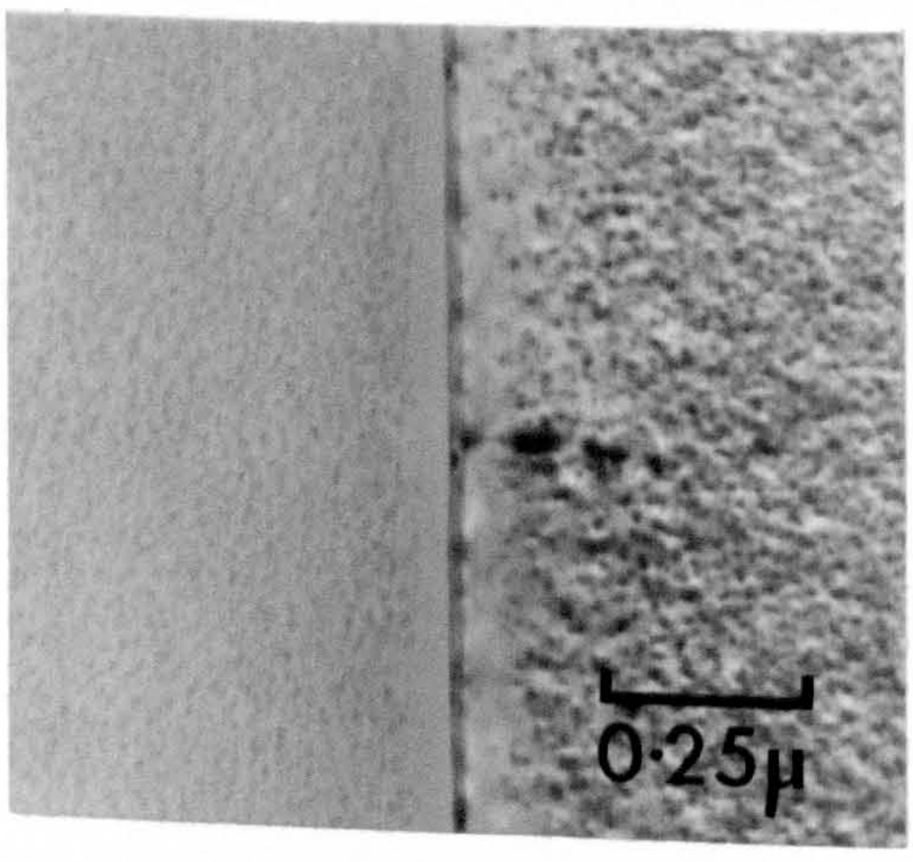

(c)

Figure 6.9 Al-17.5%Zn : The nature of the precipitation near to a grain boundary (a) after 3 days at room temperature; (b) as (a) plus 1 hour at 160°C; (c) as (a) plus $1\frac{1}{2}$ hours at 150°C.

before being subsequently aged at 160°C is illustrated by Figure 6.9(b).

The results summarized by Figure 6.7 show that, for a given pre-treatment at T_1, the p.f.z. established on subsequent ageing at 170°C is wider than that established on ageing at 160°C. This behaviour is predicted by the model and arises because the G.P. zones must grow to a larger size before they are stable in the remaining solute supersaturation associated with a higher value of T_2.

Case (2) : $T_2 < T_c$

The p.f.z. shown in Figure 6.8(b) is typical of those observed in a sample that was pre-aged at room temperature for $\frac{1}{2}$ minute before being subsequently aged at 150°C. It illustrates the case, discussed in the model above, where there is a region either side of the grain boundary where G.P. zones were not seeded during the pre-treatment and where re-stabilization of some G.P. zones has subsequently occurred at 150°C, giving rise to a local lowering of the G.P. zone density compared to that further away from the grain boundary. The narrow p.f.z. is also to be noted which, as discussed above, is believed to arise because of localised solute-depletion near to the grain boundary.

Longer times of pre-treatment at room temperature caused the "seed-free" zone established at 150°C to be progressively reduced in width and it was not detectable in samples pre-aged at room temperature for $\geqslant$ 1 hour. In samples pre-aged between 1 hour and 3 days at room temperature, before being subsequently aged at 150°C, a narrow p.f.z. was formed which appeared to be independent of pre-ageing time (Figure 6.9(c) shows an example of this in a sample that was pre-aged for 3 days). It is thought that these p.f.z's were caused primarily because of solute-depletion.

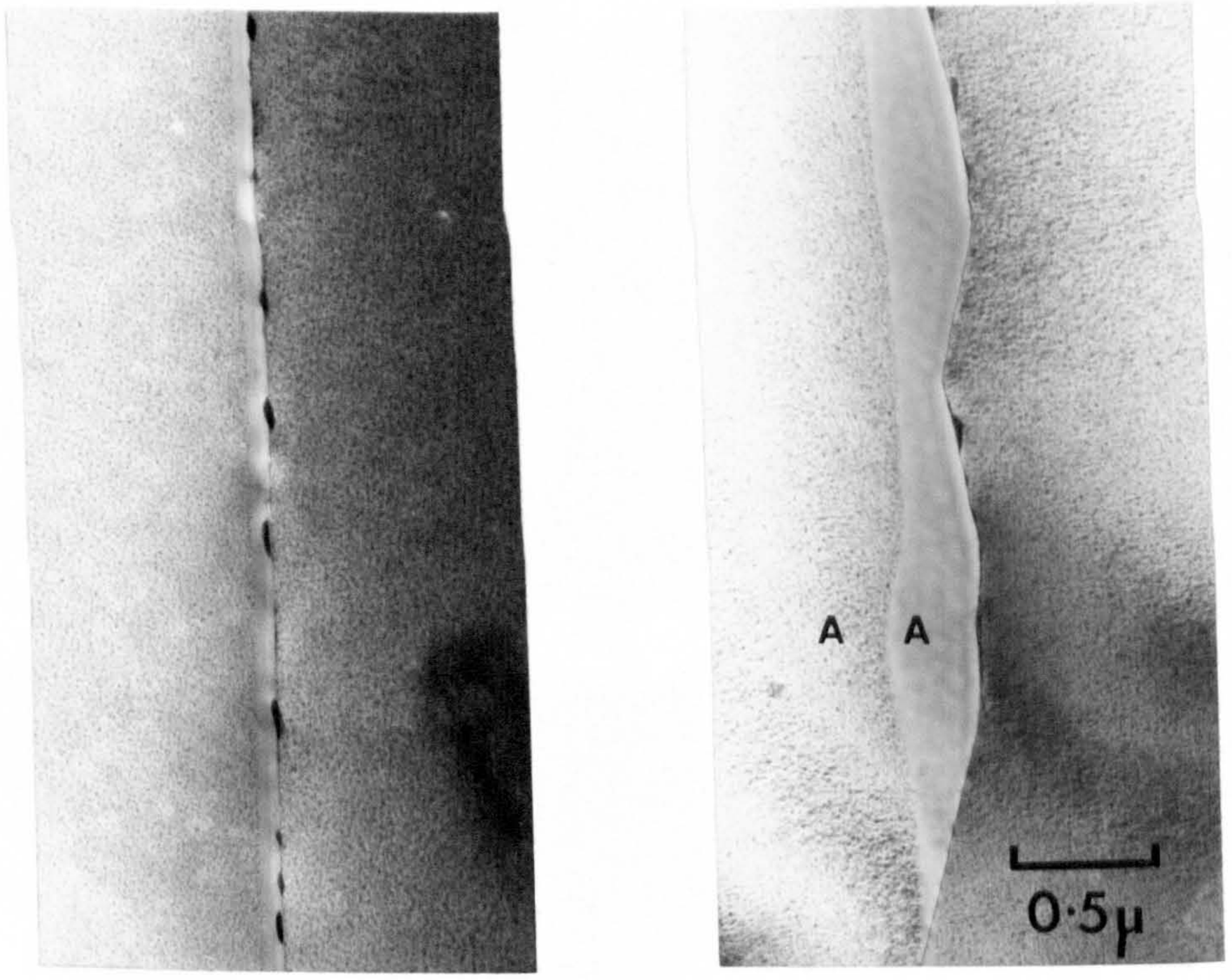

(a) (b)

Figure 6.10 Al-17.5%Zn : Asymmetrical precipitate-free zones in samples aged at 120°C for (a) 2 hours and (b) 16 hours. The two areas labelled A, in (b), were of identical crystal orientation.

6.2.3 Asymmetrical precipitate-free zones

During the work described in the previous two sections some p.f.z's were observed which were asymmetrical with respect to the grain boundaries. An example of this in a sample which was direct-quenched into oil at 120°C and aged for 3 hours is illustrated in Figure 6.10(a) (cf. Figure 6.3(b)).

These asymmetrical p.f.z's were not studied extensively, but a few interesting results were obtained with samples which were direct-quenched into Wood's metal and aged for various times. These results showed that the asymmetrical p.f.z's developed during ageing at 120°C. Apart from one isolated grain boundary which was associated with a very narrow asymmetrical p.f.z., all the many other grain boundaries which were examined in a sample which was aged for only $\frac{1}{2}$ hour at 120°C were associated with the extremely narrow symmetrical p.f.z. of the type discussed in section 6.2.1. For longer ageing times at 120°C (between 2 and 16 hours) a noticeable difference in the behaviour between high-angle and low-angle grain boundaries was observed. Many of the high-angle grain boundaries appeared to have migrated during the ageing treatment, giving rise to a wide asymmetrical p.f.z. of variable width, as exemplified by Figure 6.10(b), whereas no such behaviour was associated with low-angle boundaries. The high-angle boundaries that had only migrated a short distance ($\lesssim 0.1\mu$) were usually still straight (similar in appearance to that illustrated by Figure 6.10(a)), whereas those that had migrated a much larger distance (as in Figure 6.10(b)) were kinked and contained numerous large grain boundary precipitates which were thought to be of the equilibrium Zn phase. The extent of the migration of high-angle boundaries varied greatly, even within the same sample, but the general trend was for the migration to be more extensive in the samples which were aged for a

longer time at 120°C.

Asymmetrical p.f.z's were also observed in samples which were given a two-step ageing treatment.

It is thought that all the asymmetrical p.f.z's were associated with the beginning of discontinuous precipitation[9,10] at the high-angle grain boundaries. This phenomenon has also been called "cellular precipitation"[159,160] and the "recrystallization reaction"[11]. Also, when it was first observed by optical-metallography in Al-Cu alloys[161,162] and in Al-Zn alloys[163], it was called the "light phenomenon".

The observations reported above are completely consistent with the mechanism of discontinuous precipitation put forward by Smith[164] in which a high-angle grain boundary migrates into one or other of its adjacent grains, during which precipitates are formed along the boundary and a solute-depleted matrix, whose orientation is identical to that from which the boundary is migrating, is left behind it. The latter point was confirmed by selected-area electron diffraction and dark-field microscopy which indicated that the two regions labelled A in Figure 6.10(b) were of identical crystal orientation.

According to Cahn[160] the driving force for discontinuous precipitation is the net free energy change caused by the movement of the grain boundary. In the case considered here a large part of the free energy change was thought to be derived from the conversion of small metastable G.P. zones into large equilibrium precipitates. The redistribution of the solute atoms appeared to occur only at the grain boundary as it advanced forward and no evidence was observed to indicate that G.P. zone dissolution started ahead of the grain boundary.

The observation of discontinuous precipitation in Al-Zn alloys has been reported by several other workers[9,107,111,165,166].

6.3 CONCLUSIONS

In this Chapter the pronounced p.f.z's that were observed in the vicinity of grain boundaries in samples of Al-17.5%Zn have been described. Symmetrical p.f.z's were observed in samples that were either (1) direct-quenched to the ageing temperature or (2) given a two-step ageing treatment. Two theoretical models have been derived, based on the concepts outlined in Chapters 4 and 5, which can qualitatively explain the observed variation of p.f.z. width with ageing conditions for both types of heat treatment. Both models invoked vacancy-depletion and/or solute-depletion in the neighbourhood of the grain boundaries as the primary cause of the p.f.z's. In the case of samples that were direct-quenched and aged, it was the inhibiting effect of either, or both, of these types of depletion on the nucleation of G.P. zones that was shown to be responsible for giving rise to p.f.z's. Whereas, in the case of two-step ageing, it was the detrimental effect of these two types of depletion on the growth and stability of G.P. zones that was shown to be the controlling factor which influenced the p.f.z. width. The usefulness of the concept of a critical temperature T_c for aiding the interpretation of the observed precipitation behaviour was demonstrated.

Asymmetrical p.f.z's were also observed and these were believed to be associated with the start of discontinuous precipitation.

Finally, it should be mentioned that p.f.z's were sometimes observed within the grains around matrix dislocations and heterogeneous precipitates. It is thought that whenever a localised region of solute-depletion and/or vacancy-depletion is produced in the vicinity of a sink (e.g. a dislocation or some other heterogeneity) then the models developed above for grain boundaries will be equally applicable and a p.f.z. may be formed. An example of this behaviour is illustrated by Figure 7.2(a) and is discussed in the next Chapter.

CHAPTER 7

THE REVERSION OF G.P. ZONES IN Al-Zn ALLOYS

7.1 INTRODUCTION

The phenomenon of reversion (sometimes called retrogression or restoration) is the name given to the process whereby the changes in mechanical properties which accompany the low temperature ageing of a precipitation-hardening alloy can be destroyed temporarily if the alloy is subjected to a short high temperature anneal above the so-called "minimum reversion temperature" before being subsequently returned to the initial ageing temperature. This behaviour was first discovered by Gayler[167], in 1922, who found that the increase in hardness attained by a Duralumin alloy, when aged at room temperature, could be removed by a short anneal at a temperature above $\sim 200^{\circ}C$. A similar behaviour is now known to be exhibited by a large number of precipitation-hardening alloys (see Kelly and Nicholson[9], Guinier[13] and Hardy[168]).

Thus, from an experimental point of view, a "reversion heat treatment" is just a special kind of two-step ageing treatment. It is now widely accepted that during the reversion treatment the homogeneous precipitates that are formed during the pre-treatment at T_1 become unstable and dissolve when the temperature is raised to T_2, so that the alloy returns (almost) to a single phase solid solution (heterogeneous precipitates need not necessarily be dissolved during the reversion treatment if they are a more stable type of precipitate than the homogeneous precipitates - see later in this Chapter).

For many of the more important age-hardening alloys it is the formation of G.P. zones which gives rise to the increase in hardening

during low temperature ageing. In this case the process of reversion corresponds to a two-step heat treatment in which the G.P. zones are dissolved during the second ageing treatment.

This Chapter is concerned with the reversion of G.P. zones in Al-Zn alloys. Two-step ageing treatments are described in which a series of samples were pre-aged at a temperature T_1 for progressively longer periods of time before being subsequently treated at a higher temperature T_2 which was always above the critical temperature T_c for the particular alloy under study. Each sample was then examined by electron microscopy to see if the G.P. zones which were grown during the pre-treatment at T_1 had remained stable and continued to grow at the second ageing temperature T_2. If so, then the G.P. zones were considered to have been seeded at T_1 for growth at T_2 (see Chapters 5 and 6). On the other hand, if <u>all</u> the G.P. zones which were formed at T_1 were completely dissolved at T_2, then T_2 was considered to be above the minimum reversion temperature T_R.

The experimental results, which are described in section 7.2, yielded the important conclusion that there appears to be no unique value of the minimum reversion temperature T_R for a given composition of Al-Zn alloy, since the lowest temperature at which complete dissolution of the G.P. zones was observed to occur was found to depend upon the thermal history of the sample before the second ageing temperature. The highest value of T_R was always obtained with the longest pre-treatment at T_1. In section 7.3 an interpretation of the results is given which is based on the model[81] for two-step ageing that is described in Chapter 5. This approach is compared to other theories of reversion and it is deduced that, for a suitably long pre-treatment at T_1, the experimentally determined value of T_R may approach the G.P. zone solvus temperature $T_{G.P.}$ fairly closely, although an accurate estimate of the temperature difference

$(T_{G.P.} - T_R)$ cannot be obtained from the experimental results.

7.2 EXPERIMENTAL RESULTS

Two-step ageing treatments were carried out with samples of the Al-10%Zn, Al-17.5%Zn and Al-26%Zn alloys and the final microstructures of the heat treated samples examined by electron microscopy. As in Chapter 6, the majority of the work was carried out with the Al-17.5%Zn alloy and these results were supplemented with a few results obtained with the other two alloy compositions. Whereas in Chapter 6 the discussion concentrated on the G.P. zone distribution in the neighbourhood of grain boundaries the current discussion concentrates on the microstructure that was observed well away from the influence of grain boundaries.

The more extensive results obtained with the Al-17.5%Zn alloy are described first and these are followed by the results obtained with the other two alloys. It is emphasized at this point that in all the two-step ageing treatments described in this section the values of the second ageing temperature T_2 were all above the critical temperature T_c for the particular alloy under discussion.

7.2.1. Results obtained with the Al-17.5%Zn alloy

Series (a) : Samples which were direct-quenched to room temperature

For this series of experiments the samples were all solution treated at 560°C, direct-quenched into water at room temperature and aged for different times ranging between $\frac{1}{2}$ minute and 3 days, and then subsequently aged with T_2 at either 160°C, 165°C, 170°C, 175°C or 180°C (T_c for this alloy = 156°C $\pm$ 2°C - see Chapter 4).

At the end of each two-step ageing treatment the sample was examined to see if any of the G.P. zones which had formed during the

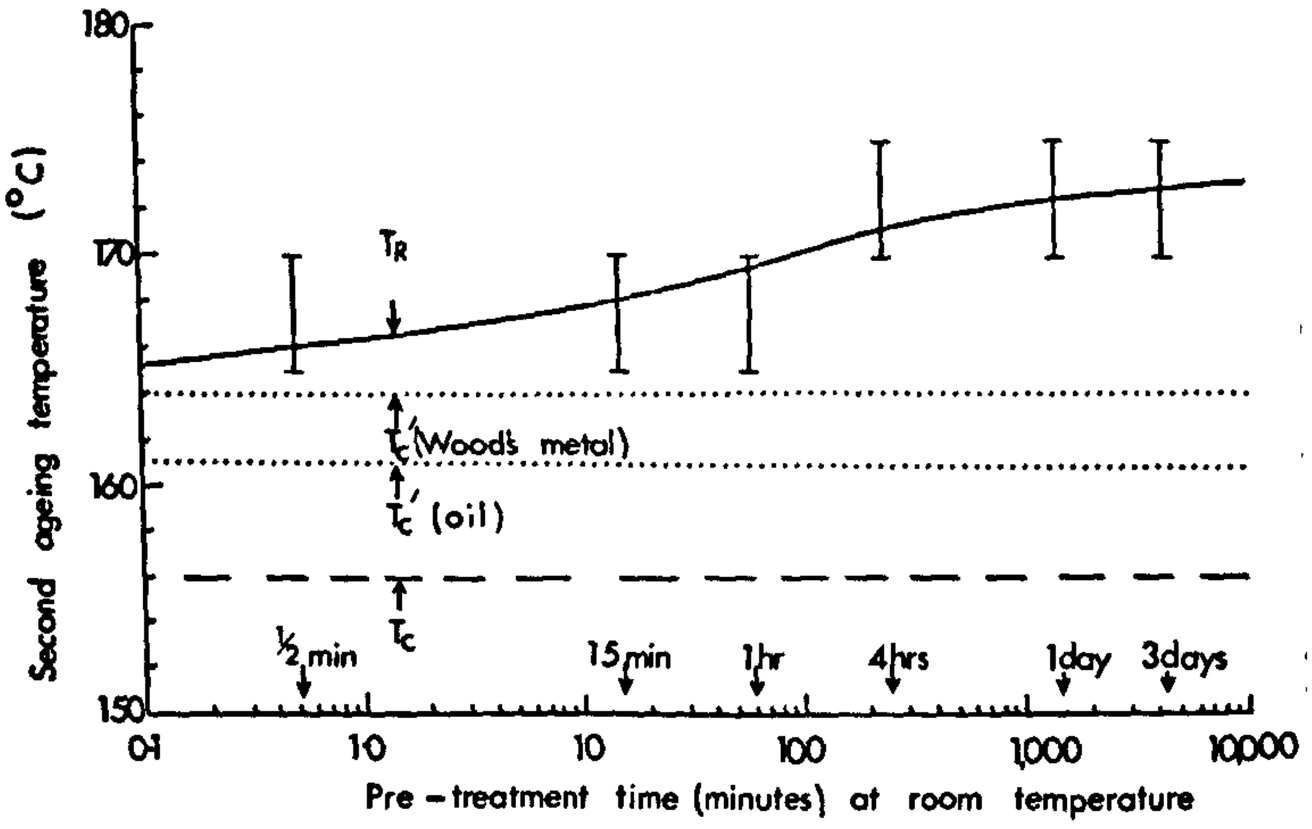

Figure 7.1 The experimentally determined variation of the minimum reversion temperature (T_R) with pre-treatment time at room temperature for an Al-17.5%Zn alloy.

pre-treatment at room temperature had remained stable and continued to grow at the second ageing temperature. The results are summarized in Table 7.1 and from this data the highest value of T_2 at which seeding was observed, and also the lowest value of T_2 at which complete dissolution of the G.P. zones was observed, can be obtained for each of the pre-treatment times at room temperature.

TABLE 7.1

Value of T_2	G.P. zones were observed at the completion of the two-step ageing treatment: Yes/No. (--- signifies no observation) Pre-treatment time at room temperature					
	$\frac{1}{2}$ min.	15 min.	1 hr.	4 hrs.	1 day	3 days
160°C	Yes	Yes	Yes	Yes	Yes	Yes
165°C	Yes	Yes	Yes	Yes	---	---
170°C	No	No	No	Yes	Yes	Yes
175°C	---	---	---	No	No	No
180°C	---	---	---	No	No	No

Clearly, the value of T_R for each pre-treatment time lies somewhere between this pair of T_2 values and an approximate minimum-reversion temperature curve can be drawn, as a function of pre-treatment time at room temperature, as shown in Figure 7.1. This graph shows the important result that a higher value of T_R was associated with a longer pre-treatment at room temperature. It is to be noted that it is thought that $T_R \simeq T'_c$ (Wood's metal) for very short pre-treatment times at room temperature, since a high vacancy supersaturation will be retained in the matrix and a negligible amount of seeding will occur because of the short time available for solute clustering. Therefore, G.P. zone formation will occur at T_2

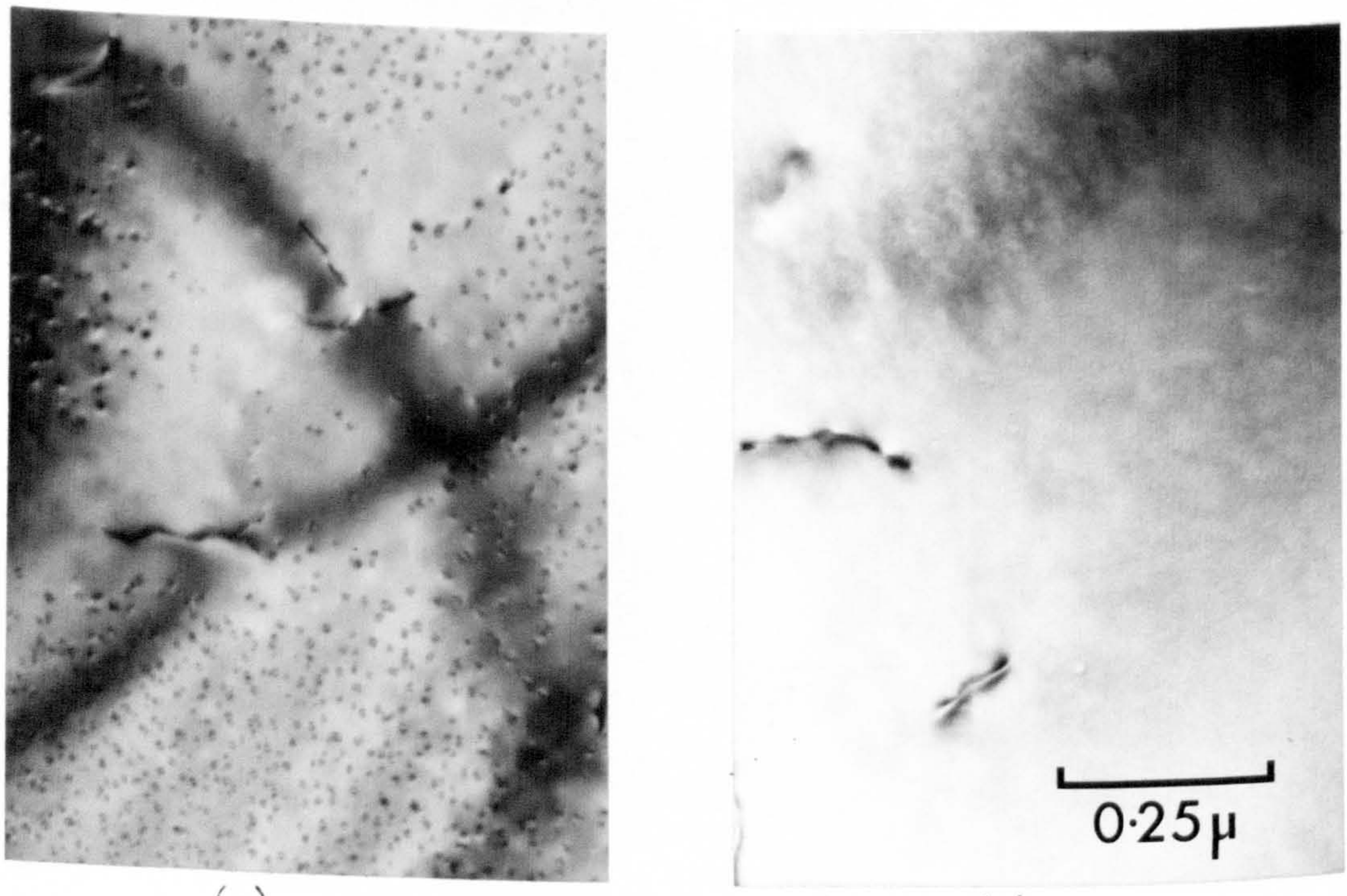

(a) (b)

Figure 7.2 Al-17.5%Zn: The final microstructure observed in samples which were direct-quenched into water at 20°C and then pre-aged at room temperature for 1 hour before being subsequently aged at (a) 165°C for 1 hour and (b) 170°C for 20 minutes.

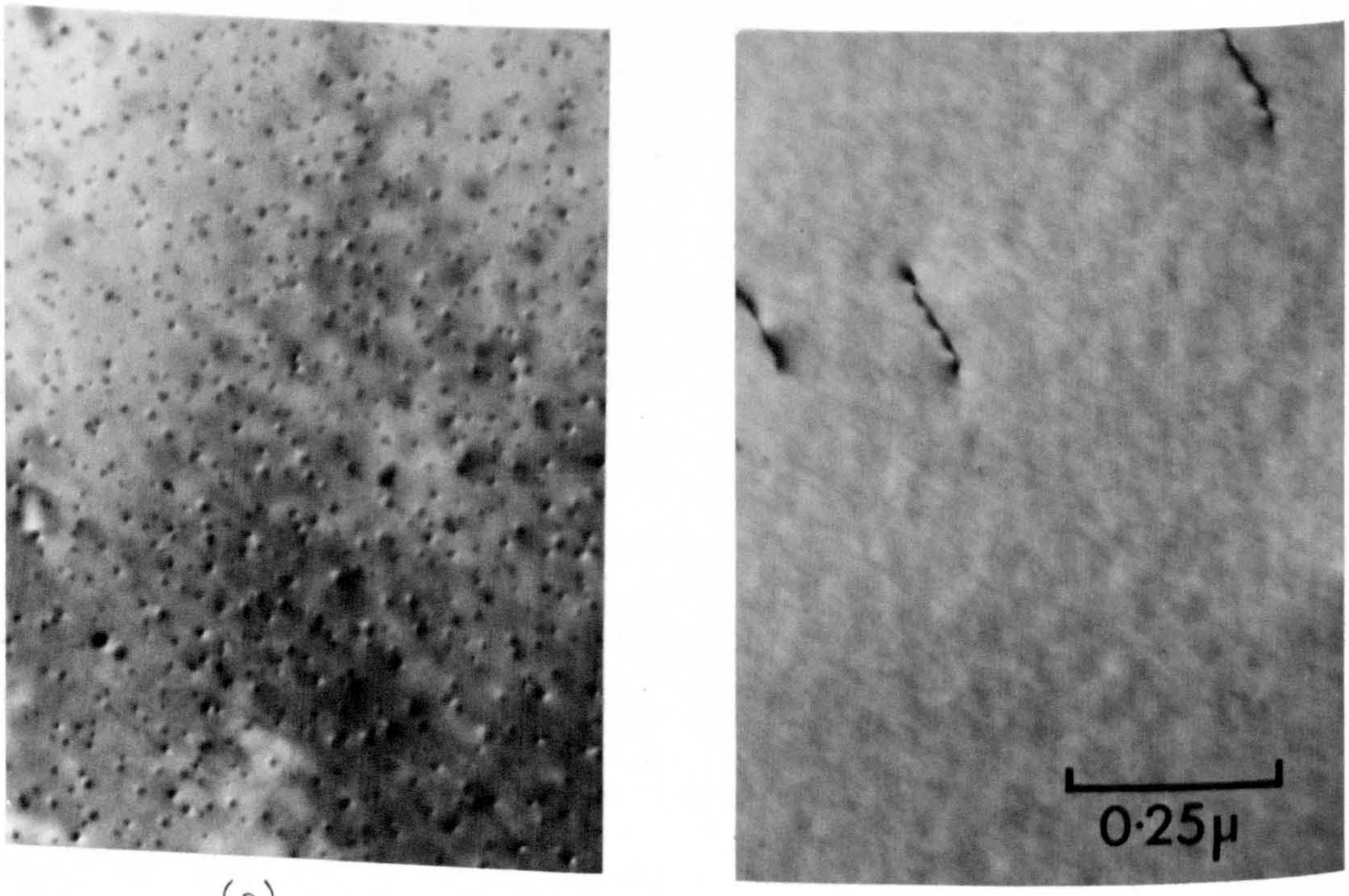

(a) (b)

Figure 7.3 Al-17.5%Zn: The final microstructure observed in samples which were direct-quenched into water at 20°C and then pre-aged at room temperature for 1 day before being subsequently aged at (a) 170°C for 20 minutes and (b) 175°C for 30 minutes.

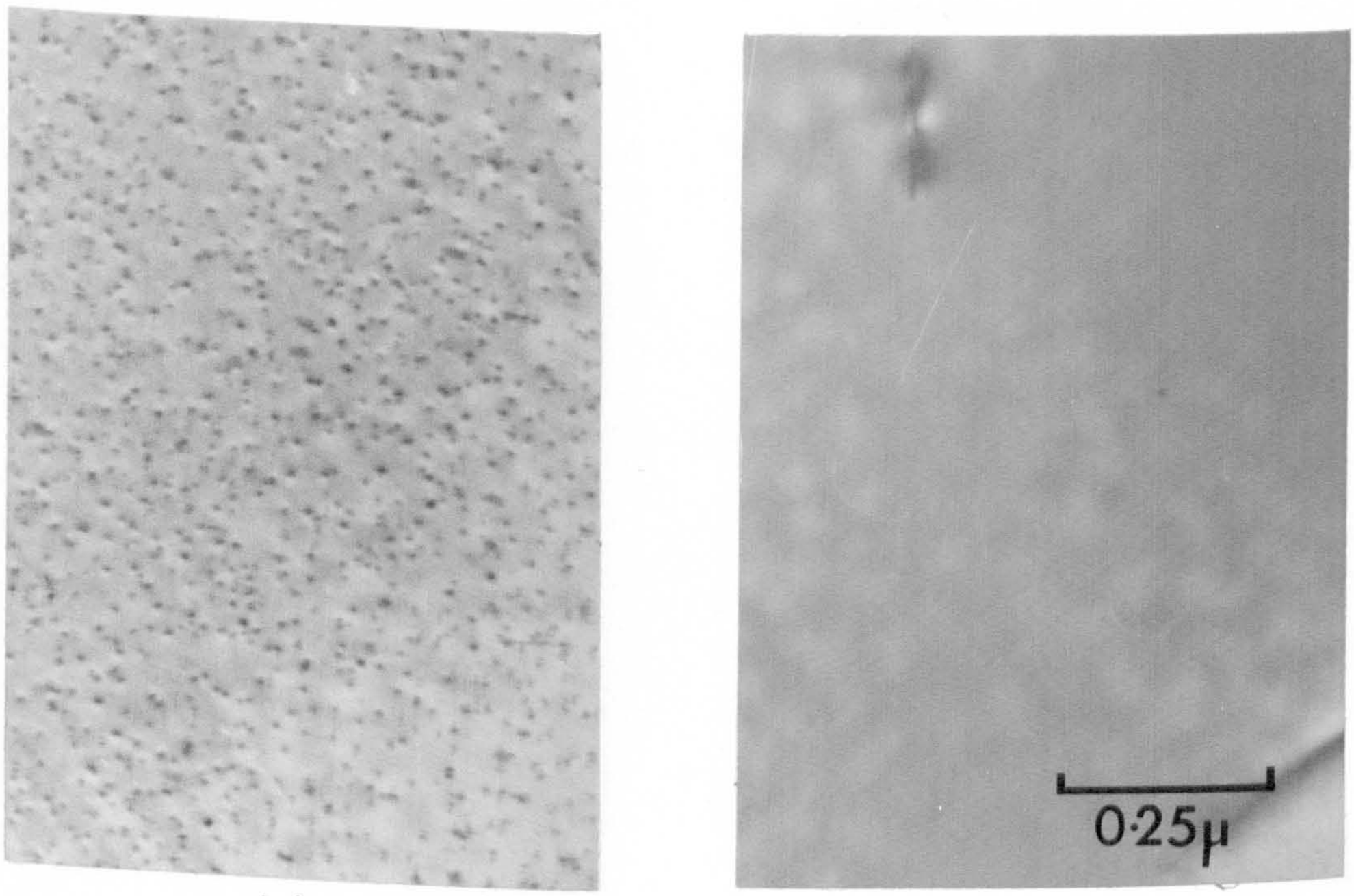

(a) (b)

Figure 7.4 Al-17.5%Zn: The final microstructure observed in samples which were step-quenched into water at 20°C and then pre-aged at room temperature for 1 day before being subsequently aged at (a) 160°C for 1 hour and (b) 170°C for 20 minutes.

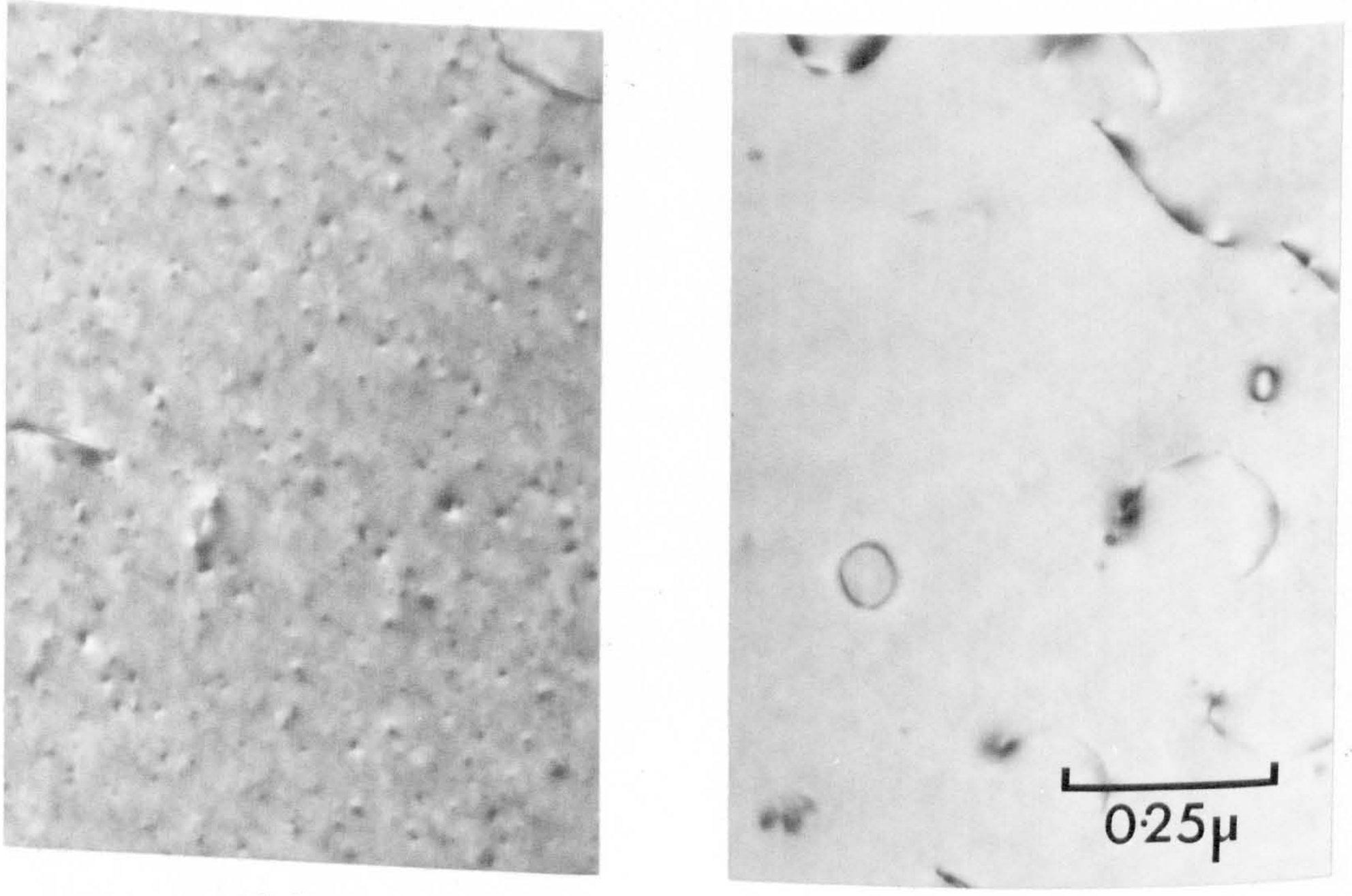

(a) (b)

Figure 7.5 Al-17.5%Zn: The final microstructure observed in samples which were direct-quenched into oil at 90°C and pre-aged for 1 hour before being subsequently aged at (a) 170°C for 30 minutes and (b) 180°C for 15 minutes.

if a sufficiently high vacancy supersaturation is present in the matrix i.e. for values of T_2 up to $\simeq T'_c$ (Wood's metal).

Figures 7.2(a) and (b) illustrate that T_R was between 165°C and 170°C after a 1 hour pre-treatment and Figures 7.3(a) and (b) illustrate that T_R was between 170°C and 175°C after pre-treatment for 1 day. A frequently observed feature in all samples that were pre-aged for a short time at room temperature before being subsequently aged at a value of T_2 where seeding occurred was the presence of a p.f.z. around some of the matrix dislocations. An example of this behaviour is shown in Figure 7.2(a). The same samples always exhibited wide grain boundary p.f.z's. The connection between p.f.z's and reversion in Al-Zn alloys is discussed in section 7.3.1.

Series (b) : Samples which were step-quenched to room temperature

For this series of experiments the samples were solution treated at 560°C, step-quenched (via 180°C for 1 minute) into water at room temperature and aged for different times ranging between 15 minutes and 3 days, and then subsequently aged with T_2 at either 160°C or 170°C. Seeding of G.P. zones was observed in all samples for which T_2 was 160°C, whereas complete dissolution of the G.P. zones occurred in all samples for which T_2 was 170°C. Figures 7.4(a) and (b) illustrate these results for T_2 at 160°C and 170°C, respectively, after a pre-treatment at room temperature for 1 day.

Thus, although 170°C was below T_R for the sample that was direct-quenched to room temperature and pre-aged for 1 day (as shown by Figure 7.3(a)) it is clear that 170°C was above T_R for the sample that was step-quenched to room temperature and pre-aged for the same length of time (as shown by Figure 7.4(a)).

Series (c) : Samples which were direct-quenched to 90°C

In the final series of heat-treatments the samples were direct-quenched into an oil bath held at 90°C and aged for different lengths of time before being subsequently aged at either 160°C, 170°C or 180°C. Pre-treatment times at 90°C of 15 min., 1 hr., 4 hrs. and 24 hrs. were examined. Seeding of G.P. zones for further growth at both 160°C and 170°C were observed for all pre-treatments, whereas complete dissolution always occurred when T_2 was 180°C. Figures 7.5(a) and (b) illustrate that, after a pre-treatment for 1 hour at 90°C, some G.P. zones were seeded for growth at 170°C whereas all G.P. zones dissolved during the treatment at 180°C. These micrographs should be compared with Figures 7.2(a) and (b).

Summary of results

The three series (a), (b) and (c) of results demonstrated that the observed value of minimum reversion temperature (T_R) for G.P. zones in an Al-17.5%Zn alloy was dependent upon the pre-ageing time at T_1, the type of quench to T_1 and the value of T_1, as follows :-

(i) Series (a) showed that, after a direct-quench to room temperature, a higher value of T_R was associated with a longer period of pre-treatment;

(ii) Series (b) showed that, after a step-quench to room temperature, the value of T_R was lower after a pre-treatment for 1 day than for the same pre-treatment following a direct-quench;

(iii) Series (c) showed that, after a direct-quench to 90°C, the value of T_R after a pre-treatment of only 15 minutes was approximately the same as that observed with a sample which was direct-quenched to room temperature and pre-aged for 1 day.

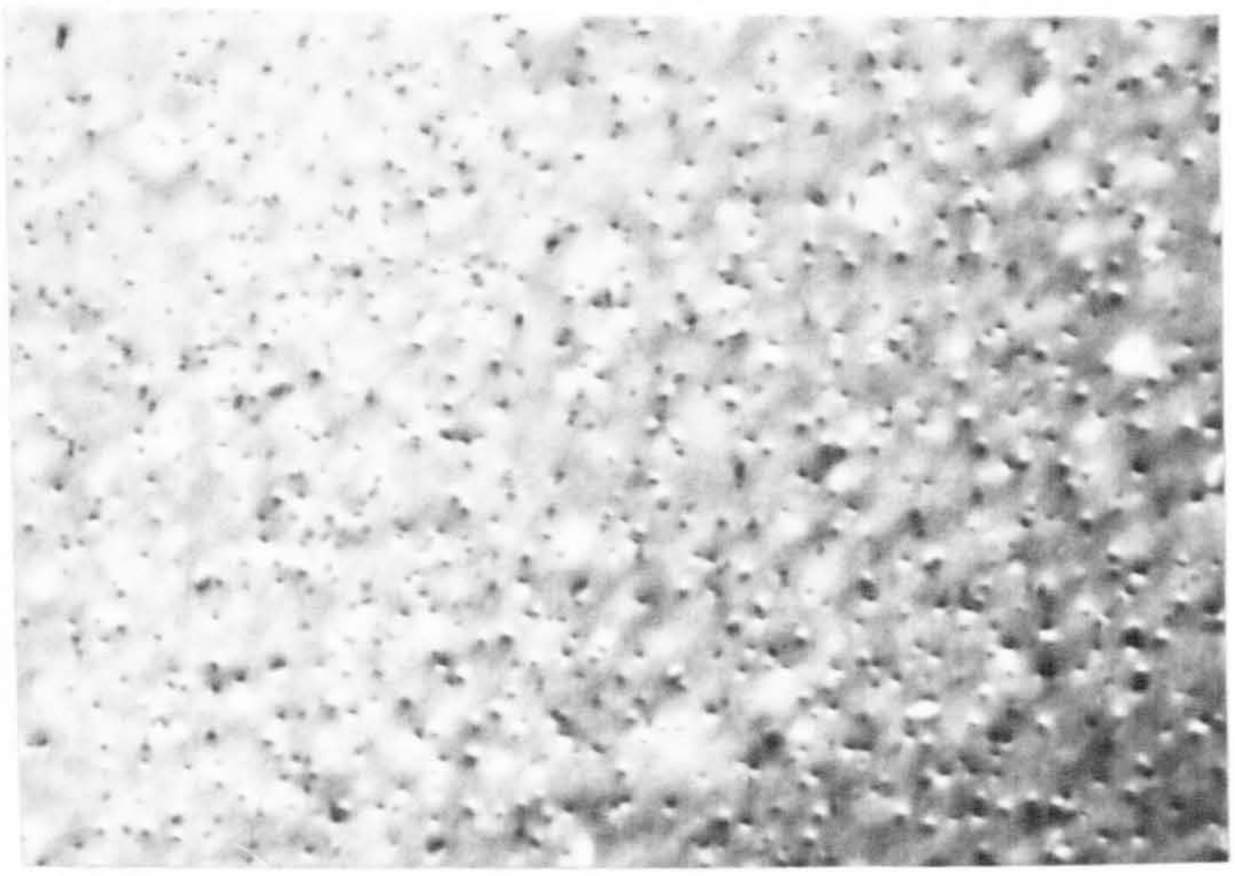

(a)

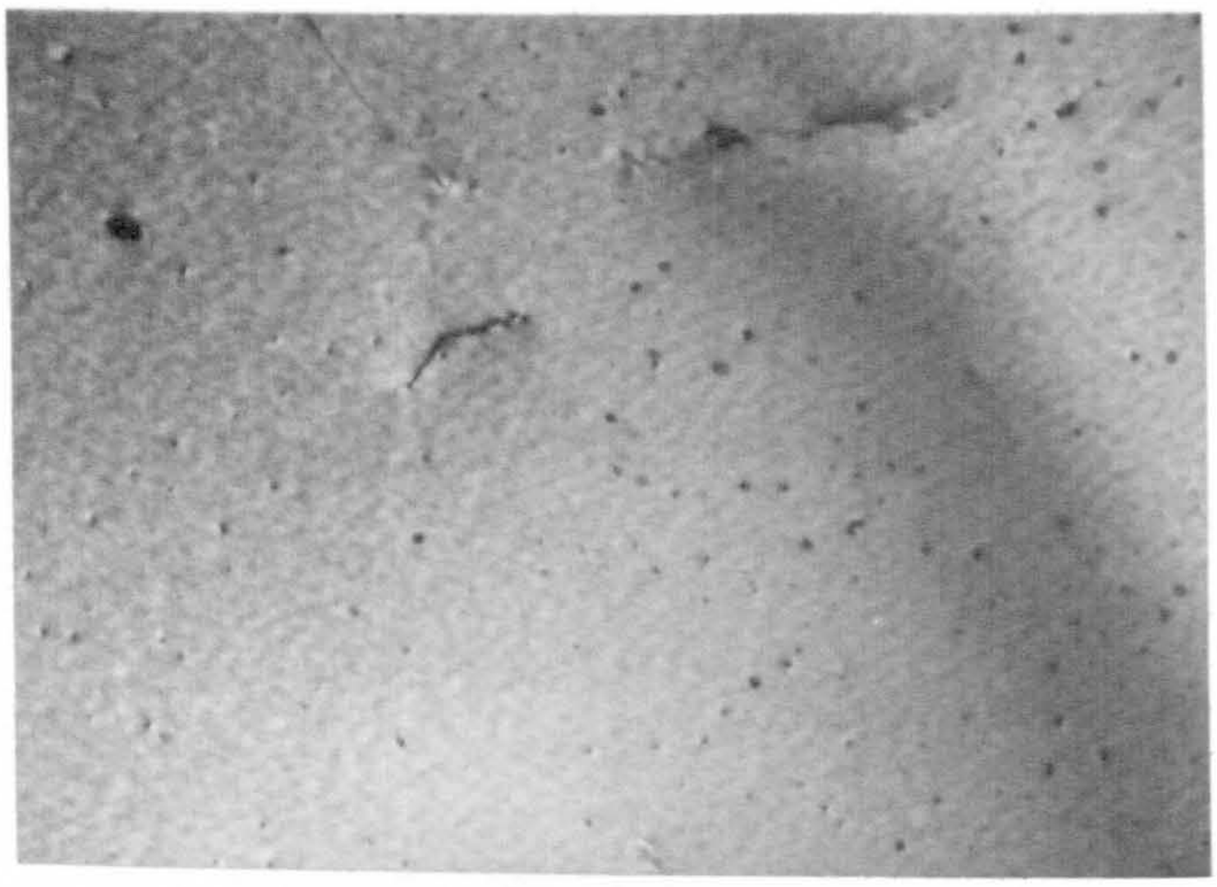

(b)

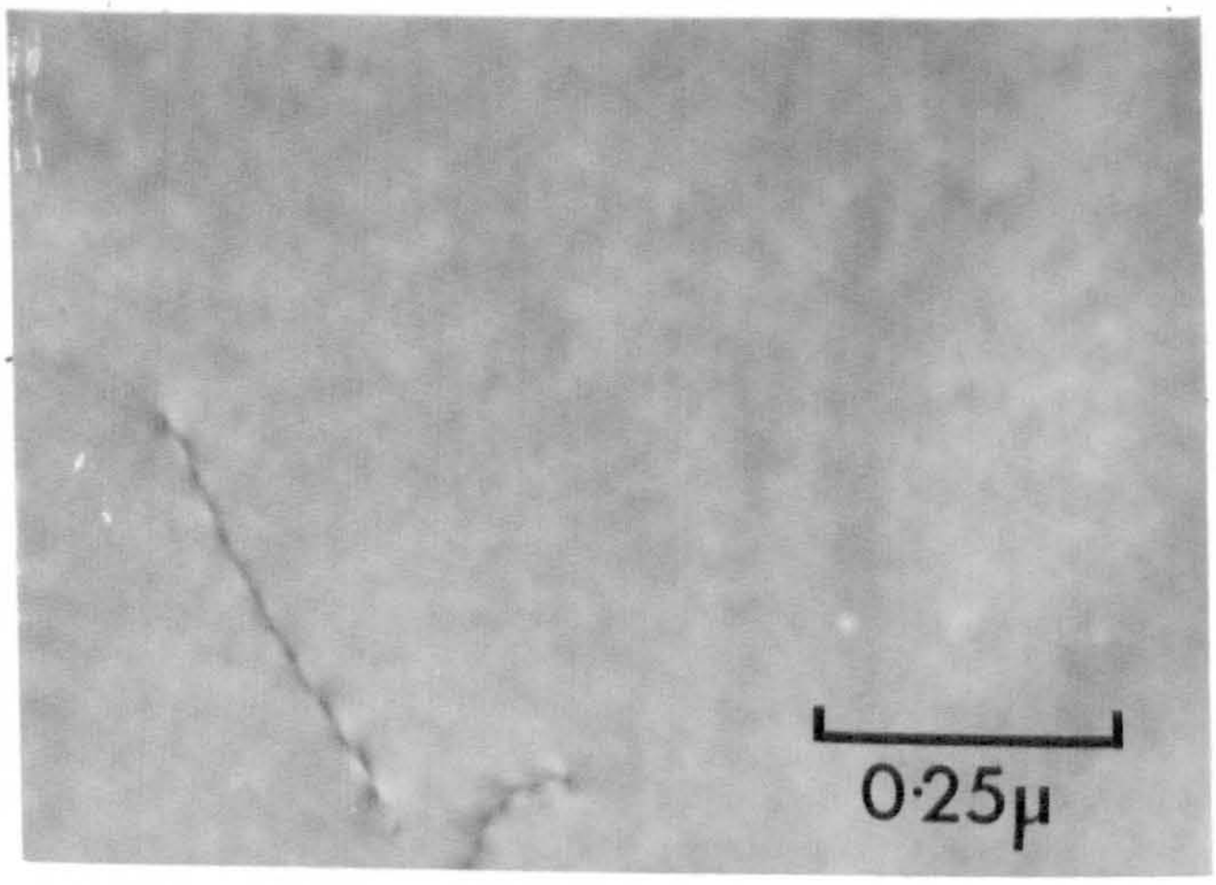

(c)

Figure 7.6 Al-10%Zn: The final microstructure observed in samples which were direct-quenched into water at 20°C and then pre-aged at room temperature for 1 hour before being subsequently aged for two weeks at (a) 98°C, (b) 110°C and (c) 115°C.

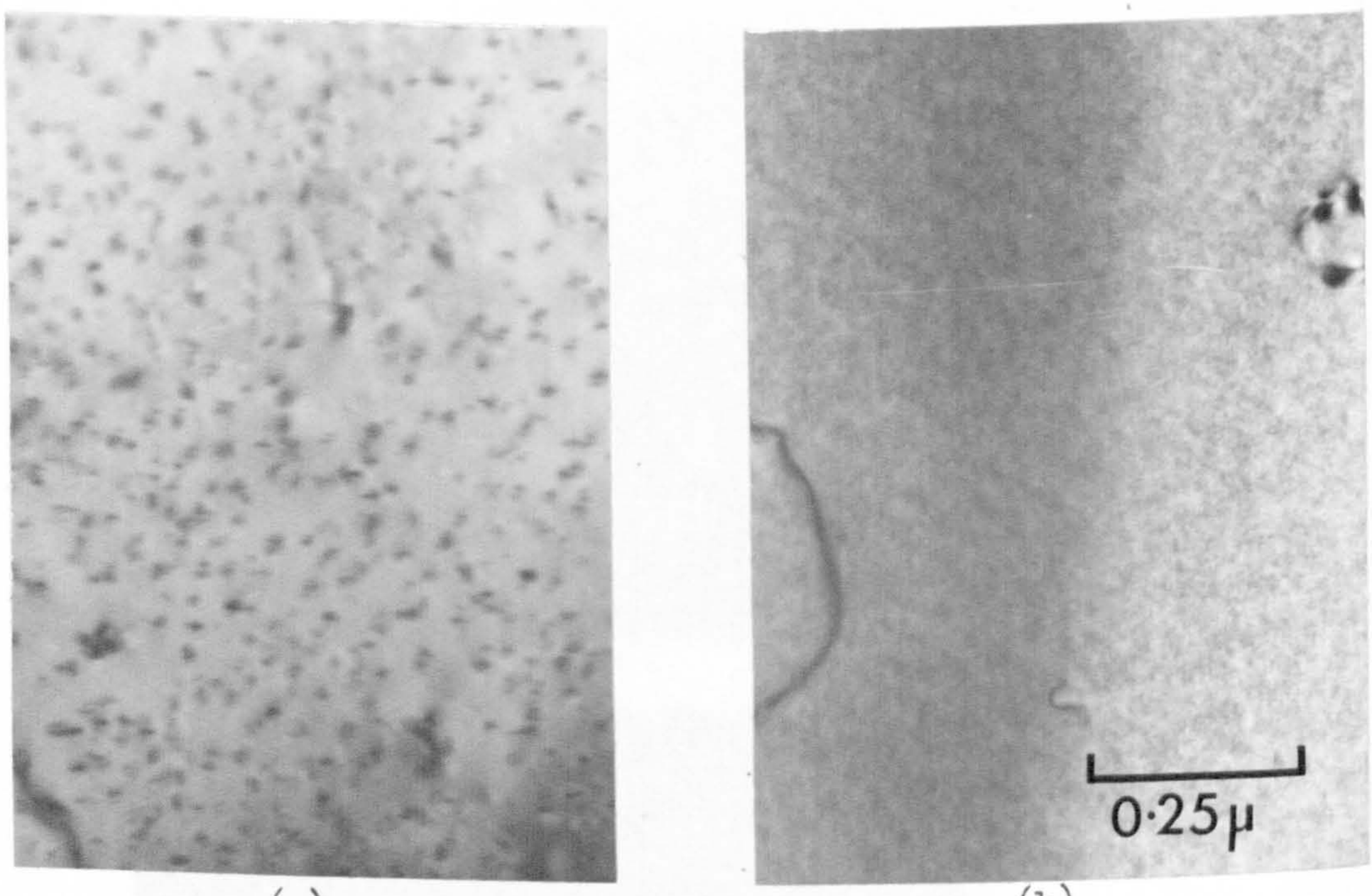

(a) (b)

Figure 7.7 Al-26%Zn: The final microstructure observed in samples which were direct-quenched into water at 20°C and then pre-aged at room temperature for 1 hour before being subsequently aged for 5 minutes at (a) 220°C and (b) 225°C.

7.2.2. Results obtained with the Al-10%Zn and Al-26%Zn alloys

(a) Al-10%Zn

Two-step ageing treatments were carried out in which samples were solution treated at 560°C, direct-quenched into water at room temperature and aged for 1 hour, and then subsequently aged at 98°C, 110°C and 115°C (T_c for this alloy = 92°C ± 4°C - see Chapter 4). The final microstructure that was observed in these samples is illustrated by Figures 7.6(a), (b) and (c), from which it can be seen that G.P. zones were seeded for growth at 98°C and 110°C, but not at 115°C. It was therefore concluded that for a pre-treatment of 1 hour at room temperature the corresponding value of T_R was between 110°C and 115°C.

(b) Al-26%Zn

Two-step ageing treatments were carried out in which samples were solution treated at 500°C, direct-quenched into water at room temperature and aged for 1 hour, and then subsequently aged at 220°C and 225°C (T_c for this alloy = 210°C ± 2°C - see Chapter 4). These results are illustrated by Figures 7.7(a) and (b). The sample for which T_2 was 220°C (Figure 7.7(a)) contained copius homogeneous precipitates which were believed to be a mixture of spherical and ellipsoidal G.P. zones (see Chapter 3). A few regions contained larger, platelet, precipitates and these were probably of the α'_R - rhombohedral phase. It was thought that the ellipsoidal G.P. zones and α'_R - precipitates were developed from the growth of spherical G.P. zones during the treatment at 220°C. The sample for which T_2 was 225°C (Figure 7.7(b)) contained no homogeneous precipitates.

Thus, for this alloy, a pre-treatment of 1 hour at room temperature yielded a value of T_R of between 220°C and 225°C.

7.3 DISCUSSION OF THE RESULTS

7.3.1 An interpretation of the results

In Chapter 5 a model for two-step ageing[81] was described and the conditions under which G.P. zones may be seeded during a pre-treatment at a temperature T_1 for further growth at a higher temperature T_2 were derived. The stability of a G.P. zone at T_2 was shown to be a function of two parameters; (a) the radius r of the G.P. zone and (b) the value of the remaining solute supersaturation i_R surrounding the zone at T_2. According to this approach a G.P. zone will only remain stable at T_2 in regions of the matrix where $r \log_e i_R > K$, where K is the temperature dependent stability constant which was defined in Chapter 5. If $T_2 > T_c$ (as it was for all the two-step ageing treatments that were described in the previous section of experimental results) then, according to this model, G.P. zones will only be stable and continue to grow if they were seeded by a sufficiently long pre-treatment at T_1.

In Chapter 6 this model was able to account adequately for the observed precipitate distribution in the neighbourhood of grain boundaries after a two-step ageing treatment. The case where $T_2 > T_c$ (see section 6.2.2.) is relevant to the reversion studies of this Chapter. It was shown that near to a grain boundary, where the growth rate of G.P. zones was appreciably slower than further away in the matrix owing to local vacancy-depletion, the G.P. zones formed during the pre-treatment at T_1 within a distance of $\pm$ w/2 of the grain boundary were too small to remain stable at T_2 and a p.f.z. of width w was formed. One way of looking at this result is to consider that T_2 was above the minimum reversion temperature for the small G.P. zones situated within a distance $\pm$ w/2 of the grain boundary, whereas for the larger G.P. zones situated outside this region the value of T_2 was below their minimum reversion temperature.

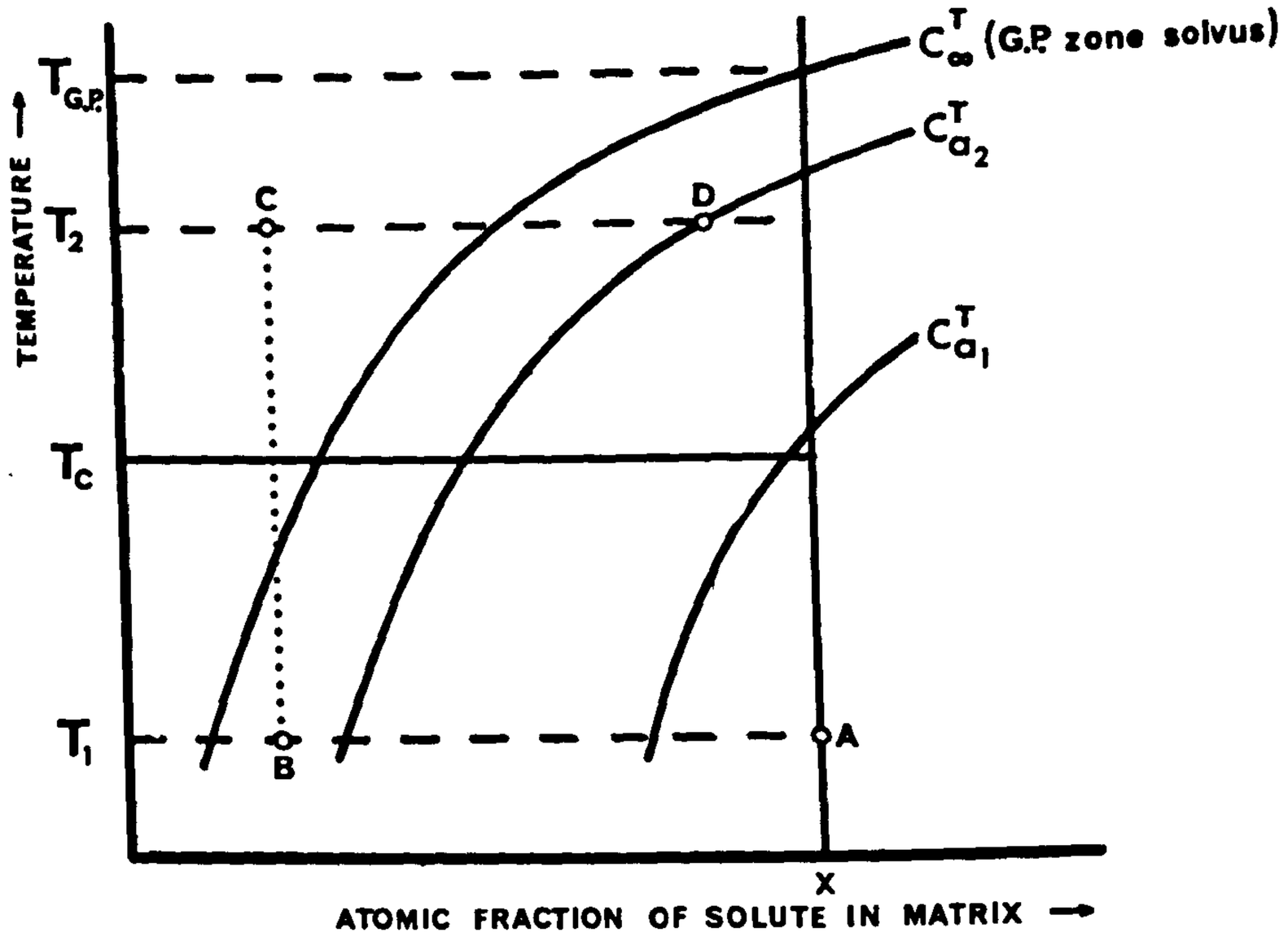

Figure 7.8 A schematic diagram showing the stability curves for zones of different sizes. The curves labelled $C^T_{a_1}$ and $C^T_{a_2}$ are for zones of radius a_1 and a_2 ($a_1 < a_2$), respectively.

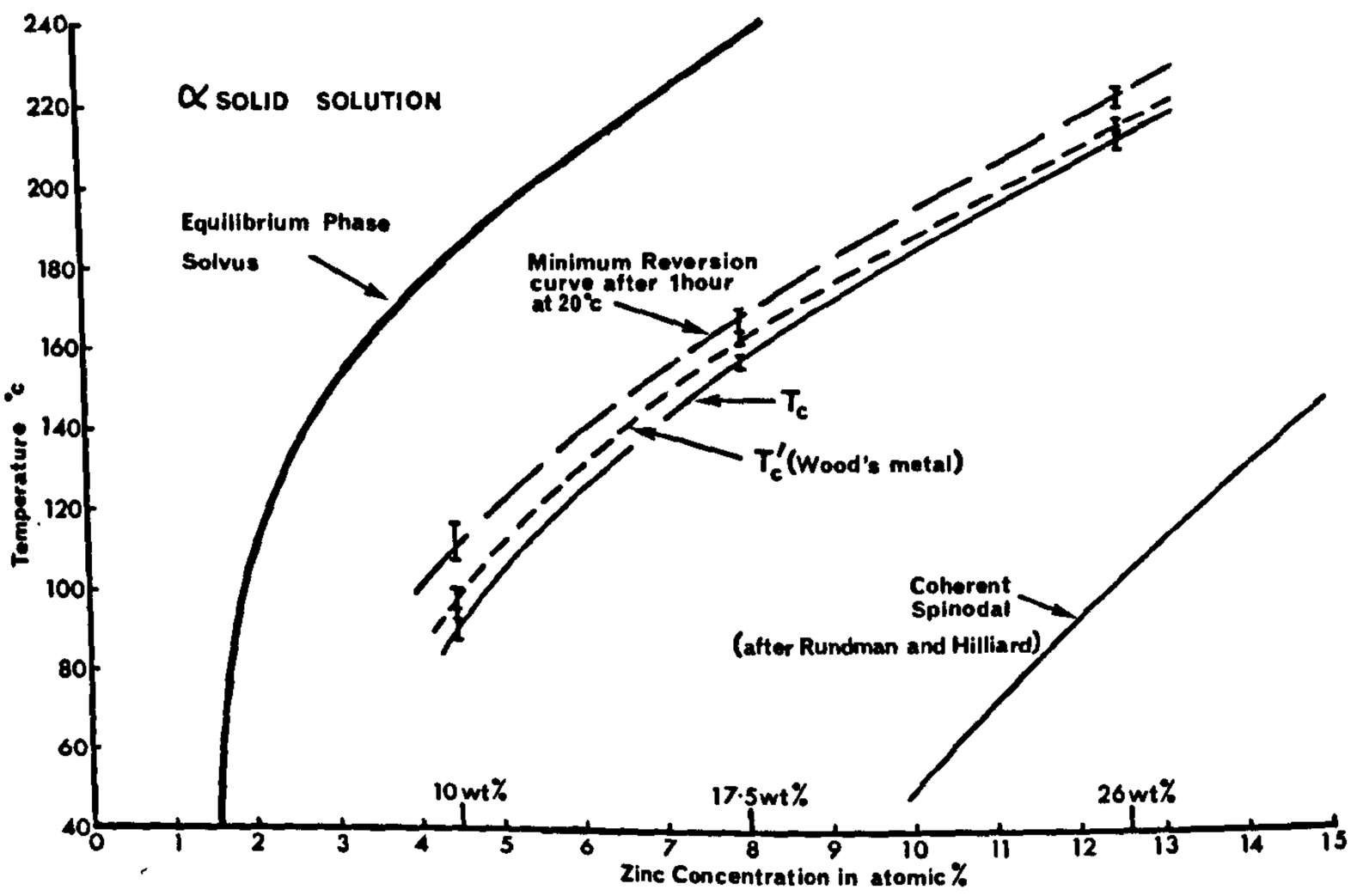

Figure 7.9 A diagram showing the relationship between the T_c and T_c'(Wood's metal) curves for Al-Zn alloys and the minimum reversion curve after a direct-quench into water at 20°C followed by a pre-treatment at room temperature for 1 hour.

Thus, the conditions under which reversion of G.P. zones occurs at a temperature T_2 are completely complementary to those required for the seeding of G.P. zones at T_2. If we define T_R^a as the minimum reversion temperature for a G.P. zone of radius a, when surrounded by a given value of matrix solute supersaturation, then it follows from the model that zones of radius $r \leq a$, when surrounded by the same matrix solute supersaturation, will dissolve at the temperature T_R^a (here, strictly, one should speak of solute clusters rather than zones since, by definition (see Chaper 1), a G.P. zone is a stable solute cluster) whereas zones of radius $r > a$ will be stable at T_R^a and will continue to grow.

For a very long pre-treatment at T_1, in which large G.P. zones are formed and the atomic fraction of solute atoms in the matrix is considerably reduced in value, a slight modification can be made to the mechanism of seeding that was discussed above. The situation is illustrated schematically by Figure 7.8. Consider a binary alloy which contains an atomic fraction X of solute atoms. If this alloy is direct-quenched to a low ageing temperature T_1 then we may represent the fully supersaturated alloy by the point A on Figure 7.8. Next, let the alloy be aged at T_1 for a long period of time during which G.P. zones are formed and the solute concentration in the matrix is considerably reduced in value (represented by the point B on the diagram). Suppose that at the end of this treatment there is a distribution in G.P. zone sizes and that a significant proportion of these have radii much larger than the value a_2. If the alloy is now up-quenched to the temperature T_2 (point C on Figure 7.8) then all the G.P. zones will initially be unstable because the point C is above the G.P. zone solvus. All the unstable G.P. zones (now more correctly called solute clusters) will start to dissolve and so feed-back solute atoms into the matrix. The process can be represented

on Figure 7.8. by the matrix solute concentration progressively increasing along the line C → D. Suppose that at the point D the alloy still contains a number of solute clusters which have radii greater than a_2. Since D is shown to be on the stability curve for solute clusters of radius a_2 then these solute clusters will become stabilised as G.P. zones. The pre-treatment at T_1 can be described as the "seeding" treatment by which these G.P. zones were seeded for growth at T_2. Clearly, the nearer is T_2 to $T_{G.P.}$ (see Figure 7.8) the less is the likelihood of this mechanism operating and all G.P. zones formed at T_1 will completely dissolve at T_2.

The results obtained by the two-step ageing experiments which were carried out on the Al-17.5%Zn alloy, which were reported in section 7.2.1, can all be rationalised if the minimum reversion temperature T_R^r is considered to be a function of both G.P. zone size r and the value of the remaining matrix supersaturation. For example, the G.P. zones will grow more slowly at room temperature after a step-quench than after a direct-quench (owing to the lower vacancy concentration). Therefore, after a given pre-treatment at room temperature, the hypothesis outlined above predicts that the observed minimum reversion temperature will be lower for the step-quench sample than for the direct-quenched sample, which was the observed behaviour. For the samples which were direct-quenched and aged at 90°C the G.P. zones will have grown more rapidly than at room temperature and, since the density of G.P. zones is lower at 90°C than at room temperature, the remaining solute supersaturation at T_2 for equivalent zone sizes grown at T_1 will be higher after pre-treatment at 90°C than after pre-treatment at room temperature. Thus, for a sample pre-aged for a short time at 90°C the observed value of minimum reversion temperature is expected to be higher than for a sample pre-aged for the same time at room temperature. This again was the observed behaviour.

Let us now consider an idealized and hypothetical two-step heat treatment in which a sample, which contains an atomic fraction X of solute atoms (see Figure 7.8), is direct-quenched to a temperature which is close to the critical temperature T_c so that only a very low density of G.P. zones is formed, and let these zones all grow to a very large size such that the effect of zone size on stability becomes negligible (see Chapter 4). It is assumed that, during the growth of these G.P. zones, the solute concentration in the matrix between the zones is not significantly reduced in value, so that at the end of this hypothetical heat-treatment we have a few very large G.P. zones surrounded by a fully supersaturated matrix. From Figure 7.8 and the theory of section 4.5.1 it will be seen that these G.P. zones will remain stable if the temperature of the sample is now raised to a value T_2 which is fractionally less than $T_{G.P.}$ but that the zones will definitely dissolve if $T_2 > T_{G.P.}$ Clearly, then even in this ideal case, T_R (where r is very large) can never exceed $T_{G.P.}$.

Since the effect of zone size on G.P. zone stability is pronounced only for very small zones it is probably only necessary to grow zones at T_1 to radii > 50 Å (see Chapter 4) for them to be considered as "the very large G.P. zones" discussed above. However, in any real two-step ageing treatment, even with a high value of T_1, the solute concentration in the matrix will always be reduced to some extent, so even with the most favourable experimental conditions the observed highest value of T_R will probably be significantly less than $T_{G.P.}$.

In the case of the Al-17.5%Zn alloy, the results obtained with samples which were pre-treated at 90°C before being subsequently aged at T_2 indicated that the highest value of T_R was between 170°C and 180°C (see section 7.2.1). It is of interest to note that the results obtained by an additional experiment, which was not reported in section 7.2.1, in which

samples were pre-aged at 150°C for 15 minutes also indicated that T_R was between 170°C and 180°C. The same result was also obtained with the samples that were pre-aged for $\geqslant$ 4 hours at room temperature. It is considered that $T_{G.P.}$ for this alloy is definitely above 170°C. However, since there appears to be no way at present of obtaining an estimate of the temperature difference ($T_{G.P.} - T_R$) it is deduced that the value of $T_{G.P.}$ cannot be obtained from these experiments.

If account is taken of the experimental error in the temperature control of T_2 then the experimentally determined values of minimum reversion temperature, for the three alloys examined, after a direct-quench and pre-age at room temperature for 1 hour can be listed as follows :-

(i) Al-10%Zn, T_R lies between 108°C and 117°C;

(ii) Al-17.5%Zn, T_R lies between 164°C and 171°C;

(iii) Al-26%Zn, T_R lies between 219°C and 226°C;

These results are all plotted on Figure 7.9 and a reasonable minimum reversion curve drawn through the experimental points. When represented in this way, the relationship between this reversion curve (which is thought to be below the G.P. zone solvus curve) and the T_c' (Wood's metal) and T_c curves is illustrated clearly.

It is emphasized that the discussion of reversion given above refers solely to G.P. zones and that if either intermediate or equilibrium precipitates are formed during the pre-treatment at T_1 then these need not necessarily dissolve if the temperature of the alloy is suddenly raised to $T_2 > T_{G.P.}$. These more stable types of precipitate may arise directly as the result of the growth and subsequent transformation of G.P. zones at T_1 or they may be nucleated independently (either homogeneously or heterogeneously) and for each type of precipitate there will be a corresponding

solvus curve[9]. The more stable the precipitate, the more displaced is its corresponding solvus curve towards higher temperatures and lower solute concentrations compared to the G.P. zone solvus[9] and therefore the higher will be its reversion temperature relative to that of a G.P. zone. For example, large grain boundary precipitates of hexagonal zinc were formed in samples of Al-17.5%Zn which were pre-aged at room temperature and these remained stable at all the values of T_2 investigated, which is not surprising since the equilibrium solvus temperature is considerably above $T_{G.P.}$ for this alloy (see Figure 7.9). The possibility exists that the minimum reversion temperature of an intermediate of equilibrium precipitate may be dependent on precipitate size, but this point was not studied in this investigation.

Finally, it should be mentioned that the ideas developed above can also provide an explanation of the phenomenon of partial-reversion, for, as the value of T_2 is increased towards T_R, the density of G.P. zones seeded for growth at T_2 progressively decreases (compare Figure 7.6(a) with Figure 7.6(b)) and, for example, the hardness of the alloy will progressively decrease towards the "as-quenched" value.

7.3.2 A general discussion of reversion

One of the earlier theories of reversion was put forward by Konobeevski[169]. His theory was in many ways similar to that discussed in section 7.3.1 above. He invoked the Gibbs-Thomson relation to deduce that an upper temperature limit for the stability of a precipitate of given size will exist, so that precipitates formed at a low temperature T_1, which are smaller than the critical size for stability at T_2, will dissolve at T_2. When formulating his theory he took as an example the equilibrium $CuAl_2$ precipitates in Al-Cu alloys and so his theory must be modified if it is applied to the reversion of G.P. zones. The two important characteristics

of a G.P. zone that must be taken into account are (1) a G.P. zone is usually completely coherent with the matrix whereas, in most cases, the equilibrium precipitate is completely incoherent, and (2) the crystal structure of a G.P. zone is metastable with respect to the crystal structure of the equilibrium phase. The first point was considered in section 4.5.1 where it was shown that if a low value of interfacial free energy is associated with a coherent, strain free, interface between a G.P. zone and the matrix, the effect of zone size on G.P. zone stability is pronounced only for zones of very small size. The second point, which was discussed in Chapter 1, leads to the concept of a G.P. zone solvus, which is located below the equilibrium solvus on the phase diagram. If these two important points are incorporated into Konobeevski's theory then the conclusions of sections 7.3.1 can be derived, i.e. that the G.P. zone size dependence of the minimum reversion temperature T_R is only pronounced for zones of very small size and that, for large zones, T_R tends towards $T_{G.P.}$.

Kelly and Nicholson[9] have criticized Konobeevski's[169] theory and say that it "cannot be correct since the minimum reversion temperature is constant for widely different zone sizes". However, very few carefully controlled experiments have been reported in the literature in which a deliberate attempt was made to detect small variations in T_R, especially for short pre-ageing treatment (it is noteworthy that Katz and Herman[170] and Katz, Krishna Rao and Herman[171] interpreted their electrical resistance measurements, which were carried out during the ageing of Al-rich Zn alloys (4 to 25 wt.%Zn), in a way which suggested that T_R increases with G.P. zone size). Also, it cannot be emphasized too strongly that according to the model of section 7.3.1 (which is essentially a modified form of Konobeevski's theory) there is no unique "critical size" which ensures G.P. zone stability, for account must always also be taken of the

value of remaining solute supersaturation surrounding the G.P. zone at T_2.

Since most experimental results have not revealed any variation of the value of T_R with thermal history of the alloy before the reversion treatment, most workers have recently followed the approach of Kelly and Nicholson[9] and have associated the minimum reversion curve with the G.P. zone solvus. In most cases the minimum reversion temperature T_R has been determined by the "hardness-reversion" technique of Beton and Rollason[48,172]. This technique usually involves pre-ageing the sample for a sufficient time at room temperature to produce significant hardening and then raising its temperature until softening occurs. The lowest temperature at which the sample reverts in hardness to the "as-quenched" value is then identified as the minimum reversion temperature. It seems likely that if only a short pre-treatment time is used, so that only very small G.P. zones are formed with an associated small increase in hardness of the sample, then it will be very difficult to detect accurately the minimum value of T_2 at which hardness-reversion occurs. When using this technique care must also be taken to ensure that hardening is not derived from sources other than G.P. zones (e.g. dislocation loops or helices[173]).

Carpenter and Garwood[174] have used the hardness-reversion technique to determine the minimum reversion temperature of Al-17.2%Zn and Al-22.5%Zn alloys, respectively. Each sample was quenched from 475°C into water at 20°C and pre-aged at room temperature for 1 hour before being subsequently aged at an elevated temperature. All samples were then quenched to room temperature and their hardness determined. A similar technique was used by Graf[175] for an Al-10%Zn alloy. The combined results of these two investigations were tabulated by Carpenter and Garwood[174] and the data is reproduced here as Table 7.2. These results are in fairly good agreement with the determinations of the minimum reversion

temperatures (after 1 hour at room temperature) which were reported in section 7.2 and which are represented in graphical form by Figure 7.9.

TABLE 7.2

The hardness-reversion results of Carpenter and Garwood[174] and Graf[175]

Zinc content of Al-Zn alloy		Minimum reversion temperature
wt.%	at.%	
10	4.5	104°C
17.2	7.9	170°C
22.5	10.7	210°C

Both Carpenter and Garwood[174] and Lasek[176] have commented on the fact that the minimum-reversion-temperature curve for Al-rich Zn alloys appears to lie slightly, but significantly, below the metastable (α- α') phase boundary which was proposed by Gerold and Schweizer[41] (see section 1.3.4 and Figure 1.6). They suggested that this is to be expected if the reversion curve is identified with the G.P. zone solvus and if the zones are thermodynamically less stable than the platelike precipitates of the α'-phase. This point is discussed in more detail in Chapter 8.

Niklewski et al[177] have used the diffuse X-ray scattering/technique to determine the minimum reversion temperature of G.P. zones formed (after an unspecified time at room temperature)in an Al-15 wt.%Zn alloy. They deduced that T_R for this alloy composition lies between 145°C and 160°C, which again is consistent with the reversion curve of Figure 7.9.

The evidence put forward by Cohen et al[133] in support of vacancy-trapping by G.P. zones in the Al-Zn system, which was briefly mentioned in section 4.5.2, can conveniently be examined at this point. They carried out a two-step ageing treatment, with an Al-28wt.%Zn alloy,

in which the sample was quenched to room temperature and naturally aged for 4 hours before being subsequently aged at 178°C for 5 minutes. They considered this to be a "reversion heat treatment", so that all G.P. zones were assumed to dissolve during the treatment at 178°C. The final microstructure of their sample, according to their published electron micrograph, was very similar to that illustrated by Figure 7.7(a) and they assumed that the contrast effects were due to dislocation loops formed by the clustering and subsequent collapse of vacancies[122,123] released from the dissolving G.P. zones during the ageing treatment at 178°C. Carpenter[134] has questioned this interpretation of the results and has pointed out that 178°C is considerably below the minimum reversion temperature[174] for this alloy composition. He suggested that the contrast effects observed by Cohen et al[133] were due to α'_R - phase platelets produced by the growth and subsequent transformation of some of the G.P. zones at 178°C. This explanation is consistent with the interpretation put forward in section 7.3.1 and the experimental results of section 7.2. It is therefore thought, in agreement with Carpenter[134], that the results of Cohen et al[133] do not provide conclusive proof of vacancy trapping by G.P. zones in the Al-Zn system.

Let us now return to the hardness-reversion technique mentioned above. Graf[178] has pointed out that complete hardness-reversion will only be exhibited by an alloy if, during the second ageing treatment, the low temperature precipitate does not act as a nucleus for a more stable phase. Holl[149, 150] and Lorimer and Nicholson[77] have discussed the possibility that G.P. zones may act as nuclei, during a second ageing treatment at an elevated temperature, for a more stable phase and, more recently, Lorimer and Nicholson[78] have published a detailed account of their model in which the factors controlling the ability of G.P. zones to transform to a precipitate (β) when the temperature of the alloy is

suddenly raised to a value $T_2 > T_{G.P.}$ are considered. A brief account of this model is given in Chapter 8. Clearly, if a high density of β-precipitates is seeded for growth at $T_2 > T_{G.P.}$ then hardness-reversion will not be observed. This illustrates the considerable care required in the interpretation of hardness- reversion experiments.

7.4 CONCLUSIONS

In this Chapter some experiments were described in which samples of Al-10%Zn; Al-17.5%Zn and Al-26%Zn were subjected to two-step ageing treatments in which $T_1 < T_c$ and $T_2 > T_c$. The object of the work was to determine the minimum value of T_2 at which all the G.P. zones formed at T_1 were dissolved. This minimum value of T_2 was identified with the so-called minimum reversion temperature T_R. The main conclusion obtained from these experiments was that T_R was not a unique temperature for a given alloy composition but depended upon the thermal history of the sample during the pre-ageing treatment at T_1. The general trend was for the value of T_R to increase as the time at T_1 was increased or as the value of T_1 was increased towards T_c. An interpretation of this result was put forward, which was based on the two-step ageing model[81] of Chapter 5, and it was deduced that, although the higher experimental values of T_R probably tended towards the value of $T_{G.P.}$, the value of $T_{G.P.}$ could not be estimated with any certainty from the experimental results.

CHAPTER 8

GENERAL DISCUSSION AND CONCLUSIONS

8.1 INTRODUCTION

During the course of the experimental work described in this dissertation the response of an Al-1.2%Mg_2Si alloy and three compositions of Al-base Zn alloy to a large number of different one-step and two-step ageing treatments was investigated. The aim of the work was two-fold : (1) to obtain a detailed knowledge of the various factors which influence the ageing behaviour of these two types of alloy and, more particularly, to determine the basic factors controlling the nucleation, growth and stability of G.P. zones in these alloys, and (2) to use these experimental results to aid the development of a model for two-step ageing which would provide a basis for predicting the response of a wide range of age-hardening alloys to two-step ageing treatments.

In Chapter 5 a summary was given of the two-step ageing model which was originally put forward by Dr. D. W. Pashley and described in detail in the paper by Pashley, Jacobs and Vietz[81]. In Chapters 4 to 7 of this dissertation many of the concepts and ideas that were discussed in the earlier model[81] were amplified and extended and it was shown that the model could be extended to account for the occurrence of grain boundary precipitate-free zones and the phenomenon of reversion in Al-Zn alloys.

The only other recent attempt at an overall description of the basic factors controlling two-step ageing behaviour has been made by Lorimer and Nicholson[77,78,79]. Their model was chiefly developed in an attempt to interpret the observed two-step ageing behaviour of Al-Zn-Mg, Al-Cu and Al-Ge alloys, although a broader aim of their work too was to derive a model that could be applied to other age-hardening alloys.

Their model differs in many respects from the model described by Pashley et al[81] and the approach taken in this dissertation. In the past, the model due to Lorimer and Nicholson[77,78,79] was referred to[81,82], for convenience, as the "thermodynamic model" in order to distinguish it from the so-called "kinetic model" of Pashley et al[81,82]. Since it is now agreed by both groups of workers[78,82] that each of the two models involves thermodynamic and kinetic considerations, this terminology will not be used here. As one of the chief aims of this Chapter is to compare and contrast these two models it is, nevertheless, useful to choose an abbreviated form for referring to the two models, as follows :-

(1) The original two-step ageing model due to Pashley (as described in the paper by Pashley et al[81])and the subsequent extensions and modifications to this model described in this dissertation will be referred to as the "Pashley-Jacobs" model and will be abbreviated to the (P-J) model.

(2). The model of Lorimer and Nicholson[77,78,79] will be referred to in an abbreviated form as the (L-N) model.

Since both the (P-J) model and the (L-N) model represent two independent attempts to describe the basic factors controlling the response of age-hardening alloys to two-step ageing treatments, it is clearly important to decide to what extent they are competitive or complementary. Lorimer and Nicholson have claimed[78] that the effects described by their model "are likely to be more important in most practical cases". The validity of this statement is examined critically in this Chapter and it is concluded below that(a) the validity of some of the concepts of the (L-N) model is questionable and (b) the (L-N) model is not sufficiently comprehensive to explain convincingly all the experimentally observed two-step ageing phenomena of Al-1.2%Mg_2Si and Al-Zn alloys.

Summaries of the (P-J) and (L-N) models are given in section 8.2, so that the important points of each model can be brought to the attention of the reader. Then, in section 8.3, a detailed discussion of certain aspects of the (P-J) and (L-N) models is given, with the general aims of ascertaining the extent to which the two models overlap and of high lighting their differences. Finally, in section 8.4, the major conclusions of the research work reported in this dissertation are summarized and some suggestions for future work are given.

8.2 SUMMARIES OF THE TWO-STEP AGEING MODELS

8.2.1 The Pashley-Jacobs model

The following summary of the (P-J) model is included at this point to remind the reader of the various concepts and ideas which were discussed in detail in Chapters 4-7. Since many aspects of the (P-J) model are discussed at length in section 8.3 only the salient points are given here.

(a) The formation of G.P. zones after quenching

According to the (P-J) model, the three important concepts which are relevant to this process are :-

(i) For an alloy of given solute concentration, quenching to any temperature T_1 that is below a certain critical temperature T_c will always lead to the formation of G.P. zones.

(ii) Under certain conditions (see (iii) below), quenching to a temperature $T_1 = T_c'$ ($> T_c$) may also lead to G.P.zone formation, provided that sufficient excess vacancies are available to aid the nucleation.

(iii) Even under the most favourable conditions, when the

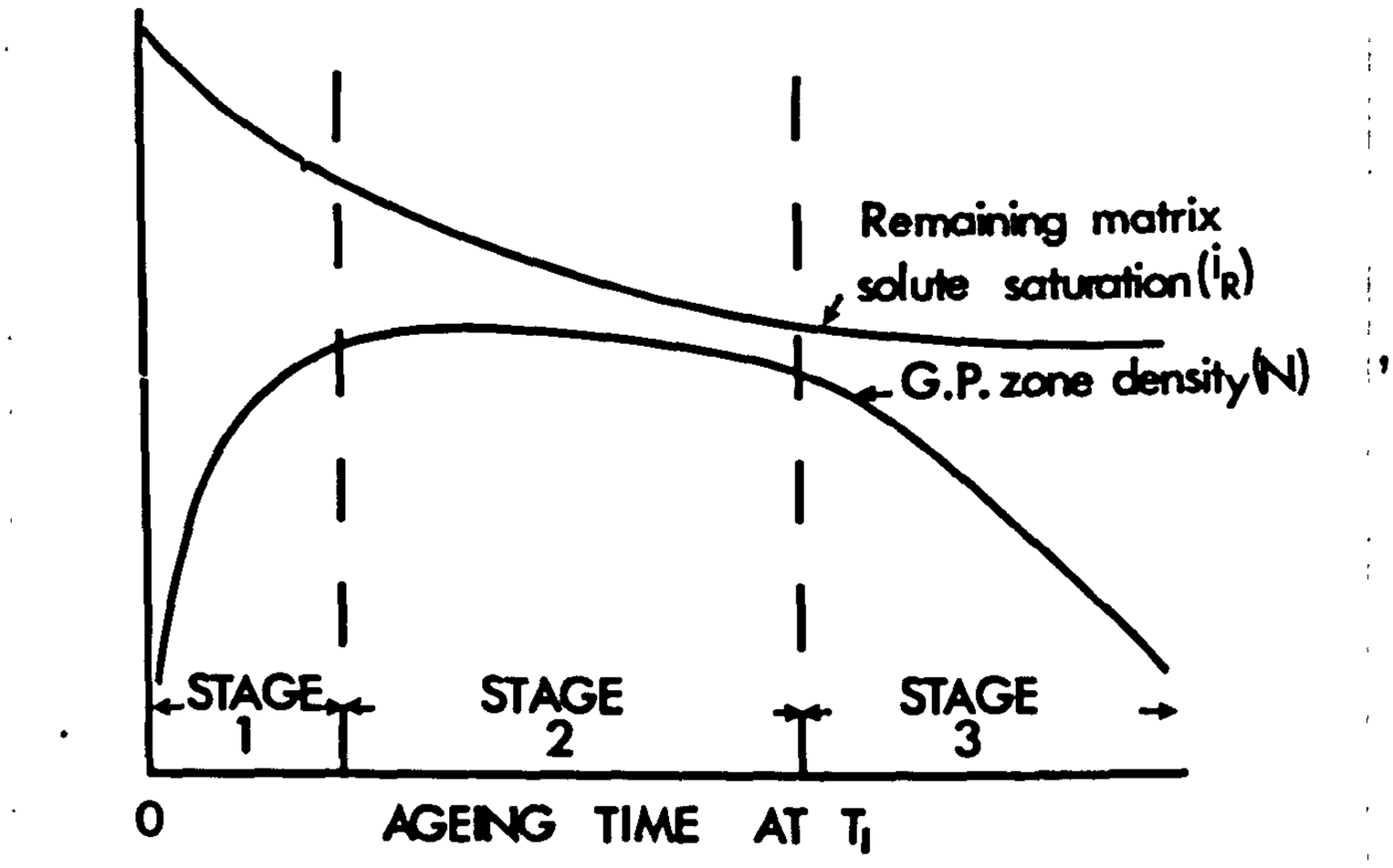

Figure 8.1 A schematic diagram showing the three stages of G.P. zone development envisaged by the Pashley-Jacobs model.

highest possible vacancy supersaturation is retained during the quench, the highest value of T_1 at which observable G.P. zone formation will occur (designated as T_c' (maximum)) may be significantly below the so-called G.P. zone solvus temperature $T_{G.P.}$.

The practical importance of the critical temperature T_c is emphasized by the (P-J) model since it is considered that its value can be determined quite accurately by means of suitable step-quenching experiments. Also, if these are carried out in conjunction with direct-quenching experiments, the difference between T_c and T_c' may be obtained. However, it is believed that the results of quenching experiments cannot be used, at present, to determine the difference between T_c (or T_c') and $T_{G.P.}$. This is an important point and it is considered again in section 8.3.

(b) <u>The growth of G.P. zones at T_1</u>

The three distinct, but overlapping, stages envisaged by the (P-J) model are illustrated schematically in Figure 8.1. The important processes which are believed to occur during each stage are given below.

Stage (1). Some G.P. zones may be nucleated during the latter part of the quench and further nucleation may occur during the initial stages of ageing. The increase in the density of G.P. zones is accompanied by a progressive decrease in the solute supersaturation in the matrix.

Stage (2). The density of G.P. zones remains approximately constant during this stage and G.P. zone growth is accompanied by the further progressive decrease in the matrix solute supersaturation. It is recognized that there will be a distribution in zone sizes during this stage, so that there will be a tendency for the larger G.P. zones to grow at the expense of the smaller ones. However, the decrease in G.P. zone density due to this process is assumed to be small.

Stage (3). Particle coarsening occurs during this final stage and the mean G.P. zone size increases while the density of G.P. zones progressively decreases.

(c) <u>The stability of G.P. zones at T_2</u>

The final problem considered by the (P-J) model concerns the factors which control the ability of G.P. zones, formed during a pre-treatment at T_1, to remain stable at a higher temperature T_2. It is assumed that the G.P. zones which are formed during ageing at T_1 are spherical in shape and that they give rise to no lattice strain. Then, as shown in Chapter 5, the Gibbs-Thomson equation may be used to derive the following stability condition for a G.P. zone of radius a at the temperature T_2:

$$a \log_e i_R > K \qquad (8.1)$$

where i_R is the value of the remaining matrix solute supersaturation (calculated with respect to the G.P. zone solvus) which surrounds the G.P. zone at T_2 and K is the value of the stability constant appropriate to T_2. Thus, the stability of a G.P. zone at T_2 depends upon two factors: (1) the size of the G.P. zone and (2) the value of the remaining solute supersaturation (the effect of introducing lattice strain around a G.P. zone is considered in section 8.3). A G.P. zone which continues to grow at T_2 is said to have been "seeded" by the pre-treatment at T_1. It is emphasized that a G.P. zone which is seeded for further growth at T_2 is considered to be identical, in all respects apart from size, to a G.P. zone formed during a pre-treatment at T_1.

Two distinct modes of behaviour are predicted by the model (see Chapter 5) depending upon whether T_2 is above or below T_c.

Mode (1) : $T_2 < T_c$

(i) For very short pre-treatments at T_1 the final size and distribution of G.P. zones after a subsequent treatment at T_2 will be very similar to that normally produced by direct-quenching and ageing at T_2.

(ii) For slightly longer pre-treatments at T_1 the size and distribution of G.P. zones established on subsequent ageing at T_2 will be on a coarser scale than that produced in a sample which is either direct-quenched to T_2 or quenched to T_1 and then immediately aged at T_2. This is the important coarsening behaviour predicted by the (P-J) model.

(iii) For long pre-treatments at T_1 a large proportion of the G.P. zones may be seeded for growth at T_2. This may, under suitable conditions, give rise to a G.P. zone distribution which is considerably finer than that produced by direct-quenching and ageing at T_2.

Mode (2) : $T_c < T_2 < T_{G.P.}$

(i) After a suitably short pre-treatment at T_1 the G.P. zones will have grown insufficiently in size to be seeded for further growth at T_2 and reversion will occur.

(ii) After a suitably long pre-treatment at T_1, some (possibly all) of the G.P. zones may have grown sufficiently in size to be seeded for further growth at T_2. For T_c' (maximum) $< T_2 < T_{G.P.}$ a significant number of G.P. zones may be seeded for further growth, whereas none can be nucleated by direct-quenching to T_2.

8.2.2 The Lorimer-Nicholson model

The purpose of this section is to acquaint the reader with the main concepts and ideas of the (L-N) model, as reported in the literature[77,78,79]. No attempt is made in this section to criticize the model, although certain points which are to be discussed in more detail in section 8.3 are indicated.

(a) <u>The formation of G.P. zones after quenching</u>

Lorimer and Nicholson considered a binary alloy for which the precipitation sequence at a low ageing temperature is

$$\alpha_{\text{supersaturated}} \rightarrow \alpha'_{\text{saturated}} + \text{G.P.zones} \rightarrow \alpha_{\text{saturated}} + \beta$$

where α and β are the two terminal solid solutions and G.P. zones are formed as a transition precipitate and where $\alpha'_{\text{saturated}} > \alpha_{\text{saturated}}$. The important concepts involved in determining if G.P. zones and /or β-precipitates are nucleated after quenching from T_S to T_1 were reported to be as follows:

(i) If T_1 is less than the β-solvus temperature T_β then the alloy is metastable with respect to β-precipitates.

(ii) If T_1 is less than the G.P. zone solvus temperature $T_{G.P.}$ then the alloy is also metastable with respect to G.P. zones (see (iii) below).

(iii) Since G.P. zones are less stable than β-precipitates then $T_{G.P.} < T_\beta$.

In their early paper[77], the upper limiting temperature for G.P. zone formation in an Al-Zn-Mg alloy (as determined by direct-quenching experiments) was identified with the G.P. zone solvus temperature $T_{G.P.}$. About a year later the work of Pashley et al[81], with an Al-1.2%Mg_2Si alloy, demonstrated the quench-rate dependence of the upper limiting temperature for G.P. zones in that alloy. Later, Lorimer and Nicholson[78] reported the same effect with Al-Cu and Al-Ge alloys and modified their model to take this effect into account. Their interpretation[78] of this behaviour focussed attention on the G.P. zone solvus temperature $T_{G.P.}$ and stated that a finite undercooling below $T_{G.P.}$ is required before G.P. zone nucleation occurs at an observable rate. This important aspect of their model is discussed again in section 8.3.

(b) <u>The growth of G.P. zones at T_1</u>

Lorimer and Nicholson adopted the Gerold model[40,41] (see

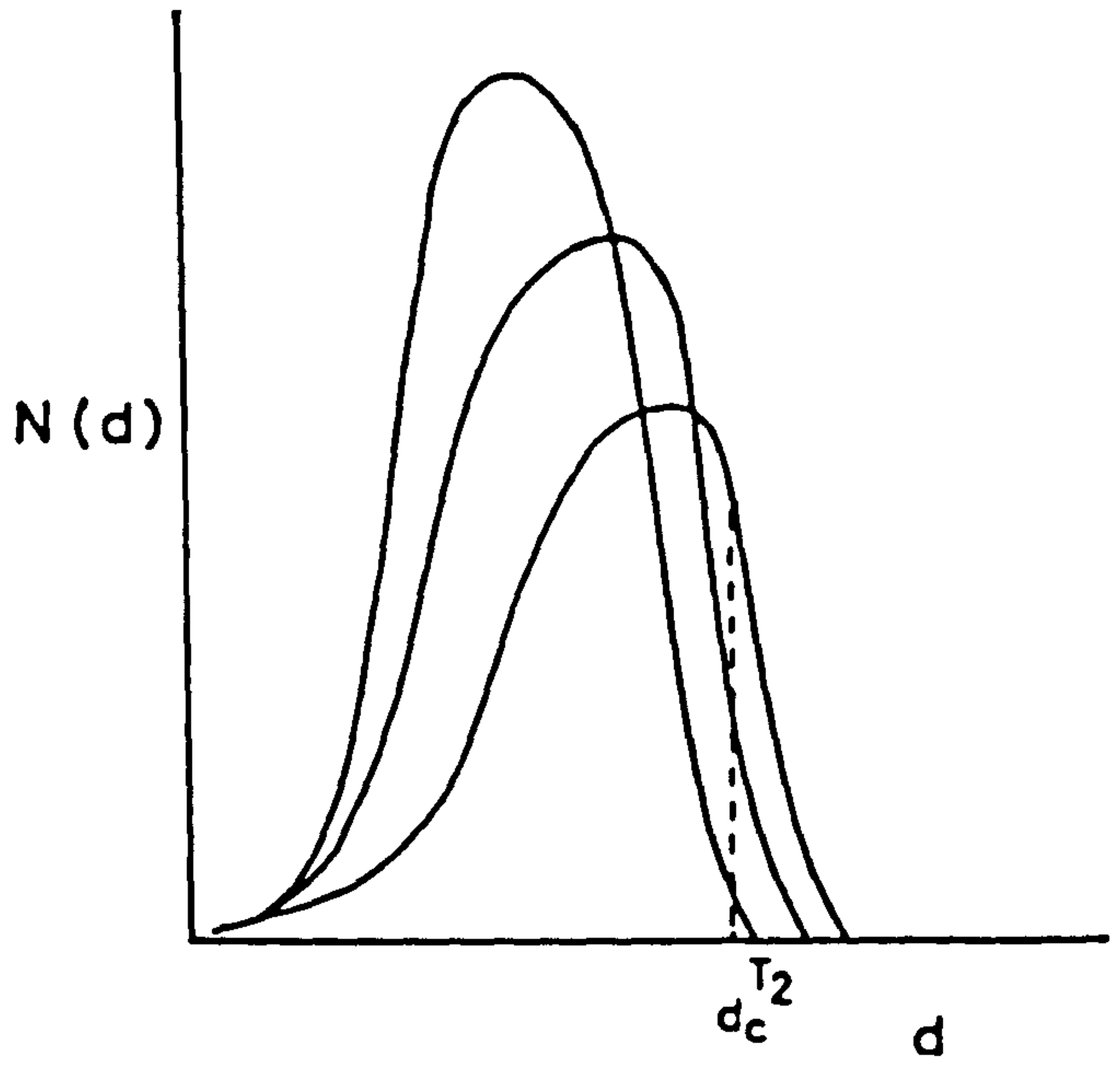

Figure 8.2 A schematic diagram (reproduced from Lorimer and Nicholson[78]) showing the variation of G.P. zone-size distribution with ageing time at T_1. N(d) is the number of G.P. zones of diameter d. According to the Lorimer-Nicholson model, all G.P. zones which are larger than $d_c^{T_2}$ are potential nuclei for precipitates at T_2.

section 1.4.3) in order to describe the development of G.P. zones at T_1 (although they said that their results were not qualitatively affected if the Guinier model[13,75] was used).

According to the (L-N) model, the size distribution of G.P. zones after any given ageing time at T_1 is determined by the amount of particle coarsening that has occurred, so that for progressively longer ageing times at T_1 the zone density decreases and the mean zone size increases (see Figure 8.2). They assumed that all excess solute atoms are incorporated within G.P. zones during ageing at T_1 and that the matrix surrounding the G.P. zones is a saturated solid solution. Thus, the mechanism of G.P. zone development according to Lorimer and Nicholson differs significantly from that proposed in the (P-J) model. This point is discussed critically in section 8.3.

(c) The stability of G.P. zones at T_2

Lorimer and Nicholson[78] concentrated on the particular case when $T_2 > T_{G.P.}$ and considered in detail the possibility of unstable G.P. zones acting as nuclei for the more stable β-phase. The following is a summary of their argument.

(i) Since $T_2 > T_{G.P.}$, all G.P. zones formed at T_1 will be unstable at T_2 and therefore will start to dissolve.

(ii) The process of dissolution will take a finite time to occur since it involves the redistribution of solute atoms within the alloy by solute diffusion. During this period the alloy contains a number of unstable solute clusters which are far larger in size than the transient thermally-activated solute fluctuations expected after a direct-quench to T_2.

(iii) The next step is the critical part of their argument, for they then postulated that those unstable solute clusters which exceed

a certain critical size can act as potential nuclei for the more stable β-phase. They also postulated that the nucleation event requires only part of the normal activation energy associated with the nucleation of β after direct-quenching to T_2 (i.e. that part associated with the transformation in crystal structure) since the change in solute concentration has already been achieved during the pre-treatment. They considered that those solute clusters which are smaller than the critical size will completely dissolve.

(iv) They then pointed out that the nucleation rate of β-precipitates will be highest immediately after the up-quench to T_2, since this is when the highest proportion of the unstable solute clusters exceed the critical size. As the ageing time at T_2 increases, the nucleation rate progressively decreases and eventually becomes negligible.

Thus, according to this model, G.P. zones may "seed" the transformation to β at a temperature $T_2 > T_{G.P.}$ (it must be emphasized that the "seeding" mechanism proposed by Lorimer and Nicholson is fundamentally different from the "seeding" of G.P. zones for further growth, at a temperature T_2 between T_c and $T_{G.P.}$, that is described in the (P-J) model). Lorimer and Nicholson also pointed out that the isothermal transformation of G.P. zones to β-precipitates can take place below $T_{G.P.}$ They did not investigate the implications of this extensively, although Lorimer[79] has used this concept to propose an explanation of the "coarsening behaviour" associated with the delayed-ageing of Al-Mg_2Si alloys. His explanation is fundamentally different from that proposed in the (P-J) model and is examined critically in section 8.3.

In order to make a qualitative estimate of the number of β-precipitates that are seeded after a given two-step treatment, Lorimer and Nicholson[78] made the assumption that the critical cluster size for

seeding ($d_c^{T_2}$) could be equated to the critical nucleus size at T_2, as given by classical homogeneous nucleation theory for direct-quenching to T_2 (although they recognised that the condition for a nucleus may actually depend upon the solute composition and defect concentration of the cluster in addition to its size). The validity of this assumption is examined in section 8.3. They then suggested that as T_2 is increased above $T_{G.P.}$ towards T_β, $d_c^{T_2}$ will become larger and so fewer β-precipitates will be seeded for a given pre-treatment at T_1. Also, as the time at T_1 is increased, or the value of T_1 is increased towards $T_{G.P.}$, the number per unit volume of G.P. zones which exceed the critical size is increased and so the density of seeded β-precipitates obtained after up-quenching and ageing at T_2 will be correspondingly increased.

8.3 A GENERAL DISCUSSION OF THE FACTORS CONTROLLING TWO-STEP AGEING

The object of this section is two-fold: (1) to examine the validity of some of the concepts and ideas of the (P-J) model, and (2) to compare and contrast critically the (P-J) model and the (L-N) model. It is convenient to divide the discussion into a number of sub-sections, each of which will concentrate on one particular phenomenon or process.

(a) The relationship between T_c and $T_{G.P.}$

Both the (P-J) and (L-N) models introduce the concept of a critical temperature above which G.P. zones are not observed to form. The (P-J) model focusses attention on the critical temperature T_c and considers that its value can be obtained quite accurately by means of step-quenching experiments. The model recognizes that G.P. zones can be formed at a temperature $T_c' > T_c$, provided that sufficient excess vacancies are available to aid the nucleation. The (L-N) model focusses attention on the G.P. zone solvus temperature $T_{G.P.}$ and recognizes that an undercooling

is necessary below $T_{G.P.}$ before a finite rate of G.P. zone nucleation can take place.

Thus, apart from a difference in emphasis, the two models are qualitatively very similar, e.g. both models predict that the experimentally observed upper limiting temperature for G.P. zone formation will be quench-rate dependent. The two models differ, however, in the significance attributed to the results obtained by direct-quenching experiments. According to the (P-J) model, the temperatures T_c and T_c' are both amenable to experimental determination whereas it is believed that the temperature difference between T_c' and $T_{G.P.}$ cannot be estimated, a priori, from direct-quenching experiments. According to the (L-N) model[78], "a detectable rate of homogeneous nucleation will occur at undercoolings below $T_{G.P.}$ of the order of 10-20°C". This is a major assumption made by Lorimer and Nicholson and the danger of applying it too rigidly is demonstrated in the following discussion.

Some of the important experimental results which were reported in Chapter 4 are summarized in Table 8.1. The marked difference in behaviour between the Al-17.5%Zn and Al-1.2%Mg_2Si is reflected in the $(T_c' - T_c)$ values. It is possible that larger values of $(T_c' - T_c)$ would be obtained with a quench that is more rapid than that provided by Wood's

TABLE 8.1

Experimental results obtained by quenching studies			
Alloy	T_c'(oil) - T_c	T_c'(salt) - T_c	T_c'(Wood's metal) - T_c
Al - 17.5%Zn	$\sim$ 5°C	-	$\sim$ 8°C
Al - 1.2%Mg_2Si	-	$\sim$ 35°C	$\sim$ 55°C

metal. In view of the different response of the two alloys to quenching it would appear difficult to make even a reliable guess at the magnitude of ($T_{G.P.}$ - T'_c (Wood's metal)) for either alloy. It could be argued that since T'_c does not appear to be very sensitive to quench-rate in the case of the Al-17.5%Zn alloy then T'_c (Wood's metal) may be close to, although still below, $T_{G.P.}$. Even so, the amount below is still more a matter of opinion than experimental fact, which is not very satisfactory. It is therefore concluded that the results of direct-quenching experiments cannot be interpreted unambiguously if they are referred to the G.P. zone solvus temperature $T_{G.P.}$, that is, unless some method other than direct-quenching can be found for determining independently the value of $T_{G.P.}$. The possibility of using reversion studies to do this is discussed below.

In Chapter 7 it was demonstrated that the minimum reversion temperature T_R is dependent upon the thermal history of the sample before the "reversion heat treatment". In <u>all</u> experiments $T_R > T'_c$ (Wood's metal) and for the Al-17.5%Zn alloy it was shown that (T_R - T'_c (Wood's metal)) $\sim$ 10°C. However, if the interpretation of reversion according to the (P-J) model is correct, then even this highest experimentally observed value of T_R may still be considerably below $T_{G.P.}$ and it is thought that the amount below cannot, at present, be estimated from the experimental results. The reason for this is that, according to the (P-J) model, the observation of complete dissolution of all G.P. zones at T_2 does not necessarily mean that $T_2 > T_{G.P.}$ but merely that the G.P. zones formed at T_1 were unstable with respect to the reduced matrix solute supersaturation at T_2. Thus, it is believed that reversion studies do not readily provide an estimate of the value of $T_{G.P.}$.

Let us now consider the experimental observation, which was reported in Chapter 4, that needle-shaped precipitates can be nucleated

on matrix dislocations in the Al-1.2%Mg_2Si system after direct-quenching to a temperature $\leqslant 330^{o}C$. Since the electron microscope images of these needle-shaped precipitates were always identical to the images of homogeneous needle-precipitates nucleated at a temperature below T_c'(Wood's metal) it is suggested that the heterogeneous and homogeneous needles may be of the same phase and may be described as the G.P. zones of the Al-Mg_2Si system. In Chapter 4 the marked catalyzing effect of some dislocations on the nucleation of the needle-shaped precipitates in this system was attributed to the ability of a dislocation of predominantly edge character to relieve partially the strain energy nucleation barrier which is believed to be associated with G.P. zone formation in this alloy. If the above interpretation of these experimental results is correct then the observations, that (1) G.P. zones can be nucleated on dislocations at temperatures up to $\sim 330^{o}C$ and (2) that they can then grow rapidly in length so that a large part of the needle is a relatively large distance from the influence of the catalyzing dislocation, suggest that $T_{G.P.} \geqslant 330^{o}C$ for this alloy. If so, then $(T_{G.P.} - T_c) \geqslant 140^{o}C$. A tentative explanation of this result is given below.

Let us ignore the effect due to lattice strain for the moment. In Chapter 4 it was mentioned that the needle-shaped zones in the Al-Mg_2Si system are thought to be partially coherent. If so, then according to the nucleation model of section 4.5.1, the higher value of interfacial free energy γ associated with the incoherent interface (as compared to the coherent interface) will result in a larger dependence of G.P. zone stability on zone size (i.e. a large matrix solute supersaturation will be required to stabilize a small zone and the effect of zone size on stability will extend to a large zone size). The stability curves for this alloy will be widely separated with respect to temperature. We can take account

of the lattice strain around the zones by reference to equation 4.8 which showed that lattice strain increases the critical size below which a zone becomes unstable with respect to a given value of matrix solute supersaturation. Thus, the stability curves will be depressed towards high solute concentrations and low temperatures. It then follows that a high solute supersaturation will be required for homogeneous G.P. zone nucleation to occur. Also, the nucleation kinetics will depend very markedly on the ability of vacancies to aid the formation of nuclei (see Chapter 4). Edge-type dislocations will provide preferential nucleation sites, especially at low solute supersaturations, by virtue of their ability to relieve partially the strain energy barrier to nucleation. Thus, in a qualitative way, the experimental results obtained by direct-quenching samples of an Al-1.2%Mg_2Si alloy can be explained.

To summarize this section, it is believed that the parameters T_c and T'_c are of great <u>practical and theoretical</u> importance for aiding the interpretation of the experimentally observed response of alloys to quenching. It is acknowledged that the concept of a G.P. zone solvus temperature $T_{G.P.}$ may in certain circumstances be useful, but it is thought that its practical significance in relation to quenching experiments is doubtful because its value cannot be readily obtained, at present, with any certainty.

(b) <u>The isothermal growth of G.P. zones at T_1</u>

In section 8.2 it was pointed out that the (P-J) and (L-N) models differ in the mechanisms describing the development of G.P. zones at T_1. In order to distinguish the differences more clearly let us re-call the so-called Guinier and Gerold models which were briefly described in section 1.4.3. According to the Guinier model[13,75], each G.P. zone is surrounded initially by a region which is depleted in solute atoms and the full solute super-

saturation is retained between these regions. Subsequent growth of the G.P. zones causes the depleted regions to overlap and the matrix solute supersaturation is progressively reduced in value. According to the Gerold model[40,41], the segregation of all excess solute atoms in the form of clusters is completed within a very short time after the quench and the subsequent isothermal growth process is entirely one of competitive growth, with the mean cluster size increasing as the density of clusters decreases.

The mechanism of G.P. zone development envisaged in the (P-J) model includes, at least in broad outline, the concepts of both the Guinier and Gerold models, but as separate stages of the growth process. In terms of the three stages of the (P-J) model, stage 1 and the beginning of stage 2 correspond approximately to the Guinier approach, whereas the latter part of stage 3 corresponds approximately to the Gerold approach. By associating the Gerold approach with the latter part of stage 3 it is assumed, as do Lorimer and Nicholson[78], that the Gerold model refers to the process of Ostwald ripening, as described by Lifshitz and Slyozov[179], Wagner[180], Oriani[181] and Greenwood[182]. During Ostwald ripening it is assumed that the matrix supersaturation is negligibly small and that a quasi-stationary particle-size distribution is maintained. It is suggested that the alloy tends progressively towards this situation during the latter part of stage 2 and the beginning of stage 3.

It is also suggested that the relevant stage for any given heat treatment will depend upon the rate of solute clustering and the duration of ageing. For example, in the case of Al-Mg_2Si alloys, the rate of solute clustering at room temperature is very slow (see Chapter 5) and continues over a period of many years. It would therefore seem reasonable to assume that for heat treatments of the order of a few hours, or even days, the solute clusters never develop beyond stage 2. In the case of an

Al-Zn sample, the initial rate of solute clustering is very rapid at room temperature in regions of the sample where the quenched-in excess vacancy concentration is high (see Chapter 1). In these regions, the G.P. zones will develop rapidly through stages 1 and 2 and further development will consist of competitive growth. It is believed, however, that the situation will be different near to a grain boundary where, due to vacancy-depletion (see Chapter 6), the growth rate of G.P. zones will be slower. The zones in this region will progress less rapidly through stage 2, so that the ageing time before the onset of competitive growth will be correspondingly increased. It therefore seems reasonable to assume that the density of G.P. zones will remain approximately constant in the vicinity of grain boundaries for fairly short ageing times, which was the assumption made in Chapter 6.

Lorimer and Nicholson[78] have claimed that their model is equally applicable if either the Guinier model or the Gerold model is adopted, although the detailed development of their model is carried out in terms of the Gerold model. Lorimer[79] pointed out that, during the early stages of ageing, "the concentration of solute in the matrix will be higher than that indicated by the equilibrium phase diagram due to the small size of the G.P. zones and the associated Gibbs-Thomson effect", which is in agreement with the (P-J) model. This point was subsequently ignored in the later paper by Lorimer and Nicholson[78] where it was assumed that, during G.P. zone growth, the matrix is a saturated solid solution and that the zones grow by a process of Ostwald ripening. Their model therefore differs from the (P-J) model, which stresses the importance of taking the remaining solute supersaturation into account and emphasizes that at all times the stability of a G.P. zone depends upon (a) its size and (b) the value of the surrounding solute supersaturation, even during Ostwald

ripening (the matrix must remain supersaturated or else all G.P. zones will dissolve). It is believed that this effect is particularly important in two-step ageing, as will be discussed below in section (c).

Finally, let us consider the possibility of spinodal decomposition occurring in Al-Zn alloys at room temperature. Rundman and Hilliard[127] have calculated the position of the coherent spinodal curve on the phase diagram for Al-rich Zn alloys (see Figure 7.9). According to their results, alloys with zinc contents $\geq$ 20 wt.%Zn can decompose spinodally at room temperature. Clearly, any attempt to develop the (P-J) model for this alloy in a quantitative way would have to consider the implications of spinodal decomposition during pre-treatment at room temperature for concentrated Al-Zn alloys.

(c) Two-step ageing

Let us first of all examine the validity of some of the assumptions made by the (P-J) model.

As discussed in Chapter 4, the assumption made by the (P-J) model that the G.P. zones are spherical in shape and give rise to no lattice strain is believed not to be valid for the early stages of ageing in the Al-Mg_2Si system, where needle-shaped G.P. zones are thought to be formed. It was suggested by Pashley et al[81] that the curvature at the ends of the needle-shaped zones will probably decrease with an increase in the size of the zone, so the same effect of zone size on zone stability (as deduced from the Gibbs-Thomson equation) is qualitatively to be expected. The effect of introducing lattice strain around a G.P. zone is to increase the critical size at which it is stable with respect to a matrix of given solute supersaturation (see Chapter 4). Thus, although a quantitative treatment would have to take the shape of the G.P. zones and the lattice strain into account, the same general effect of zone size and matrix solute

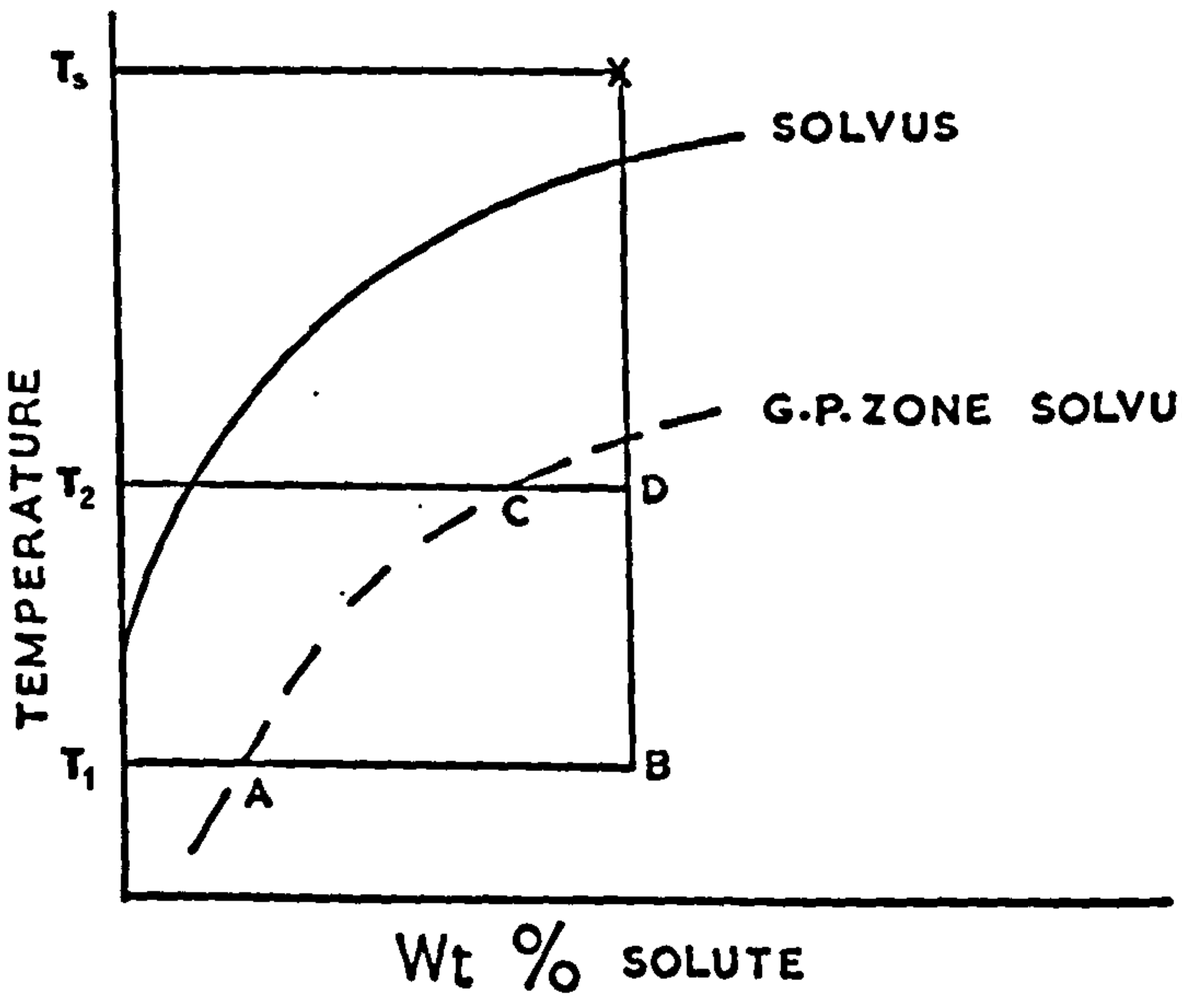

Figure 8.3 The schematic temperature-composition diagram, showing stable and metastable phase boundaries, which was used by Lorimer[79] to explain the "coarsening" behaviour of Al-Mg_2Si alloys.

supersaturation on zone stability is qualitatively to be expected.

Next, let us compare the (P-J) model with the (L-N) model and consider, in detail, the following two topics : (i) the "coarsening behaviour" observed with an Al-Mg_2Si alloy; (ii) the "seeding" mechanisms of both models.

(i) Coarsening in Al-Mg_2Si alloys

In Chapter 5 the excellent qualitative agreement between the predictions of the (P-J) model and the experimentally observed two-step ageing behaviour of Al-1.2%Mg_2Si was demonstrated. One of the significant results of this work[81] was a qualitative explanation of the "coarsening behaviour" exhibited by this alloy after a suitable heat treatment[80] with $T_1 = 20^oC$ and $T_2 = 160^oC$ (which is below T_c).

Lorimer[79] has put forward an alternative explanation of this coarsening behaviour, which is based on the (L-N) model for two-step ageing. The first point to note is that Lorimer used the direct-quenching technique to determine that the upper limiting temperature for G.P. zone formation in an Al-1.2%Mg_2Si alloy after a salt quench was $230^oC \pm 5^oC$. This is in good agreement with the results reported in Chapter 5. He identified this value of upper limiting temperature with $T_{G.P.}$, which, as explained earlier in this Chapter, is believed to be incorrect. However, this does not effect the argument qualitatively if $T_1 = 20^oC$ and $T_2 = 160^oC$. His explanation of the coarsening behaviour may be summarized as follows:-

When the temperature of the alloy is raised from T_1 to T_2 (see Figure 8.3) the equilibrium volume fraction of solute in the form of G.P. zones will decrease in the ratio CD/AB. (This essentially says, as is said in the (P-J) model, that the full solute supersaturation is lower at T_2 than at T_1 and so less solute is available to form G.P. zones). Lorimer then invokes this effect together with the concept of a "G.P. zone to precipitate" transformation to predict three distinct modes of behaviour.

(1) For a short, or low temperature, pre-treatment at T_1, all the zones will dissolve on up-quenching to T_2 and the size distribution of G.P. zones formed at T_2 will be characteristic of direct-quenching to T_2; (2) for a sufficiently long time at T_1, the zones will have reached a sufficient size to be able to transform to precipitates at T_2 before the decreased supersaturation results in their dissolution, and the final precipitate density will be higher than that produced by direct-quenching to T_2; (3) For an intermediate time at T_1 only a few zones will have reached a sufficient size to act as precipitate nuclei at T_2. These transform to precipitates (of lower free energy than the G.P. zones) which then grow at the expense of the zones and therefore decrease the matrix solute supersaturation. During ageing at T_2, zone growth is arrested (and therefore the zones will eventually dissolve) and the final precipitate distribution will be coarser than after direct-quenching to T_2.

The significant difference between this explanation and that of the (P-J) model is that it requires the G.P. zones to "seed" intermediate precipitates. However, since at the present time there is no convincing evidence which suggests that the small needle-shaped precipitates are preceded by a "G.P. zone phase", it is difficult to accept this explanation. In fact, it is emphasized that in Chapters 4 and 5 of this dissertation the needle-shaped precipitates were considered to be the G.P. zones of the Al-Mg_2Si system.

(ii) <u>The "seeding" mechanisms of both models</u>

The (P-J) model has not been developed, so far, to consider the possible consequences of a G.P. zone ⟶ intermediate precipitate transformation. The object of this section is to show that the (P-J) model can easily be extended to include this process.

Take as an example a hypothetical alloy which decomposes at a low temperature by the formation of G.P. zones, which grow in size and

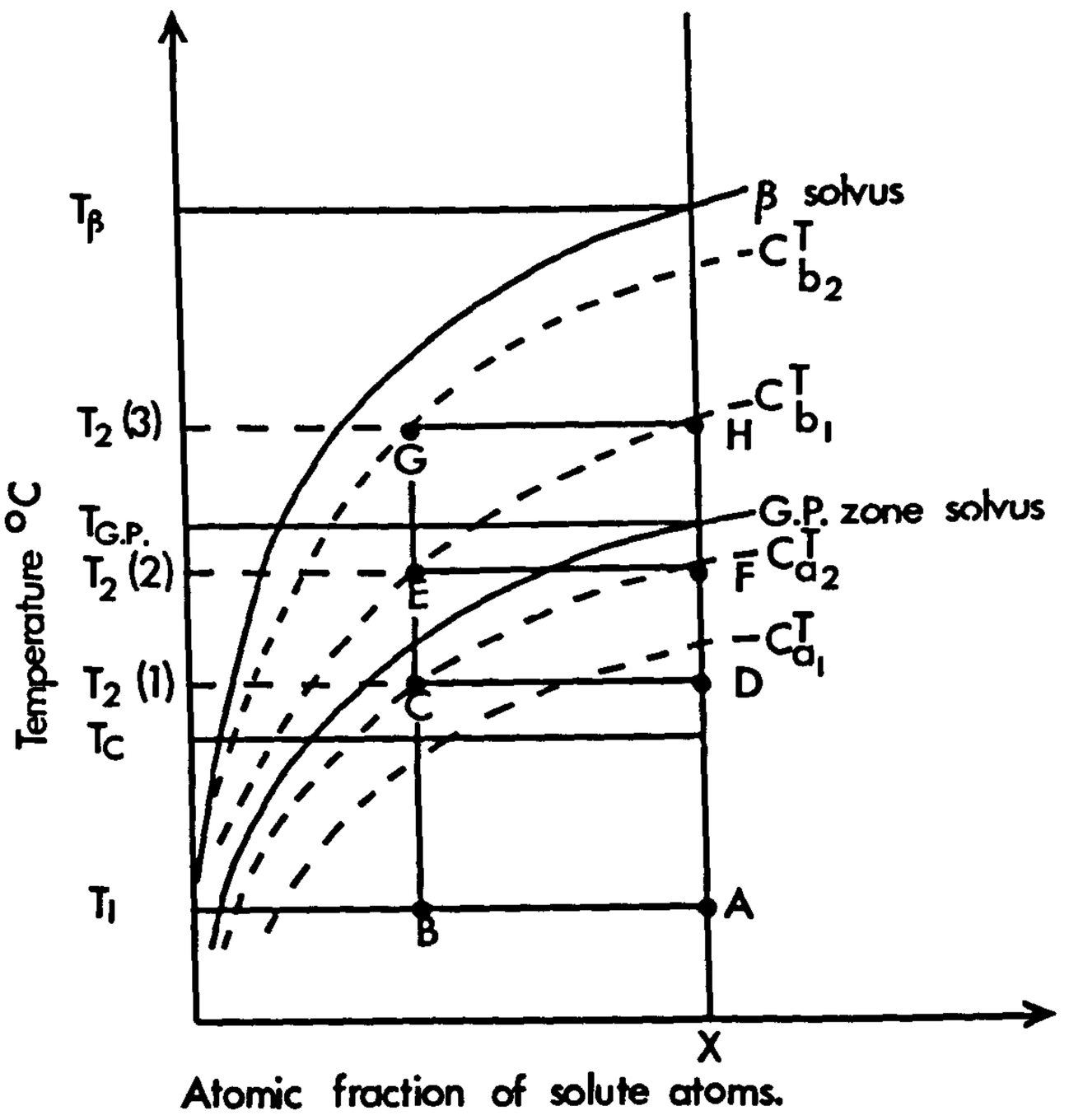

Figure 8.4 The hypothetical stability diagram (see text for further discussion).

eventually transform isothermally to a more stable β-phase (which, to be quite general, may be an intermediate or equilibrium precipitate). Let us suppose that the crystal structure of β-phase is very different from that of the matrix, so that the activation energy for the direct homogeneous nucleation of β-precipitates is high and the probability of direct β nucleation is negligible, even at a low temperature. The hypothetical metastable phase diagram for this system is shown schematically in Figure 8.4, together with some stability curves for zones and β-precipitates of small size.

Let us now develop the (P-J) model for the case of two-step ageing with $T_1 < T_c$ and $T_2 > T_c$. Consider an alloy of composition X (see Figure 8.4) which is quenched to T_1 (point A on the diagram) and then subsequently pre-aged at T_1 for a period of time during which G.P.zones are formed and the solute concentration in the matrix is reduced in value (point B on the diagram). Suppose the alloy is now up-quenched to a temperature T_2 and let us examine three particular cases where T_2 equals $T_2(1)$, $T_2(2)$ and $T_2(3)$, respectively (see Figure 8.4).

Case (1) : $T_2 = T_2(1)$

Immediately after the up-quench we may represent the solute concentration in the matrix by the point C, which is shown to lie on the $C_{a_2}^T$ stability curve for G.P. zones of radius a_2. This case has already been adequately covered by the (P-J) model (see earlier Chapters in this dissertation) and the three possible modes of behaviour at T_2 may be listed as follows:-

(1) Zones of radius $r > a_2$ will be seeded for further growth at $T_2(1)$ and these may subsequently transform to β-precipitates.

(2) Zones of radius r which is just less than a_2 will be unstable initially at $T_2(1)$ but, if the alloy also contains a large

number of zones of radius $r << a_2$ which rapidly dissolve and so increase the matrix supersaturation, these zones may subsequently become restabilized for growth at $T_2(1)$, in the manner already described in Chapter 7.

(3) If all the zones are very small (i.e. $r << a_2$) then no seeding of zones will take place. Reversion will occur, as described by the (P-J) model.

Case (2) : $T_2 = T_2(2)$

Immediately after the up-quench we may represent the matrix solute concentration by the point E on the diagram, and since E is above the G.P. zone solvus curve all the zones will be unstable initially. Two possible situations may arise during subsequent ageing at $T_2(2)$, as follows :-

(1) First of all it is to be noted that the point E is shown to be on the $C^T_{b_1}$ stability curve for β-precipitates of radius b_1. The possibility therefore arises that an unstable solute cluster of radius $r \geqslant b_1$ may be able to seed the transformation to a β-precipitate of radius $r \geqslant b_1$, which will be stable at $T_2(2)$. This is, of course, similar to the transformation process described in the (L-N) model, but in this case it occurs at a temperature $T_2 < T_{G.P.}$ (see Figure 8.4).

(2) If all the unstable solute clusters at point E have radii $r << b_1$, then the transformation to β will not occur. All the solute clusters will start to dissolve and the solute concentration in the matrix will increase along the line E $\longrightarrow$ F. If some restabilization of solute clusters occurs, as described by the (P-J) model, then a few G.P. zones may be seeded for further growth, otherwise reversion will occur.

Case (3) : $T_2 = T_2(3)$

Immediately after the up-quench we may represent the solute concentration in the matrix by the point G in Figure 8.4. Since

T_2 (3) $>$ $T_{G.P.}$, it is impossible for G.P. zones to be stable at T_2(3) and two possible modes of behaviour may occur during subsequent ageing, as follows:-

(1) All the solute clusters dissolve and reversion occurs.

(2) Since the point E lies on the $C^T_{b_2}$ stability curve for β-precipitates of radius b_2, then clusters of radius $r \geqslant b_2$ are capable of seeding the transformation to β-precipitates.

It is believed that by this simple extension to the (P-J) model, all the experimental results reported by Lorimer and Nicholson can be explained. There are, however, several points in the argument given above which warrant amplification. Let us first of all consider the "solute cluster to β-precipitate" transformation. According to the ideas outlined above the critical cluster size at which this transformation can occur is dependent upon the value of the remaining solute concentration in the matrix, as reflected by the shape of the stability curves for β-precipitates of different sizes in Figure 8.4. Thus, for a given value of T_2, the critical nucleus size increases as the solute concentration in the matrix decreases. Lorimer and Nicholson[78] did not consider the possibility that the critical nucleus size at T_2 may be dependent on the degree of matrix solute depletion which accompanies solute clustering at T_1, but assumed that the diameter of the critical nucleus ($d_c^{T_2}$ in their notation) can be equated to the critical nucleus size for the homogeneous nucleation of β after direct-quenching to T_2. Thus, the two approaches differ in this respect.

The second point which must be emphasized is that even if the size of an unstable cluster exceeds the critical size at T_2, this does not necessarily mean that the transformation to the β-phase will occur. It is believed that the (L-N) model is correct in saying that the

probability of the transformation occurring will depend upon the activation energy required for the transformation in crystal structure to take place and also upon a kinetic factor which arises because atom movement is required within the solute cluster during the transformation. However, if the model described above is correct, an additional factor which may be important is that as very small solute clusters dissolve, and so feed-back solute atoms into the matrix, the critical nucleus size for the transformation to occur will be progressively decreased. It is possible that this effect may significantly influence the nucleation rate of β-precipitates at T_2.

A third point which must be emphasized is that, as described in case (2) above, a transformation from unstable solute clusters to stable β-precipitates can occur at a temperature $T_2 < T_{G.P.}$. This is included as a precautionary note, since it is believed that the experimental observation that G.P. zones dissolve at T_2 and "seeded" β-precipitates grow does not necessarily mean that $T_2 > T_{G.P.}$.

Finally, let us consider the conditions under which the seeding of intermediate or equilibrium precipitates will be a predominant effect. It seems likely that if the temperature difference between $T_{G.P.}$ and T_β is large (i.e. the two solvus curves are widely separated) then this will be a favourable situation for the transformation to occur. At a temperature T_2 just above $T_{G.P.}$, the alloy will be highly supersaturated in solute atoms with respect to the β-solvus curve and so the critical nucleus size will be small. This condition does not necessarily mean that copious β-precipitates will be seeded at T_2, for the other factors mentioned above may be equally important. On the other hand, if the two solvus curves are very close together, then the critical nucleus size will be very large for $T_{G.P.} < T_2 < T_\beta$ and the transformation is unlikely to occur at T_2.

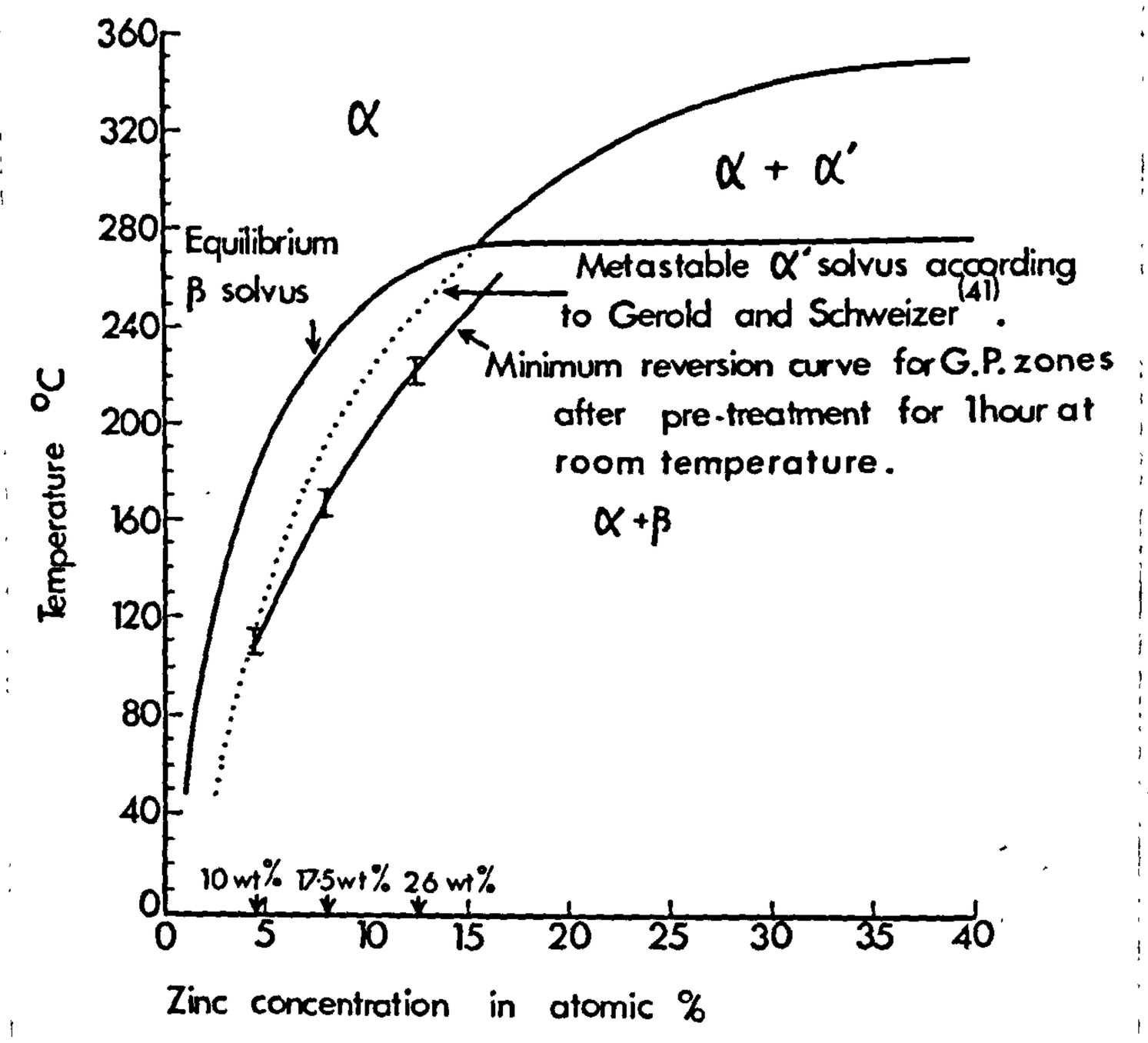

Figure 8.5 The aluminium-rich side of the Al-Zn phase diagram showing the metastable α' solvus according to Gerold and Schweizer[41] and the minimum reversion curve for G.P. zones after pre-treatment for 1 hour at room temperature.

Let us consider the Al-Zn system. According to Gerold and Schweizer[41] the metastable α' - solvus curve can be constructed on the phase diagram by extrapolating the high temperature (α - α') miscibility boundary down into the (α + β) two-phase region, as shown in Figure 8.5. Also shown in Figure 8.5 is the minimum reversion curve for G.P. zones after pre-treatment at room temperature for 1 hour, as derived in Chapter 7. Since it is thought that this reversion curve is below the G.P. zone solvus, it is believed that the α'-solvus and the G.P. zone solvus are very close together. According to the arguments given above, it is unlikely that the seeding of α' - precipitates will occur on ageing at a temperature above $T_{G.P.}$, which is consistent with the experimental results of Chapter 7. It is suggested that unstable G.P. zones are unable to seed hexagonal zinc precipitates at $T_2 > T_{G.P.}$ because a high activation energy is associated with the transformation.

Let us next consider an Al-7.4wt.%Zn-2.8wt.%Mg alloy. Lorimer and Nicholson[77] have shown that T'_c(oil) for this system is $\sim 155^{o}C$ and that G.P. zones formed at room temperature can easily seed the transformation to the intermediate η' - phase with $T_2 = 180^{o}C$. It therefore seems likely that the G.P. zone solvus and the η' -solvus are widely separated in this system, which again is consistent with the deductions described above.

8.4 CONCLUSIONS AND SUGGESTIONS FOR FUTURE WORK

In this dissertation the two-step ageing model which was originally developed by Pashley et al[81] to explain the two-step ageing behaviour of an Al-1.2%Mg_2Si alloy has been applied to a study of the two-step ageing of Al-Zn alloys and has been shown to provide an adequate interpretation of the ageing behaviour. Many aspects of the model have

been amplified and extended and the concept of stability curves for G.P. zones (or precipitates) of different sizes has been shown to be a useful way of representing the concepts of the model diagrammatically. The model has been applied to the problem of determining the basic factors controlling the width of precipitate-free zones in Al-Zn alloys and an excellent correlation between the predictions of the model and the experimental results was shown to exist. It has also been shown that the model is capable of explaining the observed reversion phenomena of Al-Zn alloys.

The Pashley-Jacobs model for two-step ageing has been compared and contrasted critically with the alternative Lorimer-Nicholson model. Despite the claim by Lorimer and Nicholson[78] that the effects described by their model "are likely to be more important in most practical cases" it is believed that the Pashley-Jacobs model can adequately explain all the experimental results reported in this dissertation and, moreover, can easily explain many of the intricate effects associated with the formation of precipitate-free zones, reversion and two step-ageing.

Both models assume that the temperature change between T_1 and T_2 is instantaneous. Experiments which are carried out with a thin foil sample that is rapidly up-quenched from T_1 to T_2 approximate to this assumption closely. It is clear that both models will have to be modified if they are applied to the two-step heat treatment of bulk samples where the heating rate between T_1 and T_2 is slower.

In their present form both models are still very qualitative and probably the most important advance that can be made in the future is to make the models more quantitative. Any success in this direction may help to clarify some of the more controversial aspects of the two models.

More quantitative experimental results would also be invaluable. For example, in Chapter 6 the assumption was made that solute-depletion

occurs in the vicinity of grain boundaries in Al-Zn alloys during the quench and, on the basis of the Pashley-Jacobs model, an estimate of the shape of the solute concentration profile was obtained. It would be useful if an independent experimental determination of this solute concentration profile could be made. At one time it was thought that the electron energy-loss technique of Cundy et al[183] would provide a suitable technique, but recently the work of Cook and Cundy[184] has shown that the Al-Zn system is not suited to electron energy-loss microanalysis because of the weak dependence of plasma energies on zinc concentration in this alloy.

Since the processes which occur during and immediately after direct-quenching from T_S to T_1 and also the processes which occur during and immediately after up-quenching from T_1 to T_2 are so vitally important with regard to the overall two-step ageing behaviour of an alloy, it is suggested that these processes should be studied in greater detail. Of particular importance is the mechanism of the phase transformations (1) stable G.P. zones → intermediate precipitates and (2) unstable G.P. zones → intermediate precipitates, since the detailed knowledge of the processes taking place during these transformations is rather vague[185]. One possible way of studying these transformations is to carry out dynamic experiments inside an electron microscope. However, in view of the many experimental difficulties and inherent limitations of this technique[85] a more profitable way of approaching this problem may probably be to use some other technique, such as X-ray small-angle scattering or the measurement of electrical resistivity changes, possibly in conjunction with electron microscopy.

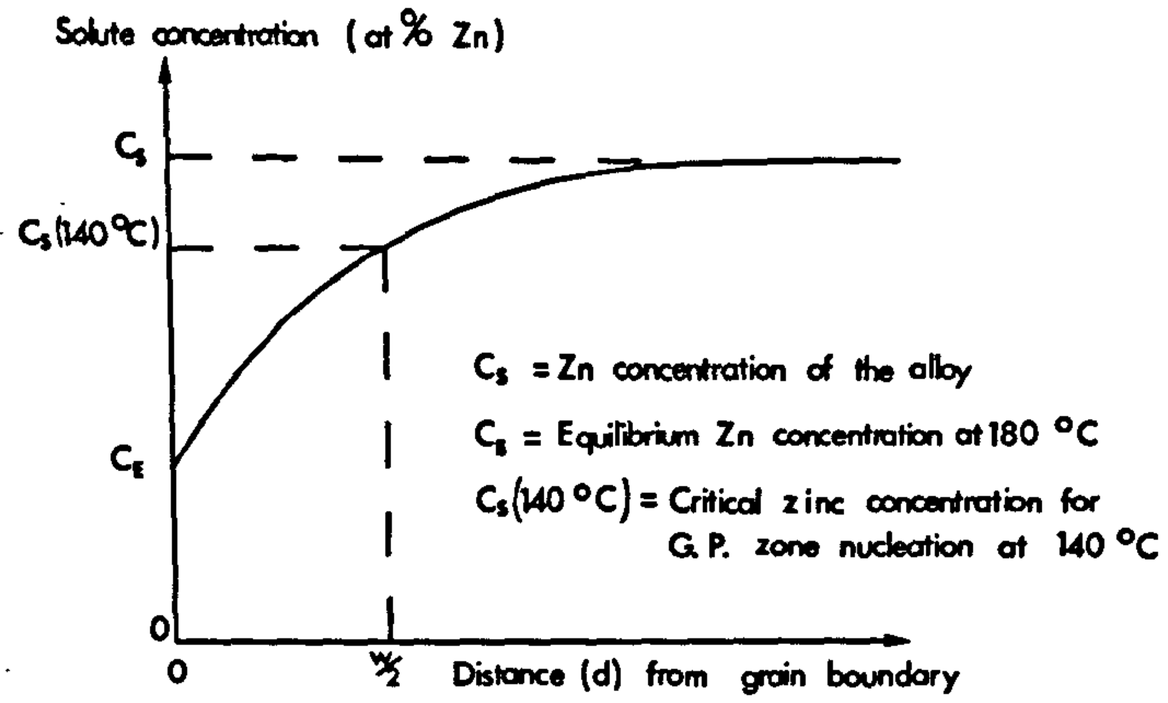

Figure A.1 A schematic diagram showing the solute-concentration profile near to a grain boundary after a holding time of t seconds at 180°C.

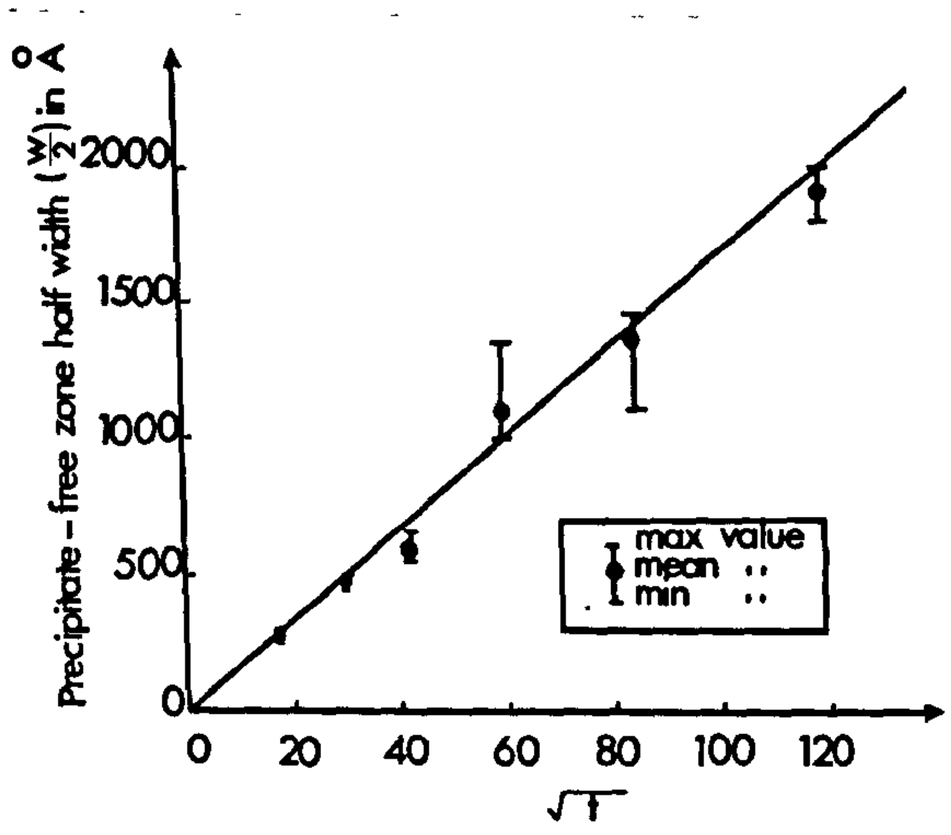

Figure A.2 A graph showing that the precipitate-free zone half-width established at 140°C was proportional to the square-root of the holding time (in seconds) at 180°C.

APPENDIX

THE DEVELOPMENT OF PRECIPITATE-FREE ZONES BY STEP-QUENCHING TO $T_1 < T_c$

In Chapter 6 some experiments were described in which samples of Al-17.5wt.%Zn (8 at.%Zn) were step-quenched from 560°C, via 180°C, to an ageing temperature T_1 = 140°C. In Figure 6.5(a) the experimentally observed p.f.z. width established during ageing at 140°C is shown plotted as a function of the holding time (in hours) at 180°C. It will be seen that wider p.f.z's were established at 140°C after longer holding treatments at 180°C. From this observation it was deduced that the longer the holding time at 180°C, the wider was the corresponding region of solute-depletion adjacent to the grain boundary. The object of this appendix is to demonstrate that the rate of solute-depletion at 180°C can be explained in terms of the diffusion of Zn atoms through the matrix, and towards the grain boundary, at the equilibrium rate.

The assumption is made that, apart from during a transient period immediately after the quench to 180°C, the Zn concentration immediately adjacent to the grain boundaries is maintained during the holding treatment at 180°C at the equilibrium value (C_E) which is characteristic of the temperature 180°C, as given by the equilibrium solvus curve of Figure 4.8. Then, after a holding time of t seconds at 180°C, the solute-concentration profile near to a grain boundary will be as illustrated schematically by Figure A.1. C_s is the full Zn concentration of the alloy (= 8 at.%Zn). The problem is similar to that of diffusion to the surface of a semi-infinite medium, whose surface concentration is maintained at a constant value C_E. If it is assumed that the diffusion coefficient D is constant (i.e. independent of both time and Zn concentration) then the equation

which gives the Zn concentration C_d at a distance d from the grain boundary after a holding time t is as follows[186,187] : -

$$\frac{C_d - C_E}{C_s - C_E} = \text{erf}\left(\frac{d}{2\sqrt{Dt}}\right) \qquad (A.1)$$

According to the model described in section 6.2.1, the edge of the p.f.z. that is formed on subsequent ageing at 140°C is defined by the distance d from the grain boundary where the local solute concentration $C_d = C_s$ (140°C), i.e. the critical solute concentration (see Chapter 6) required for G.P. zone formation at 140°C. Thus, if w is the p.f.z. width established at 140°C, after a holding treatment of t seconds at 180°C, then we may rewrite equation A.1 as

$$\frac{C_s(140^\circ C) - C_E}{C_s - C_E} = \text{erf}\left(\frac{w/2}{2\sqrt{Dt}}\right) \qquad (A.2)$$

If it is assumed that all excess-vacancies are rapidly annihilated during the holding treatment at 180°C and the very small vacancy supersaturation that is introduced by the quench from 180°C to 140°C is neglected then the value of $C_s(140^\circ C)$ can be obtained from the T_c - curve of Figure 4.8. This gives $C_s(140^\circ C)$ = 7at.%Zn. Also, C_s = 8at.%Zn and C_E = 4.3at.%Zn. By substitution of these values into equation A.2 we obtain

$$0.73 = \text{erf}\left(\frac{w/2}{2\sqrt{Dt}}\right) \qquad (A.3)$$

from which

$$\frac{(w/2)}{\sqrt{t}} = 1.56\sqrt{D} \qquad (A.4)$$

The variation of mean p.f.z. half-width ($w/2$) with holding time (t seconds) at 180°C is given in Table A.1. In Figure A.2 the p.f.z. half width is

TABLE A.1

Holding time at 180°C. t secs.	$\sqrt{t}$	Number of grain boundaries examined	p.f.z. half-width ($w/_2$) in Å		
			Mean value	Maximum value	Minimum value
300	17.3	2	265	278	255
900	30.0	2	475	500	450
1800	42.4	2	600	550	650
3600	60.0	4	1100	1350	1000
7200	84.9	5	1380	1450	1100
14400	120.0	4	1900	2000	1800

shown plotted against $\sqrt{t}$. A straight line drawn through these experimental points yields a slope $\left(\frac{w/_2}{\sqrt{t}}\right) = 1.67 \times 10^{-7} cm/sec^{\frac{1}{2}}$. Substitution of this value of $\left(\frac{w/_2}{\sqrt{t}}\right)$ into equation A.4 yields a value of the diffusion coefficient

$D \simeq 1 \times 10^{-14} cm^2/sec.$

To see if this value of D is consistent with the equilibrium diffusion coefficient of Zn in this alloy at 180°C we refer to the radio-tracer self-diffusion measurements of Hilliard et al[188]. From their results, for an alloy of Al-8at.%Zn, the activation energy $Q \simeq 27.2$ kcal/mol. and the frequency factor $D_o \simeq 0.24\ cm^2/sec.$

The equilibrium self-diffusion coefficient D_T at a temperature T°K may be calculated from the usual expression,

$$D_T = D_o \exp\left(-\frac{Q}{RT}\right) \qquad (A.5)$$

from which $D_{180°C} \simeq 2 \times 10^{-14} cm^2/sec.$ This value is in very good agreement with the experimentally determined value of $D_{180°C}$ derived above, although such good agreement is probably fortuitous.

It is therefore concluded that the solute-depletion occurred by the diffusion of Zn atoms at an equilibrium rate to the grain boundary during the holding treatment at 180°C.

REFERENCES

1. A. Wilm, Metallurgie, vol.8, 1911, p.225.

2. P.D.Merica, R.G.Waltenberg and R. Scott, Trans.AIMME, vol.64, 1920, p.41.

3. P.D.Merica, Trans. AIMME, Vol.99, 1932, p.13.

4. A.Guinier, Nature, vol.142, 1938, p.569.

5. G.D.Preston, Proc.Roy.Soc., vol.A167, 1938, p.526.

6. H.K.Hardy and T.J.Heal, Progress in Metal Physics, vol.5, 1954, p.143.

7. H.K.Hardy, J.Inst.Met., vol.77, 1950, p.457.

8. J.W.Newkirk, in 'Precipitation from solid solution ', p.6, Cleveland, Ohio, ASM, 1959.

9. A.Kelly and R.B.Nicholson, Progress in Materials Science, vol.10, 1963, p.151.

10. J.W.Christian, 'The theory of transformations in metals and alloys', Oxford, Pergamon, 1965.

11. A.H.Geisler in 'Phase transformations in solids', p.387, New York, J.Wiley, 1951.

12. A.Guinier, Acta Cryst., vol.5, 1952, p.51.

13. A.Guinier, Solid State Physics, vol.9, 1959, p.293.

14. A.H.Cottrell, 'Theoretical structural metallurgy', London, Edward Arnold, 1948.

15. R.A.Swalin, 'Thermodynamics of solids', New York, J.Wiley, 1962.

16. M.Volmer and A.Weber, Z.Phys.Chem., vol.119, 1925, p.277.

17. R.Becker and W.Döring, Ann.Phys., vol.24, 1935, p.719.

18. R.Becker, Ann.Phys., vol.32, 1938, p.128.

19. R.Becker, Proc. Phys. Soc., vol.52, 1940, p.71.

20. G.Borelius, Ann.Phys., vol.28, 1937, p.507.

21. G.Borelius, Arkiv.Mat.Astron.Fysik., vol.32A, 1945, p.1.

22. G.Borelius, Trans.AIMME, vol.191, 1951, p.477.

23. J.N.Hobstetter, Trans.AIMME, vol. 180, 1949, p.121.

24. E.Scheil, Z.Metallkunde, vol.43, 1952, p.40.

25. M.Hillert, Acta Met., vol.9, 1961, p.525.

26. J.W.Cahn and J.E.Hilliard, J.Chem.Phys., vol.31, 1959, p.688.

27. J.W.Cahn, Acta Met., vol.9, 1961, p.795.

28. J.W.Cahn, Acta Met., vol.10, 1962, p.179.

29. J.W.Cahn, J.Chem.Phys., vol.42, 1965, p.93.

30. J.W.Cahn, Trans.AIMME, vol.242, 1968, p.277.

31. W.Boas and J.K.Mackenzie, Progress in Metal Physics, vol.2, 1950, p.90.

32. H.Mykura, 'Solid surfaces and interfaces', New York, Dover Publications Inc., 1966.

33. J.Burke, 'The kinetics of phase transformations in metals', Oxford, Pergamon, 1965.

34. C.S.Smith in 'Imperfections in nearly perfect crystals', p.377, New York, J.Wiley, 1952.

35. J.W.Cahn, Acta Met., vol.10, 1962, p.907.

36. J.W.Cahn, Acta Met., vol.14, 1966, p.83.

37. J.C.Fisher, J.H.Holloman and J.G.Leschen, Ind.Eng.Chem., vol.44, 1952, p.1324.

38. J.H.Holloman and D.Turnbull, Progress in Metal Physics, vol.4, 1953, p.333.

39. V.Gerold, Aluminium, vol.37, 1961, p.583.

40. V.Gerold, Phys.Stat.Sol., vol.1, 1961, p.37.

41. V.Gerold and W.Schweizer, Z.Metallkunde, vol.52, 1961, p.76.

42. M.Hansen, 'Constitution of binary alloys', New York, McGraw-Hill, 1958.

43. G.R.Goldak and J.G.Parr, J.Inst.Met., vol.92, 1964, p.230.

44. A.A.Presnyakov, Y.A.Gorban and V.V.Chervyakova, Zhur.Fiz.Khim., vol.35, 1961, p.1289.

45. R.Baur and V.Gerold, Z.Metallkunde, vol.52, 1961, p.671.

46. R.Baur and V.Gerold, Acta Met., vol.10, 1962, p.637.

47. J.M.Silcock, T.J.Heal and H.K.Hardy, J.Inst.Met., vol.82, 1953-54, p.610.

48. R.H.Beton and E.C.Rollason, J.Inst.Met., vol.86, 1957-58, p.77.

49. A.C.Damask and G.J.Dienes, 'Point defects in metals', New York, Gordon & Breach, 1963.

50. F.S.Bradshaw and S.Pearson, Phil.Mag., vol.2, 1957, p.570.

51. G.Panseri and T.Federighi, Phil.Mag., vol.3, 1958, p.1223.

52. W.M.Lomer, 'Vacancies and other point defects', Inst.of Metals Monograph No.23, p.79. London, Inst.Metals, 1958.

53. J.Takamura, in 'Lattice defects in quenched metals', p.521, edited by R.M.J.Cotterill et al. London, Academic Press, 1965.

54. J.Takamura, in 'Physical metallurgy', p.681 edited by R.W.Cahn, Netherlands, North-Holland, 1965.

55. H.Jagodzinski and F.Laves, Z.Metallkunde, vol.40, 1949, p.296.

56. D.Turnbull and H.N.Treaftis, Acta Met., vol.5, 1957, p.534.

57. W.de Sorbo, H.N.Treaftis and D.Turnbull, Acta Met., vol.6, 1958, p.2.

58. D.Turnbull, 'Defects in crystalline solids', London, Physical Society, p.203, 1955.

59. D.Turnbull, Solid State Physics, vol.3, 1956, p.225.

60. F.Seitz in 'L'Etat Solide', p.401, Bruxelles, R.Stoops, 1952.

61. T.Federighi, Acta Met., vol.6, 1958, p.379.

62. W.de Sorbo, H.N.Treaftis and D.Turnbull, Acta Met., vol.6, 1958, p.401.

63. D.Turnbull, H.S.Rosenbaum and H.N.Treaftis, Acta Met., vol.8, 1960, p.277.

64. M.Wintenberg, Compt.Rend., vol.244, 1957, p.2800.

65. C.Panseri and T.Federighi, Acta Met., vol.8, 1960, p.217.

66. C.Panseri and T.Federighi, J.Inst.Met., vol.94, 1966, p.99.

67. S.Ceresara and P.Fiorini, Mat.Sci.Eng., vol.3, 1968, p.170.

68. E.W.Hart, Acta Met., vol.6, 1958, p.553.

69. T.Federighi and G.Thomas, Phil.Mag., vol.7, 1962, p.127.

70. G.Sines, R.Kikuchi and W.B.Grupen, J.Phys.Soc.Japan, vol.18, suppl.III, 1963, p.30.

71. W.B.Grupen and G.Sines, Acta Met., vol.13, 1965, p.527.

72. J.Okamoto and H.Kimura, Mat.Sci.Eng., vol.4, 1969, p.39; 'The mechanism of phase transformations in crystalline solids', p.79. Institute of Metals Monograph and Report Series No.33. London, Institute of Metals, 1969.

73. L.A.Girifalco and H.Herman, Acta Met., vol.13, 1965, p.583.

74. J.W.Cahn, Acta Met., vol.14, 1966, p.1685.

75. C.B.Walker and A.Guinier, Acta Met., vol.1, 1953, p.568.

76. J.D.Embury and R.B.Nicholson, Acta Met., vol.13, 1965, p.403.

77. G.W.Lorimer and R.B.Nicholson, Acta Met., vol.14, 1966, p.1009.

78. G.W.Lorimer and R.B.Nicholson, in 'The mechanism of phase transformations in crystalline solids', p.36. Institute of Metals Monograph and Report Series No.33. London, Institute of Metals, 1969.

79. G.W.Lorimer, Ph.D.Thesis, Cambridge University, 1967.

80. D.W.Pashley, J.Rhodes and A.Sendorek, J.Inst.Met., vol.94, 1966, p.41.

81. D.W.Pashley, M.H.Jacobs and J.T.Vietz, Phil.Mag., vol.16, 1967, p.51.

82. M.H.Jacobs and D.W.Pashley, in 'The mechanism of phase transformations in crystalline solids', p.43. Institute of Metals Monograph and Report Series No.33. London, Institute of Metals, 1969.

83. R.B.Nicholson, G.Thomas and J.Nutting, Brit.J.Appl.Phys., vol.9, 1958, p.25.

84. G.Thomas, 'Transmission electron microscopy of metals', New York, J.Wiley, 1962.

85. P.B.Hirsch, A.Howie, R.B.Nicholson, D.W.Pashley and M.J.Whelan, 'Electron microscopy of thin crystals', London, Butterworths, 1965.

86. R.D.Heidenreich, 'Fundamentals of transmission electron microscopy'. New York, Interscience, 1964.

87. E.H.Dix, F.Keller and R.W.Graham, Trans.AIMME, vol.93, 1931,p.404.

88. A.H.Geisler and J.K.Hill, Acta Cryst., vol.1, 1948, p.283.

89. A.Guinier and H.Lambot, Compt.Rend., vol.227, 1948, p.74.

90. A.Lutts, Acta Met., vol.9, 1961, p.577.

91. H.Lambot, Rev.Met., vol.47, 1950, p.709.

92. A.Lutts and H.Lambot, Rev.Met., vol.54, 1957, p.775.

93. A.Guinier, Acta Cryst., vol.5, 1952, p.121.

94. R.Castaing and A.Guinier, Compt.Rend., vol.227, 1949, p.1146.

95. A.Saulnier and P.Mirand, Rev.Met., vol.57, 1960, p.91.

96. G.Thomas, J.Inst.Met., vol.90, 1961-62, p.57.

97. G.Thomas, in 'Electron microscopy 1966', Proc.Sixth.Int.Congress Electron Microscopy, Kyoto, 1966, vol.1, p.389, Tokyo,Maruzen,1966.

98. M.H.Jacobs, Paper presented at Institute of Metals Conference on 'Electron Microscopy in Metallurgy', Swansea, Sept. 1967.

99. D.W.Pashley and J.Rhodes, Paper presented at Institute of Physics Conference on 'Electron microscopy', Cambridge, July 1963. (cited by R.B.Nicholson, W.C.Nixon and D.H.Warrington, Brit.J.Appl.Phys., vol.14, 1963, p.733).

100. G.C.Weatherley, Ph.D.Thesis, Cambridge University, 1966.

101. G.C.Weatherley and R.B.Nicholson, Phil.Mag., vol.17, 1968, p.801.

102. A.Guinier, Metaux, Corrosion-Usure, vol.18, 1943, p.209.

103. A.H.Geisler, C.S.Barrett and R.F.Mehl, Trans.AIMME, vol.152, 1943, p.201.

104. R.D.Garwood, A.L.Davies and G.L.Richards, J.Inst.Met., vol.88, 1959-60, p.375.

105. E.C.Ellwood, J.Inst.Met., vol.80, 1951-52, p.217.

106. R.Graf, J.Phys.Radium, vol.23, 1962, p.819.

107. M.Simerska and V.Synecek, Acta Met., vol.15, 1967, p.223.

108. W.Merz, T.R.Anantharaman and V.Gerold, Phys.Stat.Sol., vol.8, 1965, p.K5.

109. W.Merz and V.Gerold, Z.Metallkunde, vol.57, 1966, p.607.

110. W.Merz and V.Gerold, Z.Metallkunde, vol.57, 1966, p.669.

111. G.J.C.Carpenter and R.D.Garwood, Met.Sci.Journal, vol.1, 1967, p.202.

112. R.Graf and M.Lenormand, Compt.Rend., vol.259, 1964, p.3494.

113. K.Krishna Rao, H.Herman and E.Parthé, Mat.Sci.Eng., vol.1, 1966, p.162.

114. R.Ciach, Scripta Met., vol.2, 1968, p.575.

115. R.S.Leigh, Phil.Mag., vol.42, 1951, p.876.

116. V.A.Phillips and J.D.Livingston, Phil.Mag., vol.7, 1962, p.969.

117. M.F.Ashby and L.M.Brown, Phil.Mag., vol.8, 1963, p.1083.

118. M.F.Ashby and L.M.Brown, Phil.Mag., vol.8, 1963, p.1649.

119. M.Rogulic, Ph.D.Thesis, Cambridge University, 1964.

120. N.F.Mott and F.R.N.Nabarro, Proc.Phys.Soc., vol.52, 1940, p.86.

121. G.Thomas, Phil.Mag., vol.4, 1959, p.1213.

122. D.Kuhlmann-Wilsdorf, Phil.Mag., vol.3, 1958, p.125: J.Appl.Phys., vol.31, 1960, p.516.

123. P.B.Hirsch, J.Silcox, R.E.Smallman and K.H.Westmacott, Phil.Mag., vol.3, 1958, p.897.

124. A.T.Thomas, J.Inst.Met., vol.95, 1967, p.92.

125. A.J.Cornish and M.K.B.Day, J.Inst.Met., vol.97, 1969,p.44.

126. P.A.Thackery, J.Inst.Met., vol.96, 1968, p.228.

127. K.B.Rundman and J.E.Hilliard, Acta Met., vol.15, 1967, p.1025.

128. F.R.N.Nabarro, Proc.Roy.Soc., vol.A175, 1940, p.519.

129. F.R.N.Narbarro, Proc.Phys.Soc., vol.52, 1940, p.90.

130. R.G.Baker, D.G.Brandon and J.Nutting, Phil.Mag., vol.4, 1959, p.1339.

131. J.D.Embury and R.B.Nicholson, J.Austr.Inst.Met., vol.8, 1963, p.76.

132. J.L.Taylor, J.Inst.Met., vol.92, 1963-64, p.301.

133. J.B.Cohen, O.F.Kimball, M.Meshii and K.B.Rundman, Acta Met., vol.14, 1966, p.545; Scripta Met., vol.2, 1968, p.83.

134. G.J.C.Carpenter, Scripta Met., vol.2, 1968, p.77.

135. R.B.Nicholson in 'Electron microscopy and strength of crystals', p.861, edited by G.Thomas and J.Washburn, New York, Interscience, 1963.

136. J.W.Cahn, Acta Met., vol.5, 1957, p.169.

137. J.A.Nock, Iron Age, vol.159, 1947, p.48.

138. I.R.Harris and P.C.Varley, J.Inst.Met., vol.82, 1953-54,p.379.

139. M.Renouard and R.Meillat, Mem.Sci.Rev.Met., vol.57, 1960, p.930.

140. O.R.Singleton, Iron Age, vol.192, 1963, p.94.

141. P.E.Fortin, Canad.Met.Quart., vol.2, 1963, p.143.

142. P.E.Fortin, Metal Progress, vol.86, 1964, p.119.

143. H.Borchers and M.Kainz, Metall., vol.17, 1963, p.192.

144. H.Borchers and M.Kainz, Metall., vol.18, 1964, p.1045.

145. A.H.Geisler, Trans.AIMME, vol.180, 1949, p.230.

146. P.C.Varley, M.K.B.Day and A.Sendorek, J.Inst.Met., vol.86, 1957-58, p.337.

147. G.Thomas and J.Nutting, J.Inst.Met., vol.86, 1957-58, p.7; ibid vol.88, 1959-60, p.81.

148. I.J.Polmear, J.Inst.Met., vol.89, 1960-61, p.193.

149. H.A.Holl, J.Inst.Met., vol.93, 1964-65, p.364.

150. H.A.Holl, Met.Sci.Journal, vol.1, 1967, p.111.

151. N.Ryum, Acta Met., vol.16, 1968, p.327.

152. K.G.Kent, J.Inst.Met., vol.97, 1969, p.127.

153. H.S.Rosenbaum and D.Turnbull, Acta Met., vol.6, 1958, p.653; ibid, vol.7, 1959, p.664.

154. A.Saulnier, Mem.Sci.Rev.Met., vol.58, 1961, p.615.

155. A.J.Cornish and M.K.B.Day, paper presented at Inst.Metals Conference on 'Electron microscopy in metallurgy', Manchester, 1966.

156. A.J.Cornish and M.K.B.Day, J.Inst.Met., vol.97, 1969, p.44.

157. W.T.Read, 'Dislocations in crystals', New York, McGraw-Hill, 1953.

158. P.N.T.Unwin, G.W.Lorimer and R.B.Nicholson, to be published in Acta Met.

159. D.Turnbull, Acta Met., vol.3, 1955, p.55.

160. J.W.Cahn, Acta Met., vol.7, 1959, p.18.

161. M.L.V.Gayler, J.Inst.Met., vol.72, 1946, p.243.

162. I.J.Polmear and H.K.Hardy, J.Inst.Met., vol.81, 1952-53, p.427.

163. E.C.W.Perryman and J.C.Blade, J.Inst.Met., vol.77, 1950, p.263.

164. C.S.Smith, Trans.ASM, vol.45, p.533.

165. K.Krishna Rao and H.Herman, J.Inst.Met., vol.94, 1966, p.420.

166. G.Ll.Richards and R.D.Garwood, J.Inst.Met., vol.93, 1964-65, p.393.

167. M.L.V.Gayler, J.Inst.Met., vol.28, 1922, p.213.

168. H.K.Hardy, J.Inst.Met., vol.75, 1948-49, p.707.

169. S.T.Konobeevski, J.Inst.Met., vol.69, 1943, p.397.

170. L.E.Katz and H.Herman, J.Inst.Met., vol.17, 1965, p.107.

171. L.E.Katz, K.Krishna Rao and H.Herman, Trans.Indian Inst.Met., vol. 19, 1966, p.95.

172. R.H.Beton and E.C.Rollason, J.Inst.Met., vol.86, 1957-58, p.85.

173. Vad Prakash and B.R.Nijhawan, J.Inst.Met., vol.94, 1966, p.180.

174. G.J.C.Carpenter and R.D.Garwood, J.Inst.Met., vol.94, 1966, p.301.

175. R.Graf, Compt.Rend., vol.249, 1959, p.1110.

176. J.Lasek, J.Inst.Met., vol.95, 1967, p.320.

177. T.Niklewski, P.Spiegelberg and K.Sunbulli, Met.Sci.Journal, vol.3, 1969, p.23.

178. R.Graf, J.Inst.Met., vol.86, 1957-58, p.534.

179. I.M.Lifshitz and V.V.Slyozov, J.Phys.Chem.Solids, vol.19, 1961, p.35.

180. C.Wagner, Z.Elektrochem, vol.65, 1961, p.581.

181. R.A.Oriani, Acta Met., vol.12, 1964, p.1399.

182. G.W.Greenwood, 'The mechanism of phase transformations in crystalline solids', p.103. Institute of Metals Monograph and Report Series No.33. London, Institute of Metals, 1969.

183. S.L.Cundy, A.J.F.Metherell, M.J.Whelan, P.N.T.Unwin and R.B. Nicholson, Proc.Roy.Soc., vol.A307, 1968, p.267.

184. R.F.Cook and S.L.Cundy, to be published.

185. Discussion on precipitation in, 'The mechanism of phase transformations in crystalline solids',p.94. Institute of Metals Monograph and Report Series No.33,London,Institute of Metals,1969.

186. L.S.Darken, in 'Atom movements', p.1, Cleveland,Ohio,ASM, 1951.

187. Y.Adda and J.Philibert, 'La Diffusion dans les Solides',vol.1, p.142, France,Saclay(S.-et-O).Institut National Des Sciences et Techniques Nucleaires,1966.

188. J.E.Hilliard, B.L.Averbach and M.Cohen,Acta Met.,vol.7, 1959,p.86.